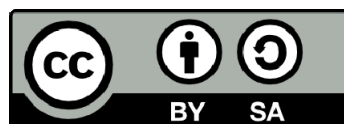




UNIVERSITAT_{DE}
BARCELONA

Advanced physiomimetic models for in vitro studies on respiratory diseases

Esther Marhuenda Segarra



Aquesta tesi doctoral està subjecta a la llicència **Reconeixement- Compartlqual 4.0. Espanya de Creative Commons.**

Esta tesis doctoral está sujeta a la licencia **Reconocimiento - Compartirlqual 4.0. España de Creative Commons.**

This doctoral thesis is licensed under the **Creative Commons Attribution-ShareAlike 4.0. Spain License.**



UNIVERSITAT DE
BARCELONA

Advanced physiomimetic models for in vitro studies on respiratory diseases

por

Esther Marhuenda Segarra

Para optar al título de doctora por la Universidad de Barcelona

Programa de Biomedicina

Línea de Ingeniería Biomédica

Directores: Isaac Almendros López y Jorge Otero Díaz

Facultad de Medicina y Ciencias de la Salud

Barcelona, Junio 2022

Esther Marhuenda

Isaac Almendros

Jorge Otero

Isaac Almendros López i Jorge Otero Díaz, professors de la Unitat de Biofísica i Bioenginyeria del Departament de Biomedicina de la Facultat de Medicina i Ciències de la Salut de la Universitat de Barcelona, i directors de la tesi doctoral de la Sra. Esther Marhuenda Segarra,

INFORMEN, sobre la participació personal de la Sra. Marhuenda Segarra en els articles científics inclosos a la seva Tesi Doctoral, que es presenta en el format de compilació d'articles. A continuació es fa referència als articles en el mateix ordre en que apareixen en la memòria de la Tesi doctoral:

Marhuenda E, Campillo N, Gabasa M, Martínez-García MA, Campos-Rodríguez F, Gozal D, Navajas D, Alcaraz J, Farré R, Almendros I. Effects of Sustained and Intermittent Hypoxia on Human Lung Cancer Cells. American Journal of Respiratory Cell and Molecular Biology, 2019. 61(4)

En aquest estudi Esther Marhuenda va desenvolupar el sistema experimental i va realitzar els experiments. També va a realitzar l'anàlisi dels resultats. A més, els resultats els va presentar en congressos nacionals i internacionals. Destacar que va ser premiat al congres de la European Respiratory Society com l'abstract més rellevant de l'assemblea de fisiologia respiratòria. Esther Marhuenda va escriure el primer esborrany de l'article i va participar en posteriors revisions.

Marhuenda E, Villarino A, Narciso ML, Camprubí-Rimblas M, Farré R, Gavara N, Artigas A, Almendros I, Otero J. Lung extracellular matrix hydrogels enhance preservation of type II phenotype in primary alveolar epithelial cells. International Journal of Molecular Sciences, 2022. 23(9).

Esther Marhuenda va ser responsable de tot el desenvolupament experimental. Va posar a punt el sistema d'aïllament de cèl·lules primàries alveolars de rata i va contribuir en el disseny dels diferents experiments. Posteriorment va fer l'aïllament i els cultius cel·lulars, va realitzar les tècniques experimentals d'anàlisi (qPCR i immunohistoquímica), i va processar les dades obtingudes. Així mateix, va tenir un paper protagonista en la redacció de l'article. *Aquest article no s'ha utilitzat ni formarà part, implícita o explícitament, de cap altra tesi doctoral.*

Marhuenda E, Villarino A, Narciso ML, Elowsson L, Almendros I, Westergren-Thorsson G, Farré R, Gavara N, Otero J. Development of a Physiometric Model of Acute Respiratory Distress Syndrome by using ECM Hydrogels and Organ-on-a-chip Devices. Frontiers in Pharmacology, 2022. Under review.

Esther Marhuenda va ser responsable de tot el desenvolupament experimental. Va posar a punt el sistema de co-cultiu de cèl·lules primàries alveolars i mesenquimals de pulmó de rata i va contribuir en el disseny dels diferents experiments. També va realitzar el setup experimental per cultivar les cèl·lules en hidrogel de matriu extracel·lular a un lung-on-a-chip on es podien sotmetre a estirament mecànic i controlar la concentració d'oxigen. També va posar a punt el model de dany inflamatori per LPS i del seu tractament amb dexametasona. Posteriorment va realitzar les tècniques experimentals d'anàlisi (ELISA i

immunohistoquímica), i va processar les dades obtingudes. Així mateix, va tenir un paper protagonista en la redacció de l'article. *Aquest article no s'ha utilitzat ni formarà part, implícita o explícitament, de cap altra tesi doctoral.*

A més, cal destacar que la Sra. Marhuenda ha col.laborat molt activament amb altres treballs de recerca del laboratori durant la realització de la seva Tesi Doctoral, com queda reflectit en la resta d'articles on la doctorand és coautora.

Així ho fem constar pels efectes que siguin pertinents davant la corresponent Comissió de Doctorat de la Universitat de Barcelona.

ISAAC
ALMENDROS
LOPEZ - DNI
77588447V

Firmado digitalmente
por ISAAC
ALMENDROS LOPEZ -
DNI 77588447V
Fecha: 2022.05.27
11:33:22 +02'00'

Isaac Almendros López



Jorge Otero Díaz

INDEX

LIST OF ABBREVIATIONS.....	6
Chapter I Introduction.....	9
1. Respiratory physiology	10
1.1 Lung extracellular matrix composition.....	10
1.2 Biomechanical properties of the extracellular matrix.....	12
1.3 Lung cell populations.....	15
1.4 Cyclic stretch.....	16
1.5 Lung immune homeostasis.....	18
2. Respiratory diseases.....	20
2.1 Obstructive Sleep Apnea.....	20
2.2 Chronic Obstructive Pulmonary Disease.	22
2.3 Overlap syndrome.....	24
2.4 ARDS.....	25
3. Main features in respiratory disease in vitro models.....	28
3.1 Hypoxic patterns.....	28
3.2 Cyclic stretch.....	30
3.3 Extracellular matrix.....	31
3.4 Cocultures.....	33
3.5 Advanced models.....	34
Chapter II Aims of the thesis.....	40
1. Aims.....	41
1.1 General aim.....	41
1.2 Specific aims.....	41
Chapter III Articles in this thesis.....	42
Chapter IV Scientific article I.....	44
Chapter V Scientific article II.....	54
Chapter VI Scientific article III.....	68
Chapter VII Results Summary.....	79
Chapter VIII Discussion.....	83
Chapter IX Conclusions.....	96
Chapter X References.....	98

Chapter XI Appendices.....	127
APPENDIX A Fabrication and calibration of chips.....	128
APPENDIX A. Isolation of primary lung cells.....	136
APPENDIX B. Cell culture on chips and lung hydrogels adhered to the chip surface.....	142

ABBREVIATION INDEX

ALI: air-liquid interface

AHI: apnea-hypopnea index

AQP: aquaporin 5

ARDS: acute respiratory distress syndrome

ATI: alveolar type I

ATII: alveolar type II

CCSP: club cell secretory protein

COPD: chronic obstructive pulmonary disease

CPAP: continuous positive airway pressure

DAD: diffuse alveolar damage

DAMPs: damage-associated molecular patterns

ECM: extracellular matrix

EHS: Engelbreth-Holm-Swarm

FA: focal adhesion

FAK: focal adhesion kinase

FBS: Fetal Bovine Serum

GAG: glycosaminoglycan

GelMA: gelatin methacryloyl

IH: intermittent hypoxia

IL-6: interleukin-6

IL-8: interleukin-8

KGF: keratinocyte growth factor

LINC: linkers of the nucleus and the cytoskeleton

LMSC: lung mesenchymal stromal cells

LPS: lipopolysaccharide

MMPs: matrix metalloproteinases

MSC: mesenchymal stromal cells

NCP: nuclear pore complex

NLRs: NOD-like receptors

NF- κ B: nuclear factor- κ B

OS: overlap syndrome

OSA: obstructive sleep apnea

PAMPs: pathogen-associated molecular pattern molecule

PDMS: polydimethylsiloxane

PDPN: podoplanin

PEEP: positive end-expiratory pressure

PHD: prolyl hydroxylase

PRR: pattern-recognition receptors

ROCK: Rho-kinase

ROS: reactive oxygen species

SCGB: secretoglobin

SH: sustained hypoxia

SF: stress fiber

SPC: surfactant protein C

SPB: surfactant protein B

TIMPs: tissue inhibitors of metalloproteinases

TLR: toll-like receptors

TNF- α : tumor necrosis factor- α

YAP: yes associated protein

Chapter I.
INTRODUCTION

1. Respiratory physiology

Lungs are complex organs with a structure composed of ≈ 300 million alveoli and an alveolar area of 140 m^2 responsible for gas exchange ¹. To accomplish this function, they need to meet a series of characteristics: specific location of different cell types specialized in certain functions, and composition and structure presenting mechanical characteristics allowing them to endure the tensile forces originated by breathing. Moreover, to ensure the correct gas exchange, the alveoli are surrounded by a capillary network. ²

1.1 Lung extracellular composition

In addition to cells, all organs present an acellular component, the extracellular matrix (ECM). It is mainly formed by fibrous proteins, glycoproteins, and proteoglycans, and it presents a unique and dynamic composition that varies depending on the tissue, the characteristics of the individual, and other physiological circumstances. Besides, the ECM can present two different structural functions. On one hand, basement membranes, composed of the basal lamina (mainly formed by glycoproteins) and the reticular lamina (mainly formed by collagen), can be found underneath the cells or covering nerves, organs, and muscles. On the other hand, interstitial matrices are composed of different proteins forming a fibrillar meshwork that gives structural support and interconnects different cell types conferring cohesiveness (Figure 1) ^{3,4}.

The ECM plays an important structural and biological role in tissues. It provides physical support to the cells and participates in the physical separation of organs and tissues. Also, it is a reservoir for secreted proteins (growth factors, ECM modifying enzymes, and ECM associated proteins). Moreover, ECM interacts with cells, thus participating in the biophysical and biochemical cell signaling. In the specific case of the lung, the extracellular matrix composition is responsible for the biophysical characteristics that allow them to constantly stretch and recoil for breathing. Although the lung ECM contains hundreds of components, most of them can be classified into structural proteins (collagen and elastin), glycoproteins, and carbohydrates (glycosaminoglycans (GAGs) and proteoglycans) (Figure 1). ³

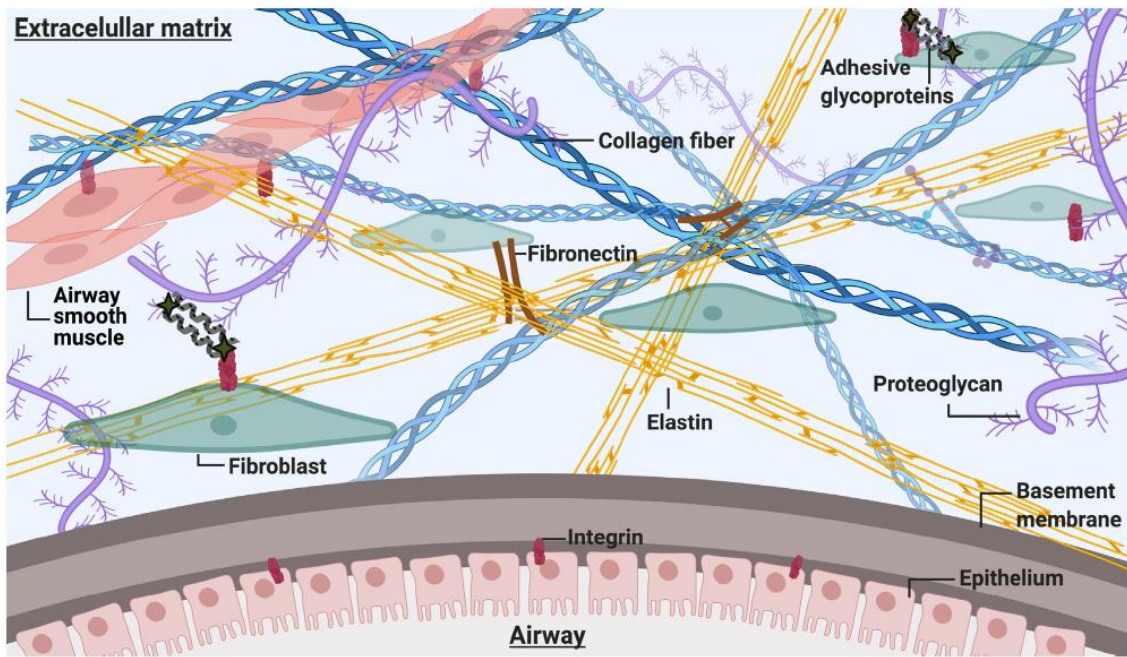


Figure 1. Composition of the lung extracellular matrix and its interaction among them and with the interstitial cells. Image from Wijsman *et al.* 2021.⁵

- **Structural proteins.** The two main structural proteins in the lung are collagen and elastin.³ The most abundant one is collagen, which gives mechanical support to the tissue for withstanding tensile forces⁶. Collagen is usually found forming fibers, but it can be also found forming sheets as a part of the basement membranes.⁷ The elastic properties of the ECM are mainly provided by another protein, elastin, due to its characteristic composition: the increased number of hydrophobic regions are hidden in the inner part of the protein in its quaternary composition. When mechanical loads are applied, these regions are exposed to the aqueous medium, and when they disappear, elastin recovers its globular conformation.⁸

- **Glycoproteins.** These proteins act as intermediaries binding proteins from the ECM among them or with the cells, contributing to forming the ECM cohesive network. Some glycoproteins, like fibrillin, also contribute to lung elasticity by covering the external part of the elastic fibers.⁹ The two main glycoproteins are laminin and fibronectin. Laminin is one of the most important components of the basal lamina, which is the specialized ECM layer below the epithelial and the endothelial cells separating them from the connective tissue, acting as a barrier. In addition to its structural role, laminin is a bridge between cells and other ECM components, influencing cell behavior and differentiation.¹⁰ Fibronectin is a large glycoprotein that maintains ECM consistency by connecting different

components and regulates cell adhesion, migration, and differentiation through the binding of cells to other proteins.⁷

- **Glycosaminoglycans.** They are polysaccharides whose main functions are to help maintain the hydration in the tissues due to their negative charge, provide resistance to mechanical loads, and participate in cell signaling. Some of the processes they are implicated in are wound repair, proliferation, cell growth regulation, and cell adhesion. Often, glycosaminoglycans are covalently bonded to polypeptides, which are known as proteoglycans.¹¹

As said before, ECM is a dynamic evolving system, that can adapt to different physiological conditions. There are some proteins specialized in the ECM remodeling to keep homeostasis: matricellular proteins, metalloproteinases (MMPs), and tissue inhibitors of metalloproteinases (TIMPs).¹² Matricellular proteins are dynamically expressed and mature and coordinate the flow of information between cells and their environment by sequestering growth factors and binding ions, inhibiting the proteases by direct binding, activating cytokines, etc. Also, they induce the detachment of the cells from the ECM. Their abundance in the ECM is dynamic, increasing during remodeling processes as a response to an injury, and during development.¹³ Metalloproteinases are a family of extracellular enzymes with proteolytic activity. Some of them are constitutively expressed but others are synthesized only under disease or remodeling situations. They play a key role in some important processes for the lung as remodeling, branching morphogenesis,¹⁴ cell migration,¹⁵ repair, matrix turnover,^{16,17} and host defense against pathogens.¹⁸

1.2 Biomechanical properties of the extracellular matrix

Topography and stiffness are the main biomechanical properties of the ECM impacting the lung tissue behavior. The stiffness of a tissue is a measure of the resistance to deformation when external forces are applied. It depends on the ECM composition, the degree of crosslinking of the fibers, and the interstitial fluids. The topography consists of the structural characteristics (architecture, geometry, size, and organization) of the tissue from the nanoscale to the macro-scale level.¹⁹

Several investigations^{20,21,22} about how biomechanical properties influence cell behavior *in vitro* have been made since this phenomenon was first reported in 1911 by Harrison²³ when studying the growth of embryonic cells on spider web fibers. He showed that topography influenced the morphogenesis and migration of cells. More recent works have also associated topography with cell

behavior as cells tend to align their cytoplasm in parallel to the pattern of the surface they grow on,^{24,21,25} and also influences their differentiation abilities²⁶. and migration velocity.^{24,21} Also, stiffness has been related to cell behavior, showing improved cell adhesion to the surface when the stiffness increases, with the consequent increase in cell spreading and size of focal adhesions.^{27,28} It also has consequences on the migration ability^{29,30,31} and cell identity as it can promote differentiation.^{32,33,29} The concentration of ligands has also been linked to the formation of FAs,^{34,35} influencing the spreading, proliferation, or differentiation^{22,36}. Increased stiffness goes usually together with an increase in ligand concentration, which makes it difficult to understand the independent contribution of both factors. However, the effects of stiffness alone have also been reported.^{37,38}

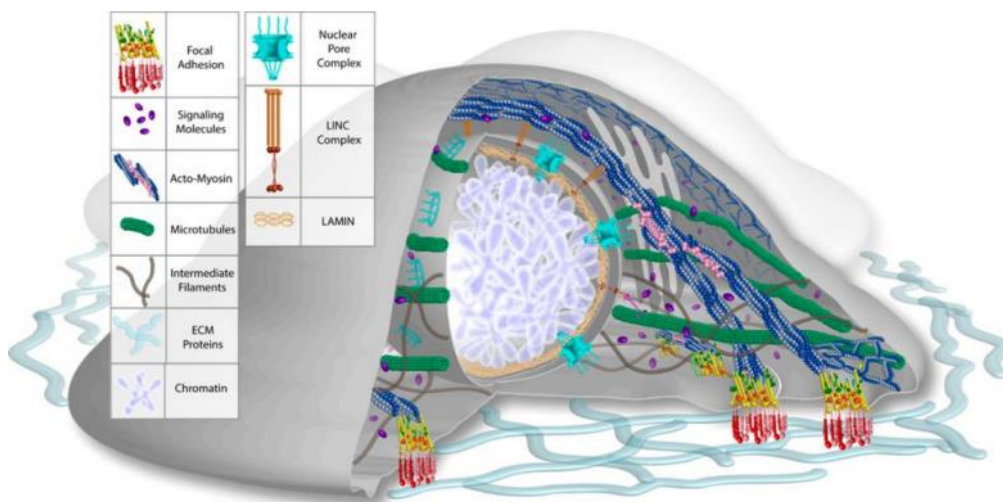


Figure 2. Signal mechanotransduction from the ECM to the nuclei through the formation of the focal adhesion complexes and the formation of the actin fibers. Image from Shams et al 2017.³⁹

Cells interact with the ECM by establishing adhesion protein complexes known as focal adhesions (FAs), formed mainly by integrins and a complex of proteins like vinculin, talin, focal adhesion kinases (FAK), and paxillin. Integrins are dimeric transmembrane proteins whose extracellular part interacts with the ECM and its intracellular part interacts with the complex of proteins that interplay with the cell cytoskeleton (figure 2)^{40 41}. The formation of the FAs is a complex and dynamic process where⁴² the Rho family of GTPases plays an important role, being Rac implicated in early events of focal complex formation, while Rho is related to the maturation of the focal adhesion.⁴³⁻⁴⁵ Rho, and more importantly, its effector Rho Kinase (ROCK), are involved in the formation of stress fibers that takes place during the maturation of FAs through the regulation of the myosin light chain phosphorylation,

which promotes the bundling of the actin filaments into stress fibers and also increases myosin ATPase activity leading to myosin contractility (Figure 3)^{46,47}. They are responsible to link the FAs to the cytoskeleton (comprised of microtubules, actin fibers, and intermediate filaments) to directly transmit the mechanical force of the ECM to the nucleus through the LINC (linkers of the nucleus and the cytoskeleton) complexes (Figure 2).^{48-51,39}

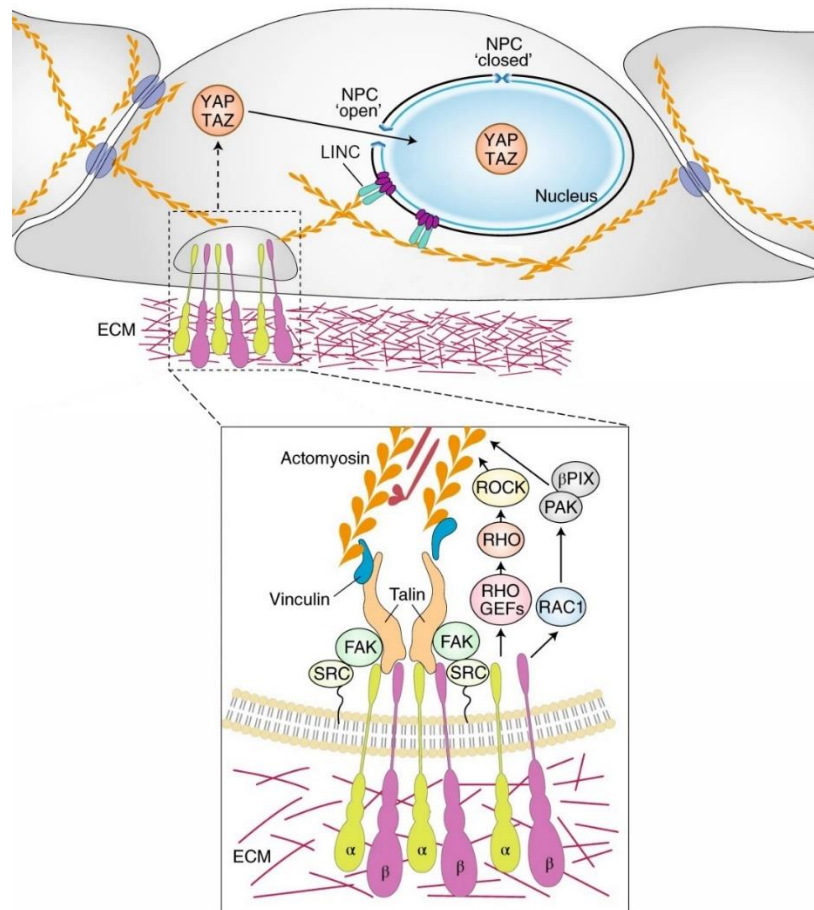


Figure 3. Integrin-mediated focal adhesions recognition of the ECM and activation of the signaling cascade that leads to actomyosin deposition. The formation of F-actin favors thanks to the LINC proteins the YAP translocation into the nuclei resulting in the transcriptionally active YAP/TAZ. Adapted from Totaro et al 2018.⁵²

As a result of the integrin-mediated ECM sensing, cells experience changes in their cytoskeleton through which it transmits the signal from the extracellular matrix to the nucleus, activating or inhibiting transcription factors, in a similar way that the chemical response can be triggered by the activation of signaling pathways and messengers in the cells.⁵³ One of the important transcription factors is the Yes-associated protein (YAP), which can translocate to the nucleus where it acts as a transcription factor through the nuclear pore complexes (NCP) due to the role of the actomyosin

fibers in modifying the nucleus shape after sensing the extracellular stiffness through the FAs (Figure 3)^{52,54}.

Through these responses, cells establish a dynamic interaction with the ECM: cells can modify or remodel the ECM (e.g secretion of metalloproteinases, collagen...), and they are affected by the properties of the matrix, which play a role in several important cellular processes.^{55,56,57,58}

1.3 Lung cell populations

Two parts can be distinguished in the mammal respiratory system: the conducting zone, which is formed by the trachea, bronchi, and bronchioles and transports the air, and the respiratory zone, which consists of the bronchioles, alveolar ducts, and alveoli, and is in charge of the gas exchange⁵⁹. The respiratory organs are formed by epithelial cells derived from embryonic endoderm, neuroectoderm, and mesoderm that cover from the trachea to the alveoli, including the bronchi and bronchioles,⁶⁰ but also present other cell types all over the different regions like endothelial, mainly forming the walls of the capillaries that cover the alveoli, and mesenchymal cells, fibroblasts, and myofibroblasts, found in the interstitium^{61,62}. The distribution of the different epithelial cells is different according to the location (figure 4). The trachea is composed of a pseudostratified epithelium specialized in warming and filtering the air obtained from the external environment and avoiding the entrance of dust and bacteria to the gas exchange area. Throughout all the airways can be found multiciliated cells which are specialized in the mucociliary clearance and basal cells that can give rise to all cell types within the airways. In the upper airway, there are also goblet cells, the main producers of mucins. As the airway becomes more distal, the epithelium becomes columnar, and goblet cells decrease in number, increasing neuroendocrine cells and club cells, involved in the response of lungs to the environment, and in the secretion of the secretoglobins and surfactant proteins, respectively^{63,61}. Finally, alveoli are formed by type I and type II alveolar epithelial cells. Alveolar type I (ATI) are squamous cells juxtaposed to the microvascular endothelial cells that surround the alveoli, so they can perform efficient gas exchange. They are specialized cells that don't present self-renewal ability and they compose 95% of the alveolar epithelium. Alveolar type II (ATII) are cuboidal cells that synthesize surfactant protein C to reduce the surface tension of the alveoli. They can act as a self-renewing stromal cell-like population that can also give rise to ATI cells⁶⁴.

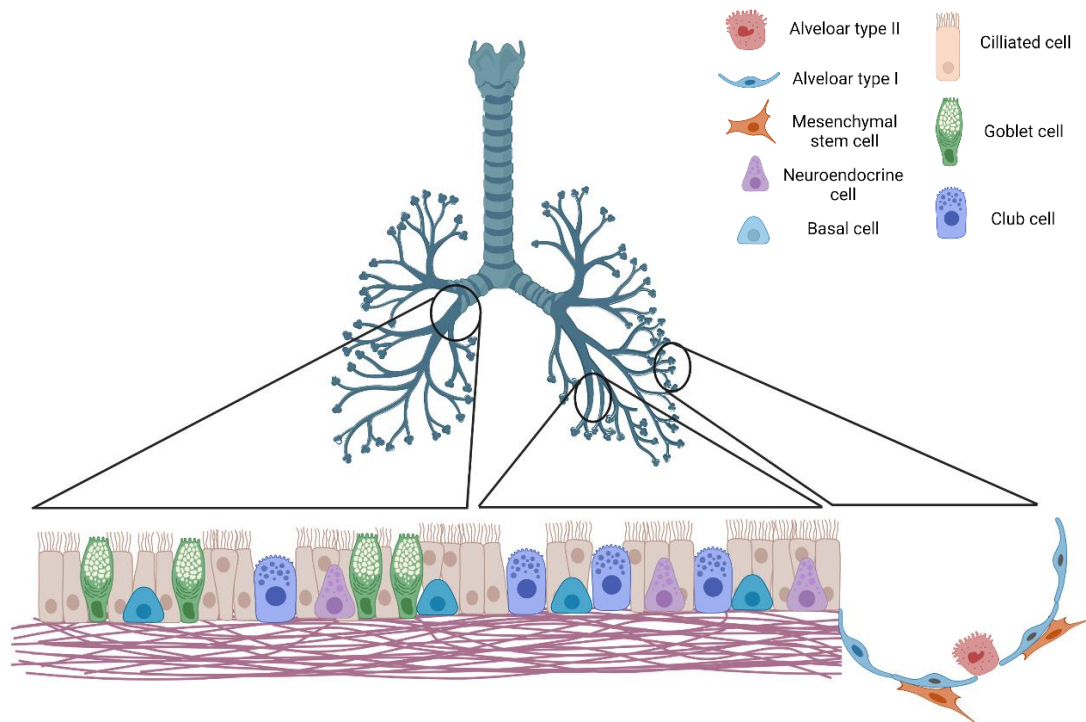


Figure 4. Cell type distribution from the proximal parts of the airways to the alveoli. Airways are formed by a pseudostratified epithelium including goblet, ciliated, club, neuroendocrine and basal cells. Alveoli are formed by a single layer of ATI and AII cells. Beneath them, there can be found mesenchymal alveolar cell. Based on images from Bennet et al 2021 and Basil et al. 2020.^{65,61}

Since the respiratory epithelium is exposed to an external source of pathogens and possibly toxic substances, there is a population of lung-resident mesenchymal stromal cells (LMSCs) whose function is to differentiate into several types of cells, contributing to the homeostasis and regeneration of the lung after injury ⁶⁶. They are cells with fibroblast-like morphology with multi-lineage differentiation capacity and specific surface markers (+CD105,+CD90, +CD73, -CD45, -CD34/CD11b, -CD79a/CD79) ^{67,68}. They have immunosuppressive abilities ^{69,70}, and the ability to differentiate to other lung cell types as shown by their ability to secrete Club cell secretory protein and aquaporin-5 under certain conditions ⁷¹. These cells play an important role in the distal epithelium, where are found in close association with AII cells, to contribute to the epithelium repair after damage, supporting cell growth, self-renewal, and differentiation ^{71,66,61}.

1.4 Cyclic stretch

Lungs are organs subjected constantly to cyclic stretch at a frequency of 10 – 20 breathings per minute (0.16 – 0.33 Hz) in the case of adult humans ⁷². These mechanical strains are key to biological function and are affected by spatially and temporary nonuniform loading and boundary conditions.

Gas exchange takes place in complex octahedron-shaped structures, with an approximate 100 μm diameter: the alveoli. They are composed of an air contact epithelial layer and endothelial cell line capillaries, separated by the extracellular matrix proteins (basement membrane). Those three components form a barrier that allows for effective gas exchange and prevents fluid leakage in the airspace⁷³. Lungs are composed of between 200 and 300 million alveoli which suppose a surface of 140 m^2 , which can increase when they inflate, thanks to their elastic properties.¹ Estimating the alveolar area is complicated due to the dependence on whether measurements are taken on inflation or deflation, the method of fixation, or the amount of surfactant⁷⁴. The transpulmonary pressure (P_T), which is the difference between the alveolar pressure and the pleural pressure, determines the volume of the lung. The stresses provoked by the P_T are transmitted to the air spaces through the tissue attachments and distend them, avoiding alveolar collapse. After the contraction of the diaphragm and the expansion of the chest wall, the alveolar pressure decreases below the atmospheric pressure, provoking the air entering the lung. The expiration is a passive process, where the elastic chest wall returns to its resting position increasing the alveolar pressure over the atmospheric pressure, and thus, the air is expired (Figure 5 A-C).⁷³

Therefore, lung cells are constantly subjected to a cyclic mechanical stimulation that plays an important role in tissue regeneration⁷⁵ and cell death^{76,77}, permeability⁷⁸, and migration⁷⁹. Also, stretch is essential in organ formation and development due to its involvement in the maturation of fetal lung muscles and epithelial cells. Different studies have related lung stretch to increased secretion of surfactant protein C during the episodic breathing movements in fetal lung development^{80,81}, the lung movement after birth, and as a consequence of mechanical ventilation⁸². Cells sense the stretch through the FAs, as explained previously, and can activate important pathways such as the MAPK signaling pathway^{83,84}. This pathway can be involved in the increased secretion of inflammatory cytokines, as several authors have claimed.⁸⁵ Like the effect of stiff substrates, cyclic stretch also provokes the formation of stress fibers and larger FAs. In fact, the subjection of cyclic stretch to cells cultured on soft substrates promotes similar results that stiff substrates in terms of focal adhesions and actin cytoskeleton remodeling⁸⁶.

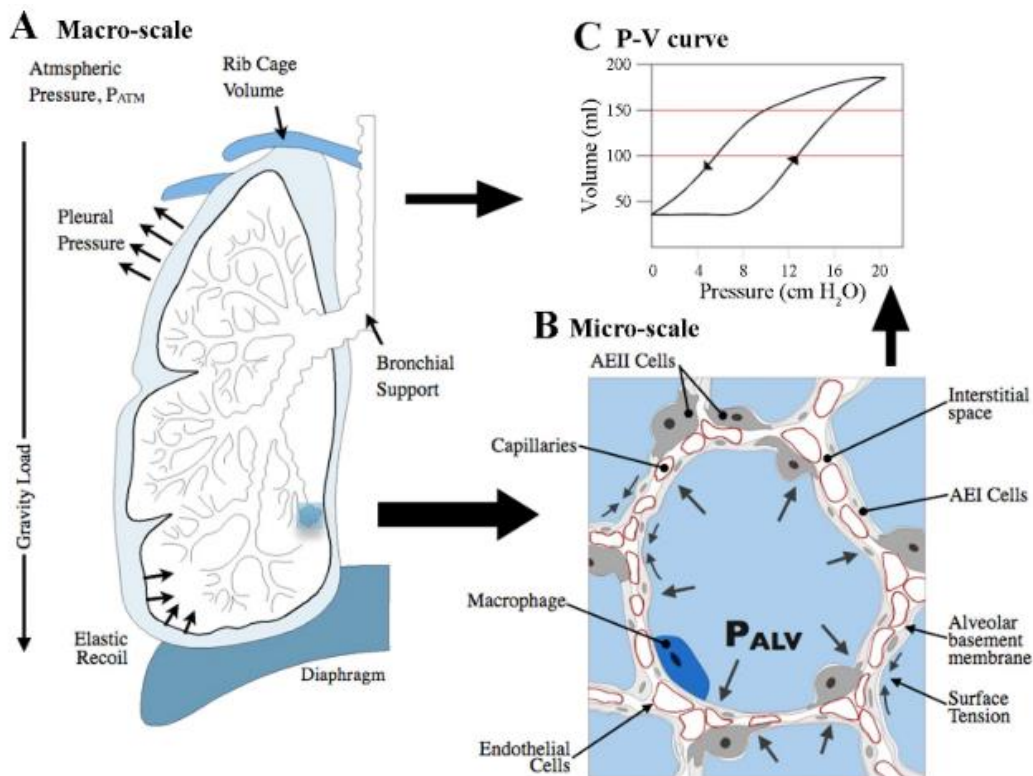


Figure 5. (A) Intrapleural pressure is the result of two opposing forces: elastic tissue and alveolar fluid surface tension pulls the lungs inwards, and the thoracic wall pulls the lungs outwards. The outward pull is slightly superior to the inward pull, maintaining the alveoli open. Upon the contraction of the diaphragm and the expansion of the chest, alveolar pressure decreases below atmospheric pressure and air goes inside the lungs. During the expiration process, the lung returns to its initial volume thanks to the elastic and recoil properties of the lung ECM in a passive process. (B) Alveolar structure formed by different type of cells. The arrows indicate the alveolar pressures (P_{ALV}). (C) P-V curve showing the hysteresis occurring in the respiration process. It is explained by the great intermolecular forces of the molecules lining the alveoli that must be broken in order to fill it with air. Image from Roan and Waters 2011.⁷³

1.5 Lung immune homeostasis

The lungs are constantly exposed to possible aggressions from the environment as the inhaled air can contain dust, microorganisms, and toxic substances. For that reason, they count on several defense mechanisms. One of them is the tight impermeable barrier that the epithelial cells of the respiratory tract form, which are bound together by tight junctions⁸⁷. These cells present different mechanisms as the presence of vili and the secretion of mucus to perform the mucociliary clearance in the upper airway⁸⁸. Some cells can secrete surfactant proteins A and D which play an important role in the immune response.^{89,90,91}

Airway epithelial cells can sense and respond to inhaled antigens through the recognition of pathogen-associated molecular patterns (PAMPs) or damage-associated molecular patterns (DAMPs)

by a conserved set of pattern-recognition receptors (PRRs). The PRRs can be classified into toll-like receptors (TLR) and NOD-like receptors (NLRs) ⁹²⁻⁹⁴. As a response to a pathogenic infection, after its recognition through the PRRs, epithelial cells can secrete a wide range of damage-associated molecular patterns proinflammatory cytokines and chemokines as TNF- α ⁹⁵, IL-1 β ⁹⁶, IL-6 ⁹⁷, IL-8, IFN- γ ⁹⁸, MCP-1 ⁹⁹, TGF- β ¹⁰⁰, GM-CSF ¹⁰¹ and CXCL5 ¹⁰². In addition, the epithelium can secrete also anti-inflammatory cytokines such as IL-10 to avoid excessive pro-inflammatory responses ¹⁰³. Apart from cytokines, epithelial cells can also protect the respiratory tract from external aggressions through the release of antimicrobial peptides known as defensins, which can directly kill bacteria, viruses, fungi, and protozoa, and inactivate toxins ¹⁰⁴⁻¹⁰⁶. Both cytokines and defensins can act as chemotactic agents for other immune cells such as monocytes, macrophages, T-cells, and dendritic cells ^{107,108}.

However, epithelial cells are not the only lung cell type capable of responding to pathogens through the secretion of cytokines. The aforementioned mesenchymal stromal cells actively participate in cytokine and chemokine production as a response to lung damage as *in vivo* and *in vitro* studies have shown ^{109,110,69}. Also, in the homeostatic lung, macrophages can be found in the interstitium (interstitial macrophages) and also in the alveoli (alveolar macrophages), in charge of phagocytosing the inhaled microorganisms and also secreting cytokines.

Briefly, the more relevant functions of the main involved cytokines are:

- IL-1 β : it induces the production of other cytokines. Its main functions are to promote ATII proliferation and to increase spreading and migration on the edge of wounds, favoring the epithelial repair. ¹¹¹ It is an early response cytokine and its expression has a role in the development of lung injury. ¹¹² It is a biomarker of bad prognosis in ARDS patients ¹¹³.
- TNF- α : it is one of the most important pleiotropic cytokines (cytokines able to exert many different types of responses, often on different cell types). Similar to IL-1 β , it induces the production of other cytokines and can promote alveolar epithelial repair. It also activates the expression of adhesion molecules and stimulates growth ^{114,111}. Its release in inflammatory processes is related to vascular endothelial damage, destruction of the barrier function, and reduction of antioxidants. ¹¹⁵
- IL-6: it's a pleiotropic cytokine that induces an inflammatory cascade reaction. It has been associated with a bad prognosis in ARDS patients, as it is a predictor of the severity of lung injury related to the CT (computerized tomography) score, and PaO₂/FiO₂ ratio. ¹¹⁶⁻¹¹⁸ Its

presence usually decreases over time during patients' recovery but it increases before worsening and before respiratory failure.¹¹⁷ It is also associated with a COPD severe phenotype.¹⁰⁸

- IL-8: its main function acts as a chemoattractant for different immune cells, especially neutrophils,¹¹⁹ and also acts as an angiogenic factor.¹²⁰ Its murine counterpart is known as MIP-2. Like IL-6, it is associated with a COPD severe phenotype.¹⁰⁸
- IL-10: it is a potent anti-inflammatory cytokine that is constitutively expressed in the alveoli and not only mediates the inhibition of other pro-inflammatory cytokines but also inhibits antigen-presenting function^{121,122,123}. It is known to present a release peak at day 1 in ARDS patients and decreases over time¹²⁴. Its reduction has been associated with increased mortality in ARDS patients¹²⁵.
- IFN- γ : it orchestrates early inflammatory events, enhancing immune-mediated injury in acute lung injury. Its main function is to activate macrophages upon viral or bacterial infection.¹²⁶

2 Respiratory diseases

2.1 Obstructive Sleep Apnea

Obstructive Sleep Apnea (OSA) is a chronic condition characterized by recurrent episodes of apnea or hypopnea, due to the complete or partial obstruction of the upper airway, respectively, during sleep. This respiratory cessation results in arousal from sleep and hypoxia and reoxygenation cycles, leading to its two major pathological traits: sleep fragmentation and intermittent hypoxia¹²⁷. People suffering from this pathology frequently present some symptoms derived from nocturnal sleep fragmentation, such as diurnal sleepiness or fatigue.¹²⁸ The apnea-hypopnea index (AHI), measured by polysomnography, represents the average number of apneic events experienced each hour during sleep. AHI is a diagnostic index for determining the presence and severity of OSA. According to it, OSA can be classified as mild (AHI between 5 and 14), moderate (AHI between 15 and 29), and severe (≥ 30). For determining OSA severity it is also useful to calculate the time that the saturation of the oxyhemoglobin in the blood is under 90%, which is known as T90.¹²⁹

The first-line treatment is the loss of body weight to reduce fat deposition around the neck and the abdomen which can cause a decrease in the pharynx lumen, and an increase in abdominal pressure.

¹³⁰ For the most severe cases, therapy with continuous positive airway pressure (CPAP) is chosen.

They can be combined with other treatments like antihypertensives. Alternatively to CPAP, there is the option of mandibular advancement devices, which keep the upper airway open to avoid collapse.¹³¹ Surgically, OSA patients can be treated by enlarging the oropharyngeal airway or by maxillofacial surgery.¹³²

The pathogenesis of OSA is multifactorial, complex and incompletely understood.¹³³ The reduced intrathoracic pressures and the activation of the sympathetic nervous system, combined with the relaxation of the throat muscles during sleep give rise to episodes of OSA. Anatomically, several factors can increase the collapsibility of the upper airway: 1) alteration of soft tissue structures, 2) abnormal craniofacial structures (retroposed mandibles, inferiorly placed hyoid bones) and 3) an excess of fat deposition. Also, the lack of pharyngeal protective reflex during sleep and the reduced neuromuscular compensation contribute to increasing pharyngeal collapsibility.¹³⁴

The hypoxic-reoxygenation episodes derived from the upper airway occlusion during sleep followed by the awakening of the patient can generate the liberation of many inflammatory mediators¹³⁵ and reactive oxygen species (ROS)¹³⁶ due to mitochondrial dysfunction, the activation of the NADPH synthase and the impairment of the nitric oxide synthase (NOS)^{137,138}. All these alterations, give rise to the existence of comorbidities, mainly cardiovascular^{139,140} or cerebrovascular diseases^{139,141}, metabolic dysregulations^{142,143} and lung cancer.^{144,145} Actually, several clinical trials associate the preexistence of OSA with a higher risk of developing lung cancer.^{146–148,149,150} The higher OSA prevalence in newly diagnosed lung cancer patients supported this relationship¹⁵¹. OSA severity is associated also with increased mortality risk in patients with III-IV lung cancer stage. Interestingly, higher values of AHI are related not only to increased mortality but also to increased HIF-1 α expression in the tumors of those patients, which is commonly used as a cancer prognosis marker^{152,153,154,155}. HIF-1 α has been related to tumor progression and resistance to therapy under both sustained and intermittent hypoxia^{152,153,154,156}. *In vitro* and *in vivo* experiments have been performed to elucidate the mechanisms linking hypoxia and the increased incidence and/or malignancy of lung cancer. Experiments performed in mice showed that IH increases tumor growth and invasiveness.¹⁵⁷ Some of the mechanisms underlying the increased malignancy as a consequence of IH could be the increased ROS produced by the hypoxic-reoxygenation cycles,¹⁴⁵ the release of exosomes promoting tumor invasion and metastasis,¹⁵⁸ and a shift to M2 phenotypes of the macrophages^{159,157}. However, despite all the knowledge and clinical improvements, sometimes the prognostic expectations do not

meet the reality ¹⁶⁰. This fact could be explained by the different mutations in each specific kind of cancer, ¹⁶¹ leading to a lack of agreement in the management of lung cancer. ^{162,163}

Cancer is not a homogeneous disease, hence we can find different histological types of cancer. Traditionally lung cancer was classified into two main divisions: small cell lung cancer (15%) and non-small cell lung cancer (85%). Due to the high heterogeneity within the second group, it has been subclassified according to its histology: adenocarcinoma, squamous carcinoma, and large cell carcinoma. ¹⁶⁴ Despite the link between OSA and lung cancer has been widely observed, little is known about how hypoxia could affect the different histological lung cancer cells and if the effect of hypoxemia derived from OSA is to accelerate the cancer progression or increase the cancer incidence.

2.2 Chronic Obstructive Pulmonary Disease

Chronic Obstructive Pulmonary Disease (COPD) is a progressive disease characterized by airflow limitation caused by abnormalities in the airways and/or the alveoli. It is usually accompanied by an inflammatory response, caused by the exposure to noxious particles. The disease is characterized by (1) oxidative stress, caused by activated inflammatory cells and noxious particles; (2) a protease/antiprotease imbalance, in part due to the excessive release of proteases by inflammatory and epithelial cells, leading to a destruction of the parenchyma; (3) and fibrosis, that can be developed by the inflammation together with small injuries.¹⁶⁵ Emphysema and chronic bronchitis are two diseases classically associated with COPD. Emphysema is the destruction of the air sacs and loss of lung parenchyma leading to a blunted blood oxygenation and a loss of flexibility and lung compliance, and its appearance is favored by all the main features of COPD previously mentioned (excess of proteases, inflammation, fibrosis, and oxidative stress).¹⁶⁶ Chronic bronchitis involves inflammation of the airways, mucus hypersecretion, and ciliary dysfunction.¹⁶⁷ Therefore, there are two main clinical phenotypes of the disease: one characterized by small airway disease (airflow obstruction phenotype), and the other with increased alveolar space destruction (emphysematous phenotype). Both, emphysema and chronic bronchitis, lead to air trapping, progressive airflow obstruction, and loss of elasticity due to an increase in the resistance of airflow and the compliance of the lungs. The consequence is the appearance of hypoxia and hypoxemia, leading to low exercise tolerance and low skeletal muscle function.^{168,165} The principal contributor to hypoxemia is ventilation/perfusion mismatch (V/Q ratio), as a result of airflow limitation and emphysematous destruction of the lung

capillary bed.¹⁶⁹ COPD patients with a predominant airflow obstruction phenotype will present a low V/Q ratio due to poor ventilation¹⁶⁹ and, on the contrary, the emphysematous phenotype will be characterized by a high V/Q ratio.¹⁷⁰

As mentioned, the inhaled noxious particles (from tobacco smoke or pollutants) play a very important role in the development of this disease. When in contact with inhaled toxins, small airways cells produce an inflammatory response. When COPD develops, this physiological response is amplified, with a consequent release of inflammatory cells and inflammatory mediators^{171,172}. These inflammatory cells are a source of oxygen and nitrogen reactive species that increase the oxidative stress created by tobacco exposure^{173,171}. This can favor inflammatory cells to release proteases (metalloproteinases) and the inactivation of antiproteases due to oxidation, creating an imbalance and favoring the destruction of the extracellular matrix that characterizes the emphysema^{174,175}.

Due to the inflammation and fibrosis, patients with COPD usually present gas trapping leading to lung hyperinflation, which translates into the reduction of FEV₁ (forced expiratory volume in 1 second) and FEV₁/FVC (forced expiratory volume in 1 second/ forced vital capacity). This hyperinflation reduces inspiratory capacity, which limits the exercise capacity of the patient¹⁷⁶. Also, gas exchange can be impaired in these patients due to the damage in the parenchyma, and together with the air trapping, can produce hypercapnia.¹⁷⁷ Mucus hypersecretion, occasionally accompanied by cough, is another symptom that some COPD patients present. It is due to the enlargement of the submucosal glands and the increase in the number of goblet cells.¹⁷⁸

The diagnosis of a COPD patient should be done by studying the clinical history (infections during childhood, presence of comorbidities like asthma, or family history of COPD), followed by a physical examination. Physical examination includes the detection of crackles or wheezing through auscultation, evidence of fatigue, or weight loss. Finally, the confirmation of the diagnosis should be done with spirometry.¹⁷⁹ The main treatment for COPD is the use of bronchodilators, which effect is the widening of the airways, reducing the hyperinflation at rest and during exercise.¹⁸⁰

Hypoxemia derived from COPD has been associated with several deleterious effects on the organism. As in OSA, there is an increase in oxidative stress by the secretion of ROS and increased NADPH oxidase function. Also, there is vasoconstriction derived from hypoxia due to the increased depolarization of pulmonary arterial smooth muscle cells, the impairment of the nitric oxide synthase, and the increase in vasoconstrictor mediators.¹⁸¹ In COPD patients is usual to find an increased

release of inflammatory mediators causing systemic inflammation. All these characteristics are usually translated into the comorbidity of other pathologies like atherosclerosis and other cardiovascular diseases,^{182,183} pulmonary hypertension,¹⁸⁴ skeletal muscle dysfunction¹⁸⁵, neurocognitive dysfunction,¹⁸⁶ and lung cancer.¹⁸⁷ In the case of lung cancer, there is increasing evidence that COPD patients are more likely to develop lung cancer (a 5-fold increase) than the general population¹⁸⁸. Several clinical trials concluded that the presence of COPD increased the risk of developing lung cancer in both smokers and non-smokers^{189,187,190,191}. Furthermore, the corticosteroids administered to COPD patients could increase lung cancer incidence.¹⁹² The tight relationship between both diseases can be due to the fact that they share common pathogenic pathways^{193,194}. The main event underlying this link is mainly the high oxidative stress that COPD patients present, which can promote DNA damage^{195,196} and the release of inflammatory mediators,¹⁷² both inductors of carcinogenesis^{197,198}. Also, some genetic mutations and polymorphisms predispose patients to suffer from both COPD and lung cancer.^{199,200} Importantly, tobacco consumption can also trigger both diseases, due to the accumulation of toxicants in the airway.^{201,202}

2.3 Overlap syndrome

COPD and OSA are both highly prevalent, and thus the coexistence of both disorders is often referred to as the overlap syndrome (OS). The incidence of OS is not well known because it can be underdiagnosed but some studies reveal a higher prevalence than would be expected by coincidence²⁰³. As explained previously, COPD patients have low oxygen levels due to the ventilation/perfusion (V/Q) mismatch resulting from progressive airflow limitation and emphysematous destruction of the pulmonary capillary bed.²⁰⁴ During the night, this condition can become more serious due to the relaxation of the intercostal muscles and reduced chest wall mobility.²⁰⁵ When it appears with concomitant OSA, the apnea episodes worsen the hypoxic level, having systemic consequences. The maintained hypoxia combined with the episodes of intermittent hypoxia in these patients increases the release of reactive oxygen species (ROS) and inflammatory mediators such as C-reactive protein, IL-6, NF- κ B, TNF- α , and IL-8.^{206,207} As both OSA and COPD are independently associated with an increased risk of suffering lung cancer, it is expected that the overlap of both diseases also gives rise to an increase in lung cancer risk.^{190,191,144,150} Several comorbidities have been associated with the overlap syndrome, however, data about its prevalence among the lung cancer population is missing

2.4 Acute Respiratory Distress Syndrome

Acute Respiratory Distress Syndrome is a life-threatening condition that was first described in 1967 as a conjunction of acute hypoxemia, reduced lung compliance, noncardiogenic pulmonary edema, difficulties in breathing, and the need for positive-pressure ventilation.²⁰⁹ It is a highly prevalent disease with high mortality rates: the prevalence of this disease in the intensive care admissions is between 10-15%, of which 80% need mechanical ventilation. Among these patients, 30% had mild ARDS, 47% had moderate ARDS, and 23% had severe ARDS.²¹⁰ The high heterogeneity in patients' symptoms made the establishment of a proper definition difficult but the most accurate one was made in 2012, considering physiological and epidemiological data as well as clinical trials. This new definition, known as the Berlin definition,²¹¹ considers ARDS patients to be those experiencing hypoxemia within 1 week of a known clinical insult or new or worsening respiratory symptoms, with bilateral opacities, or lobar/lung collapse. Also, it includes those patients that experience respiratory failure that is not fully explained by the cardiac failure or fluid overload. The value obtained by doing the ratio between the arterial oxygen pressure (PaO_2) and the inspired fraction of oxygen (FiO_2), is a useful measurement for assessing the severity of the disease. It can be classified as mild ($\text{PaO}_2/\text{FiO}_2 = 201\text{-}300$ mmHg), moderate ($\text{PaO}_2/\text{FiO}_2 = 101\text{-}200$ mmHg), and severe ($\text{PaO}_2/\text{FiO}_2 \leq 100$ mmHg).²¹¹

ARDS is the result of a wide spectrum of different risk factors that can have a pulmonary origin (direct lung insult as infection by bacteria, virus, fungi, or parasites; thoracic surgery; toxic gases inhalation; smoking; lung contusion...) or an extrapulmonary origin (indirect lung insult as non-pulmonary sepsis, blood transfusions, pancreatitis, drugs consumption...) ^{212,213}. All these insults can damage lung endothelial and epithelial cells causing diffuse alveolar damage (DAD). Epithelial cells are common to suffer sublethal injury due to for instance the bacterial pore-forming toxins, lytic viral infections, or high tidal volumes during mechanical ventilation. Inflammatory signals produced by pathogenic microorganisms also promote endothelial activation and can increase the permeability of the endothelium to allow leukocytes to travel to the wounded area. Furthermore, during this process of infection, pathogens and their toxins can produce cell-cell adhesion damage and endothelial cell apoptosis. The increased permeability and the endothelial disruption caused during the inflammatory process results in fluid leakage to the interstitium, which can infiltrate the alveoli through the damaged alveolar barrier. The resulting accumulation of fluid, proteins, neutrophils, and red blood cells inside the alveoli, is known as edema, which is the main hallmark of ARDS (figure 6). ^{214,215,216}. ARDS can be

divided into two stages according to the course of the disease: the early and the late phases. The early phase occurs within hours from the insult and is characterized by the secretion of inflammatory cytokines (IL-6, IL-1 β , IL-8, IL-10, IFN- γ , TNF- α , IL-18). It is in this early phase when DAD and edema take place, with the flooding of the alveolar space and the loss of alveolar epithelial cells. The late phase is characterized by the proliferation of fibroblasts and ATII cells, the increased deposition of the ECM, and vasculogenesis.^{217,126,218}

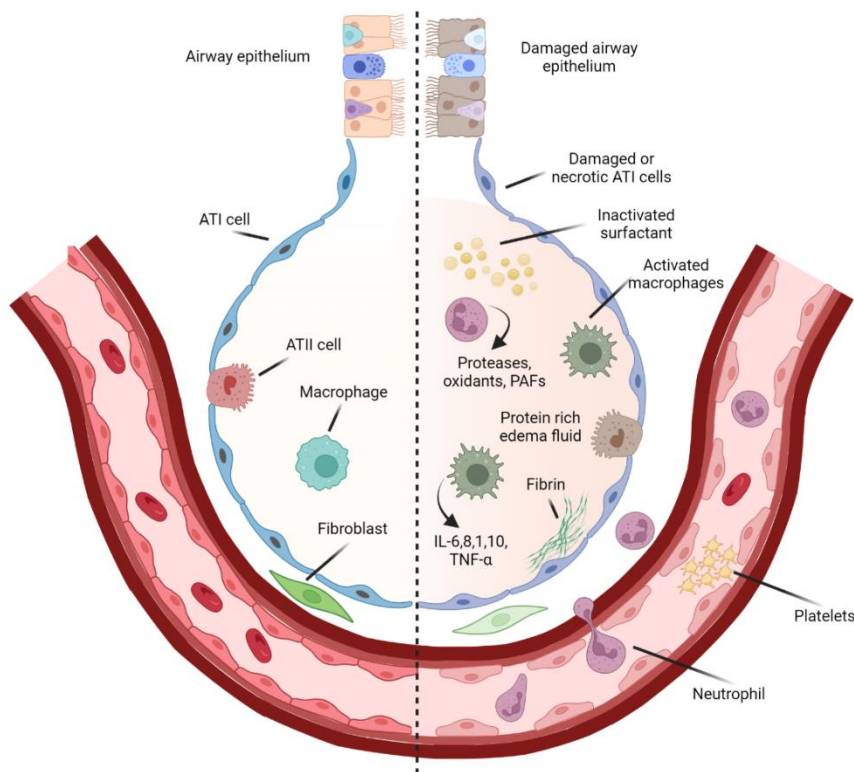


Figure 6. Schematic drawing of the mechanism of ARDS occurring in the alveoli. In the left part of the image, it is represented a healthy alveolus whereas in the right part there is a damaged alveolus. Adapted from Chen et al. 2020.²¹⁹

In addition to cell damage, ARDS-related infections have other effects such as mitochondrial dysfunction that results in hypercapnia, and alterations in the extracellular matrix, such as an increase in rigidity which decreases the compliance of the lungs. Also, the damage in the epithelium can result in an impairment in surfactant production, leading to the alveoli collapse. Altogether, combined with the cell damage, produces a ventilation-to-perfusion mismatch and an increased pulmonary dead

space caused by impaired excretion of carbon dioxide. The final physiological consequences are translated into increased hypercapnia and hypoxemia.^{220,221}

Most patients coincide with the feeling of short breath as the main symptom. Also, they usually present an elevated respiratory rate and tachycardia and need to make efforts to breathe. The main method to diagnose ARDS is image-based diagnosis. A chest radiograph can help to visualize lung edema²¹⁷.

Increasing interest in this syndrome has been developed in the past two years since ARDS is a major complication derived from infection by the highly contagious severe acute respiratory syndrome coronavirus 2 (SARS-CoV-2), the virus responsible for the coronavirus disease 2019 (COVID-19) pandemic. It has caused over 6 million deaths worldwide and more than 510 million infections, causing a global healthcare crisis.^{222,223}

ARDS patients' management is focused on the treatment of infections, respiratory support, and conservative fluid strategies. In moderate and severe ARDS cases, patients are subjected to mechanical ventilation with low tidal volumes and PEEP (positive end-expiratory pressure) ranging from 5 to 20 cmH₂O.²²⁴ Severe ARDS patients with high transpulmonary pressures are treated with neuromuscular blockade to avoid patient-ventilator desynchrony that can increase mechanical lung injury.²²⁵ For patients with mild ARDS, noninvasive respiratory support can replace mechanical ventilation to avoid the associated risks.²¹⁵ When patients do not show improvement in their symptoms, rescue therapies need to be applied. These therapies consist of the extracorporeal either oxygenation or elimination of CO₂ from blood using a membrane through which the blood is circulated.^{226,227} As pharmacological treatments, glucocorticoids have been employed to improve the inflammatory state and inhaled vasodilators to improve the ventilation-perfusion matching. However, the benefits of both treatments in terms of survival have not been demonstrated.²²⁸⁻²³⁰ In the last 50 years, only a few new drugs to treat respiratory diseases such as ARDS were subjected to clinical trial studies.²³¹ These discouraging data are explained by the fact that between 80-90% of researched drugs fail before they are even tested in clinical trials, and almost 50% of experimental drugs fail in Phase III trials.²³² Moreover, most traditional culture methods for modeling the disease *in vitro* are unrealistic, making more difficult the translation of the results to *in vivo* models. So, there is an urgent need to develop *in vitro* models to represent the physiological characteristics of the respiratory diseases, in this case, ARDS, to accelerate drug discovery and increase the success rate of the drugs that get to be tested in the clinical trials.

3 Main features in respiratory disease *in vitro* experimental models

Several efforts have been made by several research groups to better recreate *in vitro* the above-mentioned respiratory diseases. In this section, a succinct description of the main advances for *in vitro* mimicking the main typical characteristics of the lungs, such as the oxygenation patterns, cyclic stretch, interaction among cells, the use of scaffolds composed of extracellular matrix proteins, and the advances in the design of lung-on-a-chip devices for this purpose.

3.1 Hypoxic patterns

Cells and tissues in living organisms are exposed to oxygen pressures ranging from 1% to 6%.²³³ Lung alveolar cells, however, are constantly exposed to ~13% (~100 mmHg) of oxygen pressure, which is the concentration of O₂ in the air that reaches the alveoli.¹⁹ Nevertheless, most experiments are carried out under stable conditions of temperature (37 °C), humidity, and atmospheric air enriched with 5% of CO₂. The volume fraction of oxygen in the incubator is approximately 18.6% (135.2 mmHg), attending to the fraction displaced by the added CO₂ (5%) and by the partial pressure of the evaporated water.²³⁴ This supposes a hyperoxic environment for cell culture that can contribute to obtaining different results derived from non-physiologic conditions²³⁵. In addition, some diseases can promote a decrease in the oxygen levels^{236,237,237} or even promote a dynamic scenario in terms of oxygen availability.²³⁸

For studying cell behavior under different oxygen conditions, hypoxic incubators can be used.^{239,240} However, this approach presents some limitations as (1) the slow diffusion of gas through the culture medium, which can be even slower than the oxygen consumption in highly active metabolic cells leading to non-controlled hypoxic conditions, and (2) the impossibility of subjecting the cells to rapid hypoxic cycles to mimic OSA disease. Another option to subject cells to hypoxia is the use of hypoxia mimetics in the culture media. These are compounds that produce a hypoxic-like response in the cell due to the inhibition of the HIF-prolyl hydroxylases (PHDs), which are essential for HIF-1 α degradation. CoCl₂ is the most widely used and it acts through the competition with the Fe²⁺ ions necessary for the enzymatic activity of the PHDs.²⁴¹ These two aforementioned methods can be used for studying the effect of continuous hypoxia,^{239,240,242} but none of them are optimal for the study of the effects of intermittent hypoxia mimicking OSA, due to the need for rapid oxygen

variations that can be sensed by the cells. In the field of microfluidics, several devices have been created for studying the effect of the oxygen gradients, using PDMS chips with microchannels that act as a gas mixer^{243,244} or that introduce the use of oxygen scavengers²⁴⁵. For studying the effect of intermittent hypoxia, several approaches have been addressed, from the use of an oxygenated medium to the fabrication of custom-made devices. Different studies subjected different types of cells (cancer cells or macrophages) to intermittent hypoxic patterns with the use of medium previously equilibrated to the desired oxygen concentration, using gas equilibrators²⁴⁶ or oxygenated medium reservoirs.²⁴⁷ These systems could rapidly subject cells to alternate oxygenation patterns, being able to represent severe cases of OSA. However, they had the problem that cells were also subjected to shear stress, which may not be a representative cue of their physiological environment. Oppegard *et al.*²⁴⁸ designed a PDMS device that adapted to a Boyden chamber so cell migration and invasion could be studied under intermittent hypoxia. However, this device was employed for studying cells in the context of cancer and could not be used for studying intermittent hypoxia corresponding to OSA due to the long equilibration times that it presents (20 minutes). PDMS has been widely used to achieve rapid swaps in oxygen concentrations compatible with the study of IH occurring in OSA. Polak *et al* used culture plates with permeable PMDS membrane underneath, and 10-minute cycles of different hypoxic patterns were employed to study the effect of IH on insulin secretion.²⁴⁹ Campillo *et al* designed two different models of custom-made devices. The first of them, permitted the study of the effects of IH combined with different stretching patterns, corresponding to either the cardiac frequency or the respiratory frequency.²⁵⁰ The second one was employed for the study of the effect of different amplitudes and frequencies corresponding to different IH patterns in OSA.²⁵¹ Due to the elevated number of comorbidities that OSA presents, the use of these devices to explore the relationship among the different diseases is really attractive. However, only a few of them were used to study these relationships in the case of cardiovascular diseases,²⁵¹ metabolic dysregulations,²⁴⁹ and cancer.²⁴⁷ Of these three studies, the one investigating the effect of hypoxia in cancer cells used non-realistic and exaggerated ranges of hypoxia, with cycles varying from 5% to 20%. Attending to the fact that the higher oxygen pressure is found in the arterial blood and corresponds to 13%, there is a lack of information on how cancer cells can react to intermittent oxygen patterns representing those occurring in intermittent hypoxia.

3.2 Cyclic stretch

Mechanical stretch has many biological effects on lung function at the cell level but also at the organ level. It has been linked to important processes such as fetal lung growth, surfactant secretion and metabolism, cell proliferation and apoptosis, ECM and cytoskeleton turnover, alveolar-capillary permeability, and release of mediators.^{76,252,253,81,80}

In vitro stretch models have been used to study different types of cells due to the implication of stretch in different organs of the body, like the heart, the lungs, the intestines, the bladder, or the skeletal muscle contraction. For that reason, there is a need for adjusting the amplitude and frequency of strain to the parameters that best mimic the object of study, as well as for deciding if the stretch is applied uniaxial, biaxial, or equiaxially.²⁵⁴

One of the first studies performed with stretch was in 1979 on the development of skeletal myotubes in myoblasts from embryonic chickens subjected to mechanical stretch. The cells were cultured on a membrane within an expansible frame that allowed for longitudinal stretch.²⁵⁵ In the area of respiratory physiology, one of the first studies performed employing stretch was published in 1990 by Wirtz and coworkers, where authors applied hydrostatic pressure under the membranes where cells were cultured for stretching them²⁵⁶ to study the expression of surfactant proteins, which was seen to be associated with an increase in cytosolic Ca^{2+} . However, the main limitation of this pioneering study was the impossibility of subjecting cells to cyclic stretch.

Gutierrez et al used similar devices for studying the effect of stretch in the differentiation of ATII cells. They observed a significant increase in cells expressing ATI markers together with a decrease in cells expressing ATII markers when subjected to a single strain of 21%.²⁵⁷ Later on, the static stretch was related to the consequent small GTPases and Rho signaling pathway activation to an increased formation of actin stress fibers and eventually ATII-ATI transdifferentiation.²⁵⁸ Recent studies obtained similar results regarding the activation of the Rho pathway and its relationship with ATII transdifferentiation through the activation of YAP/TAZ.²⁵³ In this latter study, the authors showed the relationship between the Rho-mediated YAP/TAZ activation and the increase in ATI cell population both *in vivo* (by mice fetus tracheal occlusion) and *ex vivo* (by introducing an agarose volume superior to total lung capacity).

In the ARDS context, most of the studies performed were addressed to investigate the effect of mechanical ventilation on certain cell damage, usually induced by the use of a lipopolysaccharide

bacteriotoxin (LPS) challenge. For doing so, different magnitudes of cyclic stretch (from 5% to 30%) and frequencies (from 0.1 Hz to 0.5 Hz) were applied to different cell lines including alveolar cells, bronchial cells, macrophages, and fibroblasts. From these experiments, it was derived that the cyclic stretch alkalinized the media favoring the proliferation of bacteria related to ventilator-associated pneumonia²⁵⁹ and also induced the secretion of inflammatory cytokines^{260,261}. This increase in cytokines seems to be related to the increase in oxidative stress due to mitochondrial ROS production.²⁶⁰ The development of fibrosis associated with the mechanical ventilation was also studied as the increased ECM deposition in the fibroblast culture at high magnitudes of a stretch compared to lower magnitudes, relating these data with the protective ventilation.²⁶² All these studies give interesting data on how lung cells behave under the combined stimuli of LPS hit and cyclic stretch. However, none of them has considered the fact that under physiological conditions, alveolar cells experience a strain similar to that applied to represent mechanical ventilation. For that reason, it is important to include cyclic stretch as a parameter in *in vitro* models of lung pathologies such as ARDS. Moreover, devices to perform stretch should be combinable with the induction of different oxygenation patterns to fully represent the environment.

3.3 Extracellular matrix

Given the relevance of ECM in cell behavior, it is important to introduce the use of scaffolds with a similar composition and topography as the native tissue in the *in vitro* cultures to obtain more representative results of what is happening *in vivo*.²⁵⁴ This is interesting for studying not only the response of cells as they establish interactions with the substrate, but also it would open the door to three-dimensional culturing, especially for stromal cells. For that reason, hydrogels, which are highly hydrated polymeric materials that try to resemble the physical and/or biochemical characteristics of the ECM, are gaining popularity for cell culture. They are used for 3D culturing and have the advantage that can be easily tuned to modify some of their physicochemical characteristics to adequate them for a particular study.^{263,264,265} Hydrogels can be composed of polysaccharides, (e.g. alginate, carrageenan, agarose, or chitosan)^{263,266–268} proteins,^{269,270} or a complex amalgam of proteins derived from decellularized tissues.^{271,272} Polysaccharides have been used in the encapsulation of cells but also in the fabrication of hydrogel as a culture scaffold and as a vehicle for cell therapy or drug treatments^{273,274,275,276,277,278}. However, despite their high biocompatibility and low immunogenicity, their biochemical composition is very different from the ECM one. To make non-physiologic

polymers a more idoneous culture scaffold, polysaccharides can be mixed with proteins as the mixture between agarose and collagen I in the case of alginate for increasing the number of adhesion motifs,²⁷⁹ the modification of the mechanical properties and water holding capacity of agarose hydrogels with the addition of polydopamine,²⁸⁰ or the chitosan hydrogel by its mixture with collagen.²⁸¹ Protein-based polymers have been extensively used and their importance resides in their ability to resemble physiologic scenarios based on their biocompatibility, the cell adhesion ability they present, and their presence in the extracellular matrix.^{282,283} Among protein-based hydrogels, the most commonly used has been type I collagen, mainly because of its ease of obtaining²⁸⁴ from different sources like bovine, porcine²⁸⁵ or rat²⁸⁶. Some studies performed with the use of collagen hydrogels showed that the environment where cells are cultured on is essential in cell survival, in carrying out specific functions of a certain cell type, and even in their identity in the case of mesenchymal stromal cells, and that cells showed different behavior according to the different properties of the hydrogels in terms of biomechanical properties.^{264,287,270,288,270} Mesenchymal stromal cells have shown increased differentiation capacity in those environments more similar to their *in vivo* niche, as in the case of osteogenic differentiation in cells cultured in collagen hydrogels containing basic fibroblast growth factor²⁶⁴ or chondrogenic differentiation in those cells cultured in collagen II hydrogel versus other cultures employing collagen I or alginate²⁸⁷.

In recent years, methods for producing hydrogels from the ECM have appeared. Great advances have been made in the field of tissular bioengineering since the first ECM-derived hydrogel was fabricated²⁸⁹. As the composition and the organization of the extracellular matrix varies among tissues, there are ECM-derived hydrogels fabricated from different sources. (e.g. skin, heart, lungs, kidney...)^{271,272,290,291}. The interest in ECM-derived hydrogels resides in their potential to affect cellular behavior, even though the mechanisms through which they act are not completely understood. It seems that they can be releasing bound growth factors, cytokines, and chemokines and that they expose bioactive motifs and cryptic peptides which the cells can interact with²⁹²⁻²⁹⁵. The protocol to fabricate ECM-derived hydrogels is performed with decellularized organs obtained with a protocol consisting of different detergents. After that, the sample is freeze-dried and milled. Once the decellularized ECM powder is obtained, it is subjected to two important steps. The first one consists of the solubilization of ECM proteins into monomeric components and the second one consists of the spontaneous rearrangement of the monomeric components into a homogeneous gel by controlling the pH and the temperature. For achieving the first step, it is fundamental to digest the ECM proteins after powdering them with pepsin obtained from porcine gastric mucose. Several

protocols can be found in the literature about the diluent used for such reaction.^{296,297,289,272} The parameters (pH, temperature, salt concentration) at which the hydrogel polymerizes can be modified to change its mechanical properties.²⁹⁶ Like collagen hydrogels, lung ECM-derived hydrogels are compatible with 3D-cultured cells, showing attachment, proliferation abilities and viability.²⁷² Furthermore, mechanical properties of tissue-derived hydrogels can affect to the gene expression of the cells cultured inside, like in the higher collagen I and α -smooth muscle actin expression in the case of myofibroblast cultured in stiff hydrogels compared to soft ones.²⁹⁸

The use of hydrogels in the culture of alveolar epithelial cells was first employed by Shannon²⁹⁹ when studying the increase in the secretion of surfactant proteins of alveolar cells cultured on EHS hydrogels, in which the main composition was a mixture of proteins, mainly laminin, type IV collagen, heparan sulfate proteoglycan, and entactin. This result was very important due to the limited ability of alveolar type II cells to secrete surfactants with increasing culture times, related to the ATII-to-ATI transdifferentiation. However, the cells grew forming aggregates and were not able to create a monolayer, dampening the secretion of surfactant proteins.³² Due to the number of emerging hydrogels from different origins, it seems a promising field to investigate improvements in the alveolar cell culture. Nevertheless, not many different substrates have been tested. Some studies with the use of lung-derived hydrogels showed the suitability of this kind of substrate for the culture of induced pluripotent stem cells-derived ATII cells^{300,301} or for lung cancer cells culturing³⁰². In addition, it is an adequate tool for studying cancer invasion or resistance to therapy^{302,303}. Hydrogels are especially useful for the study of the interaction of cells due to the possibility of establishing cocultures by culturing cells inside and on top of them. The different uses of the hydrogels (e.g. cocultures, combination with other stimuli) are addressed in the next sections.

3.4 Cocultures

For *in vitro* representing the cell lung physiology is not only important the composition of the scaffold they are seeded on or in, but also the interfaces that are present in the culture. In the lung, it can be found the interaction of different tissues and also different media. For that reason, compartmentalized lung-on-a-chip devices with porous membranes have been developed allowing for the culture of different types of cells (cocultures) and different interfaces (air-liquid interface (ALI) culture). The use of cocultures is very relevant for studying infections such as the ones causing ARDS, as the alveolo-

capillary barrier can be represented. An example of this sort of model is the epithelial-endothelial (A549 or H441 - HPMEC) coculture established at different sides of a porous membrane, followed by an inflammatory hit caused by the addition of TNF- α .³⁰⁴

The use of transwells is useful to work with cocultures due to the existence of two different compartments that are connected. This tool can be used to make either submerged cocultures by adding medium to the cells on the plate and to the cells inside the transwell, or ALI cocultures, by adding medium just in the inferior compartment. Coculture of primary alveolar or bronchial cells with smooth muscle cells was subjected to TGF- β and the study of the barrier integrity, the transport of drugs, and the pharmacological response was performed.³⁰⁵ For instance, the coculture of A549 with macrophages inside a transwell has been employed for studying the inflammation produced by air contaminant particles measured as the secretion of proinflammatory mediators, cytotoxicity, and ROS.³⁰⁶

A highly advanced coculture model has recently combined the presence of three cell types in the same microfluidic device: epithelial cells, endothelial cells, and fibroblasts. For doing so, the authors distributed the cells in three different channels: the first one was cultured with epithelial cells, which were subjected to airflow after the confluence was achieved, the middle was cultured with fibroblasts, and the last one where the endothelial cells were cultured that were subjected to liquid flow.⁶⁵

3.5 Advanced models

In respiratory diseases such as ARDS, the organism responds with a highly coordinated multistep inflammatory cascade, that includes the interaction of different cell types among other factors. For that reason, the development of devices that allow the integration of different stimuli is fundamental in the study of these diseases. With this objective, cocultures have been added to compartmentalized lung-on-a-chip devices, to create more realistic models.^{307,308,309} Some devices combine stretch and coculture of different cell types to represent a realistic culture. For example, one of the first models representing the alveolo-capillary barrier was composed of a compartmentalized PDMS stretching device containing a coculture of human alveolar and epithelial cells at opposite faces of a porous PDMS membrane.³¹⁰ Stucki et al. created an epithelial-endothelial coculture separated by a porous membrane that can be subjected to three-dimensional cyclic stretch with the use of an *in vivo*-inspired micro-diaphragm.³¹¹ Other authors represented the cocultures in a more physiological

environment with the use of 3D hydrogels. Humayun et al. cocultured airway epithelial cells separated from smooth muscle cells by a thin layer of lamina propria composed of collagen I and Matrigel.³⁰⁷ Other models have been developed to include these three parameters: stretch, coculture, and hydrogels. Zamprogno et al fabricated a model to represent the alveolar epithelial-endothelial barrier through a stretchable device consisting of a thin membrane composed by a mixture of elastin and collagen that substituted the typical PDMS membrane. Primary alveolar epithelial cells (formed by ATI and ATII cells) were cultured on one side, and primary lung endothelial cells on the other side. This hydrogel that mimics the basement membrane, was suspended on a gold hexahedral mesh, forming small alcoves where cells can find a similar environment to the one found in the alveoli.³¹²

Lung-on-a-chip devices usually present a small geometry to try to mimic the *in vivo* setting. However, this has the inconvenience that the shape is limited to rectangular geometry, causing the cells to grow in 2D.³¹³ Recently, Huang et al. have overcome this disadvantage by doing an alveoli-on-a-chip that perfectly resembles the sphere geometry with a thin monolayer of epithelial cells growing on biodegradable gelatin methacryloyl (GelMA) hydrogels with similar stiffness to the human lungs. This PDMS device presented opal shape interconnected structures that stretched mimicking breathing motions (8% of strain) and were employed to study the matrix remodeling in the context of emphysema.³¹⁴

Other investigators went a step ahead and employed the hydrogels to embed cells from the extracellular matrix, giving their three-dimensionality to their culture. Barkal et al, similar to⁶⁵, represented a tri-culture model more realistically, with the use of hydrogels. They cultured the fibroblasts inside the collagen-fibrinogen hydrogels that contained channels inside, which lumens were recovered alternatively by epithelial or endothelial cells. With this model, they studied the inflammatory response and the recruitment of white cells as a response to fungal infection³⁰⁹. Similarly, Park et al placed a transwell containing epithelial cell on a decellularized sheet of extracellular matrix on a bioprinted device containing in different compartments fibroblasts and that fully represented a functional interface between the vascular network and the bronchiolar epithelium.³⁰⁸

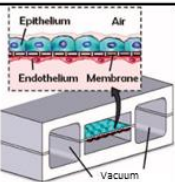
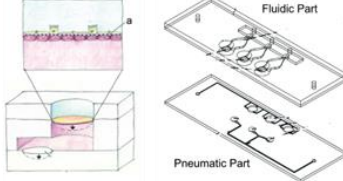
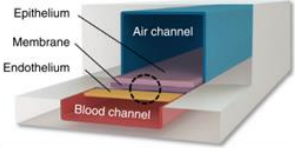
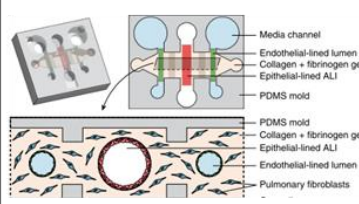
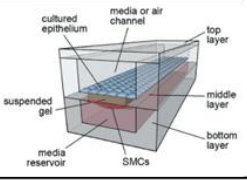
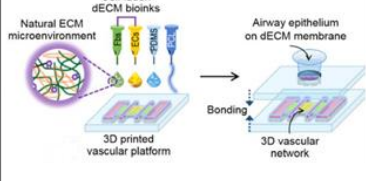
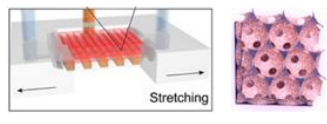
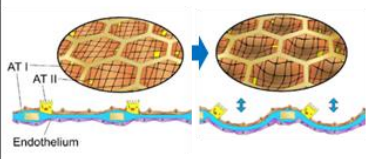
Model desing	Author	Description	Strengths	Weaknesses
	Huh et al. 2010	Epithelial-endothelial coculture at both sides of a porous membrane subjected to CS	Coculture CS	Lack of hydrogels. Commercially obtained epithelial and endothelial cells.
	Stucki et al. 2015	Epithelial-endothelial coculture at both sides of a porous membrane subjected to three-dimensional CS	Three-dimensional CS. Primary epithelial cells.	Lack of hydrogels. Lack of realistic O ₂ concentration. Commercially available endothelial cells.
	Benam et al. 2015	Epithelial-endothelial coculture at both sides of a polyester membrane coated with collagen I	Epithelial ALI culture + submerged endothelial culture. Primary epithelial cells.	Lack of CS and hydrogels. Lack of realistic O ₂ concentration. Commercially obtained endothelial cells.
	Barkal et al. 2017	Co-culture of fibroblasts, epithelial, and alveolar cells.	Tri-culture model 3D fibroblast culture. Accurate representation of the interfaces. Primary epithelial cells.	Hydrogel made of collagen I + fibrinogen. Lack of CS and realistic O ₂ concentration. Commercially obtained fibroblasts and endothelial cells.
	Humayun et al. 2018	Airway epithelial cells cocultured with smooth muscle cells separated by a collagen and Matrigel layer	Epithelial ALI culture + submerged endothelial culture	Use of rat tail collagen I + Matrigel. Lack of CS and realistic O ₂ concentration. Commercially obtained cells.
	Park et al. 2018	Transwell containing epithelial cells on a decellularized ECM sheet placed in a well with 3D cultured fibroblasts / endothelial cells	Tri-culture model with 3D fibroblast culture. Tissue derived bioink.	3D culture of endothelial cells, not representing the vascular endothelial barrier. Lack of CS and realistic O ₂ concentration. Commercially obtained cells
	Huang et al. 2021	Epithelial cell monolayer on sphere-like structures made of GelMA.	Representation of small sphere geometry resembling alveoli. Three-dimensional CS	Not realistic ECM: use of GelMA. Lack of coculture and realistic O ₂ concentration
	Zamprogno et al. 2021	Epithelial-endothelial cell monolayer cultured on both sides of a collagen-elastin membrane suspended in a hexagonal gold mesh	Combination of three parameters: three-dimensional CS, coculture (endothelial-epithelial barrier), and hydrogels. Primary epithelial cells.	Not realistic ECM nor realistic O ₂ concentration. Commercially obtained endothelial cells.

Table 1. Summary of the main advanced models from 2010 to 2021.

These advanced physiomic models are important tools in the advance in the study of diseases and the research of new treatments. However, they present some limitations like the absence of cyclic stretch or the use of commercially available cells instead of using freshly obtained primary cells in most of them. All of them are performed under non-physiological oxygen concentrations (hyperoxia), which could be altering the cellular responses, especially in those studies where ROS was measured as a result of the inflammatory hit. In most of these models, there is the representation of the alveolo-capillary barrier, due to the importance of the study of the permeability properties. However, the wide majority of them do not include 3D culturing for representing the interaction of the stromal cells and the epithelium. However, this is especially important in the context of inflammation due to the immune properties of MSC. Furthermore, these models use hydrogels that are not derived from the extracellular matrix coming from the same organ of the cells they use (except³⁰⁸). The use of specific-tissue derived hydrogels is an interesting tool to include in the creation of novel physiomic models to study diseases due to the accurate representation of the cellular environment.

Chapter II.
AIMS OF THE THESIS

1. Aims

1.1 General aim

The general objective of this thesis is the development of physiometric models to reproduce specific traits of the cell environment for representing *in vitro* scenarios that are closer to physiological or pathological conditions.

1.2 Specific aims

- I. To study how different oxygenation patterns representing common respiratory diseases affected lung cancer cell *in vitro* behavior in terms of proliferation and expression of EpCAM protein.
- II. To study the effect that the use of lung extracellular matrix-derived hydrogels as scaffold can exert on cell cultures.
 - a. To study its effect on primary alveolar type II cells in terms of phenotype maintenance compared to traditional methods.
 - b. To investigate its anti-inflammatory effect in an advanced physiometric ARDS model.
- III. To investigate the interactions of alveolar cells with lung mesenchymal stem cells (LMSCs) in an advanced inflammatory *in vitro* ARDS model.
- IV. To investigate the effects of physiological cyclic stretch in the inflammatory process on the established coculture for the ARDS physiometric model.

Chapter III.
ARTICLES IN THIS THESIS

The scientific articles included in this thesis, in which the Ph.D. candidate was the first author, are here listed in relation to the Aims of the thesis.

Aim I. To study how different oxygenation patterns representing common respiratory diseases affected lung cancer cell in vitro behavior in terms of proliferation and expression of EpCAM.

- **Marhuenda E**, Campillo N, Gabasa M, Martínez-García MA, Campos-Rodríguez F, Gozal D, Navajas D, Alcaraz J, Farré R, Almendros I. Effects of Sustained and Intermittent Hypoxia on Human Lung Cancer Cells. *Am J Respir Cell Mol Biol.* 2019 Oct; 61(4):540-544. IF= 6.914 Q1

Aim IIa. To study the effect of lung extracellular matrix-derived hydrogels on primary alveolar type II cells in terms of phenotypic maintenance compared to traditional methods.

- **Marhuenda E**; Villarino A; Narciso M; Camprubí-Rimblas M; Farré R; Núria Gavara; Artigas A; Almendros I; Otero J. Lung Extracellular Matrix Hydrogels Enhance Preservation of Type II Phenotype in Primary Alveolar Epithelial Cells. *Int. J. Mol. Sci.* 2022, 23(9), 4888. IF = 5.924 Q1

Aim IIb, III, IV. To investigate the anti-inflammatory properties of lung extracellular matrix-derived hydrogels in an advanced physiologic ARDS model. To investigate the interactions of alveolar cells with lung mesenchymal stem cells (LMSCs) in an advanced inflammatory in vitro ARDS model. To investigate the effects of physiological cyclic stretch on the coculture and its possible role in the inflammatory process.

- **Marhuenda E**; Villarino A; Narciso M; Elowsson L; Almendros I; Westergren-Thorsson; Farré R; Gavara N; Otero J. Development of a Physiologic Model of Acute Respiratory Distress Syndrome by using ECM Hydrogels and Organ-on-a-chip Devices. Submitted for publication and under revision.

Chapter IV.
SCIENTIFIC ARTICLE I

Stephan Pleschka, Ph.D.
Institute of Medical Virology
Giessen, Germany

and
Justus-Liebig University Giessen
Giessen, Germany

Werner Seeger, M.D.
Universities of Giessen and Marburg Lung Center
Giessen, Germany

Excellence Cluster Cardio-Pulmonary Institute
Giessen, Germany

Max Planck Institute for Heart and Lung Research
Bad Nauheim, Germany

and
Instituto de Investigación en Biomedicina de Buenos Aires
Buenos Aires, Argentina

Andreas Günther, M.D.
Susanne Herold, M.D., Ph.D.*
Universities of Giessen and Marburg Lung Center
Giessen, Germany

and
Excellence Cluster Cardio-Pulmonary Institute
Giessen, Germany

*S.H. is Deputy Editor of *AJRCMB*. Her participation complies with American Thoracic Society requirements for recusal from review and decisions for authored works.

†Corresponding author (e-mail: susanne.herold@innere.med.uni-giessen.de).

References

- Mauad T, Hajjar LA, Callegari GD, da Silva LF, Schout D, Galas FR, *et al*. Lung pathology in fatal novel human influenza A (H1N1) infection. *Am J Respir Crit Care Med* 2010;181:72–79.
- Herold S, Steinmueller M, von Wulffen W, Cakarova L, Pinto R, Pleschka S, *et al*. Lung epithelial apoptosis in influenza virus pneumonia: the role of macrophage-expressed TNF-related apoptosis-inducing ligand. *J Exp Med* 2008;205:3065–3077.
- Högner K, Wolff T, Pleschka S, Plog S, Gruber AD, Kalinke U, *et al*. Macrophage-expressed IFN- β contributes to apoptotic alveolar epithelial cell injury in severe influenza virus pneumonia. *PLoS Pathog* 2013;9:e1003188.
- Li CC, Wang XJ, Wang HR. Repurposing host-based therapeutics to control coronavirus and influenza virus. *Drug Discov Today* 2019;24:726–736.
- Korfei M, Ruppert C, Mahavadi P, Henneke I, Markart P, Koch M, *et al*. Epithelial endoplasmic reticulum stress and apoptosis in sporadic idiopathic pulmonary fibrosis. *Am J Respir Crit Care Med* 2008;178:838–846.
- Kim HJ, Jeong JS, Kim SR, Park SY, Chae HJ, Lee YC. Inhibition of endoplasmic reticulum stress alleviates lipopolysaccharide-induced lung inflammation through modulation of NF- κ B/HIF-1 α signaling pathway. *Sci Rep* 2013;3:1142.
- Kim SR, Kim DI, Kang MR, Lee KS, Park SY, Jeong JS, *et al*. Endoplasmic reticulum stress influences bronchial asthma pathogenesis by modulating nuclear factor κ B activation. *J Allergy Clin Immunol* 2013;132:1397–1408.
- Wang Y, Wu ZZ, Wang W. Inhibition of endoplasmic reticulum stress alleviates cigarette smoke-induced airway inflammation and emphysema. *Oncotarget* 2017;8:77685–77695.
- Hetz C. The unfolded protein response: controlling cell fate decisions under ER stress and beyond. *Nat Rev Mol Cell Biol* 2012;13:89–102.
- Hrncius ER, Liedmann S, Finkelstein D, Vogel P, Ganseborn S, Samarasinghe AE, *et al*. Acute lung injury results from innate sensing of viruses by an ER stress pathway. *Cell Reports* 2015;11:1591–1603.
- Roberson EC, Tully JE, Guala AS, Reiss JN, Godburn KE, Pociask DA, *et al*. Influenza induces endoplasmic reticulum stress, caspase-12-dependent apoptosis, and c-Jun N-terminal kinase-mediated transforming growth factor- β release in lung epithelial cells. *Am J Respir Cell Mol Biol* 2012;46:573–581.
- Hassan IH, Zhang MS, Powers LS, Shao JQ, Baltrusaitis J, Rutkowski DT, *et al*. Influenza A viral replication is blocked by inhibition of the inositol-requiring enzyme 1 (IRE1) stress pathway. *J Biol Chem* 2012;287:4679–4689.
- Atkins C, Liu Q, Minthorn E, Zhang SY, Figueroa DJ, Moss K, *et al*. Characterization of a novel PERK kinase inhibitor with antitumor and antiangiogenic activity. *Cancer Res* 2013;73:1993–2002.
- Okada T, Haze K, Nadanaka S, Yoshida H, Seidah NG, Hirano Y, *et al*. A serine protease inhibitor prevents endoplasmic reticulum stress-induced cleavage but not transport of the membrane-bound transcription factor ATF6. *J Biol Chem* 2003;278:31024–31032.
- Heindryckx F, Binet F, Ponticos M, Rombouts K, Lau J, Kreuger J, *et al*. Endoplasmic reticulum stress enhances fibrosis through IRE1 α -mediated degradation of miR-150 and XBP-1 splicing. *EMBO Mol Med* 2016;8:729–744.
- Lawson WE, Cheng DS, Degryse AL, Tanjore H, Polosukhin VV, Xu XC, *et al*. Endoplasmic reticulum stress enhances fibrotic remodeling in the lungs. *Proc Natl Acad Sci USA* 2011;108:10562–10567.
- Nureki SI, Tomer Y, Venosa A, Katzen J, Russo SJ, Jamil S, *et al*. Expression of mutant Sftpc in murine alveolar epithelia drives spontaneous lung fibrosis. *J Clin Invest* 2018;128:4008–4024.
- Guenther A, Krauss E, Tello S, Wagner J, Paul B, Kuhn S, *et al*. The European IPF registry (eurIPFreg): baseline characteristics and survival of patients with idiopathic pulmonary fibrosis. *Respir Res* 2018;19:141.

Copyright © 2019 by the American Thoracic Society

Effects of Sustained and Intermittent Hypoxia on Human Lung Cancer Cells

To the Editor:

Lung cancer is the most commonly diagnosed solid malignancy and the leading cause of mortality among all cancers (1). It is well established that lung cancer usually coexists with chronic obstructive pulmonary disease (COPD), as both diseases feature previous exposures to tobacco smoke. Moreover, recent data suggest a potential link between lung cancer and other respiratory diseases. For instance, Cabezas and colleagues found that \sim 50% of patients with lung cancer also suffered from moderate to severe obstructive sleep apnea (OSA) (2), and Dreher and colleagues described a similarly high prevalence of OSA in patients with newly diagnosed lung cancer (3).

Tumor hypoxia has been widely associated with poor prognosis in several types of cancer (4). Thus, episodically low systemic oxygen levels caused by most respiratory diseases (e.g., COPD, interstitial lung disease, asthma, OSA, and obesity hypoventilation syndrome) could contribute to tumor progression. Indeed, lung cancer is more aggressive in patients with COPD (5), and the magnitude of intermittent hypoxia (IH) in OSA was recently linked to both cancer incidence and cancer mortality (6). Interestingly, experimental studies have described enhanced malignant

Supported in part by the Spanish Society of Pneumology and Thoracic Surgery (595/2017), the Spanish Ministry of Economy and Competitiveness (SAF2017-85574-R, DPI2017-83721-P, and SAF2016-79527-R), Fundació Privada Cellex, and the National Institutes of Health (1R01HL130984).

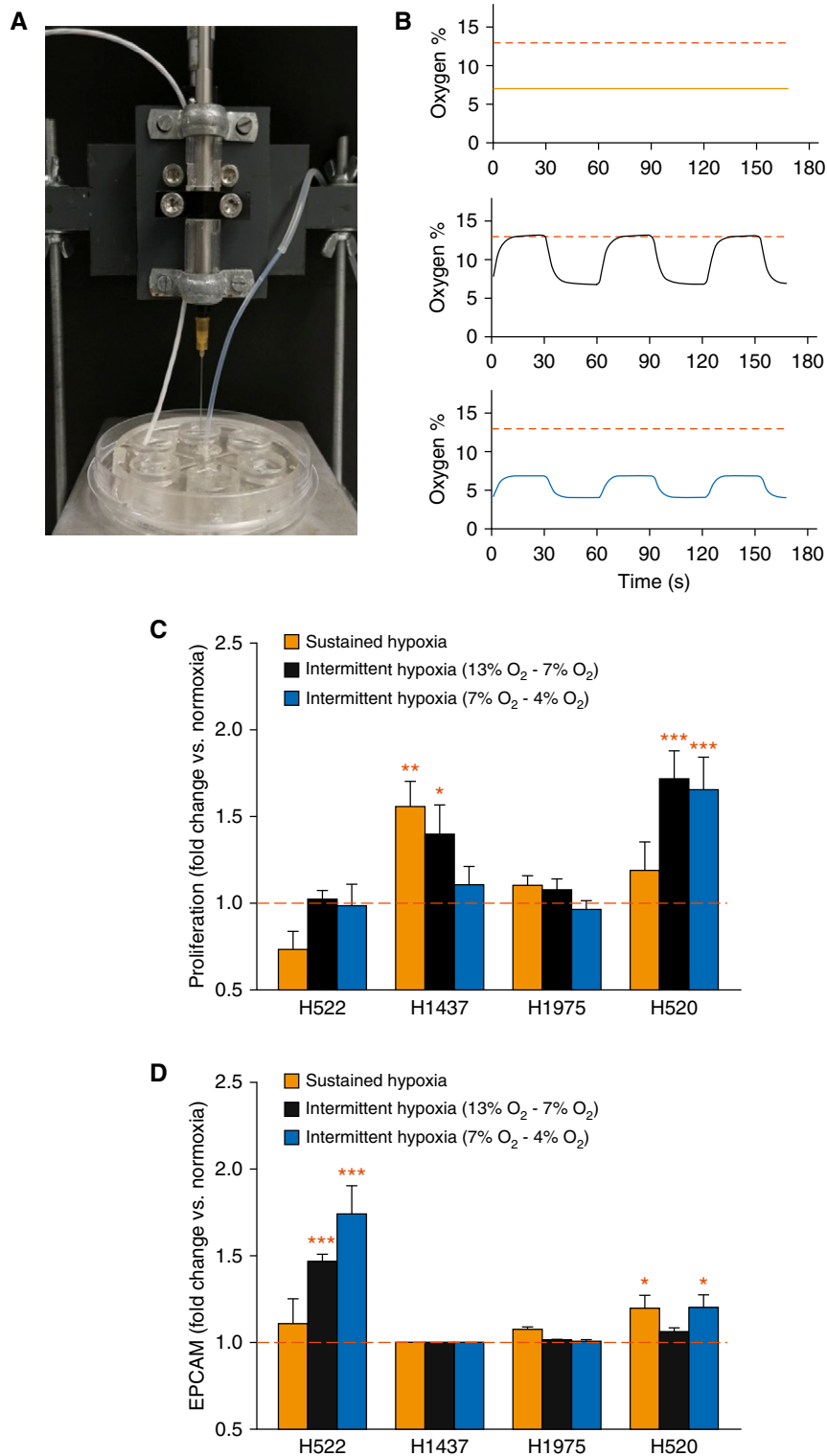


Figure 1. (A) A custom-made lab-on-a-chip reliably generates the different hypoxia patterns. Real-time oxygen levels were measured by introducing an optical oxygen sensor into the cellular layer. (B) Oxygen profiles applied to lung cancer cells in comparison with sustained normoxic levels (dashed red lines; 13% O₂). Time scales in seconds. Top: sustained hypoxia mimicking a patient presenting with impaired lung function (7% O₂). Center: intermittent hypoxia mimicking severe obstructive sleep apnea (cycles of 30 s of 13% O₂ followed by 30 s of 7% O₂). Bottom: intermittent hypoxia mimicking the overlap syndrome (cycles of 30 s of 7% O₂ followed by 30 s of 4% O₂). (C) Cellular proliferation computed as fold changes in the number of cells versus normoxia (dashed red line). (D) Fold-change expression of epithelial cell adhesion molecule (EPCAM) for all experimental groups versus normoxia (dashed red line). Data are presented as mean \pm SE. * P < 0.05, ** P < 0.01, and *** P < 0.001.

properties of lung cancer in response to both sustained hypoxia (SH) and IH (7–9). These observations are therefore translationally relevant, as the high prevalence of OSA in the general population makes its coexistence with other respiratory diseases very probable, and the co-occurrence of these two conditions (sometimes termed overlap syndrome) can elicit a more severe nocturnal hypoxemia (10). However, the potential link between hypoxia and major subtypes of lung cancer remains largely unexplored.

In this context, we report our findings from a study investigating the effect of different patterns of hypoxia on a panel of cell lines harboring representative oncogenic mutations of the most prevalent histological subtypes of non-small cell lung cancer (adenocarcinoma and squamous cell carcinoma), including p53 and endothelial growth factor receptor (EGFR). Specifically, H522, H1437 (human adenocarcinoma; p53 mutant and EGFR wild-type), H1975 (human adenocarcinoma; p53 mutant, EGFR mutant), and H520 (human squamous cell lung cancer; p53 mutant, EGFR wild-type) cells were exposed for 48 hours to either normoxia (13% O₂, which corresponds to normal arterial blood oxygen levels), SH (7% O₂, mimicking a patient presenting with impaired lung function), or two types of IH (oscillating between 13% and 7% to mimic moderate OSA, and oscillating between 7% and 4%, which would correspond to the overlap syndrome). Cells were subjected to each profile by using a recently described lung-on-a-chip setup (11), to reproduce the high frequency of IH (60 cycles/h) that occurs in patients with severe OSA (12) (Figure 1). Cell proliferation and expression of epithelial cell adhesion molecule (EpCAM), which has been associated with lung cancer cell survival (13), were quantified by flow cytometry. Differences between the effects induced by the various hypoxic patterns as applied on each cancer cell type were assessed by two-way ANOVA. In a second set of experiments ($n = 5$), the protein localization of hypoxia-inducible factor 1 α (HIF-1 α) to the nucleus as an indicator of its activation was estimated by immunofluorescence as previously described (11). Briefly, after gas exposure, cells were fixed and stained with rabbit anti-HIF-1 α (Novus Biologicals) antibody and DAPI (Sigma-Aldrich). Five epifluorescence images were acquired with an inverted microscope using a 20 \times Plan Fluor multi-immersion objective (0.75 NA) for each experiment. The total cellular fluorescence of HIF-1 α was measured by adjusting Huang's thresholding to subtract the background and delimit cells. The nuclear intensity of HIF-1 α was estimated from the

nuclear outlines identified by the DAPI channel. Cytoplasmic HIF-1 α was calculated by subtracting the nuclear intensity from the whole-cell intensity. Finally, the translocation of HIF-1 α to the nuclei was estimated as the nuclear/cytoplasmic fluorescence intensity ratio.

Figure 1 shows that different hypoxic profiles differentially stimulated cell proliferation in most cancer cell lines and EpCAM expression in selected cell lines. In terms of tumor cell proliferation, the most severe hypoxic IH pattern, corresponding to the overlap syndrome, only enhanced the proliferation of squamous cell carcinoma (H520) ($\sim 66\%$, $P < 0.001$), whereas the IH profile mimicking OSA alone enhanced the tumor cell growth rate in H520 cells ($\sim 72\%$, $P < 0.001$) and H1437 adenocarcinoma cells ($\sim 40\%$, $P = 0.043$) compared with that observed in normoxic control conditions. Application of SH promoted an increase in tumor cell proliferation ($\sim 56\%$, $P = 0.005$) in only one of the cancer cell types (H1437, adenocarcinoma). However, none of the hypoxic profiles elicited measurable changes in the proliferative rates of the two other adenocarcinoma cell lines (i.e., H522 and H1975). Similarly, EpCAM showed heterogeneous responses among the different human lung cancer cell types. As shown in Figure 1, H522 cells increased EpCAM expression under IH stimuli ($\sim 47\%$, $P < 0.001$, and $\sim 74\%$, $P < 0.001$ for IH mimicking OSA and overlap syndrome, respectively). The H520 squamous cell carcinoma cell line also exhibited increased EpCAM expression in response to SH ($\sim 20\%$, $P = 0.014$) and IH mimicking the overlap syndrome ($\sim 20\%$, $P = 0.021$) when compared with normoxia. However, the two other adenocarcinoma cell lines used, H1437 and H1975, failed to display any detectable changes in EpCAM. Thus, these results suggest that EpCAM expression in response to hypoxic stimuli is largely uncorrelated with both the p53/EGFR status and the histologic subtype. The only significant changes in HIF-1 α activation were observed in H1437 and H1975 lung cancer cells: $\sim 20\%$ ($P = 0.022$) and 2.6-fold ($P = 0.047$) increases when cells were exposed to IH mimicking the overlap syndrome compared with normoxia, respectively (Table 1).

Our *in vitro* experiments in human lung cancer cells provide new evidence in support of the clinical data that link lung cancer malignancy with other respiratory diseases (5, 6). Most importantly, our data also suggest that the response of lung cancer cells may depend, at least in part, on the presentation of the hypoxic stimulus (8). Moreover, these results are in accord with previous findings that SH and IH exposures promoted different

Table 1. Nuclear/Cytoplasmic Ratio of Hypoxia-Inducible Factor 1 α Fluorescence for Each Cell Line and Hypoxic Condition Compared with 13% Normoxia

	H522		H1437		H1975		H520	
	Mean \pm SE	P Value	Mean \pm SE	P Value	Mean \pm SE	P Value	Mean \pm SE	P Value
13% O ₂	0.70 \pm 0.11		1.13 \pm 0.03		0.91 \pm 0.03		2.84 \pm 0.28	
13–7% O ₂	2.63 \pm 0.86	0.098	1.38 \pm 0.10	0.059	1.27 \pm 0.30	0.319	3.18 \pm 0.37	0.266
7% O ₂	0.97 \pm 0.16	0.261	1.35 \pm 0.16	0.208	1.72 \pm 0.35	0.078	2.70 \pm 0.15	0.629
7–4% O ₂	0.92 \pm 0.06	0.090	1.36 \pm 0.09	0.022	2.39 \pm 0.55	0.047	2.78 \pm 0.26	0.883

P values, paired *t* test; $n = 5$.

growth rates in a murine lung Lewis carcinoma cell line (LLC1) (7). Here, we found that the behavior of cancer cells depended on the magnitude of hypoxia during IH oscillations (13–7% O₂ vs. 7–4% O₂). It is expected that different frequencies with similar oscillations could modulate the response of lung cancer cells, as was previously reported for melanoma (14). Furthermore, other potential factors, such as host immunity and aging, could also modulate the malignant properties of lung cancer cells in a specific hypoxic environment (7, 15).

Thus, it is important to devote further efforts to identify the target lung cancer cell types that are susceptible to hypoxia-mediated regulation, and particularly those that are affected by profiles such as those represented by IH. In this context, information on these specific issues and an improved understanding of the underlying mechanisms could potentially guide future epidemiological/clinical studies aimed at detecting incipient relationships between lung cancer and other respiratory diseases. Mechanistically, these potential relationships are likely to be complex and involve specific cancer cell mutations that are ultimately responsible for the increased cancer progression observed in response to hypoxia. Studying the effects of different hypoxic profiles in lung cancer could help investigators elucidate the roles played by COPD, OSA, and other respiratory diseases in the initiation and progression of lung cancer, thus providing the opportunity to design novel personalized therapies. ■

Author disclosures are available with the text of this letter at www.atsjournals.org.

Acknowledgment: The authors thank Miguel Ángel Rodríguez for technical support, and Luca Roz and Giulia Bertolini for helpful discussions.

Esther Marhuenda, B.Sc.
Noelia Campillo, Ph.D.
Marta Gabasa, Ph.D.
Universitat de Barcelona
Barcelona, Spain

Miguel Angel Martínez-García, M.D., Ph.D.
Hospital Universitario y Politécnico La Fe
Valencia, Spain

Francisco Campos-Rodríguez, M.D., Ph.D.
Hospital Universitario de Valme, IBIS
Seville, Spain

and
Centro de Investigación Biomédica en Red de Enfermedades Respiratorias
Madrid, Spain

David Gozal, M.D., Ph.D.
University of Missouri School of Medicine
Columbia, Missouri

Daniel Navajas, Ph.D.
Jordi Alcaraz, Ph.D.
Universitat de Barcelona
Barcelona, Spain
Centro de Investigación Biomédica en Red de Enfermedades Respiratorias
Madrid, Spain
and
Barcelona Institute of Science and Technology
Barcelona, Spain

Ramon Farré, Ph.D.
Isaac Almendros, Ph.D.*
Universitat de Barcelona
Barcelona, Spain
Centro de Investigación Biomédica en Red de Enfermedades Respiratorias
Madrid, Spain
and
Institut d'Investigacions Biomèdiques August Pi i Sunyer
Barcelona, Spain

ORCID ID: 0000-0002-1998-9379 (I.A.).

*Corresponding author (e-mail: isaac.almendros@ub.edu).

References

- Bray F, Ferlay J, Soerjomataram I, Siegel RL, Torre LA, Jemal A. Global cancer statistics 2018: GLOBOCAN estimates of incidence and mortality worldwide for 36 cancers in 185 countries. *CA Cancer J Clin* 2018;68:394–424.
- Cabezas E, Perez-Warnisher MT, Troncoso MF, Gomez T, Melchor R, Pinillos EJ, et al. Sleep disordered breathing is highly prevalent in patients with lung cancer: results of the sleep apnea in lung cancer study. *Respiration* 2019;97:119–124.
- Dreher M, Krüger S, Schulze-Olden S, Keszei A, Storre JH, Woehrle H, et al. Sleep-disordered breathing in patients with newly diagnosed lung cancer. *BMC Pulm Med* 2018;18:72.
- Muz B, de la Puente P, Azab F, Azab AK. The role of hypoxia in cancer progression, angiogenesis, metastasis, and resistance to therapy. *Hypoxia (Auckl)* 2015;3:83–92.
- Young RP, Hopkins RJ. Estimating overdiagnosis of lung cancer. *Ann Intern Med* 2013;158:635.
- Campos-Rodríguez F, Martínez-García MA, Martínez M, Duran-Cantolla J, Peña MdeL, Masdeu MJ, et al.; Spanish Sleep Network. Association between obstructive sleep apnea and cancer incidence in a large multicenter Spanish cohort. *Am J Respir Crit Care Med* 2013;187:99–105.
- Almendros I, Wang Y, Becker L, Lennon FE, Zheng J, Coats BR, et al. Intermittent hypoxia-induced changes in tumor-associated macrophages and tumor malignancy in a mouse model of sleep apnea. *Am J Respir Crit Care Med* 2014;189:593–601.
- Almendros I, Wang Y, Gozal D. The polymorphic and contradictory aspects of intermittent hypoxia. *Am J Physiol Lung Cell Mol Physiol* 2014;307:L129–L140.
- Hunyor I, Cook KM. Models of intermittent hypoxia and obstructive sleep apnea: molecular pathways and their contribution to cancer. *Am J Physiol Regul Integr Comp Physiol* 2018;315:R669–R687.
- Owens RL, Malhotra A. Sleep-disordered breathing and COPD: the overlap syndrome. *Respir Care* 2010;55:1333–1344, discussion 1344–1346.
- Campillo N, Jorba I, Schaedel L, Casals B, Gozal D, Farré R, et al. A novel chip for cyclic stretch and intermittent hypoxia cell exposures mimicking obstructive sleep apnea. *Front Physiol* 2016;7:319.
- Farré R, Almendros I, Montserrat JM, Gozal D, Navajas D. Gas partial pressure in cultured cells: patho-physiological importance and methodological approaches. *Front Physiol* 2018;9:1803.
- Hase T, Sato M, Yoshida K, Girard L, Takeyama Y, Horio M, et al. Pivotal role of epithelial cell adhesion molecule in the survival of lung cancer cells. *Cancer Sci* 2011;102:1493–1500.
- Yoon DW, So D, Min S, Kim J, Lee M, Khalmuratova R, et al. Accelerated tumor growth under intermittent hypoxia is associated with hypoxia-inducible factor-1-dependent adaptive responses to hypoxia. *Oncotarget* 2017;8:61592–61603.
- Torres M, Campillo N, Nonaka PN, Montserrat JM, Gozal D, Martínez-García MA, et al. Aging reduces intermittent hypoxia-induced lung

carcinoma growth in a mouse model of sleep apnea. *Am J Respir Crit Care Med* 2018;198:1234–1236.

Copyright © 2019 by the American Thoracic Society

Muc5b Enhances Murine Honeycomb-like Cyst Formation

To the Editor:

Idiopathic pulmonary fibrosis (IPF) is a devastating lung disease characterized by physiologic restriction and progressive, ultimately fatal, respiratory failure. These functional changes are caused by fibrotic interstitial remodeling, alveolar destruction, and bronchiolization or “honeycombing” of the distal airspaces. IPF affects almost 0.5% of the U.S. population over the age of 65, and its prevalence is increasing (1). The strongest risk predictor for developing IPF is the minor allele of the polymorphism rs35705950, a promoter variant upstream of the polymeric mucin *MUC5B* (2, 3). Variant rs35705950 is associated with increased *MUC5B* expression, suggesting that excessive *MUC5B* protein may play a role in the pathobiology of IPF. *MUC5B* is a dominant feature of human honeycomb cysts (HCs) (4, 5), which are composed of a stratified columnar epithelium comprising mucus and ciliated cells over a layer of cytokeratin 5 (KRT5)-expressing basal cells. We hypothesized that *MUC5B* was involved in HC formation.

Recently it was reported that influenza A infection (H1N1) promotes structural remodeling consistent with HCs in mice (6). Formation of these structures is contingent on mobilization of progenitor “pods” of Krt5-expressing cells (5–7). Using a previously published RNA sequencing Gene Expression Omnibus data set (GSE83467) comparing unstimulated murine progenitors to mobilized Krt5-expressing cells, we found that *Muc5b* was upregulated in Krt5 cells after H1N1 infection (fold change = 4.59; 95% confidence interval, 4.58–4.60; two biological replicates). We suspected that *Muc5b* might also be a feature of murine HCs. Given our recent findings that *Muc5b* modulates fibrosis in bleomycin-treated mice (8), we additionally wanted to determine whether honeycombing could be detected after bleomycin injury, and whether this was dependent on *Muc5b*.

Mice (8–12 wk old) were exposed to H1N1 or intratracheal bleomycin. Two models were used for bleomycin exposure. In the single-dose model, mice were administered 2.5 U/kg bleomycin intratracheally on day 0, and harvested after 10 weeks. In the repeat bleomycin model, mice were administered 2.5 U/kg, 1.25 U/kg, and 1.25 U/kg intratracheally on days 0, 7, and 14, and harvested at 7 weeks. For H1N1 infection, mice were intranasally administered 10^4 PFU of lab-adapted influenza A H1N1 PR 8/34 (ATCC) in 20 μ l of

PBS and harvested after 10 weeks unless specified otherwise. Control studies were performed with UV-irradiated H1N1. Mice who failed to lose >5% body weight after injury in either model were excluded, and those who lost 20% body weight without recovery were killed in accordance with the policies of the University of Colorado Denver Institutional Animal Care and Use Committee. BAL, hydroxyproline (HP), immunohistochemical analysis, and *Muc5b* dot blot were performed as described previously (9).

Mice injured with H1N1 demonstrated significant increases in *Muc5b* protein over baseline 4 weeks after infection (Figure 1A). In preliminary experiments, we were able to identify significant bronchiolization of distal airspaces consistent with HC formation as early as 4 weeks and as late as 30 weeks after H1N1 infection (not shown). At 10 weeks after infection, we noted expansive areas of HCs (Figure 1D, asterisk, top left); however, no significant differences in fibrosis above UV controls were measured by HP (Figure 1B) or second-harmonic two-photon microscopy (not shown). In contrast to human IPF, the HCs were relatively small and uniform; however like IPF they were marked by a close association with Krt5⁺ basal cells and filled with copious *Muc5b* (Figure 1C, asterisk, top right). Previous authors have observed mobilization of Krt5 cells after bleomycin exposure, presaging the development of HCs (6). Bleomycin-exposed mice also showed upregulated *Muc5b* gene expression (9) and elevated airway *Muc5b* (Figure 1A). We observed that bleomycin-injured mice also had Krt5-associated cystic structures (Figure 1C, asterisk, bottom left). These structures were full of *Muc5b*, consistent with HCs (Figure 1C, asterisk, bottom right). In contrast to the H1N1 model, however, bleomycin-injured mice developed significant ($P < 0.005$) interstitial fibrosis based on HP (Figure 1B), consistent with published reports (8, 9).

Single-dose bleomycin injury leads to fibrosis that peaks at 21 days and then is believed to resolve. To investigate whether this resolution extends to HCs, we injured mice once with bleomycin and quantified cysts after 10 weeks, at which point total lung collagen content resolves to baseline and is indistinguishable from saline-treated controls (HP data not shown). We found that instead of resolving in a manner consistent with fibrotic lung injury, single-dose bleomycin-injured mice retained a minimal (but detectable) fraction of HCs (Figures 1D and 1E). We applied an unbiased point-counting approach to estimate the volume fraction of cystic regions from thin sections of injured mouse lung. These measurements were also used to calculate the total lung volume using the Cavalieri method (9). We then selected points overlying cystic areas at random, overlaid an additional grid, and quantified the number of cysts and number of points per cyst. The total HC burdens of all models of lung injury are compared in Figure 1E.

To address the role of *Muc5b* expression in HC development, we determined the functional consequences of altering *Muc5b* levels on HC formation in transgenic mice. *Muc5b*-overexpressing mice (*SFTPC-Muc5b* [referred to as SPC-*Muc5b*] and *Scgb1a1-Muc5b*

Supported by National Heart, Lung, and Blood Institute grants F32 HL134243-01A1 (J.S.K.), R01 HL080396 (C.M.E.), and R33 HL120770 and UH3 HL123442 (D.A.S., I.V.Y., E.D., M.I.S., T.O., C.D.C., J.H., L.A.H., A.E., and C.E.H.).

EXTENDED INFORMATION FOR THE THESIS REPORT

Detailed Methods

Chip fabrication

The PDMS chip was composed of two different parts: the upper part, with six wells that compose the culture chamber, and the lower part, with also six wells, that is concentrically placed with the upper one, which is the gas chamber. Both are separated by a PDMS membrane permeable to gases, where the cells are cultured. In the center, a tube goes through both parts, which is the inlet tube through which the gas will go and will reach the lower part of the membrane. Each PDMS part is fabricated with the help of negative molds for each part that are designed with the Ultimaker Cura software (Ultimaker, Utrecht, Netherlands) and printed with an Ultimaker S5 3D printer (Ultimaker, Utrecht, Netherlands) in polycarbonate material. Detailed protocol for chip fabrication is accurately explained in the appendixes at the end of the thesis.

Cell culture and oxygenation patterns

Cells (300.000 cells/well) were cultured on fibronectin coated PDMS membrane with RPMI (Gibco, Massachusetts,U.S) medium supplemented with 5% of a mixture of penicillin, streptomycin and amphotericin(Gibco, Massachusetts,U.S), 10% Fetal Bovine Serum (FBS) (Gibco, Massachusetts,U.S) and 5% glutamine (Gibco, Massachusetts,U.S), and were exposed to the gas stimuli for 48 hours. Detailed methodology for coating the PDMS membrane is explained in the appendixes at the end of the thesis. Four different groups were studied with different gas mixtures applied with servo-controlled gas blender (Gas Blender 100 Series, MCQ Instruments, Rome, Italy): (1) 13% O₂, 5% CO₂, 82% N₂; (2) 7% O₂, 5% CO₂, 88% N₂; (3) cycles of 30 seconds of 13% O₂, 5% CO₂, 82% N₂ and 7% O₂, 5% CO₂, 88% N₂, alternatively, and (4) cycles of 30 seconds of 7% O₂, 5% CO₂, 88% N₂ and 4% O₂, 5% CO₂, 91% N₂ alternatively. The exact mixture of gases for both continuous and intermittent patterns was controlled by the software Oxygen Gas Mixture Creator (MCQ Instruments, Rome, Italy).

Immunochemistry

Immunochemistry was performed at the end-point of the experiment. Briefly, the cells were fixed in 4% of paraformaldehyde for 15 minutes. Blocking solution was added for 45 minutes prior to the addition of the primary antibody Rabbit anti-HIF-1A (Novus Biologicals, Cambridge, UK), and the subsequent addition of the secondary anti-rabbit (goat)-Alexa 488 (Jackson ImmunoResearch Laboratories Inc., West Grove, PA). The primary antibody was left overnight at 4°C, and the secondary antibody was left 2h at 37°C. Nuclear counterstain was performed with NucBlue (ThermoFisher, Massachusetts, US). Epifluorescence images were taken with an inverted microscope using a 20x Plan Fluor Multi-immersion objective (0.75 NA). Images belonging to the same run were obtained the same day employing the same exposure and illumination settings.

Image processing

Images were processed with ImageJ Software as previously described by Campillo ³¹⁵. Briefly, three images per condition and run of the experiment were selected. Total fluorescence of the HIF-1A was measured by adjusting to an adequate threshold to subtract background and adjusting a watershed segmentation to delimit cells. HIF-1 α nuclear fluorescence was obtained by measuring the fluorescence within the outlines previously selected in the DAPI channel with the pertinent threshold. Cytoplasmic HIF-1 α fluorescence intensity was obtained by subtracting the nuclear signal to the total cellular signal. Results were presented as the ratio of the fluorescence in the nuclei divided by the fluorescence in the cytoplasm. The mean ratio of each image was calculated from that obtained from all the cells. Then, the result of each run of experiments was assessed by computing the mean of the three images.

Flow cytometry assay

Cells were detached from the PDMS membrane by incubating them with 500 μ l/well of trypsin (Gibco, Massachusetts, U.S) for 5 minutes after washing the culture medium with PBS 1X. The reaction was stopped with 2 mL of culture medium. Resuspended cells were stained with fluorophore-conjugated EpCAM antibody (BD Bioscience, Franklin Lakes, New Jersey, U.S), and viable cells were selected by staining them with Fixable Viability Dye (BD Bioscience, Franklin Lakes, New Jersey, U.S). Finally, cells were fixed with paraformaldehyde (4%). Labeled cells were analyzed on a

FACS Canto II cytometer using GACS Diva 5.5 software (BD Biosciences, San Jose, CA) and analyzed by FlowJo software (Tree Star, San Carlos, CA).

Statistics

Data are reported as mean \pm SE and statistical analysis was performed with Sigma Plot (Systat Software, San Jose, CA). Two-way ANOVA was employed for assessing the differences of EpCAM expression and proliferation among groups and Paired t-test was used for studying the HIF-1A and for the differences in proliferation and EpCAM expression between 13% O₂ and 20% O₂.

Additional Results

Raw data of EpCAM expression

The absolute expression of EpCAM marker is expressed in the table below. It can be observed that its expression varies among the cell lines employed, independently of their histologic subtype. Squamous cell line H520 showed high expression and adenocarcinoma cell line H1975 showed almost 100% of expression. These two cell lines presented higher sensibility to hypoxia in terms of proliferation, indicating that EpCAM cell marker could be involved in this process.

	H522	H1437	H1975	H520
13% O₂	11.04 \pm 2.21	99.53 \pm 0.34	58.78 \pm 2.83	75.50 \pm 5.43
13-7% O₂	16.22 \pm 1.58	99.78 \pm 0.04	59.67 \pm 1.65	80.17 \pm 4.28
7% O₂	12.47 \pm 3.39	99.88 \pm 0.04	68.73 \pm 2.44	97.52 \pm 0.80
7-4% O₂	19.7 \pm 2.83	99.85 \pm 0.08	64.52 \pm 1.79	97.95 \pm 0.96

Table 2. Absolute values of the percentage of positive EpCAM cells obtained by flow cytometry.

Differences between “traditional normoxia” and physioxia.

In the previous experiments, the normoxia group was defined as 13% of oxygen, which corresponds to the concentration of oxygen at which the lung epithelium is exposed. Therefore, the normoxia employed in this study will correspond to the physioxia. When comparing the EpCAM expression

at the values that usually are considered normoxia, namely 20%, with the physioxia (13%) it can be observed that there are changes that reach statistical significance in one of the cell lines (H522) employed (table 3). These differences are bigger in cell number, showing a decrease in cell growth that is statistically significant in the case of H1437 and H520 (table 4).

	H522		H1437		H1975		H520	
	Mean±SE	P Value	Mean±SE	P Value	Mean±SE	P Value	Mean±SE	P Value
20% O₂	18.20± 0.94	0.0009	99.77± 0.04	0.169	60.25± 0.69	0.165	78.62± 1.24	0.1888
13% O₂	11.04± 0.91		99.53± 0.14		58.78± 1.16		75.50± 2.22	

Table 3. Percentage of EpCAM positive cells assessed by flow cytometry at traditional normoxia (20% O₂) and at physioxia (13% O₂).

	H522		H1437		H1975		H520	
	Mean SE	P Value	Mean SE	P Value	Mean SE	P Value	Mean SE	P Value
20% O₂	113100± 13530	0.4186	43200± 2341	0.0187	184600± 13270	0.3261	26590± 2347	0.001
13% O₂	106300± 8267		28550± 5534		178000± 13990		18190± 1801	

Table 4. Cell number assessed by flow cytometry at traditional normoxia (20% O₂) and at physioxia (13% O₂).

Chapter V.
SCIENTIFIC ARTICLE II



Communication

Lung Extracellular Matrix Hydrogels Enhance Preservation of Type II Phenotype in Primary Alveolar Epithelial Cells

Esther Marhuenda ^{1,2,†} , Alvaro Villarino ^{1,†}, Maria Leonor Narciso ^{1,3} , Marta Camprubí-Rimblas ^{2,4} , Ramon Farré ^{1,2,5} , Núria Gavara ^{1,2,3} , Antonio Artigas ^{2,4} , Isaac Almendros ^{1,2,5} and Jorge Otero ^{1,2,3,*}

- ¹ Unitat de Biofísica i Bioenginyeria, Facultat de Medicina i Ciències de la Salut, Universitat de Barcelona, 08036 Barcelona, Spain; marhuenda.esther@gmail.com (E.M.); alvaro.villarino.romero@gmail.com (A.V.); mnarciso@ibecbarcelona.eu (M.L.N.); rfarre@ub.edu (R.F.); ngavara@ub.edu (N.G.); ialmendros@ub.edu (I.A.)
- ² CIBER de Enfermedades Respiratorias, 28029 Madrid, Spain; mcamprubi@tauli.cat (M.C.-R.); aartigas@tauli.cat (A.A.)
- ³ The Institute for Bioengineering of Catalonia (IBEC), The Barcelona Institute of Science and Technology (BIST), 08028 Barcelona, Spain
- ⁴ Corporació Sanitària Universitària Parc Tauli, I3PT, Universitat Autònoma de Barcelona, 08193 Sabadell, Spain
- ⁵ Institut d'Investigacions Biomèdiques August Pi i Sunyer, 08036 Barcelona, Spain
- * Correspondence: jorge.otero@ub.edu
- † These authors contributed equally to this work.



Citation: Marhuenda, E.; Villarino, A.; Narciso, M.L.; Camprubí-Rimblas, M.; Farré, R.; Gavara, N.; Artigas, A.; Almendros, I.; Otero, J. Lung Extracellular Matrix Hydrogels Enhance Preservation of Type II Phenotype in Primary Alveolar Epithelial Cells. *Int. J. Mol. Sci.* **2022**, *23*, 4888. <https://doi.org/10.3390/ijms23094888>

Academic Editors: Athanasios G. Papavassiliou, Patrick C. Baer and Ralf Schubert

Received: 27 March 2022

Accepted: 26 April 2022

Published: 28 April 2022

Publisher's Note: MDPI stays neutral with regard to jurisdictional claims in published maps and institutional affiliations.



Copyright: © 2022 by the authors. Licensee MDPI, Basel, Switzerland. This article is an open access article distributed under the terms and conditions of the Creative Commons Attribution (CC BY) license (<https://creativecommons.org/licenses/by/4.0/>).

Abstract: One of the main limitations of in vitro studies on lung diseases is the difficulty of maintaining the type II phenotype of alveolar epithelial cells in culture. This fact has previously been related to the translocation of the mechanosensing Yes-associated protein (YAP) to the nuclei and Rho signaling pathway. In this work, we aimed to culture and subculture primary alveolar type II cells on extracellular matrix lung-derived hydrogels to assess their suitability for phenotype maintenance. Cells cultured on lung hydrogels formed monolayers and maintained type II phenotype for a longer time as compared with those conventionally cultured. Interestingly, cells successfully grew when they were subsequently cultured on a dish. Moreover, cells cultured on a plate showed the active form of the YAP protein and the formation of stress fibers and focal adhesions. The results of chemically inhibiting the Rho pathway strongly suggest that this is one of the mechanisms by which the hydrogel promotes type II phenotype maintenance. These results regarding protein expression strongly suggest that the chemical and biophysical properties of the hydrogel have a considerable impact on the transition from ATII to ATI phenotypes. In conclusion, culturing primary alveolar epithelial cells on lung ECM-derived hydrogels may facilitate the prolonged culturing of these cells, and thus help in the research on lung diseases.

Keywords: extracellular matrix; hydrogels; alveolar cells; type II phenotype; YAP

1. Introduction

The fundamental questions on the precise mechanisms underlying alveolar epithelial cells (AECs) damage and epithelium repair in relevant diseases, such as acute respiratory distress syndrome or chronic obstructive pulmonary disease, are still unsolved. Although it is well-known that the alveolar epithelium is repaired by the proliferation of type II AECs (ATII), which differentiate into type I phenotype cells (ATIs), the involved mechanisms are still poorly understood [1]. In fact, a limitation hampering translational studies in lung diseases is the difficulty of maintaining the type II phenotype of primary AECs in vitro. Indeed, it is widely known that ATII-to-ATI transdifferentiation occurs very quickly in vitro; thus, primary type II AECs neither adequately proliferate, nor can be subcultured under conventional culture conditions [2].

To extend the maintenance of the type II AECs proliferative phenotype in vitro, it was proposed to coat the culture plates with hydrogels, such as Matrigel, resembling the

extracellular matrix (ECM) [3]. Moreover, pioneering studies on subculturing strategies for primary ATII cells [4] employed inhibitors of Rho kinases, as the connection between the activation of the Rho pathway and cell mechanosensing of the ECM is well-established [5]. However, although the relationship between ATII phenotype maintenance in vitro and culturing cells on ECM-like substrates was proposed three decades ago [6], the problem remains open, probably because no hydrogels derived from lung ECM were available.

Interestingly, based on an initial report for obtaining hydrogels from the ECM of decellularized lungs [7], we have recently described a procedure for preparing such hydrogels by exclusively using lung ECM, with no need to add potentially toxic external cross-linkers [8]. If used as a culture substrate, this hydrogel, which realistically mimics the native lung ECM, could be particularly well-suited for providing a physiomimetic microenvironment to primary AECs. Therefore, we hypothesized that a lung ECM-based hydrogel would slow down the ATII-to-ATI transdifferentiation mediated by the inhibition of the Rho pathway, resulting in a decrease in F-actin polymerization and the formation of focal adhesions, as well as nuclear YAP activation [9–11].

2. Results

2.1. Primary Alveolar Epithelial Cells Form Monolayers on Lung-Derived Hydrogels

Isolated AECs were grown either in lung-derived hydrogels or plates for four days. Cells were able to form a monolayer on a lung-derived hydrogel, as shown in bright-field images in Figure 1. Differences in the morphology of the cells as a function of the substrate were also noticeable as shown by confocal images in Figure 2. Throughout the culture, cells on plates started to show a more flattened shape as well as larger cytoplasm (cells cultured on plates presented, in general, sizes about 5 times larger than cells cultured on hydrogels), and the presence of vacuoles was noticeable. On the contrary, AECs cultured on hydrogels showed cuboidal shapes, and even their microvilli, a phenotypical characteristic of ATII cells [12], could be distinguished. Cells cultured on plates formed monolayers faster (day 3 vs. day 4).

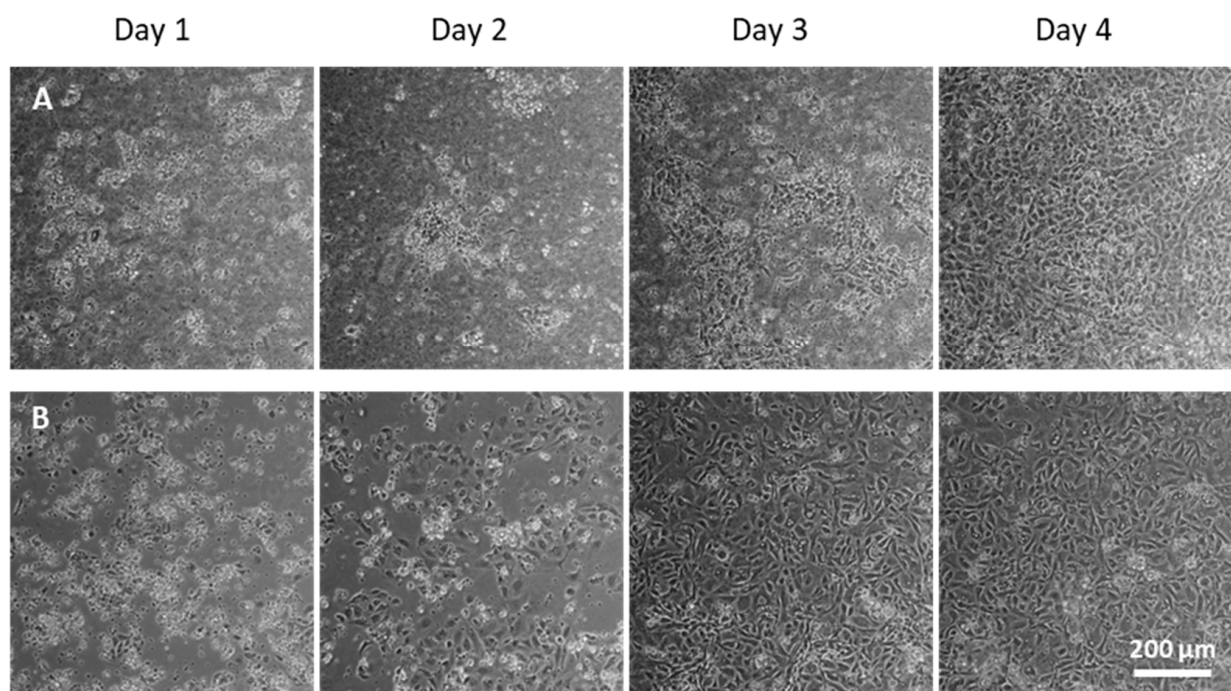


Figure 1. Rat primary alveolar cells were cultured either on porcine lung-derived hydrogel (A) or on a plate (B). Bright field images were taken every 24 h from day 1.

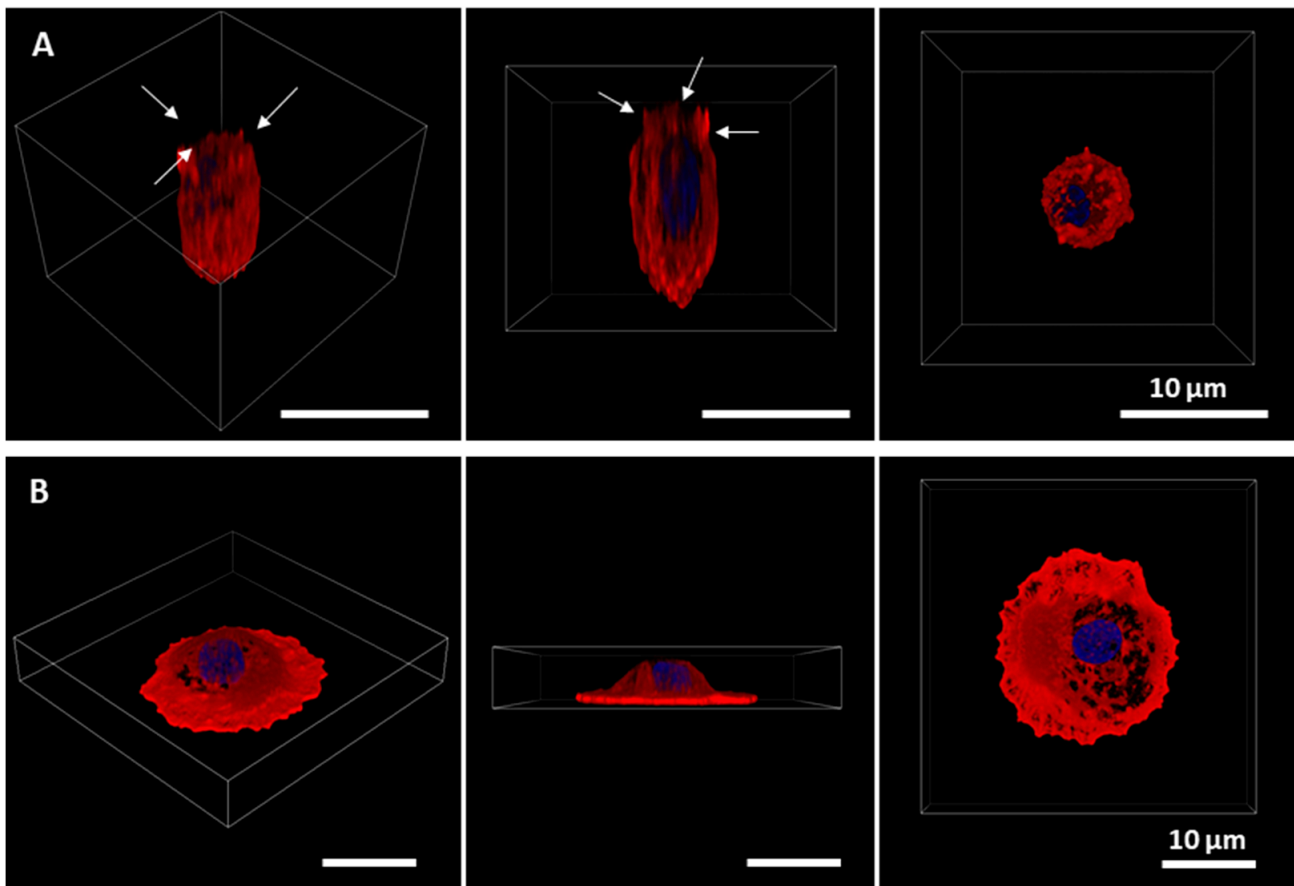


Figure 2. Three-dimensional representation of primary alveolar type II cells cultured for three days on hydrogel (A) and on a plate (B). Nuclei are stained in blue and actin cytoskeleton in red. In the case of the hydrogel-cultured cell, it can be distinguished by a cuboidal morphology and the presence of microvilli, indicated by arrows. In the case of the cell cultured on a plate, a more spread out and wider cytoplasm can be observed showing increased size.

2.2. Culture of Alveolar Epithelial Cells on Lung-Derived Hydrogels Preserves the Expression of Type II Markers for Longer Periods

The results of the genetic expression of ATI and AII typical markers (from day 2 to 5) are shown in Figure 3A. The gene expression of *sftpc* and *sftpb* decreased over time. There was a significant increase in AII markers (surfactant proteins B and C) at earlier times (day 2 and day 3) in cells cultured on lung-derived hydrogels. There was no increase in ATI markers over time in cells cultured on hydrogels, in contrast to cells cultured on plates, where the expression of *pdpn* and *aqp5* increased with time (classical ATI markers). These results show that the AII phenotype and gene expression levels were maintained for longer in lung-derived hydrogels. The results from immunostaining are shown in Figure 3B–E, revealing that the differential expression of surfactant protein C caused by the substrate was noticeable not only at the gene expression level, but also at the protein level. SPC expression was higher in cells cultured on lung hydrogels compared to that of cells cultured on a plate, as shown by the immunostainings. Furthermore, culture time affected cells differently depending on the substrate they were cultured on. Indeed, cells cultured on lung hydrogel were able to maintain the SPC expression over time, whereas cells cultured on a plate rapidly lost this ability.

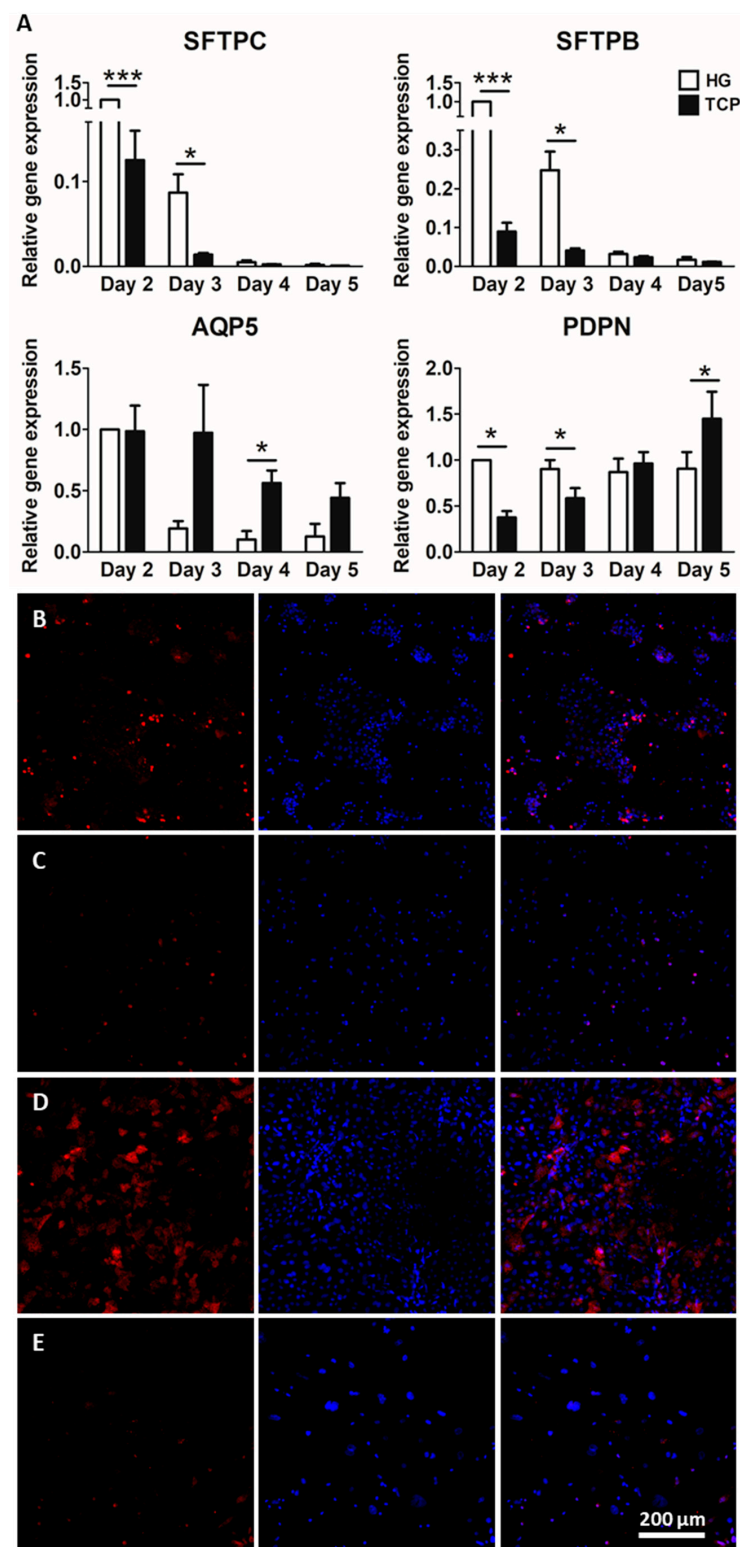


Figure 3. ATII cells were cultured either on hydrogel (HG) or a tissue culture plate (TCP). ATII typical marker surfactant proteins C (*sftpc*) and B (*sftpb*) and ATI typical marker aquaporin 5 (*aqp5*), podoplanin (*pdpn*) were studied at different time points (from day 2 to day 5) by qPCR (A). Relative gene expression is shown. Expression of surfactant protein C (SPC) was studied using immunofluorescence on ATII cells cultured on hydrogel at day 2 (B) and day 4 (D) and on a plate at day 2 (C) and day 4 (E). * $p < 0.05$, *** $p < 0.001$.

2.3. Culture of Primary Alveolar Epithelial Cells in Lung-Derived Hydrogels Inhibits Type II-to-Type I Transdifferentiation by Altering the Hippo/Rho Pathway

Since YAP is a key mechanotransduction protein, its expression was studied in cells cultured on hydrogels or plates for three days (Figure 4A,B). In cells cultured on hydrogels, the YAP protein was located mainly in the cytoplasm, which indicates that it was being phosphorylated and subsequently degraded. In contrast, in cells cultured on plates, nuclear active YAP was observed. Specifically, there was a two-fold increase in the amount of nuclear YAP when cells were cultured on a plate compared to that of cells cultured on hydrogels, indicating a higher transcriptional activity in the first group (Figure 4C).

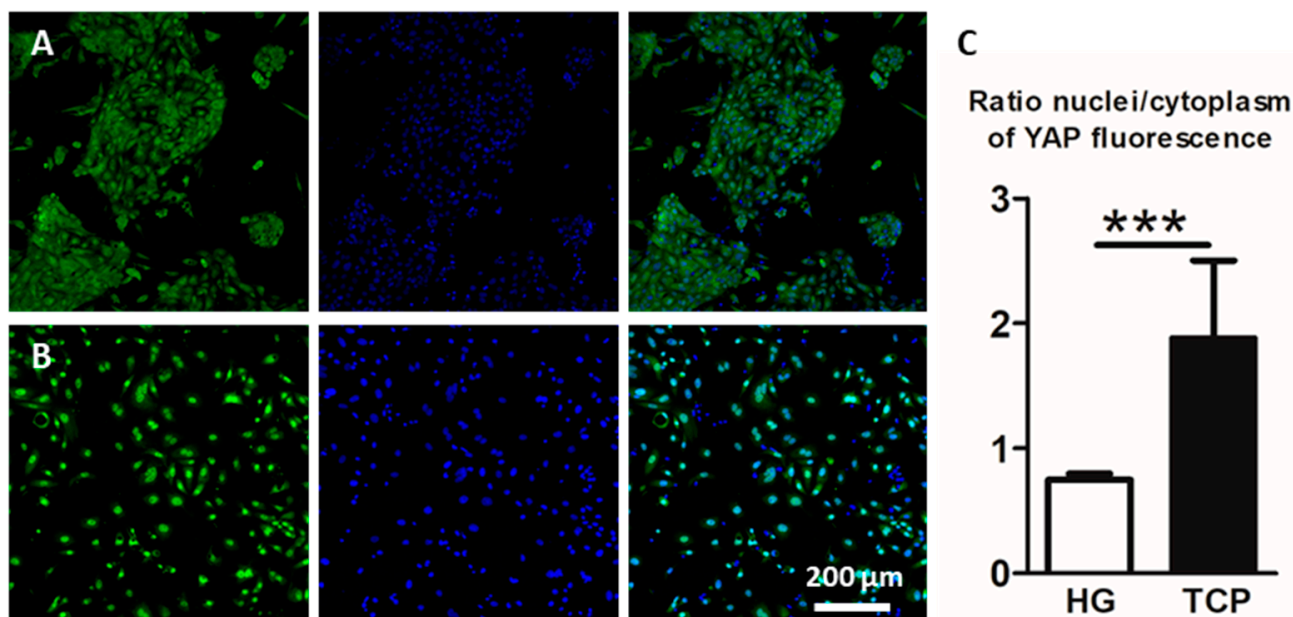


Figure 4. Alveolar type II cells were cultured on hydrogel (A) or on a plate (B) and stained for YAP protein (green). YAP nuclear and cytoplasmic expressions were quantified and expressed as the nuclei/cytoplasm fluorescence ratio in both conditions hydrogel (HG) and tissue culture plate (TCP) (C), *** $p < 0.001$.

Owing to the role of focal adhesions (FAs) and the actin cytoskeleton in sensing extracellular matrix cues and transmitting them to the cell, the expressions of actin and paxillin, which is one of the proteins comprising FAs, were studied. Both were reported to be implicated in the hippo pathway, by inhibiting it and promoting the YAP nuclear expression. In cells cultured for three days on lung-derived hydrogels, a poor focal adhesion assembly was observed by the paxillin immunostaining. Moreover, no stress fibers were formed as indicated by the phalloidin staining (Figure 5A). On the contrary, in cells that were cultured for three days on a plate, assembled paxillin and stress fibers were clearly observed (Figure 5B). The role of Rho, which is involved in the maturation of focal adhesions and YAP regulation [13,14] was studied by the use of the ROCK inhibitor (Y27632). The results show that it could play a role in the maintenance of the ATII phenotype, as reflected by an increase in SPC in conventional culture ($p = 0.02$) (Figure 5D) together with a decrease in focal adhesion size ($p = 0.001$) (Figure 5D), suggesting that the use of HGs as a substrate for AECs culture could be inhibiting the Rho pathway, and thus allowing for type II phenotype maintenance.

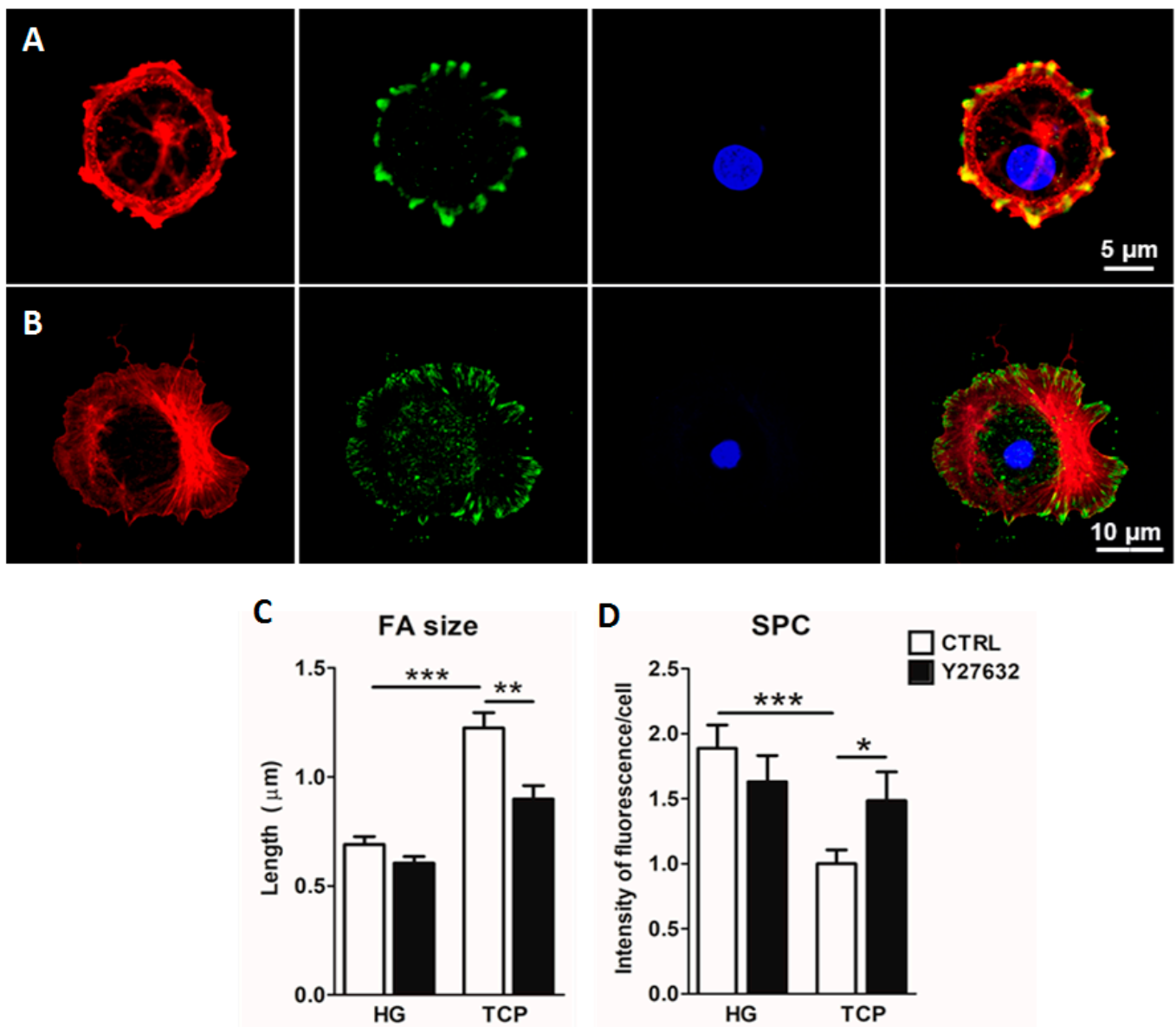


Figure 5. Representative images of focal adhesions (FAs) in cells cultured on hydrogels (A) and plate (B). Red: phalloidin, green: paxillin, blue: nuclei. Quantification of the FA length (C) and the intensity of surfactant protein C (SPC) of alveolar type II cultured on hydrogels for 3 days with (Y27632) and without (CTRL) the addition of the ROCK inhibitor (D), * $p < 0.05$, ** $p < 0.01$, *** $p < 0.001$.

2.4. Primary Alveolar Epithelial Cells Cultured on Lung-Derived Hydrogels Can Be Subcultured

The potential ability to subculture primary ATII cells was studied. Cells were cultured for 3 days on lung hydrogels and, after that time, lung-derived hydrogels were digested with collagenase, and cells were seeded again on plates. Sixteen hours later, they were immunostained for typical epithelial (EpCAM) and ATII (SFTPC) markers (Figure 6). Subcultured cells were positive for both, EpCAM and SFTPC markers. These results indicate that lung-derived hydrogels allow for primary AECs subculture.

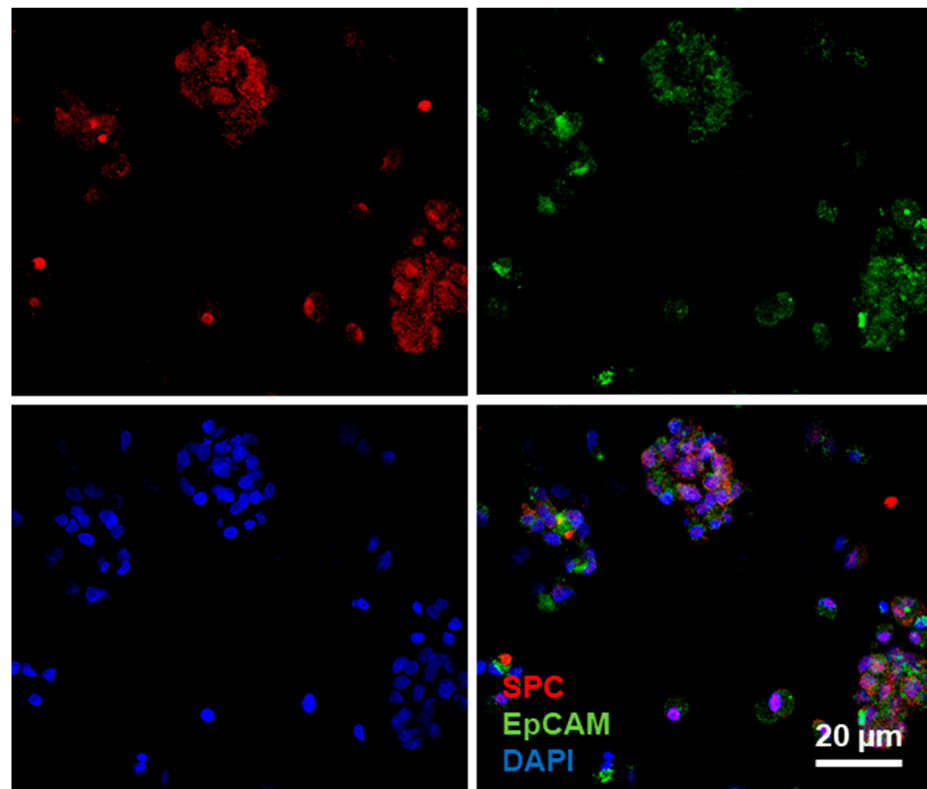


Figure 6. Alveolar type II cells were cultured on hydrogels for three days. After that time, they were subcultured on plates and stained for surfactant protein C (red) and EpCAM (green).

3. Discussion

We have provided evidence that using lung-derived ECM hydrogels as a culture substrate allows the maintenance of the type II phenotype in primary AECs to be enhanced. Moreover, our results for YAP and when using ROCK inhibitors on cells cultured on lung hydrogels, which preserve several proteins from their native organs [7], suggest that the biophysical properties of the hydrogel have a high impact on cell mechanosensing pathways, thereby playing a role in the maintenance of type II phenotype. This first-time study culturing cells on lung ECM-derived hydrogels, which was carried out in rat primary AECs as a proof of concept, opens the door for further research in primary human AECs, with a potential future impact on cell therapies for diseases such as pulmonary fibrosis and acute lung injury [15,16].

Similar results to those obtained in the present study were provided by Shannon and coworkers [6], who conducted the first study showing the importance of the protein content of the substrate in the maintenance of ATII morphology and phenotype. The main limitation of that first study was the inability of the cells to form a monolayer, which is easily accomplished in our lung-derived hydrogel. Since then, efforts have been made to improve the ability to maintain the ATII phenotype, which has only been achieved by media supplementation [3,17–19]. Both the biochemical and physical properties of the substrate are involved in cell behavior. It is worth noting that cells formed a monolayer slower in hydrogels than on plates, which could be due to the fact that cells proliferate quicker on the plate or that the ATII-to-ATI transdifferentiation allows for a faster substrate coverage, as ATI cells are much larger in size. In view of the differing stiffness of the hydrogels when compared to the culture plate and the cuboidal morphology of the cells, differences in their cytoskeleton distribution and the formation of focal adhesions, which are key points in the crosstalk of cell-ECM, were expected. Cells cultured on hydrogels showed shorter focal adhesions that correlated with a decreased YAP translocation to the nuclei. YAP is an important transcription factor that is implied in the regulation of several genes, and it

is reported to be associated with inflammatory and epithelial damage situations in vivo where the ATII-to-ATI transdifferentiation is required [20,21]. In this case, YAP nuclear location of cells cultured on a plate could be triggering the differentiation in the ATI cell population. As Rho is implicated in the maturation of focal adhesions [14], and previous authors have pointed to it as a key factor in the transdifferentiation process [4,22], its role was studied. The determination of the individual contribution of different Rho proteins would be highly interesting. However, as it would be complex [14], we studied this effect through its inhibition using Y27632. The obtained results support the implication of Rho in the ATII phenotype, as its inhibition produced an increase in SPC and decrease in FAs only in cells cultured on a plate. The origin of this inhibition of the Rho pathway, although out of the scope of the present work, is probably related to the complex molecular composition of lung-derived hydrogels and their biomechanical properties.

Primary ATII cells have previously been subcultured [4] by coculturing them with fibroblasts as feeder cells and with the addition of the Rho inhibitors. The role of fibroblasts in maintaining the ATII phenotype is not exactly known but it could be that they work as a source of the keratinocyte growth factor (KGF). The addition of KGF has been used by other authors to increase the phenotypic features of ATII cells [3,19], and in turn, to inhibit Rho kinases, which are shown to play a key role in the ATII-to-ATI transdifferentiation [22]. In our case, the use of lung-derived hydrogels as substrates for culturing allows these cells to be subcultured without the use of additional chemicals or cocultures. Therefore, culturing primary alveolar epithelial cells on lung ECM-derived hydrogels may facilitate the prolonged culturing of these cells, and thus help in the research of lung diseases. However, more research should be carried out regarding the number of possible passages, especially considering that factors different from the ATI-to-ATII transdifferentiation would limit the time that these primary cells could be maintained in vitro. Further research is also needed to determine which components of ECM-derived hydrogels have more impact on the maintenance of the type II phenotype in vitro. As the extracellular matrix used to produce hydrogels in the present work was obtained from lung tissue, it is expected that some key biochemical and biophysical factors specific to the lung are being preserved in the process of hydrogel production. The identification of these factors, although out of the scope of the present work, would allow the development of novel optimized scaffolds for the in vitro culture of pulmonary cells.

4. Materials and Methods

Unless otherwise specified, all reagents were purchased from ThermoFisher Scientific (Waltham, MA, USA) or Sigma-Aldrich (Saint Louis, MO, USA).

4.1. Decellularized Lung Extracellular Matrix Hydrogels Preparation

Lung-derived hydrogels were prepared by following a previously described protocol [23]. Briefly, porcine lungs were decellularized by consecutive perfusion of the following reagents through the vasculature and the airways: 0.1% Triton X-100 and 2% SDC for 24 h at 4 °C, and NaCl 1 M and DNase solution for 1 h at 4 °C. Three washes of milliQ water were performed between consecutive reagent perfusion, and a last wash of PBS 1X was carried out. Decellularized lungs were cut into small pieces, freeze-dried (Telstar Lyoquest-55 Plus, Terrassa, Spain) and milled in liquid N₂ (SPEX SamplePrep, Metuchen, NJ, USA). The obtained powder was resuspended at 20 mg/mL in 0.01 M HCl and pepsin digested at a 1/10 proportion under magnetic stirring at room temperature for 16 h. To produce hydrogels, the digested solution was pH-adjusted to 7.4 ± 0.4 by using 0.1 M NaOH and incubated at 37 °C for 20 min.

4.2. Primary Alveolar Epithelial Cells Isolation

The procedure was approved by the Ethical Board for Animal Research of the University of Barcelona, in compliance with regional, national and European regulations. Rat lungs were obtained from 180–250 g Sprague Dawley male rats. The animals were intraperi-

toneally anesthetized with 1 g/kg urethane and euthanized by exsanguination. AECs were isolated following a protocol described in [24]. Briefly, lungs were perfused with saline through the pulmonary artery and were resected en bloc. Three bronchioalveolar lavages were performed with 10 mL of PBS 1X to remove alveolar macrophages. Then, lungs were digested with 50 mL of 0.25% of trypsin through the airways for 30 min, cut into small pieces, and digested in a 100 units/mL DNase solution. The resulting suspension was filtered through a 100 μ m and a 40 μ m mesh and centrifuged through a Percoll (GE HealthCare, Chicago, IL, USA) gradient at 500 \times g for 20 min. The band containing ATII cells was recovered and digested using 20 units/mL of DNase. The resulting solution was centrifuged for 15 min at 500 \times g, and the pellet was resuspended in DCCM-1 (Biological Industries, Kibbutz Beit Haemek, Israel) medium and cultured for 1 h. Subsequently, medium containing ATII non-adherent cells was recovered and centrifuged for 10 min at 800 \times g. Cells were finally counted and seeded either on 24-well culture plates or on top of lung-ECM hydrogels.

4.3. Rho Kinase Inhibition Assay

For the inhibition of the Rho pathway, Y27638 (10 μ M) was added to the medium for 24 h.

4.4. Reverse Transcription qPCR

For studying the expression of ATI and ATII markers, cells were cultured either on plastic or lung-derived hydrogels for different times, and RNA was subsequently extracted from samples by employing the RNeasy kit (Qiagen, Hilden, Germany). The cDNA was obtained by a reverse transcription-polymerase chain reaction (TaqMan Reverse Transcription Reagents, Invitrogen, Waltham, MA, USA) according to the manufacturer's instructions. The expression level of surfactant protein C (*sftpc*), surfactant protein B (*sftpb*), aquaporin 5 (*aqp5*) and podoplanin (*pdprn*) was studied using the Taqman Fast Advanced Master Mix and the TaqMan Gene Expression Assays in a StepOnePlus thermocycler (Applied Biosystems, Waltham, MA, USA). The expression level of genes was normalized to the constitutively expressed gene PPIA and calculated using the $2^{-\Delta\Delta C_t}$ method [25].

4.5. Immunohistochemistry and Image Processing

For immunohistochemistry experiments, cells were fixed with 4% paraformaldehyde for 30 min. Primary antibodies were incubated overnight, and secondary antibodies were incubated for 2 h at 37 °C. Nuclei were stained with Hoechst 33342. To avoid unspecific binding, especially in the hydrogel samples, a blocking buffer consisting of 2% BSA (Thermo Fisher, MA, USA) diluted in PBS 1X (Gibco, MA, USA) was employed for 40 min. Primary antibodies employed were rabbit anti-SFTPC (Invitrogen, Waltham, MA, USA), mouse anti-YAP (Santa Cruz Biotechnology, Dallas, TX, USA) and EpCAM (Miltenyi, Bergisch Gladbach, Germany). Secondary antibodies used were goat anti-rabbit cy5 (Abcam, Cambridge, UK) and goat anti-mouse Alexa Fluor 488 (Abcam, Cambridge, UK). Images were acquired with a Nikon Confocal Eclipse Ti microscope using a 20 \times Plan Fluor Multi-immersion objective (0.75 NA) in the case of the SFTPC, EpCAM and YAP staining with a 10 \times objective (0.3 NA) for the bright field images, and a 100 \times objective (1.45 NA) for the paxillin and actin images. Nuclear images were obtained at 450 nm when illuminating the sample at 408 nm. Samples were excited at 488 nm and acquired at 515 nm for YAP, EpCAM and Paxillin images, and excited at 543.5 nm and acquired at 605 nm for SFTPC and actin stains.

For the analysis of YAP images, five images per condition were randomly selected and analyzed using a blind procedure with ImageJ Software. Quantification of the ratio nuclear fluorescence/cytoplasmic fluorescence was assessed following a previously described procedure [26] with slight modifications. To calculate the total cell fluorescence, a triangle threshold was employed, and the integrated fluorescence was calculated in the YAP channel. For calculating the YAP nuclear fluorescence, the perimeter of the nuclei was delimited by

the Huang threshold in the DAPI channel. After that, the resulting mask was redirected to the YAP channel and the integrated intensity contained in the nuclear perimeter was obtained. To calculate the cytoplasmic fluorescence, the differences in the intensities in the total cell and in the nuclei were calculated.

For focal adhesion length measurements, five representative adhesions per cell in paxillin stainings at the cell edge were manually quantified with Image J Software.

4.6. Statistical Analysis

Data are expressed as mean \pm SE unless stated otherwise. Statistical analysis was performed with Graphpad Prism software. Differences in ATI/ATII markers gene expression and YAP nuclear/cytoplasmic expression were analyzed using paired *t*-test. A *p*-value < 0.05 was considered significant.

Author Contributions: Conceptualization, E.M., I.A. and J.O.; Formal analysis, E.M., A.V., A.A., R.F., I.A. and J.O.; Funding acquisition, R.F., I.A., N.G. and J.O.; Investigation, E.M., A.V., I.A. and J.O.; Methodology, E.M., A.V., M.L.N., M.C.-R., I.A. and J.O.; Project administration, R.F., I.A. and J.O.; Resources, N.G., A.A., R.F., N.G., I.A. and J.O.; Software, E.M., M.L.N. and N.G.; Supervision, I.A. and J.O.; Writing of original draft, E.M. and J.O. All authors have read and agreed to the published version of the manuscript.

Funding: This research was funded by the Spanish Ministry of Science, Innovation and Universities, grants numbers SAF2017-85574-R, DPI2017-83721-P, PID2019-108958RB-I00, and PGC2018-097323-A-I00, and by European Union's Horizon 2020, Marie Skłodowska-Curie, grant 821772.

Institutional Review Board Statement: Animal experiments were approved by the Ethical Committee for Animal Research of the University of Barcelona.

Data Availability Statement: Data supporting the findings of this study are available from the corresponding authors upon reasonable request.

Acknowledgments: The authors wish to thank Miguel A. Rodríguez from the Unit of Biophysics and Bioengineering for his excellent technical assistance.

Conflicts of Interest: The authors declare no conflict of interest.

References

1. Sun, T.; Huang, Z.; Zhang, H.; Posner, C.; Jia, G.; Ramalingam, T.R.; Xu, M.; Brightbill, H.; Egen, J.G.; Dey, A.; et al. TAZ is required for lung alveolar epithelial cell differentiation after injury. *JCI Insight* **2019**, *5*, 128674. [[CrossRef](#)] [[PubMed](#)]
2. Dobbs, L.G. Isolation and culture of alveolar type II cells. *Am. J. Physiol.* **1990**, *258 Pt 1*, L134–L147. [[CrossRef](#)] [[PubMed](#)]
3. Rice, W.R.; Conkright, J.J.; Na, C.L.; Ikegami, M.; Shannon, J.M.; Weaver, T.E. Maintenance of the mouse type II cell phenotype in vitro. *Am. J. Physiol. Lung Cell Mol. Physiol.* **2002**, *283*, L256–L264. [[CrossRef](#)] [[PubMed](#)]
4. Bove, P.F.; Dang, H.; Cheluvvaraju, C.; Jones, L.C.; Liu, X.; O'Neal, W.K.; Randell, S.H.; Schlegel, R.; Boucher, R.C. Breaking the in vitro alveolar type II cell proliferation barrier while retaining ion transport properties. *Am. J. Respir. Cell Mol. Biol.* **2014**, *50*, 767–776. [[CrossRef](#)] [[PubMed](#)]
5. Seo, J.; Kim, J. Regulation of Hippo signaling by actin remodeling. *BMB Rep.* **2018**, *51*, 151–156. [[CrossRef](#)]
6. Shannon, J.M.; Emrie, P.A.; Fisher, J.H.; Kuroki, Y.; Jennings, S.D.; Mason, R.J. Effect of a reconstituted basement membrane on expression of surfactant apoproteins in cultured adult rat alveolar type II cells. *Am. J. Respir. Cell Mol. Biol.* **1990**, *2*, 183–192. [[CrossRef](#)]
7. Pouliot, R.A.; Young, B.M.; Link, P.A.; Park, H.E.; Kahn, A.R.; Shankar, K.; Schneck, M.B.; Weiss, D.J.; Heise, R.L. Porcine Lung-Derived Extracellular Matrix Hydrogel Properties Are Dependent on Pepsin Digestion Time. *Tissue Eng. Part C Methods* **2020**, *26*, 332–346. [[CrossRef](#)]
8. Falcones, B.; Sanz-Fraile, H.; Marhuenda, E.; Mendizábal, I.; Cabrera-Aguilera, I.; Malandain, N.; Uriarte, J.J.; Almendros, I.; Navajas, D.; Weiss, D.J.; et al. Bioprintable Lung Extracellular Matrix Hydrogel Scaffolds for 3D Culture of Mesenchymal Stromal Cells. *Polymers* **2021**, *13*, 2350. [[CrossRef](#)]
9. Das, A.; Fischer, R.S.; Pan, D.; Waterman, C.M. YAP Nuclear Localization in the Absence of Cell-Cell Contact Is Mediated by a Filamentous Actin-dependent, Myosin II- and Phospho-YAP-independent Pathway during Extracellular Matrix Mechanosensing. *J. Biol. Chem.* **2016**, *291*, 6096–6110. [[CrossRef](#)]
10. Chen, Q.; Rehman, J.; Chan, M.; Fu, P.; Dudek, S.M.; Natarajan, V.; Malik, A.B.; Liu, Y. Angiocrine Sphingosine-1-Phosphate Activation of S1PR2-YAP Signaling Axis in Alveolar Type II Cells Is Essential for Lung Repair. *Cell Rep.* **2020**, *31*, 107828. [[CrossRef](#)]

11. Kim, N.G.; Gumbiner, B.M. Adhesion to fibronectin regulates Hippo signaling via the FAK-Src-PI3K pathway. *J. Cell Biol.* **2015**, *210*, 503–515. [[CrossRef](#)] [[PubMed](#)]
12. Ito, H.; Uchida, T.; Makita, K. Interactions between rat alveolar epithelial cells and bone marrow-derived mesenchymal stem cells: An in vitro co-culture model. *Intensive Care Med. Exp.* **2015**, *3*, 53. [[CrossRef](#)] [[PubMed](#)]
13. Pennarossa, G.; Paffoni, A.; Ragni, G.; Gandolfi, F.; Brevini, T.A.L. Rho Signaling-Directed YAP/TAZ Regulation Encourages 3D Spheroid Colony Formation and Boosts Plasticity of Parthenogenetic Stem Cells. *Adv. Exp. Med. Biol.* **2020**, *1237*, 49–60. [[CrossRef](#)]
14. Warner, H.; Wilson, B.J.; Caswell, P.T. Control of adhesion and protrusion in cell migration by Rho GTPases. *Curr. Opin. Cell Biol.* **2019**, *56*, 64–70. [[CrossRef](#)] [[PubMed](#)]
15. Lopez-Rodriguez, E.; Gay-Jordi, G.; Knudsen, L.; Ochs, M.; Serrano-Mollar, A. Improved Alveolar Dynamics and Structure After Alveolar Epithelial Type II Cell Transplantation in Bleomycin Induced Lung Fibrosis. *Front. Med.* **2021**, *8*, 640020. [[CrossRef](#)]
16. Serrano-Mollar, A.; Gay-Jordi, G.; Guillamat-Prats, R.; Closa, D.; Hernandez-Gonzalez, F.; Marin, P.; Burgos, F.; Martorell, J.; Sánchez, M.; Arguis, P.; et al. Safety and Tolerability of Alveolar Type II Cell Transplantation in Idiopathic Pulmonary Fibrosis. *Chest* **2016**, *150*, 533–543. [[CrossRef](#)]
17. Griffin, M.; Bhandari, R.; Hamilton, G.; Chan, Y.C.; Powell, J.T. Alveolar type II cell-fibroblast interactions, synthesis and secretion of surfactant and type I collagen. *J. Cell Sci.* **1993**, *105 Pt 2*, 423–432. [[CrossRef](#)]
18. Buckley, S.; Driscoll, B.; Anderson, K.D.; Warburton, D. Cell cycle in alveolar epithelial type II cells: Integration of Matrigel and KGF. *Am. J. Physiol.* **1997**, *273 Pt 1*, L572–L580. [[CrossRef](#)]
19. Wang, J.; Edeen, K.; Manzer, R.; Chang, Y.; Wang, S.; Chen, X.; Funk, C.J.; Cosgrove, G.P.; Fang, X.; Mason, R.J. Differentiated human alveolar epithelial cells and reversibility of their phenotype in vitro. *Am. J. Respir. Cell Mol. Biol.* **2007**, *36*, 661–668. [[CrossRef](#)]
20. Chen, W.; Zhuo, Y.; Duan, D.; Lu, M. Effects of Hypoxia on Differentiation of Mesenchymal Stem Cells. *Curr. Stem. Cell Res. Ther.* **2020**, *15*, 332–339. [[CrossRef](#)]
21. LaCanna, R.; Liccardo, D.; Zhang, P.; Tragesser, L.; Wang, Y.; Cao, T.; Chapman, H.A.; Morrisey, E.E.; Shen, H.; Koch, W.J.; et al. Yap/Taz regulate alveolar regeneration and resolution of lung inflammation. *J. Clin. Investig.* **2019**, *129*, 2107–2122. [[CrossRef](#)] [[PubMed](#)]
22. Foster, C.D.; Varghese, L.S.; Gonzales, L.W.; Margulies, S.S.; Guttentag, S.H. The Rho pathway mediates transition to an alveolar type I cell phenotype during static stretch of alveolar type II cells. *Pediatr. Res.* **2010**, *67*, 585–590. [[CrossRef](#)] [[PubMed](#)]
23. Pouliot, R.A.; Link, P.A.; Mikhael, N.S.; Schneck, M.B.; Valentine, M.S.; Kamga Gninzeko, F.J.; Herbert, J.A.; Sakagami, M.; Heise, R.L. Development and characterization of a naturally derived lung extracellular matrix hydrogel. *J. Biomed. Mater. Res. A* **2016**, *104*, 1922–1935. [[CrossRef](#)] [[PubMed](#)]
24. Guillamat-Prats, R.; Camprubi-Rimblas, M.; Puig, F.; Herrero, R.; Tantinyà, N.; Serrano-Mollar, A.; Artigas, A. Alveolar Type II Cells or Mesenchymal Stem Cells: Comparison of Two Different Cell Therapies for the Treatment of Acute Lung Injury in Rats. *Cells* **2020**, *9*, 1816. [[CrossRef](#)]
25. Livak, K.J.; Schmittgen, T.D. Analysis of Relative Gene Expression Data Using Real-Time Quantitative PCR and the 2[−]ΔΔCT Method. *Methods* **2001**, *25*, 402–408. [[CrossRef](#)]
26. Marhuenda, E.; Campillo, N.; Gabasa, M.; Martínez-García, M.A.; Campos-Rodríguez, F.; Gozal, D.; Navajas, D.; Alcaraz, J.; Farré, R.; Almendros, I. Effects of Sustained and Intermittent Hypoxia on Human Lung Cancer Cells. *Am. J. Respir. Cell Mol. Biol.* **2019**, *61*, 540–544. [[CrossRef](#)]

Chapter VI.
SCIENTIFIC ARTICLE III

Development of a Physiomimetic Model of Acute Respiratory Distress Syndrome by using ECM Hydrogels and Organ-on-a-chip Devices

1 Esther Marhuenda^{1,2,†}, Alvaro Villarino^{1,†}, Maria Narciso^{1,3}, Linda Elowsson⁴, Isaac
2 Almendros^{1,2,5}, Gunilla Westergren-Thorsson⁴, Ramon Farré^{1,2,5}, Núria Gavara^{1,2,3}, Jorge
3 Otero^{1,2,3*}

4 ¹Unitat de Biofísica i Bioenginyeria. Facultat de Medicina i Ciències de la Salut. Universitat de
5 Barcelona, Barcelona, Spain.

6 ²CIBER de Enfermedades Respiratorias, Instituto de Salud Carlos III, Madrid, Spain.

7 ³The Institute For Bioengineering of Catalonia. The Barcelona Institute of Science and Technology,
8 Barcelona, Spain.

9 ⁴Lund University, Lund, Sweden.

10 ⁵Institut d'Investigacions Biomèdiques August Pi i Sunyer, Barcelona, Spain.

11

12 [†]Equally contributed to the work

13 * **Correspondence:**

14 Jorge Otero, Ph.D.

15 jorge.otero@ub.edu

16 **Keywords: ARDS, lung-on-a-chip, extracellular matrix, hydrogels, mesenchymal stromal cells,**
17 **alveolar epithelial cells, inflammation.**

18 **Abstract**

19 Acute Respiratory Distress Syndrome is one of the more common fatal complications in COVID-19,
20 being characterized by a highly aberrant inflammatory response. Pre-clinical models to study the
21 effect of cell therapy and anti-inflammatory treatments have not been able to give a comprehensive
22 understanding of the disease due to its high complexity. In this work, we present a novel
23 physiomimetic *in vitro* model for Acute Respiratory Distress Syndrome based on the use of lung
24 extracellular matrix-derived hydrogels and organ-on-a-chip devices. Primary alveolar epithelial cells
25 were cultured on top hydrogels fabricated of previously decellularized lung tissue, containing
26 primary lung mesenchymal stromal cells until forming monolayers. Then, cyclic stretch was applied
27 to mimic breathing, and inflammatory response was induced by using a bacteriotoxin hit. Having
28 mimicked the inflamed breathing lung environment, we assessed the effect of an anti-inflammatory
29 drug (i.e dexamethasone) by the study of secretion of the most relevant inflammatory cytokines. To
30 better identify key players in our model, the impact of the individual factors (cyclic stretch,
31 decellularized lung hydrogel scaffold and the presence of mesenchymal stromal cells) was studied
32 separately. Results showed that the developed advanced physiomimetic model presented a more
33 reduced inflammatory response than traditional models, which is in line with what is expected from
34 the response commonly observed in patients. Further, from the different stimuli, it was observed that
35 the use of extracellular matrix hydrogels obtained from decellularized lungs had the greatest impact

36 on the change of the inflammatory response. The developed model opens then the door for further *in*
37 *vitro* studies with a better-adjusted response to the inflammatory hit and more robust results in the
38 test of different drugs or the use of cell therapy.

39 1 Introduction

40 Acute Respiratory Distress Syndrome (ARDS), commonly caused by bacterial or viral pneumonia
41 (Matthay et al. 2019), is characterized by lung parenchymal damage from increased endothelial and
42 epithelial permeability (non-cardiogenic pulmonary edema) (Staub 1981). ARDS mortality is
43 approximately 25-40% and the only treatment is primarily supportive with lung-protective ventilation
44 (Brower et al. 2000). Major efforts in the medical community are focused mostly on the prevention
45 of the injury (Yadav, Thompson, and Gajic 2017) since, although numerous pharmacologic
46 strategies have been successful in animal studies, few trials have shown a clinical benefit in terms of
47 mortality (Ballard-Croft et al. 2012). On the other hand, cell therapies based on the use of
48 mesenchymal stromal cells (MSCs) have started to show certain efficacy although the mechanisms
49 involved in the processes are still to be determined (Laffey and Matthay 2017). Moreover, during the
50 COVID-19 pandemic, ARDS has been reported as a common complication that dramatically
51 increased the mortality of patients (Wu et al. 2020). The aberrant inflammatory response of these
52 patients (which is known as the cytokine storm) has been correlated with the severity of the disease
53 and has become one of the main therapeutic targets (L.D. Chen et al. 2020). Nevertheless, neither *in*
54 *vitro* nor *in vivo* available models realistically recreate the complex pathophysiology of ARDS
55 (Huppert and Matthay 2017). Therefore, there is an urgent need to develop models with higher
56 physiological relevance to understand the inflammatory processes related to ARDS, the impact of
57 cell therapy (Nonaka et al. 2020), and the use of anti-inflammatory drugs (Trivedi, Verma, and
58 Kumar 2020). Conventional ARDS *in vitro* models mainly consist of the application of an
59 inflammatory hit (usually by the use of a bacteriotoxin) to a monolayer of pulmonary epithelial or
60 endothelial cells (Cabrera-Benítez et al. 2016). The problem with these conventional models is that
61 they do not fully mimic the complex three-dimensional microarchitecture or the extracellular matrix
62 (Burgess et al. 2016) (ECM) stiffness experienced by cells *in vivo*. Moreover, lung cells *in vivo* are
63 subjected to mechanobiological signals such as those induced by the cyclic stretch associated with
64 breathing or mechanical ventilation.

65 Two different technologies have recently gained popularity for creating physiomimetic models to
66 recreate the ECM (Busch, Lorenzana, and Ryan 2021) and the mechanobiological signals *in vitro*: 3D
67 cell cultures (Habanjar et al. 2021) and organ-on-a-chip devices (Mertz, Ahmed, and Takayama
68 2018; Benam, Burgess, and Stewart 2021). Indeed, it has been shown that lung ECM can be obtained
69 from the decellularization of the native tissues with detergents and enzymes (Nonaka et al. 2014), and
70 then pulverized and reconstituted in form of hydrogels suitable for 3D cell culture (Pati and Cho
71 2017). On the other hand, organ-on-a-chip devices (Bassi et al. 2021) try to recreate the physical
72 microenvironment of living organs *in vitro*. In the specific case of a lung-on-a-chip, devices with
73 control over the cyclic stretch and oxygenation have been developed (Campillo et al. 2016; D. Huh et
74 al. 2013). In the present work, the aim was to merge these two frontier technologies (3D ECM
75 hydrogels and lung-on-a-chip-devices) to develop an advanced physiomimetic *in vitro* model of
76 ARDS for the study of inflammatory processes and how they are related to MSCs therapies. Using
77 such advanced model, we have tested the individual contribution of cyclic stretch and lung ECM, and
78 the effect of lung-resident MSCs to the secretion of inflammation-related cytokines after bacterial
79 lipopolysaccharide (LPS) challenge, as well as the effect of treatment with an anti-inflammatory drug
80 (dexamethasone).

81 2 Materials and Methods

82 All the reagents were obtained from Sigma Aldrich, Missouri, USA unless otherwise specified.

83 2.1 Decellularized extracellular matrix hydrogels

84 Lung hydrogels were developed from porcine lungs by following the protocol described in (Falcones
85 *et al.* 2021). Briefly, porcine lungs were decellularized by perfusion through the trachea and the
86 vasculature 0.1% with Triton X-100 and 2% of sodium deoxycholate for 24 hours each, and DNase
87 and 1M NaCl for one hour each. Decellularized lungs were afterward frozen at -80 °C, freeze-dried
88 (Telstar Lyoquest-55 Plus, Terrassa, Spain) and milled in liquid N₂ (SPEX SamplePrep, New Jersey,
89 USA) to obtain a fine powder. The resulting ECM powder was digested at a concentration of 20
90 mg/mL in HCl 0.01 M with porcine gastric mucosa pepsin at a 10:1 concentration at room
91 temperature for 16 hours. To produce the hydrogels, the digested solution was pH-adjusted to 7.4 ±
92 0.4 by using 0.1 M NaOH and incubated at 37 °C for 20 minutes.

93 2.2 Lung-on-a-chip devices fabrication

94 The designed lung-on-a-chip devices were composed of 3 parts containing 6 holes, each one located
95 concentrically to conform to the wells (Figure 1). A video with detailed instructions for fabricating a
96 similar chip is open-source available in the [supplementary material](#) of (23). The upper part of the
97 device, which was separated from the other two parts by a 380 µm thick gas permeable
98 polydimethylsiloxane (PDMS) membrane (Gel-Pak, Hayward, CA, USA), was the culture chamber
99 (cells and culture medium). The two other parts had channels in their lower part to allow for gas
100 efflux (gas chamber). Gas entered the chip through a small tube inserted in a central tiny hole that
101 perforates the culture chamber and the first part of the gas chamber. The air was distributed through
102 the radial channels of the middle PDMS piece (upper part of the gas chamber) and diffused to the
103 cells through the lower part of the membrane. Gas exited the chip through the radial channels of the
104 lower PDMS piece (lower part of the gas chamber), coming back to the center of the chip, where gas
105 found an exit through the perforated petri dish where the chip was located (Figure 1).

106 Once the gas had abandoned the chip, it was conducted through a tube to a proportional valve that
107 opened and closed at 0.2 Hz frequency (mimicking the human physiological breathing rate). When
108 the valve became closed, the flexible PDMS membrane deflected until reaching a surface strain of up
109 to 10%. The pressure inside the system was alleviated by a leakage, that consisted of a small diameter
110 tube (ID = 0.56 mm) (Cole Parmer, Illinois, USA) placed between the outlet of the chip and the
111 proportional valve. The length of the leakage tube was individually adjusted for each fabricated chip
112 to obtain the desired strain for a given pressure.

113 To fabricate the devices, negative molds of the parts were designed with the Ultimaker Cura software
114 (Ultimaker, Utrecht, Netherlands) and printed with an Ultimaker S5 3D printer (Ultimaker, Utrecht,
115 Netherlands) in polycarbonate material. PDMS prepolymer was mixed in a proportion 10:1 with the
116 curing agent (Sylgard 184 kit, Dow Corning, MI) and poured into the previously printed molds. The
117 resulting mixture was degassed in a bell jar vacuum desiccator (Kartell Labware, Noviglio, Italy) for
118 45 minutes and then placed in an oven (Selecta, Barcelona, Spain) for 2 hours at 65 °C. PDMS parts
119 were carefully removed from the molds and the middle and the upper parts were perforated in the
120 center with an awl for further introduction of the inlet tube. The middle and lower parts were bonded
121 together concentrically after the activation of their surfaces with a hand-held corona (Electro Technic
122 Products, Chicago, IL) at proximity (~5mm) for one minute at the highest voltage. PDMS membrane
123 was also treated with the corona and attached to the already formed gas chamber, as previously

ARDS-on-a-chip

124 indicated. The upper part (culture chamber) was attached to the PDMS membrane surface by using
125 non-polymerized PDMS and then placed in the oven for 60 minutes at 65°C. In the meantime, a 60
126 cm² petri dish (Techno Plastic Products AG, Trasadingen, Switzerland) was perforated in the center
127 with a driller (1 cm diameter). The PDMS chip was then placed on the perforated petri dish and
128 adhered by using non-polymerized PDMS. A 1.06 mm (ID) inlet tube (Cole Parmer, Illinois, USA)
129 was inserted in the central hole and sealed with non-polymerized PDMS. The whole assembled chip
130 was placed in the oven for 60 minutes at 65°C. Lastly a polycarbonate 3D-printed funnel-like piece
131 was attached with glue to the lower part of the petri dish to connect the outlet tube.

132 PDMS membranes of the devices fabricated for 3D cell culture were treated for proper adhesion of
133 the hydrogels. Briefly, PDMS membranes were activated by introducing the chips in a plasma
134 cleaner (PDC-002, Harrick Scientific Products Inc., Pleasantville, NY) for 2 minutes at maximum
135 voltage and then introduced in the culture hood under the UV light for 10 minutes to sterilize the
136 surface. APTES 10% was then added for 1 hour and 5mM genipin (Challenge Bio Products Co,
137 Taiwan) for 45 minutes. After each reagent, 3 PBS 1X washes of 5 minutes each were made. Finally,
138 the chip was left to dry overnight.

139 **2.3 Experimental setup and devices calibration and characterization**

140 **2.3.1 Experimental setup**

141 To support the specific gas mixture to the cultured cells, servo-controlled gas blenders (McQ,
142 Virginia, USA) controlled by the Software Gas Mixture Creator (McQ, Virginia, USA) were
143 employed. Previously humidified air went inside the chip through the inlet tube and distributed
144 through the channels to reach the PDMS membranes where the cells were cultured. Then, the gas
145 abandoned the chip through the outlet tube. After removing the humidity of the air, the conducting
146 tube was connected to a valve for stretch amplitude and frequency control by using an incorporated
147 pressure sensor (176PC14HD2, Honeywell, New Jersey, USA).

148 **2.3.2 Measurement of oxygen diffusion through 3D hydrogels**

149 All the measurements were acquired inside a cell incubator, at 100% humidity and 37°C. Prior the
150 measurements, chips were ventilated with 100% N₂ for 30 minutes to displace the existent O₂ in the
151 hydrogel. An optical fiber oxygen sensor (Pyroscience, Aachen, Germany) was calibrated following
152 the manufacturer's instructions and attached to a specifically designed holder that allowed for
153 micrometric-resolution vertical positioning. Measurements were performed with the sensor tip
154 introduced 300 μm in the hydrogel. The gas mixture was changed to room air (20% O₂ and 80% N₂),
155 to measure the oxygen diffusion time through the hydrogel. Measurements were repeated for
156 different distances (100 μm steps) (Colom et al. 2014) and the diffusion time constant τ was
157 calculated.

158 **2.3.3 Membrane and hydrogels strain calibration and characterization**

159 The membrane deformation was calculated by modeling it as a spherical cup shape, where linear
160 strain varies slightly across the membrane but circumferential strain decreases parabolically to zero at
161 the clamped edge (Campillo et al. 2016). The membrane experiences an equibiaxial linear strain (ϵ)
162 that can be calculated as follows: the vertical deflection of the spherical cap (h) was calculated by the
163 difference in height assessed with phase-contrast imaging using a confocal microscope with a
164 motorized 10x objective, while the radius (r) was known from chip design. The strain of the
165 membrane was calibrated for different gas pressures by using equation 1:

166
$$\varepsilon = \frac{2}{3} \left(\frac{h}{r} \right)^2 \quad (1)$$

167 To assess that the stretch of the membrane was transmitted to the cells through the hydrogels, the
 168 latter were coated with 2 μm -diameter fluorescent carboxylated beads (Invitrogen, Oregon, USA).
 169 Epifluorescence images were taken at different pressures with the 10x objective, and the
 170 displacement of the beads was computed by ImageJ as described in (Campillo *et al.* 2016).

171 **2.4 Cells isolation and culture protocols**

172 Primary lung mesenchymal stromal cells (LMSCs) and type 2 alveolar epithelial cells (ATIIIs) were
 173 isolated from ~180-250 g male Sprague-Dawley rats by following protocols described in (da Silva
 174 Meirelles, Chagastelles, and Nardi 2006) and (Guillamat-Prats *et al.* 2020) respectively, which were
 175 approved by the Ethical Committee for Animal Research of the University of Barcelona.

176 For LMSCs extraction, rats were anesthetized with 1g/kg urethane and euthanized by exsanguination
 177 through abdominal aorta excision. Lungs were perfused with 50 mL of PBS 1X through the right
 178 ventricle of the beating heart after cutting the left atrium. Lungs were excised *en bloc* with the heart.
 179 Lungs were sectioned into small pieces and digested in 10 mL of 250 U / mL collagenase (Gibco,
 180 Massachusetts, USA) solution prepared in DMEM with 10% HEPES for 1 h at 37 °C under agitation.
 181 The resulting solution was filtered by a 250 μm mesh and then centrifuged at 400 g for 10 minutes
 182 (Rotina 380R, Hettich, Tuttlingen, Germany). The obtained pellet was resuspended in red blood cell
 183 lysis buffer (RBC) (BioLegend, San Diego, CA, USA) and was incubated at 4 °C for 7 minutes.
 184 After that time, the reaction was stopped by adding PBS 1x. Finally, cells were centrifuged at 350 g
 185 for 5 minutes and cultured in T-75 flasks for expansion. LMSCs up to passage 7 were used for the
 186 experiments.

187 For ATIIIs extraction, lungs were perfused with saline through the pulmonary artery and were
 188 resected *en bloc*. Five bronchioalveolar lavages were performed with 10 mL of PBS 1X to remove
 189 the alveolar macrophages. Then, the lungs were digested with 50 mL of 0.25% of trypsin through the
 190 airways for 30 minutes. Lungs were cut into small pieces, digested in a 100 units/mL DNase, and
 191 filtered through a 100 μm and a 40 μm mesh. The filtered suspension was centrifuged through a
 192 percoll (GE HealthCare, Illinois, USA) gradient at 500 g for 20 minutes. The band containing the
 193 ATIIIs was recovered and digested by using DNase (20 units / mL). The solution was centrifuged for
 194 15 minutes at 500 g. Then, the pellet was resuspended in DCCM-1 (Biological Industries, Kibbutz
 195 Beit Haemek, Israel) medium and cultured for 1 hour. After that time, the medium containing ATII
 196 non-adherent cells was recovered and centrifuged for 10 minutes at 800 g. Cells were counted,
 197 seeded in the lung-on-a-chip devices and cultured in supplemented DCCM-1 medium (1% penicillin,
 198 streptomycin and amphotericin, 1% glutamine and 10% FBS).

199 **2.5 Acute Respiratory Distress Syndrome-on-a-chip model**

200 For the 3D culture, $3 \cdot 10^5$ cells/mL of LMSC were resuspended in 500 μL of lung ECM pregel before
 201 jellification. Then, hydrogels were formed by placing the chips in the incubator for 20 minutes before
 202 adding 500 μL of supplemented DCCM-1. ATII cells were then cultured at a density of 10^6 cells/well.
 203 All the experiments were performed at physiological oxygen levels (13%).

204 A description of the experimental groups is shown in Figure 3: three groups were cultured in each
 205 device (co-culture of ATIIIs and L-MSCs in 3D hydrogels, ATIIIs cultured on top of hydrogels and
 206 ATII cultured over the membrane). Half of the devices were subjected to cyclic stretch and half of

ARDS-on-a-chip

207 the devices were subjected to an LPS inflammatory hit (L2630 from *Escherichia Coli*, 1 µg / mL).
208 Groups with co-cultures and cyclic stretch are referred to as ‘advanced physiomimetic model’ (AM)
209 while 2D cultures of ATIIIs will be referred to as ‘traditional model’ (TM). Cells were cultured under
210 stretch for a total of 72 hours (static conditions were maintained for the stretch controls groups), and
211 the LPS hit was applied for 16 hours. At the end of the experiment, the supernatants were collected
212 for subsequent analysis. In the experiments involving the effect of an anti-inflammatory drug, 100
213 nM of dexamethasone was added for 32 hours.

214 **2.6 Multiplex ELISA Analysis**

215 ProcartaPlex Multiplex Immunoassays of the collected supernatants were performed according to the
216 manufacturer's instructions (ThermoFisher, Massachusetts, USA) for the following cytokines:
217 macrophage inflammatory protein-2 (MIP-2), interleukins 1-beta, 6, and 10 (IL-1β, IL-6, IL-10),
218 gamma interferon (INF-γ), alpha tumor necrosis factor (TNF-α), and vascular endothelial growth
219 factor (VEGF). Data were acquired with the Magpix (Luminex, Texas, USA) and processed using the
220 ProcartaPlex Analysis App Software (ThermoFisher, Massachusetts, USA).

221 **2.7 Immunohistochemistry**

222 For the immunofluorescence experiments, cells were fixed with 4% paraformaldehyde for 30
223 minutes. Primary antibodies were incubated overnight, and secondary antibodies were incubated for
224 2 hours at 37 °C. Nuclei were stained with Hoechst 33342 (ThermoFisher, Massachusetts, USA). To
225 avoid unspecific binding, especially in the hydrogels, a blocking buffer consisting of 2% BSA
226 (ThermoFisher, Massachusetts, USA) diluted in PBS 1X (Gibco, Massachusetts, USA) was
227 employed for 40 minutes, and after the primary antibody incubation, three washes of 5 minutes under
228 orbital agitation were made. The primary antibodies employed were rabbit anti-EpCAM, and mouse
229 anti-Vimentin, and the secondary antibody were goat anti-rabbit cy5 and goat anti-mouse Alexa
230 Fluor 488. All antibodies were purchased from Abcam (Cambridge, UK). Images were taken with
231 Nikon Confocal Eclipse Ti using a 20X Plan Fluor Multi-immersion objective (0.75 NA). Samples
232 were excited at 488 nm and acquired at 515 nm, for Vimentin images, and excited at 543.5 nm and
233 acquired at 605 nm for EpCAM staining. Nuclear images were obtained at 450 nm when illuminating
234 the sample at 408 nm

235 **2.8 Statistical analysis**

236 Data are expressed as mean ± SE. Statistical analysis was performed with Prism software (GraphPad
237 Software, California, US). Differences in cytokine expression were studied using Student's t-test,
238 except in those cases where they did not follow a normal distribution, where a Mann-Whitney test
239 was performed instead. Normal distribution of the samples was calculated by using a Kolmogorov-
240 Smirnov test. Differences were considered significant for p-values < 0.05.

241 **3 Results**

242 **3.1 Lung-on-a-chip device characterization**

243 Three-dimensional images of the ATIIIs monolayer on top of the ECM hydrogels with LMSCs
244 cultured inside (Advanced model if stretched) are shown in Figure 4A. The efficient oxygen
245 diffusion through the hydrogel when changing from 0% O₂ to 20% O₂ is shown in Figure 4B, where
246 measurements were taken at different depths inside the hydrogel and compared with those acquired
247 without hydrogel (culture medium) to study whether O₂ was able to diffuse through the whole

248 thickness. Measurements acquired with the fibre optic oxygen sensor showed that the time constant τ
 249 for the non-hydrogel measurement (just diffusion in the PDMS membrane) was ≈ 10 s, being
 250 increased by 40% for 300-200 μm depths and by 80% for 100 μm depth. This indicates that the lung-
 251 derived hydrogels present a coefficient of diffusion for O_2 that is quite similar to that of water,
 252 indicating that these hydrogels are suitable compatible with the three-dimensional culture and the
 253 precise control of oxygen partial pressure (Farré *et al.* 2018). Figure 4C, shows the measured strain
 254 experienced by the PDMS membrane when compared with the actual strain measured at the surface
 255 of the hydrogels calculated by the displacement of the attached fluorescent microbeads. It was
 256 observed that the strain applied to the flexible membrane was transmitted to the attached hydrogel 3D
 257 structures following a linear relationship with the applied pressure.

258 **3.2 Response of the developed advanced physiometric model to the inflammatory hit**

259 The developed advanced model was subjected to an LPS endotoxin hit and the release of
 260 inflammatory mediators was studied. LMSCs were cultured three-dimensionally while ATII were
 261 cultured on the top of the hydrogel forming a monolayer, and cyclic stretch was applied. ELISA
 262 results obtained on the secretion of cytokines for the advanced model developed when LPS endotoxin
 263 was added to the cultures are shown in Figure 5. The inflammatory hit produced a statistically
 264 significant increase in the secretion of inflammation-related cytokines IL-10 (8-fold; $p = 0.003$), IL-6
 265 (2-fold; $p = 0.02$), IL-1 β (10-fold; $p = 0.0081$) and TNF- α (3.5-fold; $p = 0.0023$) while no statistical
 266 difference was found in the secretion of VEGF, MIP-2 α and IFN- γ .

267 Differences in the inflammatory response of the developed advanced model, when compared to the
 268 traditional 2D culture model are shown in Figure 6. Results are expressed as the ratio of the cytokines
 269 secreted with and without LPS within each group (TM or AM) to compare how both models are
 270 responsive. For all the measured cytokines, the response of the advanced model to the inflammatory
 271 hit was lower than in the traditional model; statistically significant differences were found for IL-10
 272 (4-fold-fold; $p = 0.015$), IL-6 (29.5-fold-fold $p = 0.024$), MIP-2 α (2.4-fold $p = 0.0022$), and TNF- α
 273 (6.5-fold-fold; $p = 0.0014$).

274 **3.3 Effects of 3D culture of mesenchymal stromal cells in hydrogels and cyclic stretch**

275 To study the effect of cyclic stretch alone in the physiometric model, four different groups were
 276 compared (with and without CS, each of which with and without LPS). Results in Figure 7 show the
 277 ratio of the amount of cytokines secreted with and without LPS either in the presence or absence of
 278 cyclic stretch. Cyclic stretch showed no impact on the response of the advanced physiometric
 279 model to the inflammatory hit (Figure 7). However, when studying the effect of CS in the absence of
 280 LPS, a statistically significant increase in the secretion of VEGF and a decrease in the secretion of
 281 IFN- γ (2-fold $p = 0.046$; 2-fold/0.55-fold, $p = 0.02$ respectively, data not shown) was observed when
 282 cyclic stretch was applied.

283 The contribution of the lung hydrogel and the embedded LMSCs after application of the LPS hit was
 284 studied in three groups, as shown in Figure 8: (1) ATII on PDMS under cyclic stretch (AM – HG –
 285 LMSCs), (2) ATII on hydrogel under cyclic stretch (AM – LMSCs), and (3) ATII-LMSCs coculture
 286 in hydrogel subjected to cyclic stretch (AM). The effect of hydrogel significantly attenuated the
 287 secretion of all the cytokines but VEGF in response to the LPS endotoxin, showing inflammatory-
 288 suppressive properties. On the other hand, the presence of LMSCs significantly over-attenuated the
 289 secretion of IL-6 (7-fold; $p = 0.0098$) and promoted IFN- γ secretion (1.7-fold $p = 0.032$).

290 **3.4 Response to dexamethasone**

ARDS-on-a-chip

291 Results on the secretion of cytokines when dexamethasone was added to the developed advanced
292 model are shown in Figure 9. The treatment induced a trend to recover the levels of cytokine
293 expression observed before the inflammatory hit in TNF- α and IFN- γ , and a significant decrease of
294 secretion of IL-10 (3.7-fold decrease, $p = 0.0014$) and IL-1 β (3.2-fold decrease $p=0.0407$).

295 4 Discussion

296 Experimental *in vitro* models of severe respiratory diseases such as ARDS are important to better
297 understand the basic pathophysiologic mechanisms involved and the potential effects of drug
298 treatments. However, the conventional model based on cells cultured on a plate is an extreme
299 simplification of the microenvironment experienced by cells *in vivo* and has shown its limitations
300 when trying to mimic *in vivo* results. Therefore, there is nowadays an urgent need for improved
301 models which are more realistic in reproducing the physical, chemical and biological conditions of
302 cells in the lung. The work presented herein shows the feasibility of developing a physiometric
303 model for *in vitro* ARDS studies by the combined use of organ-on-a-chip technologies and ECM-
304 derived hydrogels for 3D cell culture. Specifically, the response of the developed model to an
305 endotoxin-mediated inflammatory hit showed marked differences compared to the traditional plastic-
306 based 2D models, the latter apparently overestimating the cytokine response. In this context, the
307 advanced model (3D architecture with biophysical stimuli) described herein is a novel contribution to
308 setting more physiometric approaches for studying the mechanisms of ARDS and of potential
309 treatments.

310 The developed model overcomes previous limitations of *in vitro* studies on ARDS by recreating a
311 physiometric environment and by using epithelial and stromal cells in co-culture. Device molds
312 were fast prototyped by 3D printing, hence the dimensions of the devices can be easily modified
313 depending on the requirements of each study. The developed chips were compatible with optical
314 microscopy, which eased the calibration of the membrane stretch as a function of the applied
315 pressure. This aspect opens the door for future studies incorporating real-time imaging of the cultured
316 cells in the experiments. We incorporated 3D cultures into the lung-on-a-chip devices developed by
317 attaching cell-laden ECM hydrogels to the PDMS stretchable membrane previously treated with
318 APTES and genipin. No detachment of the hydrogels from the membrane was observed during the
319 experiments. Still, there was an open question for lung-derived ECM hydrogels for organ-on-a-chip
320 devices regarding oxygen diffusivity and stretch transmission from the device to the 3D scaffold
321 (Otero et al. 2021). Oxygen was expected to diffuse quickly in the hydrogels as they are composed
322 mainly of water, and results obtained in the experiments conducted here confirmed that hypothesis.
323 The diffusion of oxygen have been shown to highly impact cell response (E. Marhuenda et al. 2019),
324 thus results obtained in our experiments demonstrate the suitability of their use of three-dimensional
325 culturing. Regarding the transmission of the stretch from the membrane to the hydrogel we observed
326 that it was correctly transmitted to the 3D hydrogel by measuring distances between beads, a method
327 adapted from 2D cultures stretch calibration (Treat et al. 2004). Nevertheless, it should be noted that
328 changing the geometries and the mechanical properties of the hydrogels could modify this stretch
329 transmission, especially if the hydrogels were softer (as they usually are when using lower ECM
330 powder concentrations in their preparation) (Pouliot et al. 2016; de Hilster et al. 2020; Martinez-
331 Garcia et al. 2021). In our case, the results showed that in the developed physiometric model the 3D
332 co-cultures were oxygenated and stretched similarly as in traditional 2D cultures. In this way, the
333 analysis of the contribution of the 3D microarchitecture can be more robustly analyzed from the
334 conducted experiments (Nonaka et al. 2016).

335 The present study was conducted with freshly isolated rat alveolar cells and primary rat lung
336 mesenchymal stromal cells. The use of primary cells is highly advantageous in comparison to
337 previous works where cancer cell lines or immortalized ATIIIs that have lost some of their typical
338 characteristics were employed (X.X. Chen et al. 2019; Abate et al. 2010; Willis et al. 2005). The
339 possibility of using primary ATIIIs was eased by the employment of lung derived hydrogels, which
340 are more suitable substrates for cell culture than culture plates, allowing alveolar cells not only to
341 form monolayers but also to maintain the secretion of surfactant B and C proteins for longer times
342 (Esther Marhuenda et al. 2022), which is of high importance when studying ARDS (S. Wang, Li, et
343 al. 2021). The results obtained using primary alveolar cells are expected to be more easily
344 translational than those using A549 cells (X.X. Chen et al. 2019), which are usually used as a
345 surrogate of ATIIIs in *in vitro* studies. Also, all the experiments shown herein were performed at
346 physiological oxygen concentrations (13%) (Wild et al. 2005; Brahim-Horn and Pouysségur 2007),
347 avoiding that cells were subjected to the typical hyperoxic conditions in traditional culture settings
348 (20% oxygen), which can induce the secretion of oxygen reactive species (Stuart et al. 2018) thereby
349 potentially altering the inflammatory response to LPS challenge and to drug treatment.

350 Results on the inflammatory response of the developed advanced physiologic model to a
351 traditional inflammatory hit (i.e. LPS) modeling ARDS were in line with what has been observed in
352 previous *in vitro* and *in vivo* studies (J.W. Huh et al. 2018; Voiriot et al. 2017; J. Li et al. 2020;
353 Cabrera-Benítez et al. 2016; Peñuelas et al. 2013). As expected, the inflammatory response observed
354 in the developed advanced model was attenuated with respect to the traditional one, indicating that
355 the presence of LMSCs and the incorporation of different biophysical stimuli are playing a protective
356 role in the response to an endotoxin hit. The overresponse observed in traditional models can be then
357 explained by the fact that cells are cultured on petri dishes, which have very different physical
358 properties and biochemical environment than the model developed herein. Interestingly, the fact that
359 our model is less sensitive to the LPS hit could ease the development of future studies with different
360 endotoxin doses with the aim to model different degrees of disease severity.

361 By separately studying the contribution of the different stimuli, very interesting data were obtained
362 regarding the decreased responsiveness to the inflammatory challenge. No significant differences
363 were observed in the secretion of cytokines by the effect of cyclic stretch alone. This could be due to
364 the fact that the impact of cyclic stretch in a physiologic model is moderated and shielded by the
365 rest of the factors present in the advanced model. The anti-inflammatory effect of cyclic stretch has
366 been previously reported (Fang et al. 2018) in a much more responsive model, and this is what was
367 also observed in our control experiments in 2D. It has been also reported to impact cell fate in
368 alveolar and mesenchymal cells (Heise et al. 2011). On the other hand, culturing cells in lung ECM-
369 derived hydrogels was the factor having major importance in the attenuation of the inflammatory
370 response in the developed model. Culturing cells using a substrate with lung parenchyma-like
371 stiffness (Falcones et al. 2021) and a more physiologic and complex biochemical composition
372 seem to offer primary alveolar cells and lung mesenchymal stromal cells a protective environment
373 that attenuated the inflammatory response. On the other hand, the LMSCs played an important role in
374 the inflammatory context, due to the cytokine secretion themselves, but also to the interaction with
375 the epithelial monolayer. As previously reported (X.X. Chen et al. 2019), the presence of LMSCs in
376 the model altered the inflammatory response but, interestingly, the results showed that the effect of
377 lung hydrogel itself has a much greater impact than the presence of LMSCs.

378 The main problem in correlating the cytokine expression from results obtained *in vitro* and *in vivo*, is
379 the fact that most *in vitro* cultures are performed under quite unrealistic conditions, attending to the
380 complex physiological biochemical and biophysical environment and more importantly, to the

381 interactions of different cell types (J. Li et al. 2020; Cabrera-Benítez et al. 2016). The expression of
382 IL-10, IL-8 (its murine counterpart is MIP-2 α), and IL-6 have a high clinical significance in ARDS
383 patients, as high values of these cytokines are clearly related with the severity of the disease. IL-6 has
384 special interest due to the link between its increase and a fatal prognosis, being related to the
385 increased lung compliance, the altered levels of Pao₂/Fio₂, and the need of mechanical ventilation (J.
386 Wang, Yang, et al. 2021; Stukas et al. 2020). Nowadays, the lack of a gold-standard treatment for the
387 ARDS patients is a matter of concern. Glucocorticoids such as dexamethasone are often used to
388 improve ARDS patients' outcomes, but there is still controversy about its benefits in all patients,
389 mainly owing to the heterogeneity in the population receiving the treatment. For example, only
390 severe cases of disease caused by COVID benefited from short-term low-dose treatment (Sterne et al.
391 2020; van Paassen et al. 2020). In addition, it is broadly accepted that MSCs present
392 immunomodulatory properties, and as such, they have been proposed as a therapy for ARDS
393 (Guillamat-Prats et al. 2020; Liu et al. 2020). However, little is known about how the presence of
394 dexamethasone can modify these immunomodulatory properties. Results presented herein, although
395 limited, suggest that the effect of drugs such as dexamethasone should be better studied *in vitro* by
396 using physiomimetic models like the developed in the present work. Studies with dexamethasone-
397 treated epithelial cells in much more responsive 2D models showed a decrease in the
398 proinflammatory cytokines (Y. Chen et al. 2021; Patil et al. 2018), but the results presented in this
399 work are the first ones conducted in a 3D model with a more physiological responsiveness to the LPS
400 hit. Regarding MSCs, results are more controversial: while some *in vitro* studies have shown a
401 decrease in cytokines and chemokines secreted by cytokine-stimulated LMSCs under dexamethasone
402 effects (Wallace et al. 2001; Kim, Cheng, and Kim 1999), *in vivo* studies point that dexamethasone
403 could be abrogating the anti-inflammatory effect of MSC (X. Chen et al. 2014; D. Wang et al. 2018).
404 This impairment of the LMSC anti-inflammatory properties by dexamethasone could explain why in
405 the developed model a drastic decrease in the proinflammatory cytokines was not observed: while
406 dexamethasone was decreasing the secretion of proinflammatory cytokines by epithelial cells, it
407 could be impairing the anti-inflammatory properties of LMSCs. Therefore, the levels of cytokines
408 measured in the advanced model may be the result of a balance, showing a scenario much more
409 similar to what is occurring *in vivo*, which was the major aim of the developed physiomimetic model
410 for ARDS. The results obtained here were more aligned with some *in vivo* studies performed in rats,
411 where LPS showed an increase in the cytokine expression while the treatment with dexamethasone
412 decreased these levels, but not completely recovering the levels prior the LPS hit (Qin and Qiu 2019;
413 L. Li, Whiteman, and Moore 2009).

414 In conclusion, this work suggests that the developed physiomimetic model of ARDS-on-a-chip
415 responds to an LPS challenge and partially recovers the secretion of cytokines after anti-
416 inflammatory drug treatment. Thus, this novel model opens the door for further *in vitro* research on
417 the development of different therapeutic strategies for ARDS treatment. Although it is impossible
418 that any *in vitro* model fully mimics the inflammatory process occurring in the lungs during ARDS,
419 the advanced model describes herein is a step forward. The model allows for studying how alveolar
420 epithelial cells respond to an inflammatory stimulus and how the resident lung mesenchymal stromal
421 cells can play a role in it. Moreover, it is a versatile model facilitating that different cell types could
422 be included to further studying crosstalk mechanisms among the different players involved in the
423 inflammatory process of ARDS. Interestingly, the possibilities in tuning the model makes it suitable
424 for expanding its use to study in detail respiratory diseases other than ARDS, including applications
425 in high-throughput drug testing for new treatment developments.

426 5 Conflict of Interest

427 The authors declare that the research was conducted in the absence of any commercial or financial
428 relationships that could be construed as a potential conflict of interest.

429 **6 Author Contributions**

430 Conceptualization, E.M., N.G., R.F. and J.O.; Formal analysis, E.M., A.V., G.W., R.F., N.G., I.A.
431 and J.O.; Funding acquisition, R.F., I.A., N.G. and J.O.; Investigation, E.M., A.V., N.G., I.A. and
432 J.O.; Methodology, E.M., A.V., M.L.N., L.E., N.G., R.F., I.A. and J.O.; Project administration, R.F.,
433 I.A., N.G. and J.O.; Resources, N.G., R.F., I.A. and J.O.; Software, E.M., M.L.N. and N.G.;
434 Supervision, R.F., N.G. and J.O.; Writing of original draft, E.M. and J.O. All authors have read and
435 agreed to the published version of the manuscript.

436 **7 Funding**

437 This research was funded by Spanish Ministry of Science, Innovation and Universities, grants
438 numbers SAF2017-85574-R, DPI2017-83721-P, PID2019-108958RB-I00, and PGC2018-097323-A-
439 I00, and by European Union's Horizon 2020, Marie Skłodowska-Curie, grant 821772.

440 **8 Acknowledgments**

441 The authors wish to thank Mr. Miguel A. Rodríguez from the Unit of Biophysics and Bioengineering
442 for his excellent technical assistance.

443 **9 References**

- 444 Abate, W., A. A. Alghaithy, J. Parton, K. P. Jones, and S. K. Jackson. 2010. "Surfactant lipids
445 regulate LPS-induced interleukin-8 production in A549 lung epithelial cells by inhibiting
446 translocation of TLR4 into lipid raft domains." *J Lipid Res* 51 (2): 334-44.
447 <https://doi.org/10.1194/jlr.M000513>. <https://www.ncbi.nlm.nih.gov/pubmed/19648651>.
- 448 Ballard-Croft, C., D. Wang, L. R. Sumpter, X. Zhou, and J. B. Zwischenberger. 2012. "Large-animal
449 models of acute respiratory distress syndrome." *Ann Thorac Surg* 93 (4): 1331-9.
450 <https://doi.org/10.1016/j.athoracsur.2011.06.107>.
451 <https://www.ncbi.nlm.nih.gov/pubmed/22244649>.
- 452 Bassi, G., M. A. Grimaudo, S. Panseri, and M. Montesi. 2021. "Advanced Multi-Dimensional
453 Cellular Models as Emerging Reality to Reproduce." *Int J Mol Sci* 22 (3).
454 <https://doi.org/10.3390/ijms22031195>. <https://www.ncbi.nlm.nih.gov/pubmed/33530487>.
- 455 Benam, K. H., J. K. Burgess, and A. G. Stewart. 2021. "Editorial: Accelerated Translation Using
456 Microphysiological Organoid and Microfluidic Chip Models." *Front Pharmacol* 12: 827172.
457 <https://doi.org/10.3389/fphar.2021.827172>. <https://www.ncbi.nlm.nih.gov/pubmed/35046832>.
- 458 Brahim-Horn, M. Christiane, and Jacques Pouyssegur. 2007. "Oxygen, a source of life and stress."
459 *FEBS Letters* 581 (19): 3582-3591.
460 <https://doi.org/https://doi.org/10.1016/j.febslet.2007.06.018>.
461 <https://doi.org/10.1016/j.febslet.2007.06.018>.
- 462 Brower, R. G., M. A. Matthay, A. Morris, D. Schoenfeld, B. T. Thompson, A. Wheeler, and Acute
463 Respiratory Distress Syndrome Network. 2000. "Ventilation with lower tidal volumes as
464 compared with traditional tidal volumes for acute lung injury and the acute respiratory
465 distress syndrome." *N Engl J Med* 342 (18): 1301-8.

ARDS-on-a-chip

- 466 <https://doi.org/10.1056/NEJM200005043421801>.
467 <https://www.ncbi.nlm.nih.gov/pubmed/10793162>.
- 468 Burgess, J. K., T. Mauad, G. Tjin, J. C. Karlsson, and G. Westergren-Thorsson. 2016. "The
469 extracellular matrix - the under-recognized element in lung disease?" *J Pathol* 240 (4): 397-
470 409. <https://doi.org/10.1002/path.4808>. <https://www.ncbi.nlm.nih.gov/pubmed/27623753>.
- 471 Busch, S. M., Z. Lorenzana, and A. L. Ryan. 2021. "Implications for Extracellular Matrix
472 Interactions With Human Lung Basal Stem Cells in Lung Development, Disease, and Airway
473 Modeling." *Front Pharmacol* 12: 645858. <https://doi.org/10.3389/fphar.2021.645858>.
474 <https://www.ncbi.nlm.nih.gov/pubmed/34054525>.
- 475 Cabrera-Benítez, N. E., E. Pérez-Roth, Á Ramos-Nuez, I. Sologuren, J. M. Padrón, A. S. Slutsky, and
476 J. Villar. 2016. "Inhibition of endotoxin-induced airway epithelial cell injury by a novel
477 family of pyrrol derivatives." *Lab Invest* 96 (6): 632-40.
478 <https://doi.org/10.1038/labinvest.2016.46>. <https://www.ncbi.nlm.nih.gov/pubmed/26999659>.
- 479 Campillo, N., I. Jorba, L. Schaedel, B. Casals, D. Gozal, R. Farré, I. Almendros, and D. Navajas.
480 2016. "A Novel Chip for Cyclic Stretch and Intermittent Hypoxia Cell Exposures Mimicking
481 Obstructive Sleep Apnea." *Front Physiol* 7: 319. <https://doi.org/10.3389/fphys.2016.00319>.
482 <https://www.ncbi.nlm.nih.gov/pubmed/27524971>.
- 483 Chen, L. D., Z. Y. Zhang, X. J. Wei, Y. Q. Cai, W. Z. Yao, M. H. Wang, Q. F. Huang, and X. B.
484 Zhang. 2020. "Association between cytokine profiles and lung injury in COVID-19
485 pneumonia." *Respir Res* 21 (1): 201. <https://doi.org/10.1186/s12931-020-01465-2>.
486 <https://www.ncbi.nlm.nih.gov/pubmed/32727465>.
- 487 Chen, X., Y. Gan, W. Li, J. Su, Y. Zhang, Y. Huang, A. I. Roberts, Y. Han, J. Li, Y. Wang, and Y.
488 Shi. 2014. "The interaction between mesenchymal stem cells and steroids during
489 inflammation." *Cell Death Dis* 5: e1009. <https://doi.org/10.1038/cddis.2013.537>.
490 <https://www.ncbi.nlm.nih.gov/pubmed/24457953>.
- 491 Chen, X. X., L. Tang, Z. H. Han, W. J. Wang, and J. G. Meng. 2019. "Coculture with bone marrow -
492 derived mesenchymal stem cells attenuates inflammation and apoptosis in lipopolysaccharide
493 -stimulated alveolar epithelial cells via enhanced secretion of keratinocyte growth factor and
494 angiopoietin - 1 modulating the Toll-like receptor-4 signal pathway." *Mol Med Rep* 19 (3):
495 1891-1902. <https://doi.org/10.3892/mmr.2019.9836>.
- 496 Chen, Y., C. Zhang, C. X. Xiao, X. D. Li, Z. L. Hu, S. D. He, X. J. Xiao, and F. Xu. 2021.
497 "Dexamethasone can attenuate the pulmonary inflammatory response via regulation of the
498 lncH19/miR-324-3p cascade." *J Inflamm (Lond)* 18 (1): 1. [https://doi.org/10.1186/s12950-
499 020-00266-0](https://doi.org/10.1186/s12950-020-00266-0). <https://www.ncbi.nlm.nih.gov/pubmed/33413425>.
- 500 Colom, A., R. Galgoczy, I. Almendros, A. Xaubet, R. Farré, and J. Alcaraz. 2014. "Oxygen diffusion
501 and consumption in extracellular matrix gels: implications for designing three-dimensional
502 cultures." *J Biomed Mater Res A* 102 (8): 2776-84. <https://doi.org/10.1002/jbm.a.34946>.
503 <https://www.ncbi.nlm.nih.gov/pubmed/24027235>.
- 504 da Silva Meirelles, L., P. C. Chagastelles, and N. B. Nardi. 2006. "Mesenchymal stem cells reside in
505 virtually all post-natal organs and tissues." *J Cell Sci* 119 (Pt 11): 2204-13.
506 <https://doi.org/10.1242/jcs.02932>. <https://www.ncbi.nlm.nih.gov/pubmed/16684817>.
- 507 de Hilster, R. H. J., P. K. Sharma, M. R. Jonker, E. S. White, E. A. Gercama, M. Roobeek, W.
508 Timens, M. C. Harmsen, M. N. Hylkema, and J. K. Burgess. 2020. "Human lung extracellular

- 509 matrix hydrogels resemble the stiffness and viscoelasticity of native lung tissue." *Am J*
510 *Physiol Lung Cell Mol Physiol* 318 (4): L698-L704.
511 <https://doi.org/10.1152/ajplung.00451.2019>.
512 <https://www.ncbi.nlm.nih.gov/pubmed/32048864>.
- 513 Falcones, B., H. Sanz-Fraile, E. Marhuenda, I. Mendizábal, I. Cabrera-Aguilera, N. Malandain, J. J.
514 Uriarte, I. Almendros, D. Navajas, D. J. Weiss, R. Farré, and J. Otero. 2021. "Bioprintable
515 Lung Extracellular Matrix Hydrogel Scaffolds for 3D Culture of Mesenchymal Stromal
516 Cells." *Polymers (Basel)* 13 (14). <https://doi.org/10.3390/polym13142350>.
517 <https://www.ncbi.nlm.nih.gov/pubmed/34301107>.
- 518 Fang, X. Z., Y. L. Ge, M. Li, T. F. Huang, Z. Yang, and J. Gao. 2018. "Preconditioning of
519 physiological cyclic stretch inhibits the inflammatory response induced by pathologically
520 mechanical stretch in alveolar epithelial cells." *Exp Ther Med* 15 (2): 2172-2176.
521 <https://doi.org/10.3892/etm.2017.5611>. <https://www.ncbi.nlm.nih.gov/pubmed/29434821>.
- 522 Farré, R., I. Almendros, J. M. Montserrat, D. Gozal, and D. Navajas. 2018. "Gas Partial Pressure in
523 Cultured Cells: Patho-Physiological Importance and Methodological Approaches." *Front*
524 *Physiol* 9: 1803. <https://doi.org/10.3389/fphys.2018.01803>.
525 <https://www.ncbi.nlm.nih.gov/pubmed/30618815>.
- 526 Guillamat-Prats, R., M. Camprubí-Rimblas, F. Puig, R. Herrero, N. Tantinyà, A. Serrano-Mollar, and
527 A. Artigas. 2020. "Alveolar Type II Cells or Mesenchymal Stem Cells: Comparison of Two
528 Different Cell Therapies for the Treatment of Acute Lung Injury in Rats." *Cells* 9 (8).
529 <https://doi.org/10.3390/cells9081816>.
- 530 Habanjar, O., M. Diab-Assaf, F. Caldefie-Chezet, and L. Delort. 2021. "3D Cell Culture Systems:
531 Tumor Application, Advantages, and Disadvantages." *Int J Mol Sci* 22 (22).
532 <https://doi.org/10.3390/ijms222212200>. <https://www.ncbi.nlm.nih.gov/pubmed/34830082>.
- 533 Heise, R. L., V. Stober, C. Cheluvvaraju, J. W. Hollingsworth, and S. Garantziotis. 2011. "Mechanical
534 stretch induces epithelial-mesenchymal transition in alveolar epithelia via hyaluronan
535 activation of innate immunity." *J Biol Chem* 286 (20): 17435-44.
536 <https://doi.org/10.1074/jbc.M110.137273>. <https://www.ncbi.nlm.nih.gov/pubmed/21398522>.
- 537 Huh, D., H. J. Kim, J. P. Fraser, D. E. Shea, M. Khan, A. Bahinski, G. A. Hamilton, and D. E.
538 Ingber. 2013. "Microfabrication of human organs-on-chips." *Nat Protoc* 8 (11): 2135-57.
539 <https://doi.org/10.1038/nprot.2013.137>. <https://www.ncbi.nlm.nih.gov/pubmed/24113786>.
- 540 Huh, J. W., W. Y. Kim, Y. Y. Park, C. M. Lim, Y. Koh, M. J. Kim, and S. B. Hong. 2018. "Anti-
541 inflammatory Role of Mesenchymal Stem Cells in an Acute Lung Injury Mouse Model."
542 *Acute Crit Care* 33 (3): 154-161. <https://doi.org/10.4266/acc.2018.00619>.
543 <https://www.ncbi.nlm.nih.gov/pubmed/31723879>.
- 544 Huppert, L. A., and M. A. Matthay. 2017. "Alveolar Fluid Clearance in Pathologically Relevant
545 Conditions." *Front Immunol* 8: 371. <https://doi.org/10.3389/fimmu.2017.00371>.
546 <https://www.ncbi.nlm.nih.gov/pubmed/28439268>.
- 547 Kim, C. H., S. L. Cheng, and G. S. Kim. 1999. "Effects of dexamethasone on proliferation, activity,
548 and cytokine secretion of normal human bone marrow stromal cells: possible mechanisms of
549 glucocorticoid-induced bone loss." *J Endocrinol* 162 (3): 371-9.
550 <https://doi.org/10.1677/joe.0.1620371>. <https://www.ncbi.nlm.nih.gov/pubmed/10467228>.
- 551 Laffey, John G., and Michael A. Matthay. 2017. "Fifty Years of Research in ARDS. Cell-based
552 Therapy for Acute Respiratory Distress Syndrome. Biology and Potential Therapeutic Value."

- 553 *American journal of respiratory and critical care medicine* 196 (3): 266-273.
 554 <https://doi.org/10.1164/rccm.201701-0107CP>. <https://pubmed.ncbi.nlm.nih.gov/28306336>.
 555 <https://www.ncbi.nlm.nih.gov/pmc/articles/PMC5549868/>.
- 556 Li, Jiansheng, Yanqin Qin, Yulong Chen, Peng Zhao, Xuefang Liu, Haoran Dong, Wanchun Zheng,
 557 Suxiang Feng, Xiaoning Mao, and Congcong Li. 2020. "Mechanisms of the
 558 lipopolysaccharide-induced inflammatory response in alveolar epithelial cell/macrophage co-
 559 culture." *Exp Ther Med* 20 (5): 76. <https://doi.org/10.3892/etm.2020.9204>.
 560 <https://doi.org/10.3892/etm.2020.9204>.
- 561 Li, Ling, Matthew Whiteman, and Philip K. Moore. 2009. "Dexamethasone inhibits
 562 lipopolysaccharide-induced hydrogen sulphide biosynthesis in intact cells and in an animal
 563 model of endotoxic shock." *Journal of Cellular and Molecular Medicine* 13 (8b): 2684-2692.
 564 <https://doi.org/https://doi.org/10.1111/j.1582-4934.2008.00610.x>.
 565 <https://doi.org/10.1111/j.1582-4934.2008.00610.x>.
- 566 Liu, S., D. Peng, H. Qiu, K. Yang, Z. Fu, and L. Zou. 2020. "Mesenchymal stem cells as a potential
 567 therapy for COVID-19." *Stem Cell Res Ther* 11 (1): 169. [https://doi.org/10.1186/s13287-020-](https://doi.org/10.1186/s13287-020-01678-8)
 568 [01678-8](https://doi.org/10.1186/s13287-020-01678-8). <https://www.ncbi.nlm.nih.gov/pubmed/32366290>.
- 569 Marhuenda, E., N. Campillo, M. Gabasa, M. A. Martínez-García, F. Campos-Rodríguez, D. Gozal,
 570 D. Navajas, J. Alcaraz, R. Farré, and I. Almendros. 2019. "Effects of Sustained and
 571 Intermittent Hypoxia on Human Lung Cancer Cells." *Am J Respir Cell Mol Biol* 61 (4): 540-
 572 544. <https://doi.org/10.1165/rcmb.2018-0412LE>.
 573 <https://www.ncbi.nlm.nih.gov/pubmed/31573339>.
- 574 Marhuenda, Esther, Alvaro Villarino, Maria L. Narciso, Marta Camprubí-Rimblas, Ramon Farré,
 575 Núria Gavara, Antonio Artigas, Isaac Almendros, and Jorge Otero. 2022. "Lung Extracellular
 576 Matrix Hydrogels Enhance Preservation of Type II Phenotype in Primary Alveolar Epithelial
 577 Cells." *International Journal of Molecular Sciences* 23 (9).
 578 <https://doi.org/10.3390/ijms23094888>.
- 579 Martínez-García, F. D., R. H. J. de Hilster, P. K. Sharma, T. Borghuis, M. N. Hylkema, J. K.
 580 Burgess, and M. C. Harmsen. 2021. "Architecture and Composition Dictate Viscoelastic
 581 Properties of Organ-Derived Extracellular Matrix Hydrogels." *Polymers (Basel)* 13 (18).
 582 <https://doi.org/10.3390/polym13183113>. <https://www.ncbi.nlm.nih.gov/pubmed/34578013>.
- 583 Matthay, M. A., R. L. Zemans, G. A. Zimmerman, Y. M. Arabi, J. R. Beitler, A. Mercat, M.
 584 Herridge, A. G. Randolph, and C. S. Calfee. 2019. "Acute respiratory distress syndrome." *Nat*
 585 *Rev Dis Primers* 5 (1): 18. <https://doi.org/10.1038/s41572-019-0069-0>.
- 586 Mertz, D. R., T. Ahmed, and S. Takayama. 2018. "Engineering cell heterogeneity into organs-on-a-
 587 chip." *Lab Chip* 18 (16): 2378-2395. <https://doi.org/10.1039/c8lc00413g>.
 588 <https://www.ncbi.nlm.nih.gov/pubmed/30040104>.
- 589 Nonaka, P. N., B. Falcones, R. Farre, A. Artigas, I. Almendros, and D. Navajas. 2020. "Biophysically
 590 Preconditioning Mesenchymal Stem Cells Improves Treatment of Ventilator-Induced Lung
 591 Injury." *Arch Bronconeumol (Engl Ed)* 56 (3): 179-181.
 592 <https://doi.org/10.1016/j.arbres.2019.08.014>.
 593 <https://www.ncbi.nlm.nih.gov/pubmed/31748133>.
- 594 Nonaka, P. N., J. J. Uriarte, N. Campillo, E. Melo, D. Navajas, R. Farré, and L. V. Oliveira. 2014.
 595 "Mechanical properties of mouse lungs along organ decellularization by sodium dodecyl

- 596 sulfate." *Respir Physiol Neurobiol* 200: 1-5. <https://doi.org/10.1016/j.resp.2014.04.008>.
597 <https://www.ncbi.nlm.nih.gov/pubmed/24837837>.
- 598 Nonaka, P. N., J. J. Uriarte, N. Campillo, V. R. Oliveira, D. Navajas, and R. Farré. 2016. "Lung
599 bioengineering: physical stimuli and stem/progenitor cell biology interplay towards
600 biofabricating a functional organ." *Respir Res* 17 (1): 161. [https://doi.org/10.1186/s12931-](https://doi.org/10.1186/s12931-016-0477-6)
601 [016-0477-6](https://doi.org/10.1186/s12931-016-0477-6). <https://www.ncbi.nlm.nih.gov/pubmed/27894293>.
- 602 Otero, J., A. Ulldemolins, R. Farré, and I. Almendros. 2021. "Oxygen Biosensors and Control in 3D
603 Physiometric Experimental Models." *Antioxidants (Basel)* 10 (8).
604 <https://doi.org/10.3390/antiox10081165>. <https://www.ncbi.nlm.nih.gov/pubmed/34439413>.
- 605 Pati, F., and D. W. Cho. 2017. "Bioprinting of 3D Tissue Models Using Decellularized Extracellular
606 Matrix Bioink." *Methods Mol Biol* 1612: 381-390. [https://doi.org/10.1007/978-1-4939-7021-](https://doi.org/10.1007/978-1-4939-7021-6_27)
607 [6_27](https://doi.org/10.1007/978-1-4939-7021-6_27). <https://www.ncbi.nlm.nih.gov/pubmed/28634957>.
- 608 Patil, R. H., M. Naveen Kumar, K. M. Kiran Kumar, R. Nagesh, K. Kavya, R. L. Babu, G. T.
609 Ramesh, and S. Chidananda Sharma. 2018. "Dexamethasone inhibits inflammatory response
610 via down regulation of AP-1 transcription factor in human lung epithelial cells." *Gene* 645:
611 85-94. <https://doi.org/10.1016/j.gene.2017.12.024>.
612 <https://www.ncbi.nlm.nih.gov/pubmed/29248584>.
- 613 Peñuelas, O., E. Melo, C. Sánchez, I. Sánchez, K. Quinn, A. Ferruelo, F. Pérez-Vizcaíno, A. Esteban,
614 D. Navajas, N. Nin, J. A. Lorente, and R. Farré. 2013. "Antioxidant effect of human adult
615 adipose-derived stromal stem cells in alveolar epithelial cells undergoing stretch." *Respir*
616 *Physiol Neurobiol* 188 (1): 1-8. <https://doi.org/10.1016/j.resp.2013.04.007>.
617 <https://www.ncbi.nlm.nih.gov/pubmed/23643709>.
- 618 Pouliot, R. A., P. A. Link, N. S. Mikhael, M. B. Schneck, M. S. Valentine, F. J. Kamga Gninzeko, J.
619 A. Herbert, M. Sakagami, and R. L. Heise. 2016. "Development and characterization of a
620 naturally derived lung extracellular matrix hydrogel." *J Biomed Mater Res A* 104 (8): 1922-
621 35. <https://doi.org/10.1002/jbm.a.35726>. <https://www.ncbi.nlm.nih.gov/pubmed/27012815>.
- 622 Qin, Mengting, and Zhongpeng Qiu. 2019. "Changes in TNF- α , IL-6, IL-10 and VEGF in rats with
623 ARDS and the effects of dexamethasone." *Exp Ther Med* 17 (1): 383-387.
624 <https://doi.org/10.3892/etm.2018.6926>. <https://doi.org/10.3892/etm.2018.6926>.
- 625 Staub, N. C. 1981. "Pulmonary edema due to increased microvascular permeability." *Annu Rev Med*
626 32: 291-312. <https://doi.org/10.1146/annurev.me.32.020181.001451>.
627 <https://www.ncbi.nlm.nih.gov/pubmed/7013669>.
- 628 Sterne, J. A. C., S. Murthy, J. V. Diaz, A. S. Slutsky, J. Villar, D. C. Angus, D. Annane, L. C. P.
629 Azevedo, O. Berwanger, A. B. Cavalcanti, P. F. Dequin, B. Du, J. Emberson, D. Fisher, B.
630 Giraudeau, A. C. Gordon, A. Granholm, C. Green, R. Haynes, N. Heming, J. P. T. Higgins, P.
631 Horby, P. Jüni, M. J. Landray, A. Le Gouge, M. Leclerc, W. S. Lim, F. R. Machado, C.
632 McArthur, F. Meziani, M. H. Møller, A. Perner, M. W. Petersen, J. Savovic, B. Tomazini, V.
633 C. Veiga, S. Webb, J. C. Marshall, and WHO Rapid Evidence Appraisal for COVID-19
634 Therapies (REACT) Working Group. 2020. "Association Between Administration of
635 Systemic Corticosteroids and Mortality Among Critically Ill Patients With COVID-19: A
636 Meta-analysis." *JAMA* 324 (13): 1330-1341. <https://doi.org/10.1001/jama.2020.17023>.
637 <https://www.ncbi.nlm.nih.gov/pubmed/32876694>.
- 638 Stuart, J. A., J. Fonseca, F. Moradi, C. Cunningham, B. Seliman, C. R. Worsfold, S. Dolan, J.
639 Abando, and L. A. Maddalena. 2018. "How Supraphysiological Oxygen Levels in Standard

ARDS-on-a-chip

- 640 Cell Culture Affect Oxygen-Consuming Reactions." *Oxid Med Cell Longev* 2018: 8238459.
641 <https://doi.org/10.1155/2018/8238459>. <https://www.ncbi.nlm.nih.gov/pubmed/30363917>.
- 642 Stukas, S., R. L. Hoiland, J. Cooper, S. Thiara, D. E. Griesdale, A. D. Thomas, M. M. Orde, J. C.
643 English, L. Y. C. Chen, D. Foster, A. R. Mitra, K. Romano, D. D. Sweet, J. J. Ronco, H. D.
644 Kanji, Y. R. Chen, S. L. Wong, C. L. Wellington, and M. S. Sekhon. 2020. "The Association
645 of Inflammatory Cytokines in the Pulmonary Pathophysiology of Respiratory Failure in
646 Critically Ill Patients With Coronavirus Disease 2019." *Crit Care Explor* 2 (9): e0203.
647 <https://doi.org/10.1097/CCE.000000000000203>.
648 <https://www.ncbi.nlm.nih.gov/pubmed/33063041>.
- 649 Trepap, X., M. Grabulosa, F. Puig, G. N. Maksym, D. Navajas, and R. Farré. 2004. "Viscoelasticity
650 of human alveolar epithelial cells subjected to stretch." *Am J Physiol Lung Cell Mol Physiol*
651 287 (5): L1025-34. <https://doi.org/10.1152/ajplung.00077.2004>.
652 <https://www.ncbi.nlm.nih.gov/pubmed/15246973>.
- 653 Trivedi, N., A. Verma, and D. Kumar. 2020. "Possible treatment and strategies for COVID-19:
654 review and assessment." *Eur Rev Med Pharmacol Sci* 24 (23): 12593-12608.
655 https://doi.org/10.26355/eurrev_202012_24057.
656 <https://www.ncbi.nlm.nih.gov/pubmed/33336780>.
- 657 van Paassen, J., J. S. Vos, E. M. Hoekstra, K. M. I. Neumann, P. C. Boot, and S. M. Arbus. 2020.
658 "Corticosteroid use in COVID-19 patients: a systematic review and meta-analysis on clinical
659 outcomes." *Crit Care* 24 (1): 696. <https://doi.org/10.1186/s13054-020-03400-9>.
660 <https://www.ncbi.nlm.nih.gov/pubmed/33317589>.
- 661 Voirirot, G., K. Razazi, V. Amsellem, J. Tran Van Nhieu, S. Abid, S. Adnot, A. Mekontso Dessap,
662 and B. Maitre. 2017. "Interleukin-6 displays lung anti-inflammatory properties and exerts
663 protective hemodynamic effects in a double-hit murine acute lung injury." *Respir Res* 18 (1):
664 64. <https://doi.org/10.1186/s12931-017-0553-6>.
665 <https://www.ncbi.nlm.nih.gov/pubmed/28424078>.
- 666 Wallace, S. R., M. M. Oken, K. L. Lunetta, A. Panoskaltis-Mortari, and A. M. Masellis. 2001.
667 "Abnormalities of bone marrow mesenchymal cells in multiple myeloma patients." *Cancer* 91
668 (7): 1219-30. [https://doi.org/10.1002/1097-0142\(20010401\)91:7<1219::aid-
669 cncr1122>3.0.co;2-1](https://doi.org/10.1002/1097-0142(20010401)91:7<1219::aid-cncr1122>3.0.co;2-1). <https://www.ncbi.nlm.nih.gov/pubmed/11283920>.
- 670 Wang, D., Y. Q. Sun, W. X. Gao, X. L. Fan, J. B. Shi, and Q. L. Fu. 2018. "An in Vitro and in Vivo
671 Study of the Effect of Dexamethasone on Immunoinhibitory Function of Induced Pluripotent
672 Stem Cell-Derived Mesenchymal Stem Cells." *Cell Transplant* 27 (9): 1340-1351.
673 <https://doi.org/10.1177/0963689718780194>.
674 <https://www.ncbi.nlm.nih.gov/pubmed/30056763>.
- 675 Wang, J., X. Yang, Y. Li, J. A. Huang, J. Jiang, and N. Su. 2021. "Specific cytokines in the
676 inflammatory cytokine storm of patients with COVID-19-associated acute respiratory distress
677 syndrome and extrapulmonary multiple-organ dysfunction." *Virol J* 18 (1): 117.
678 <https://doi.org/10.1186/s12985-021-01588-y>.
679 <https://www.ncbi.nlm.nih.gov/pubmed/34088317>.
- 680 Wang, S., Z. Li, X. Wang, S. Zhang, P. Gao, and Z. Shi. 2021. "The Role of Pulmonary Surfactants
681 in the Treatment of Acute Respiratory Distress Syndrome in COVID-19." *Front Pharmacol*
682 12: 698905. <https://doi.org/10.3389/fphar.2021.698905>.
683 <https://www.ncbi.nlm.nih.gov/pubmed/34267664>.

- 684 Wild, J. M., S. FICHELE, N. Woodhouse, M. N. Paley, L. Kasuboski, and E. J. van Beek. 2005. "3D
685 volume-localized pO₂ measurement in the human lung with ³He MRI." *Magn Reson Med* 53
686 (5): 1055-64. <https://doi.org/10.1002/mrm.20423>.
687 <https://www.ncbi.nlm.nih.gov/pubmed/15844148>.
- 688 Willis, B. C., J. M. Liebler, K. Luby-Phelps, A. G. Nicholson, E. D. Crandall, R. M. du Bois, and Z.
689 Borok. 2005. "Induction of epithelial-mesenchymal transition in alveolar epithelial cells by
690 transforming growth factor-beta1: potential role in idiopathic pulmonary fibrosis." *Am J*
691 *Pathol* 166 (5): 1321-32. [https://doi.org/10.1016/s0002-9440\(10\)62351-6](https://doi.org/10.1016/s0002-9440(10)62351-6).
692 <https://www.ncbi.nlm.nih.gov/pubmed/15855634>.
- 693 Wu, C., X. Chen, Y. Cai, J. Xia, X. Zhou, S. Xu, H. Huang, L. Zhang, C. Du, Y. Zhang, J. Song, S.
694 Wang, Y. Chao, Z. Yang, J. Xu, D. Chen, W. Xiong, L. Xu, F. Zhou, J. Jiang, C. Bai, J.
695 Zheng, and Y. Song. 2020. "Risk Factors Associated With Acute Respiratory Distress
696 Syndrome and Death in Patients With Coronavirus Disease 2019 Pneumonia in Wuhan,
697 China." *JAMA Intern Med* 180 (7): 934-943.
698 <https://doi.org/10.1001/jamainternmed.2020.0994>.
699 <https://www.ncbi.nlm.nih.gov/pubmed/32167524>.
- 700 Yadav, H., B. T. Thompson, and O. Gajic. 2017. "Fifty Years of Research in ARDS. Is Acute
701 Respiratory Distress Syndrome a Preventable Disease?" *Am J Respir Crit Care Med* 195 (6):
702 725-736. <https://doi.org/10.1164/rccm.201609-1767CI>.
703 <https://www.ncbi.nlm.nih.gov/pubmed/28040987>.
- 704

Figure Captions

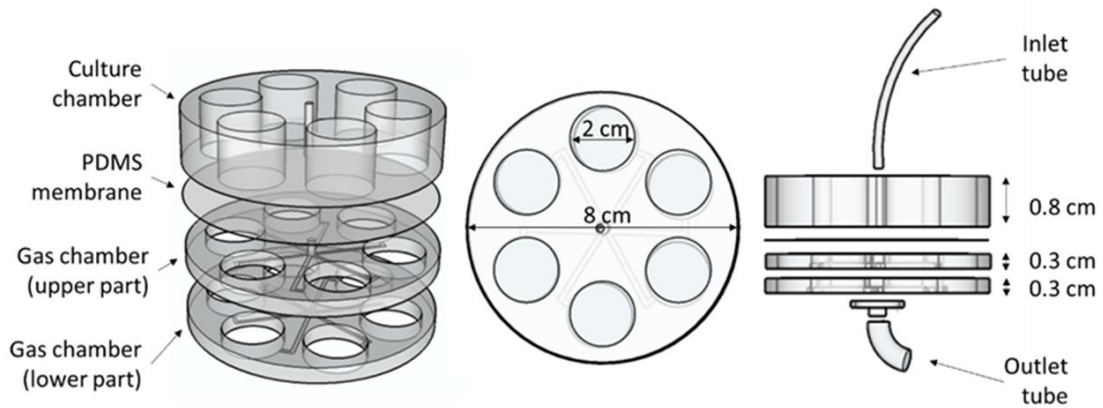


Figure 1. Chip design. Dimensions and different parts of the chip can be observed in this 3D representation. The upper part forming the culture chamber and the two lower parts forming the gas chamber can be easily distinguished, separated by the PDMS membrane.

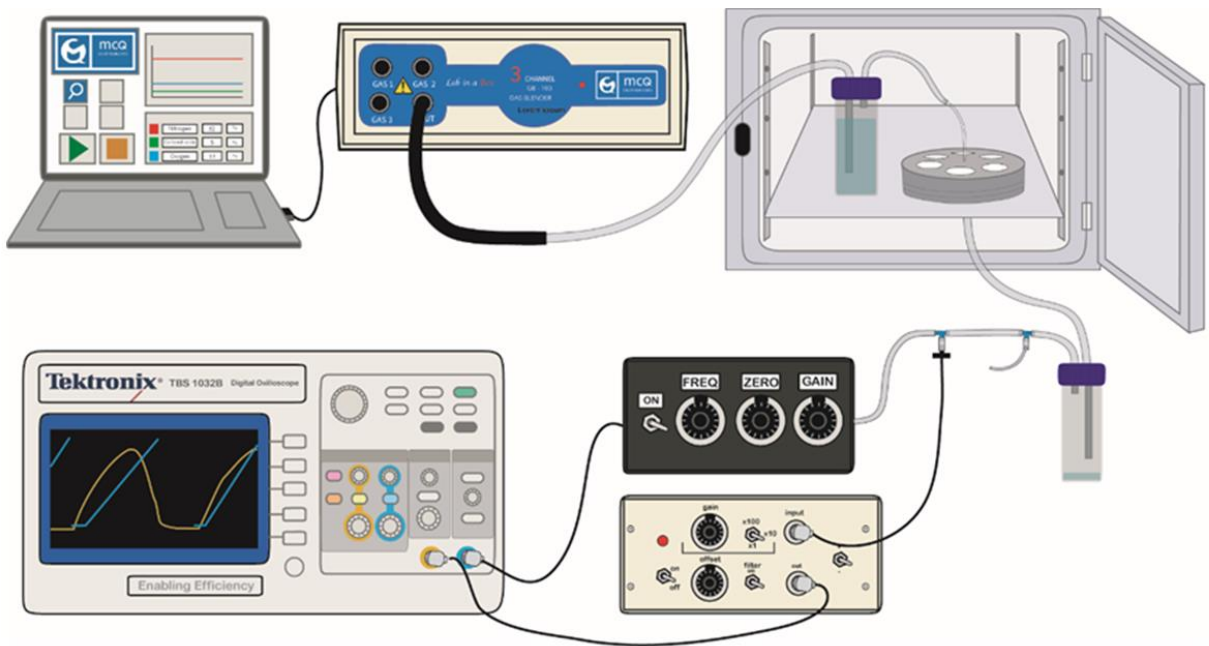


Figure 2. Experimental setup. The drawing shows how the air path from the gas blender, controlled by the software, to the valve, through the chip and the two water traps to initially humidify and finally de-humidify the gas. Cyclic stretch-generating pressure is measured along the experiment with the pressure sensor, the signal transducer and the oscilloscope.

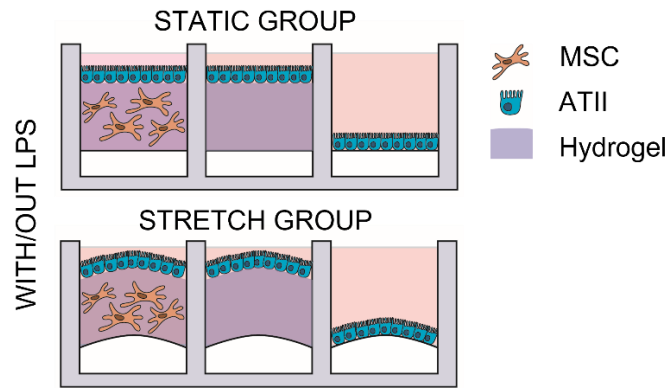


Figure 3. Four different experimental groups were designed. In every chip, three different cultures were performed: ATII-LMSC cocultured with/out 3D-cultured LMSC and an ATII monolayer on the hydrogels; ATII single culture monolayer on the hydrogel; and single culture ATII monolayer on the PDMS membrane. In every run of experiments, four chips were used, each of which was subjected to different conditions: static group, static group with an LPS hit, cyclic stretch group, and cyclic stretch group with an LPS hit.

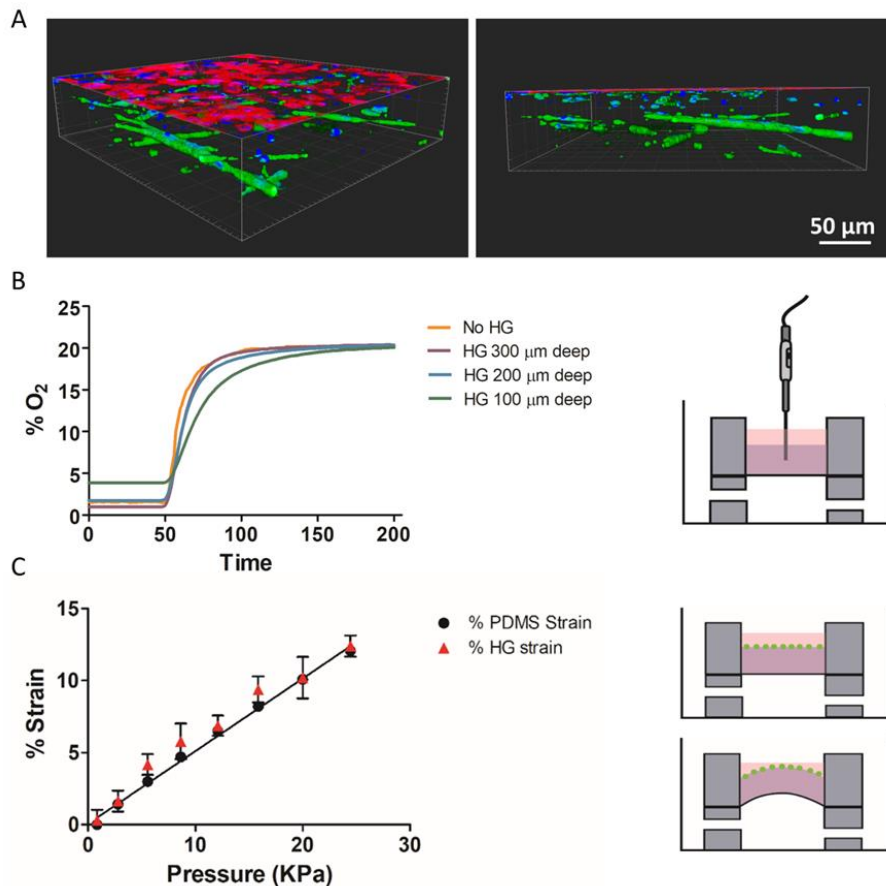


Figure 4. (A) Confocal images of the alveolar monolayer on top of the ECM hydrogels with LMSCs cultured inside. Alveolar cells (red) are stained for EpCAM and MSCs (green) are stained for vimentin (B) Oxygen diffusion measurements at different depths of the hydrogel and liquid medium (No HG). (C) Measured deformation of the membrane and the attached hydrogel at different pressures.

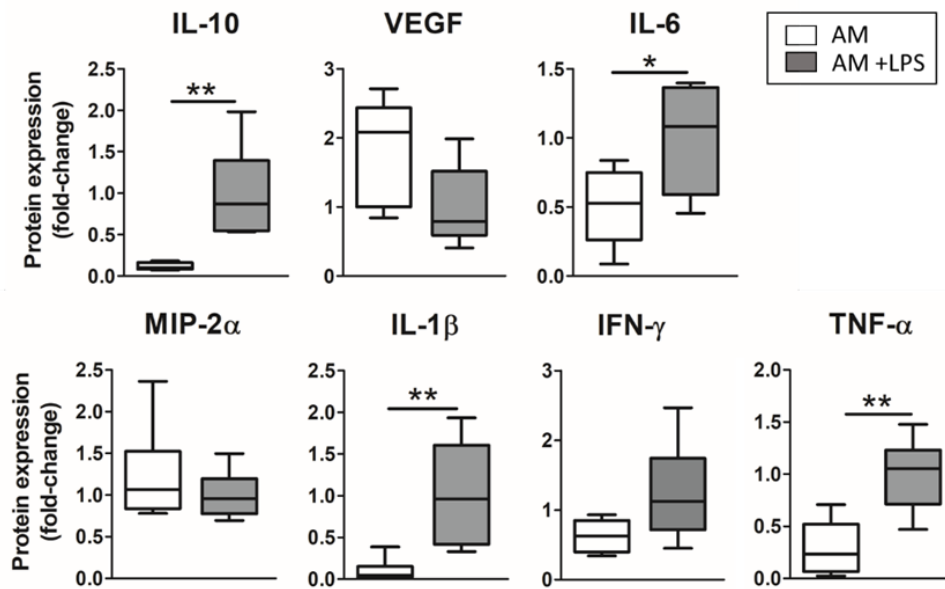


Figure 5. Response to LPS endotoxin of the developed advanced model (3D cultured LMSC in lung hydrogel with ATII cultured on top, subjected to cyclic stretch – Advanced Model).

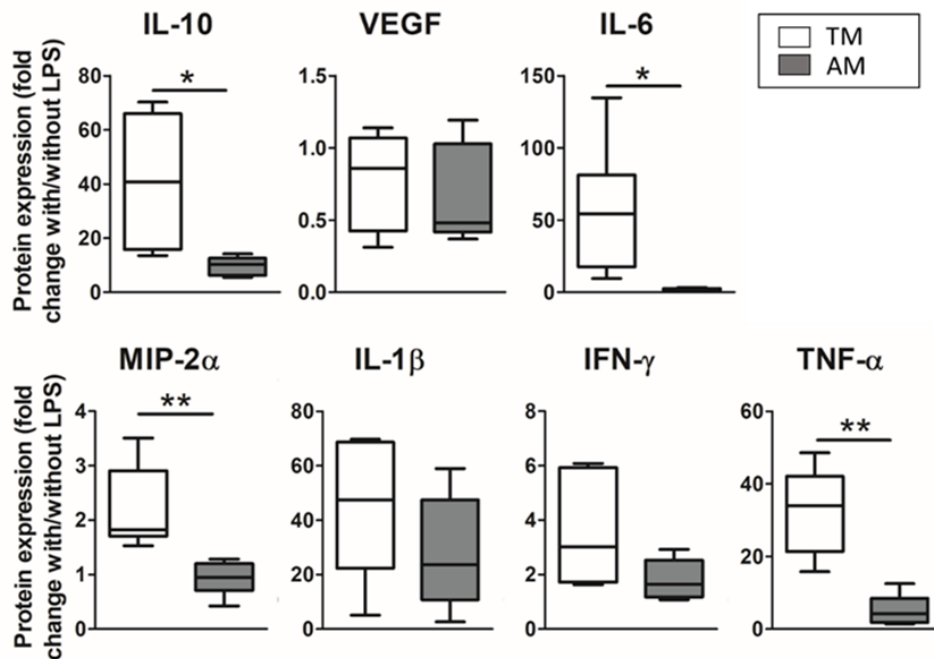


Figure 6. Different magnitude response of the advanced model (ATII cultured on hydrogels with 3D-cultured LMSC inside) compared to a traditional 2D culture model (ATII cell cultured on PDMS). Results were expressed as the ratio of cytokines expressed with/out the LPS hit, for either the traditional model or the advanced model.

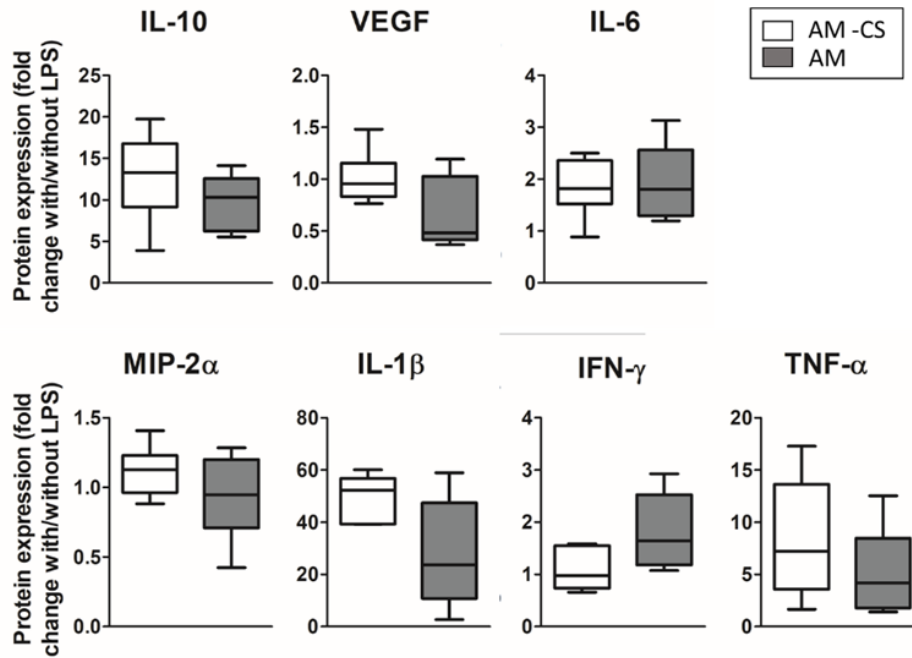


Figure 7. Effect of cyclic stretch. No statistical difference was observed in the secretion of inflammatory cytokines.

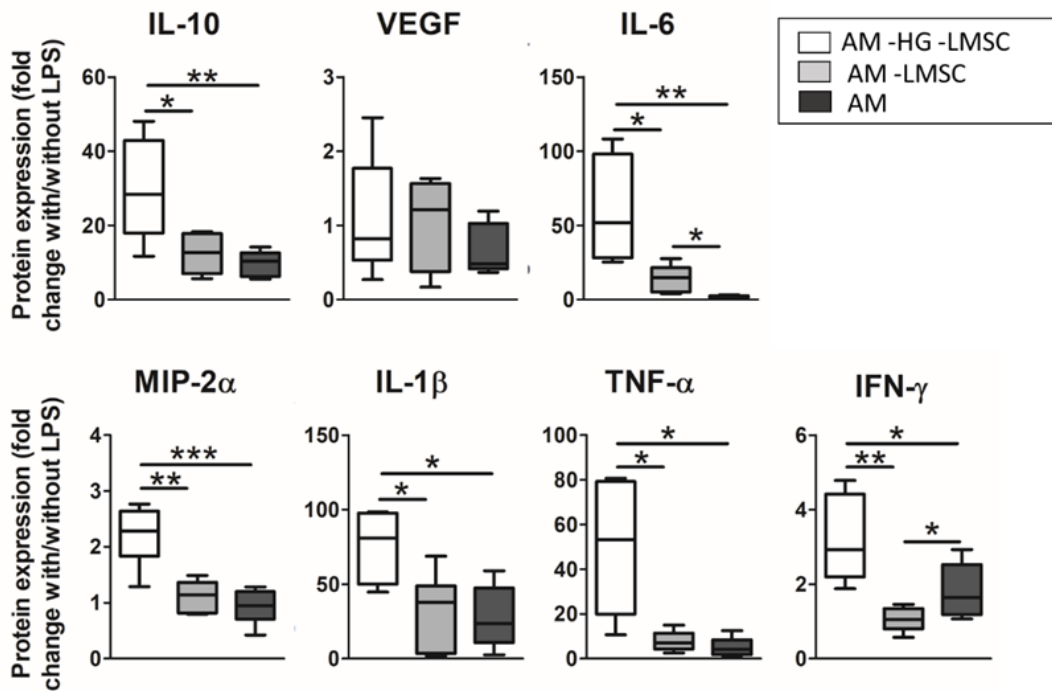


Figure 8. Effect of LMSC and hydrogel on the secretion of cytokines. Three groups were studied: ATII on PDMS with cyclic stretch (AM-HG-LMSC), ATII on hydrogel with cyclic stretch (AM-LMSC), and ATII on hydrogel with 3D LMSC cultured inside in the presence of cyclic stretch (AM).

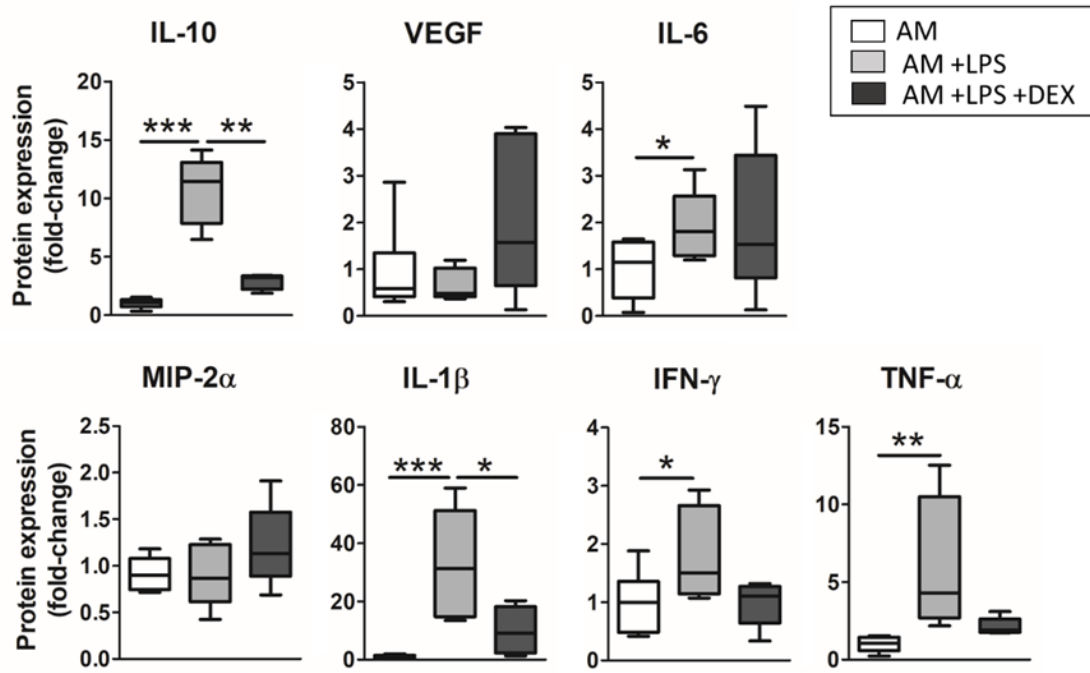


Figure 9. Anti-inflammatory effects of dexamethasone were studied in the advanced model. There was observed a general trend in recovering the expression levels observed before the inflammatory hit, which were statistically significant in the case of IL-10 and IL-1 β .

Chapter VII.
RESULTS SUMMARY

RESULTS SUMMARY

Three different research articles have been included in this thesis. The general goal of them was to study respiratory diseases *in vitro* in an optimized physiometrical way. In the first work of the thesis, cancer cells were cultured on a custom-made PDMS device that allowed us to subject them to different oxygen concentrations, mimicking those present in the lungs of patients with different respiratory diseases like OSA (13% - 7% O₂), COPD (7% O₂), or the OS (7%-4% O₂). The second part was focused on the construction of a physiometrical ARDS *in vitro* model.

The first study showed that response to hypoxia was very heterogeneous among the cell types studied. Results showed that only two cell lines were responsive to hypoxia in terms of proliferation. H1437 increased their proliferation by a ~56% (p=0.005) under sustained hypoxia and by a ~40% (p=0.043) under mild intermittent hypoxia, while H520 increased it by ~66% (p<0.001) and a ~72% (p<0.001) under severe and mild intermittent hypoxia respectively. Similarly, the response in terms of EpCAM expression, which has been related to a worse prognosis in several types of cancer, was heterogeneous. H522 showed increased EpCAM expression under intermittent hypoxia, both under the severe stimuli (~74% p<0.001) and the mild one (by ~47%, p<0.001). The squamous cell line, in contrast, increased its expression under sustained hypoxia (by ~20%, p=0.014) and under severe intermittent hypoxia (by ~20%, p=0.021).

Trying to relate these results with the expression of hypoxia-inducible factor 1 α (HIF-1 α), we performed immunostainings and calculated the ratio of nuclear expression / cytoplasmic expression. Only H1437 and H1975 expressed increased (HIF-1 α) (1.15-fold change p= 0.022 and 2.6-fold change p=0.047, respectively) in the group subjected to severe intermittent hypoxia. Interestingly, H520 do not show any significant increase in (HIF-1 α) due to its constitutive expression.

Although it was not the scope of the study, differences in terms of EpCAM expression and in terms of proliferation when cultured under traditional normoxia (20%) or physioxia (13%) were observed. Specifically, EpCAM was overexpressed (1.6-fold; p = 0.0009) in H522 cells when cultured at 20% O₂ compared to 13% O₂. In the case of H1437, cells showed an increase in proliferation (1.5-fold; p = 0.0187) when cultured under 20% O₂ indicating that the oxygen excess influences the proliferation and the expression of EpCAM in some cell lines.

Before performing the lung-on-a-chip experiment, the hydrogel on the primary alveolar type II cells phenotype was studied. To this end, cells were cultured on lung-derived hydrogels, and typical ATI

and ATII cell markers were studied. Cells cultured on hydrogels showed higher expression of ATII typical markers at 48 hours and at 72 hours according to qPCR studies and immunostainings. Also, confocal images showed that cells presented cuboidal morphology on lung hydrogel whereas its morphology was more flattened when cultured on plate. These results could be indicating that hydrogels provide more long-lasting maintenance of the ATII phenotype than traditional culture methods. Moreover, as the formation of focal adhesions and stress fibers are fundamental to the sensing of the ECM, immunostaining of paxillin and actin showed that cells cultured on lung hydrogel showed less and shorter FAs together with fewer stress fibers, indicating that mechanotransduction processes may be taking place. In keeping with these results, YAP presented lower (~ 0.4 -fold; $p < 0.0001$) nuclear translocation in hydrogel cultures. To investigate the possible link of these results with the Rho pathway, a Rho inhibitor (Y27632) was used. As a result of the inhibition of the Rho pathway, cells cultured on plate increased the synthesis of surfactant protein C (1.16-fold; $p = 0.0258$) together with a decrease in FAs length (0.73-fold; $p = 0.014$), whereas this effect cannot be seen in cells cultured on hydrogel. This could indicate that cells cultured on hydrogel already have the Rho pathway inactivated by the hydrogel. Finally, cells cultured on hydrogel showed the ability to be subcultured from hydrogel to plate, maintaining the ATII markers.

For implementing the ARDS *in vitro* model, primary alveolar type II (ATII) cells and lung mesenchymal stem cells were extracted from rat lungs and cocultured (2D culture for ATII and 3D culture for MSC) on lung-derived hydrogels that were placed on a chip subjected to cyclic stretch (frequency = 0.2 Hz), at 13% O₂. Oxygen was correctly transmitted through the hydrogels as the time constant for the oxygen diffusion increased by $\sim 40\%$ when the oxygen was measured 200-300 μm deep in the hydrogel, and an $\sim 80\%$ at 100 μm deep, showing results very similar to water diffusion. The stretch was also correctly transmitted through the hydrogels as shown by the displacement of fluorescent beads attached to the surface of the hydrogel. An LPS endotoxin hit was added to simulate lung inflammation occurring in several respiratory diseases, such as, for instance, ARDS. Cytokine expression was measured by multiplex ELISA assay. Results showed that LPS produced an increase in IL-10 (8-fold; $p = 0.003$), IL-6 (2-fold; $p = 0.02$), IL-1 β (10-fold; $p = 0.0081$) and TNF- α (3.5-fold; $p = 0.0023$) cytokines. Cyclic stretch did not show any remarkable increase or decrease in the cytokines of our model. When comparing the effect of the cytokines produced by LPS in the physiometric model and in the traditional model (single culture of ATII on culture plate) we observed that the physiometric model showed a lower response to LPS, especially remarkable in IL-10 (4-fold; $p = 0.015$), IL-6 (29.5-fold; $p = 0.024$), MIP-2 α (2.4-fold; $p = 0.0022$), and TNF- α (6.5-

fold; $p = 0.0014$). This effect can be explained by the effect of the hydrogel and the coculture of mesenchymal stem cells, that showed to decrease the secretion of IL-10 (3-fold, $p = 0.007$ and 2.5-fold, $p = 0.017$ compared to hydrogel with and without LMSC, respectively), MIP-2 α (2.4-fold, $p = 0.0004$, and 2-fold, $p = 0.0011$, compared to hydrogel with and without LMSC, respectively), IL-6 (31-fold $p = 0.0098$, and 4.3-fold, $p = 0.031$ compared to hydrogel with and without LMSC, respectively), IFN- γ (1.8-fold, $p = 0.032$, and 3-fold, $p = 0.0031$) compared to hydrogel with and without LMSC, respectively), and TNF- α (10-fold, $p = 0.011$, and 6.5-fold, $p = 0.015$), compared to hydrogel with and without LMSC, respectively). Moreover, the LMSC per se also caused a decrease in the cytokines secretion, which is statistically significant in the case of IL-6, by decreasing 7-fold in the group with the LMSC when compared to the group with hydrogel.

Chapter VIII.
DISCUSSION

In living organisms, cells live and interact with a specific environment, different for each tissue. Cells establish complex crosstalk with the environment which is crucial for their physiological behavior.⁴ In several pathologies, the environment experiences changes which can contribute to the course of the disease. In the specific case of the lung, the environment is formed by proteins which give the organ biophysical properties or elasticity and recoil necessary to perform its function.³ Conventional lung *in vitro* models, which are based on traditional cell culture methods, are highly limited to studying the critical factors that contribute to recreating the lung microenvironment (e.g. oxygen patterns, mechanical stimulation through the cyclic stretch, the interaction of different types of cells within the culture or the presence of a complex scaffold composed by proteins with realistic mechanical properties). Due to these limitations, the results obtained from *in vitro* experiments are very difficult to translate to the *in vivo* behavior of the different respiratory diseases. This is an important issue that is favoring the existent lack of correlation from pre-clinical to clinical trials in the study of several lung pathologies. In this thesis, microenvironmental aspects of the lung cell niche have been reproduced as closely as novel technologies (organ-on-a-chip and extracellular matrix hydrogels) allow, to develop more realistic physiomimetic *in vitro* models to study respiratory diseases.

The first chapter of the thesis explores the effect of different oxygenation patterns in the growth of four different cell lines of lung cancer. Hypoxia is one of the hallmarks of solid tumors and it has implications for resistance to drugs and tumor development as it alters gene expression,^{316,317} produces angiogenesis,³¹⁸ and favors malignant progression through epithelial-mesenchymal transition.^{152,153} Some respiratory pathologies are characterized by lower oxygen availability which has been associated with a higher incidence of lung cancer. Despite this correlation has been widely observed in clinical trials,^{319,150,320,321} it is not clear how different oxygenation patterns derived from these respiratory diseases can modulate cancer malignancy. In the present thesis, four different cancer cell lines representing the two more common histological subtypes were chosen to study if there was a homogeneous response inside each histological subtype or a relationship with the main driver mutations and its response to hypoxia. We employed 13% O₂ as the normoxic (physioxic) group which is much more realistic than the 21% used in previous studies. Different tissues are subjected to different oxygen tensions, being the most highly oxygenated the lungs reaching as much as 13%³²². Therefore, the proliferation of cancer cells and the expression of EpCAM cell marker as a poor prognosis marker was studied in cancer cells subjected to realistic oxygen pressures, representing different pathological conditions.

EpCAM is a cell adhesion protein expressed by most epithelial cells and the corresponding tumor cells. Actually, it is one of the most highly and frequently expressed tumor-associated antigens, and it is found in a wide range of epithelial cancers, including lung cancer.^{323,324,325} EpCAM is involved in adhesion, differentiation and cell proliferation,^{326,327} and its overexpression has been associated to cancer malignancy.^{328,329} The results showed how H520 and H522 experienced an increase in EpCAM expression when subjected to some of the hypoxic stimuli. From these cell lines, only H520 showed an increase in proliferation. This could indicate an absence of a relationship between both factors. However, when paying attention to the absolute data, it can be observed that the cell lines with higher values in EpCAM (H1437, where almost 100% of cells were expressing EpCAM in physioxia, and H520, where ~75% of cells were expressing EpCAM in physioxia) are the most responsive to hypoxia in terms of proliferation.

HIF-1 α is a hypoxia-inducible factor that acts as a transcription factor, and it is involved in the adaptative response to hypoxia. It is ubiquitously expressed in all cell types, and in the presence of oxygen, it is rapidly hydroxylated and degraded. In the absence of oxygen, it is translocated to the nuclei where it acts activating hundreds of target genes.³³⁰ Its response usually confers to the cell survival advantages in hypoxic environments, as HIFs are related to tumor progression, invasion, angiogenesis, metastasis, and resistance to therapy.^{152,153,154} However, its expression has also been related to decreased proliferation.³³¹⁻³³³ Our results showed that HIF-1 α is significantly increased only in the cell group subjected to the most severe intermittent hypoxia, which is the one that reaches the lowest oxygen tensions among all the groups. The cell lines that are affected by this increase are H1437 and H1975. However, H1975 does not show a statistically significant increase in proliferation, while H1437 group subjected to the most severe intermittent hypoxia is the only one that does not show an increase in proliferation. Therefore, our results do not show a link between the higher nuclear activity of HIF-1 α and proliferation rates. Moreover, in the case of the squamous cell line H520, it is observed a high ratio nuclei/cytoplasm in all the groups, indicating a HIF-1 α constitutively active. This is not an isolated case, since it is common to find dysregulated pathways in cancer cells that confers them some survival and adaptative advantages.³³⁴ This increased activity of HIF-1 α in H520 neither can be related to the increase in proliferation of the intermittent hypoxic groups due to the lack of differences in HIF-1 α translocation among the different hypoxic stimuli applied. Attending to the higher proliferation of these cells and H1437 cells under hypoxia, we could think that there can be other mechanisms involved in the increased proliferation as a result of the hypoxia apart from HIF-1 α .

Other *in vitro* studies using hypoxia, however, employed one or two cell lines to extrapolate the observed behavior to the whole histologic subtype.³³⁵ Our results suggest that these kinds of generalizations may not be accurate in attending to the great variability among cancer cell lines, even within a certain histologic subtype. Moreover, most studies compared the hypoxic stimuli with a non-physiologic normoxic group, using 20% oxygen.^{335–337} Such high oxygen values should be considered hyperoxia and can be promoting changes that do not replicate real normoxic processes. However, a limitation of the study is that the cells used were commercially available cell lines. This limits the translation of the results, and also the response to hypoxia is expected to be lower than those cells isolated from heterogeneous tumors can show. Studies are showing that cells isolated from a hypoxic environment had a higher response to hypoxia than those that were subjected to a hypoxic environment directly.³³⁸

Our results showed that the response of lung cancer cells to a hypoxic environment strongly depends on each cell type. In particular, some cell lines seem to be more sensitive to chronic and intermittent hypoxia increasing their proliferation. Furthermore, the expression of EpCAM is upregulated by SH and IH conditions in some types of lung cancer cells. Derived from the present study, it can be extracted that lung cancer cells' behavior is hardly predictable and respond mainly to specific mutations of each cell line. Despite this study did not show a clear correlation between histological subtype and increased lung malignancy as a response to the hypoxic stimuli, more studies should be made in the direction of the individualization of patient treatment, especially in such heterogeneous disease like cancer.

Another key factor in cell behavior is the material where they are cultured. As the physical properties of traditional plastic substrates (usually coated with certain proteins or peptides to facilitate integrin-mediated adhesions) are highly non-physiologic, different natural or synthetic biocompatible scaffolds have been used for the 2D or 3D cultures. These novel scaffolds resembling the mechanics or the biochemical properties of tissues and organs have shown important advantages compared to traditional culture methods.^{287,339,340,341} In the case of primary alveolar cells, this has special relevance as they have the limitation of the rapid transdifferentiation towards a non-proliferative phenotype when cultured *in vitro*.^{342,343} One of the first studies trying to overcome this limitation was performed by Shannon and coworkers,²⁹⁹ who cultured alveolar cells on substrates derived from the basement membrane from the Engelbreth-Holm-Swarm (EHS) tumor. They observed an increased transcription and secretion of surfactant proteins A and B, and a discrete increase in the secretion of surfactant protein C. However, the main limitation of this study was the inability of the cells to form

a monolayer together with a limited proliferation capacity.^{344,345} In the second chapter of the present thesis, the effect of culturing primary alveolar epithelial cells on porcine lung-derived hydrogels³⁴⁶ was studied. The effects of culturing these cells on the scaffolds developed by Falcones and coworkers (including the Ph.D candidate of the present thesis) were similar to those obtained by Shannon: cells maintained the expression of type II phenotype-specific markers (SPC and SPB) for longer times than cells cultured on plates, as shown by qPCR and immunofluorescence staining. There were also differences in type I phenotype-related markers, which were observed to increase in cells cultured on plates, especially as the culture time increased: while the expression of *aqp5* was lost over time in both substrates (although in the hydrogel was lost earlier), *pdpn* was maintained in cells cultured on hydrogels but it increased on cells cultured on a plate, thus indicating a transdifferentiation process towards the type I phenotype. Interestingly, unlike alveolar epithelial cells cultured on EHS hydrogels, cells cultured on lung-derived hydrogel were able to form monolayers, which is a great advance in comparison with the previous studies, mainly because the apical part of the cells won't be oriented towards inside the lumen, but towards the medium, and surfactant proteins can be released easily.³⁴⁴

The mechanisms involved in ATII-to-ATI differentiation remain obscure as it seems that different cellular pathways are implicated in phenotype changes. Previous works have related specific effects to some proteins that compounded the EHS hydrogel. For instance, in studies conducted with hepatocytes, has been reported that type I collagen can promote the stabilization of preexisting mRNA, and proteoglycans and glycosaminoglycans are involved in supporting normal levels of tissue-specific gene transcription^{347,348,349}. This is of special relevance in the developed physiomimetic model in the present thesis due to the composition of the lung ECM-derived hydrogels. Moreover, it is likely that the mechanical properties of these hydrogels also play a fundamental role in cell fate, so ATII phenotype maintenance is due to a combination of diverse factors. Plates coated with proteins that composed EHS hydrogels did not exert the same effect on alveolar cells phenotype as the EHS hydrogels,²⁹⁹ so the composition is not the only factor. On the other hand, the mechanical cues provided by a three-dimensional substrate alone did not provide such benefits, as Matrigel showed improved growth of ATII cells compared to growth factor reduced Matrigel even in presence of keratinocyte growth factor (KGF),³⁵⁰ which is known to impact in the conservation of the type II phenotype.^{351,342} In all these above studies, scientists hypothesized that the preservation of the cuboidal shape of the alveolar cells is essential for them to keep the type II phenotype. The main reason is that shape would be related to the establishment of focal adhesions and the distribution of the cytoskeleton.²⁹⁹ The results presented herein especially support this hypothesis by showing a

decreased formation of stress fibers and the formation of shorter focal adhesions in cells cultured on hydrogels, which could be related to the transmission of the mechanical forces to the cells and could have consequences on the preservation of their cuboidal morphology. Our results also showed that the culture of ATII cells on hydrogels, provided higher ability to keep their surfactant secretion together with the changes in morphology and cytoskeleton. Furthermore, these cells showed a decreased YAP translocation to the nuclei compared to their plate-culture counterparts. Several authors have related the cell geometry, which is also associated the F-actin expression, to the YAP activity: more spread cells present higher F-actin expression and a more active YAP. These authors also observed higher proliferation rates.^{352,353} *In vivo* experiments provided strong evidence that involves YAP in the transdifferentiation process. Situations where lungs are subjected to mechanical stresses and damage where the repopulation of the epithelia is needed such as pneumonectomy^{354,253}, bacterial infection^{355,356} or static stretch^{258,354,253} have shown to promote the ATII to ATI cell differentiation together with an increase the YAP nuclear activation. In our results, YAP showed higher transcriptional activity in the cells cultured on plates, where they also presented more spread morphology and more decreased ATII cell markers and increased ATI markers. This is coincident with the bigger focal adhesions and increased F-actin fibers. Actually, some authors found that the inhibition of F-actin by capping and severing proteins inhibits YAP translocation to the nuclei,^{353,357,352,358} and interestingly, similar results have been obtained through the inhibition of Rho.^{357,352} Conversely, constitutive expression of RhoA of transfected cells, induced not only higher values of YAP and TAZ mRNA expression, but also higher nuclei translocation.³⁵⁹ The link between the expression of SPC and the Rho pathway has been supported by Foster *et al.* They observed *in vitro* a relationship between the increase of stress fibers, which results from the activation of the Rho-GTP/ROCK pathway, and the type II-type I phenotype transdifferentiation.²⁵⁸ To check if the Rho pathway had an impact on the ATII phenotype in our experiments, a Rho inhibitor was used. It has been commonly employed in the literature to study the numerous implications of the Rho pathway.^{253,360,357,258} In our studies, it impacted the length of focal adhesions formed (immunostained by paxillin) and the secretion of SPC as quantified from immunostaining experiments, confirming its involvement in phenotype maintenance. These latter results confirmed previous qualitative immunostaining results and qPCR analysis, showing that surfactant protein C was more highly expressed in cells cultured on hydrogels. The effect of the Rho inhibitor on cells cultured on hydrogels barely presented any effect in terms of SPC expression or focal adhesion length. On the contrary, in cells cultured on plates, results when inhibiting Rho were more similar to ones obtained when cells

were cultured on the hydrogels: there was an increase of SPC expression and a decrease on the length of the focal adhesions formed by the cells. Similar results have been reported *in vivo* and *in vitro* relating the inhibition of the Rho pathway with a decreased ATII to ATI differentiation.^{253,258} Taking all together, our results indicate that the lung-derived hydrogel we employed is a potential better scaffold to culture primary alveolar epithelial cells attending to the increased maintenance of ATII phenotype as shown by its cuboidal morphology and its higher SPC secretion. This improvement in ATII phenotype seems to be orchestrated by the partial inhibition of the Rho pathway the hydrogel is producing in the cells.

How to perform serial subculture of primary alveolar epithelial cells is still an issue that remains to be elucidated. As of today, the most advanced system to subculture these cells was developed by Bove *et al.*³⁴³ consisting in the coculture with feeder cells (fibroblasts, that were likely secreting KGF), in the presence of ROCK inhibitor. However, it was observed an increase of ATI cell markers upon subculturing and the arrest of the proliferation. In contrast, when using lung ECM-derived hydrogels, we observed that cells kept their key markers upon subculture, but as they were cultured on tissue culture plastic they eventually lose their typical markers too. Nevertheless, further investigations are needed to increase the adhesion of the cells on the hydrogels, which is currently the main limitation in terms of subculturing the cells.

ATIIs can respond to infections or injuries and release cytokines and chemokines that recruit leukocytes to the sites of damage and activate these cells to generate an immune response.^{361,362} In the third part of the thesis, we developed a physiometric ARDS model incorporating ATIIs and LMSCs. For doing so, a custom-made PDMS device was fabricated for studying the inflammatory process. An ATII-LMCS coculture was established on lung-derived hydrogels, subjected to cyclic stretch, and to simulate the characteristic inflammation of ARDS, a lipopolysaccharide hit was added to the culture medium. Representative cytokines secreted to the medium were measured with multiplex ELISA.

In the developed physiometric model, 10% of stretch, which is among the physiological ranges (~5% to ~15%)³¹⁰, at 0.2 Hz which is the respiratory frequency³¹⁰ was used to mimic strains caused by breathing. The proposed model showed a lower response in terms of cytokine expression after 24 hours of LPS hit than the traditional model. In more simple and traditional models, cells are cultured on a plate—in our case were cultured on PDMS due to the requirements of the experimental setting—usually, in the absence of cyclic stretch and at a hyperoxic oxygen concentration. Given the

different responses to the inflammatory hit of the two models, a detailed analysis of every factor was made. After 24 hours, no significant effect of cyclic stretch was observed in terms of the expression of cytokines. As the effect caused by the LPS causes such a great increase in cytokine secretion, the effect of cyclic stretch, if any, is completely shielded by the inflammatory hit. It is also important to note that the stretch applied here was within the physiological range, so it is not unexpected that there was not a special contribution in terms of inflammation. Other studies reported an increase in cytokine secretion when higher strains were used.^{74,363} Other authors explored the effect of variable strains in ATII cells and they found out that it was more effective in terms of increasing the SPC than cyclic strain with constant amplitude.⁸¹ Interestingly, varying the amplitude during the cyclic stretch was reported to have an impact also in the inflammatory response by decreasing the release of the proinflammatory cytokines by ATII cells.³⁶⁴ Our results, however, did not show significant differences in terms of cytokines secretion, which confirmed what Huang *et al.* had previously observed in an advanced physiometric *in vitro* model when culturing hAECs under cyclic stretch among the physiological ranges in terms of strain and frequency.³¹⁴

Another factor that could be affecting the ATII phenotype is interaction with LMSC. Several *in vitro* studies using transwells demonstrated that MSCs can exert a paracrine effect on other cells by secreting soluble factors to the medium^{365,366,367,368}. In the context of lung epithelial cells, it has been observed not only the anti-inflammatory effect of MSC,^{369,69} but also the repair of injured cells as shown by the decrease of permeability has been reported.³⁷⁰ MSCs exerted all these effects on the other cells by the secretion of several factors such as cytokines or KGF, which also play a role in the infections by favoring bacterial clearance.³⁷⁰ Moreover, KGF has been used previously to promote the maintenance of ATII phenotype.^{343,371,372} Given the inflammatory nature of ARDS, the study in the third part of the present thesis focused on the effect of LMSC-ATII interaction and its impact on inflammation-related cytokine secretion. In agreement with the literature, we observed a tendency in the decrease of cytokines when LMSC were present. However, the presence in the model of hydrogel acting as another potent anti-inflammatory factor shielded part of these results. Actually, only the secretion of IL-6 cytokine was statistically decreased by the presence of LMSCs. Conversely, the presence of IFN- γ in the medium tended to increase with the presence of LMSCs. Despite of the accepted anti-inflammatory nature of MSC, it has been reported that they can secrete cytokines classically considered as pro-inflammatory as IFN- γ , TNF- α , IL-1 β .³⁷³ The element with greater impact in the decrease of the inflammatory response in the advanced model was the lung-derived hydrogel used as a scaffold for the culture of the cells. It had great relevance in the physiometric cultures

because, as observed, lung-derived hydrogels not only favored the maintenance of the type II phenotype in alveolar epithelial cells, but also prevented the exaggerated response to an inflammatory stimulus observed in conventional 2D models in plates. The main hypothesis here is that hydrogels represent a way of culturing cells much more similar to the physiological environment in terms of biochemical composition and mechanical properties. So, it was expected that cells cultured on lung-derived hydrogels that are exposed to an LPS hit were less susceptible to it than cells that are cultured on a stiff plastic culture plates. This is of especial relevance in primary cells that are subjected to a stressful isolation process such as the ones used in the present works. Furthermore, lung-derived hydrogels are composed mainly by collagens and other structural proteins, glycoproteins and glycosaminoglycans²⁷² but they also contain bioactive peptides resulting from the enzymatic process during the fabrication of the hydrogel, which are known as matrikines.³⁷⁴ They can play an important role in processes like cancer,^{375,376} inflammation,^{377,378} or fibrosis³⁷⁹. Also, growth factors and other small molecules that are expected to be participating in the cell signaling.

ARDS is a serious disease that lacks standardized treatment and the results that are given by the clinical trial regarding the use of corticosteroids are often contradictory.^{380,381} The ARDS model presented in this thesis has several advantages over the 2D single-cell culture model so its use for studying the effect of drugs in the resolution of the disease is promising. For that reason, we used it for studying the effect of dexamethasone, a commonly used anti-inflammatory drug. It was observed that the addition of dexamethasone produced an overall decrease in cytokine secretion, despite it is not significant in all of them. Several *in vivo* studies showed similar results.^{382,383} The anti-inflammatory effect of dexamethasone is widely accepted in the epithelial cells,^{384,385} but controversial results have been obtained when it comes to studying its effects on MSC, as some *in vivo* results showed how the treatment with dexamethasone and cell therapy with MSC as a treatment for ARDS did not have synergistic nor summative effects.^{386,387} It is also important to consider the effect of dexamethasone on cell types other than epithelial, as during lung damage different kinds of pulmonary cells are implicated in the process of repairing and resolving the inflammation. MSCs have an important role in this scenario,^{69,367} thus it is important to study how a given drug affects its immunomodulatory properties. The study presented in this thesis encompassed the global effect of dexamethasone on the epithelial and mesenchymal cells, including the interactions among them.

As most of the traditional culture-based models do not replicate the key biological aspects of the human lungs and do not reflect the responses that cells have *in vivo*, there is a trend of increasing the number of studies performed in more physiomimetic *in vitro* models. However, completely

mimicking the physiological environment is still a challenge. Oxygen level is the most widely wrongly used parameter as the vast majority of the studies are performed under actual hyperoxic conditions (20% O₂). As it has been shown in this thesis, cells cultured under oxygen levels that are usually employed (20 %) show different behavior when compared to realistic normoxic oxygen levels (13 %). In an attempt to include the cell interactions in the results, cocultures have been performed, especially those combining alveolar cells and endothelial cells, in order to represent the alveolo-capillary barrier^{313,304}. Others have represented the interaction between alveoli and parenchymal cells³⁰⁵. Cocultures are interesting to study the inflammatory processes that occur in some respiratory diseases because cell interaction and paracrine signaling are important in inflammatory processes. Usually, the inflammatory hit is assessed with the use of bacteria,^{388,309} LPS,^{313,389} or the addition of pro-inflammatory cytokines^{304,369}. Another commonly represented stimuli that it has been reported to participate in the inflammatory process is a cyclic stretch^{364,74}. Several commercially available cell-stretching devices have been launched to the market,^{390,391} providing a high number of possibilities for studying the different effects of this stimulus on several cell cultures. However, these devices present certain limitations since they are built to work in a specific range of stimulation parameters (waveform, frequency, and amplitude). Besides, they cannot be easily modified to incorporate new parameters, as they do not allow performing compartmentalized cultures for using different cells, nor they do not allow for the oxygen concentration modulation. For that reason, custom-made devices have been developed in the field of respiratory diseases, integrating cyclic stretch and cocultures to study inflammatory processes.^{388,311} Both studies^{388,311} realistically represent the alveolo-capillary barrier but they fail to represent realistic interfaces that can be achieved by the use of hydrogels. From all the studies found in the literature that are performed with the use of hydrogels, we should remark on the one performed by Barkal and coworkers³⁰⁹ where they studied the interaction of three cell types each of which was cultured in the pertinent interface: stromal cells were 3D-cultured within the hydrogel, alveolar cells were cultured in the air-liquid interface, and endothelial cells were submerged. However, this model could be improved by the addition of cyclic stretch and the presence of shear stress in the endothelial culture by circularizing the medium. Other authors employed hydrogels to represent the alveolar environment.^{312,392,307,313} However, none of them obtained the ECM from decellularized organs, meaning that their hydrogels did not represent the biochemical composition of the lung. Moreover, they were only employed as a scaffold to culture cells on, but none of them were used for studying the interactions between stromal cells and epithelial cells.

Most of the previous studies in the field presented the limitation of using commercially-available immortalized cell lines^{309,304} or even A549.^{304,259,306,69,385} Primary alveolar epithelial cells exhibit limited proliferation ability and cannot be expanded by a standard passaging strategy.³⁹³ This aspect together with the costly isolation protocols makes it a great deal for researchers to choose the use of commercially available cells. However, they do not fully represent the features of the cells found *in vivo*. More importantly, most of the current protocols for immortalizing the cells are based on viral vectors, which can cause the induction of proinflammatory responses, so results obtained using immortalized cell lines are not fully trustworthy, especially in the field of the inflammatory diseases³⁹³. Cell lines behave differently from primary cells as shown by studies performed by Wang³⁹⁴, where they found differences in cell morphology and the formation of tight junctions and cilia between immortalized and primary swine tracheal cells. In the specific case of A549, which is usually the surrogate for ATII cells, they present several characteristics that prove the differences between them. They do not express some of the characteristic ATII markers as surfactant proteins C^{395,396} and A,³⁹⁵ phosphatase alkaline activity³⁹⁶ or ALP.^{397,396} They also present altered architecture and barrier properties³⁹⁸ with a decrease in transepithelial resistance.³⁹⁷ Attending to their tumorigenic origin, they also present an altered metabolism, giving different responses than primary cells to stimuli^{393,399}. So even if a model accurately represents environmental factors such as stretch or cell interactions, results are hard to translate to an *in vivo* scenario if they are not obtained with primarily isolated cells. Our experiments tried to be as representative of the real scenario as possible, for that reason, we tried to get rid of confounding factors that could affect the results.

The main limitation of the studies performed in this thesis is the use of cells and ECM derived from animal sources. The next step would be to build the ARDS model with cells coming from human lungs cultured on hydrogels derived from human lungs. This would give more clinically interesting data and could be useful for drug testing. Also, it is interesting to find out if the behavior of human ATII cells is the same as rat ATII cells when cultured on hydrogels in terms of phenotype maintenance. Another future perspective is to improve cell adhesion to the hydrogels for improving the yield of the subculture process. For doing that, two different approaches can be followed: the stiffness can be increased (always among the physiological parameters) by increasing the concentration of the hydrogel or the surface can be added with laminin or other proteins. After these modifications, the preservation of the ATII phenotype should be confirmed. Moreover, more experiments can be done trying to elucidate which is the mechanism through which porcine lung-derived hydrogels favor the preservation of the ATII phenotype.

The presented ARDS model exhibits a complex environment for culturing cells with several stimuli taking place at the same time. For that reason, and given the already studied effect of the hydrogel in the ATII phenotype, it could be interesting to evaluate other factors that could be also playing a part. Variable stretch, as well as the coculture of ATII with fibroblasts, seems to increase the secretion of SPC. Given that evidence, it is worthy to study the effect of the combination of physiological cyclic stretch and the presence of lung-derived hydrogel as well as the possible role of MSC in ATII phenotype maintenance. In the case of the lung cancer study, the technology used in this work could be applied to cells derived from patient biopsies so the behavior of a certain tumor could be predicted and would help the individualized treatment of each patient.

The work presented in this thesis contributes to the increasingly more valued field of physiomimetic modeling, in which pathologies are studied in the most realistic possible manner. These approaches allow a faster and more efficient translation of results from *in vitro* research to the clinical setting.

Chapter IX.
CONCLUSIONS

- I. Lung cancer cells responded in a very heterogeneous way to the hypoxic stimuli independently of the histologic subtype to which they belonged, as evidenced by the culture in a custom-made PDMS chip to perform different oxygenation patterns mimicking respiratory diseases (COPD, OSA, and OS).
 - a. Different oxygenation patterns have different effects on lung cancer cells proliferation: sustained hypoxia increases proliferation in H1437 cells, mild intermittent hypoxia in H1437 and H520, and severe intermittent hypoxia in H520.
 - b. EpCAM expression is also altered under mild intermittent hypoxia in the case of H522, H522, under severe intermittent hypoxia in the case of H520 and H522, and under sustained hypoxia in the case of H520.
 - c. Culturing cells under hyperoxic conditions (20% O₂) can induce altered growth and expression of cell markers in comparison to physioxic conditions (13% O₂).
- II. Lung extracellular matrix-derived hydrogels can be used as scaffold for culturing primary alveolar type II cells under more physiometric conditions.
 - a. Alveolar cells are able to create a monolayer on lung-derived hydrogels.
 - b. Alveolar cells can maintain the phenotype for longer periods of time when cultured on lung-derived hydrogels compared to tissue culture plates shown by the cuboidal shape and the secretion of surfactant protein C.
 - c. Rho pathway seems to be implied in the ATII-to-ATI transdifferentiation process. Hydrogels inhibit the Rho pathway, thus favoring longer maintenance of ATII phenotype.
- III. A novel physiometric *in vitro* model for studying ARDS involving hydrogels, cyclic stretch, cocultures, and an inflammatory hit has been validated.
 - a. The cyclic stretch and the oxygen concentration are correctly transmitted to the 3D cocultures
 - b. The new physiometric model is less responsive to the inflammation than traditional cultures, so it resembles more accurately what happens *in vivo*.
 - c. The use of hydrogels as a scaffold for culturing cells exerts anti-inflammatory properties on the epithelial-mesenchymal coculture
 - d. Lung mesenchymal cells exert a moderate anti-inflammatory role.
 - e. Dexamethasone exerts an anti-inflammatory role in the inflammatory context of the new physiometric model.

Chapter X.
REFERENCES

1. Hedenstierna G, Borges JB, Webb A, et al. Normal physiology of the respiratory system Chapter: Normal physiology of the respiratory system Oxford Textbook of Critical Care (2 ed.) Normal physiology of the respiratory system Key points. 2016. doi:10.1093/med/9780199600830.001.0001
2. Weibel ER. It Takes More than Cells to Make a Good Lung. *Am J Respir Crit Care Med*. 2013;187(4):342-346. doi:10.1164/RCCM.201212-2260OE
3. Burgstaller G, Oehrle B, Gerckens M, White ES, Schiller HB, Eickelberg O. The instructive extracellular matrix of the lung: Basic composition and alterations in chronic lung disease. *Eur Respir J*. 2017;50(1). doi:10.1183/13993003.01805-2016
4. Zhou Y, Horowitz JC, Naba A, et al. Extracellular matrix in lung development, homeostasis and disease. *Matrix Biol*. 2018;73:77-104. doi:10.1016/j.matbio.2018.03.005
5. Wijsman PC, van Smoorenburg LH, de Bruin DM, et al. Imaging the pulmonary extracellular matrix. *Curr Opin Physiol*. 2021;22. doi:10.1016/j.COPHYS.2021.05.007
6. Senior RM, Bielefeld DR, Abensohn MK. The effects of proteolytic enzymes on the tensile strength of human lung. *Am Rev Respir Dis*. 1975;111(2):184-188. doi:10.1164/ARRD.1975.111.2.184
7. Mouw JK, Ou G, Weaver VM. Extracellular matrix assembly: a multiscale deconstruction. *Nat Rev Mol Cell Biol*. 2014;15(12):771-785. doi:10.1038/nrm3902
8. Li B, Alonso DO V, Bennion BJ, Daggett V. Hydrophobic Hydration Is an Important Source of Elasticity in Elastin-Based Biopolymers. 2001. doi:10.1021/ja010363e
9. Ramirez F, Sakai LY, Dietz HC, Rifkin DB. Fibrillin microfibrils: Multipurpose extracellular networks in organismal physiology. *Physiol Genomics*. 2005;19:151-154. doi:10.1152/PHYSIOLGENOMICS.00092.2004/ASSET/IMAGES/LARGE/ZH70300406391002.JPG
10. Arends F, Lieleg O. *Biophysical Properties of the Basal Lamina: A Highly Selective Extracellular Matrix*. (Travascio F, ed.). IntechOpen; 2016. doi:10.5772/62519
11. Souza-Fernandes AB, Pelosi P, Rocco PRM. Bench-to-bedside review: The role of glycosaminoglycans in respiratory disease. *Crit Care*. 2006;10(6):237. doi:10.1186/CC5069
12. Greenlee KJ, Werb Z, Kheradmand F. Matrix Metalloproteinases in Lung: Multiple, Multifarious, and Multifaceted. *Physiol Rev*. 2007;87(1):69-98. doi:10.1152/physrev.00022.2006
13. Bornstein P. Matricellular proteins: An overview. *J Cell Commun Signal*. 2009;3(3-4):163-165. doi:10.1007/s12079-009-0069-z
14. Pohl M, Sakurai H, Bush KT, Nigam SK. Matrix metalloproteinases and their inhibitors regulate in vitro ureteric bud branching morphogenesis. *Am J Physiol - Ren Physiol*. 2000;279(5 48-5). doi:10.1152/AJPRENAL.2000.279.5.F891/ASSET/IMAGES/LARGE/H21100134006.JPG
15. Herrera I, Cisneros J, Maldonado M, et al. Matrix metalloproteinase (MMP)-1 induces lung alveolar epithelial cell migration and proliferation, protects from apoptosis, and represses mitochondrial oxygen consumption. *J Biol Chem*. 2013;288(36):25964-25975. doi:10.1074/JBC.M113.459784

16. Holmbeck K, Bianco P, Caterina J, et al. MT1-MMP-deficient mice develop dwarfism, osteopenia, arthritis, and connective tissue disease due to inadequate collagen turnover. *Cell*. 1999;99(1):81-92. doi:10.1016/S0092-8674(00)80064-1
17. Wysocki AB, Staiano-Coico L, Grinnell F. Wound fluid from chronic leg ulcers contains elevated levels of metalloproteinases MMP-2 and MMP-9. *J Invest Dermatol*. 1993;101(1):64-68. doi:10.1111/1523-1747.EP12359590
18. Hong J-S, Greenlee KJ, Pitchumani R, et al. Dual Protective Mechanisms of Matrix Metalloproteinases 2 and 9 in Immune Defense against *Streptococcus pneumoniae*. *J Immunol*. 2011;186(11):6427-6436. doi:10.4049/JIMMUNOL.1003449
19. Yang Y, Wang K, Gu X, Leong KW. Biophysical Regulation of Cell Behavior—Cross Talk between Substrate Stiffness and Nanotopography. *Engineering*. 2017;3(1):36-54. doi:10.1016/J.ENG.2017.01.014
20. Yang L, Gao Q, Ge L, et al. Topography induced stiffness alteration of stem cells influences osteogenic differentiation. *Biomater Sci*. 2020;8(9):2638-2652. doi:10.1039/D0BM00264J
21. Ge L, Yang L, Bron R, Burgess JK, Rijn P van. Topography-Mediated Fibroblast Cell Migration Is Influenced by Direction, Wavelength, and Amplitude. *ACS Appl Bio Mater*. 2020;3(4):2104-2116. doi:10.1021/ACSABM.0C00001
22. Zhan X. Effect of matrix stiffness and adhesion ligand density on chondrogenic differentiation of mesenchymal stem cells. *J Biomed Mater Res Part A*. 2020;108(3):675-683. doi:10.1002/JBM.A.36847
23. Harrison RG. On the stereotropism of embryonic cells. *Science (80-)*. 1911;34(870):279-281. doi:10.1126/SCIENCE.34.870.279
24. Kaiser JP, Reinmann A, Bruinink A. The effect of topographic characteristics on cell migration velocity. *Biomaterials*. 2006;27(30):5230-5241. doi:10.1016/J.BIOMATERIALS.2006.06.002
25. Biela SA, Su Y, Spatz JP, Kemkemer R. Different sensitivity of human endothelial cells, smooth muscle cells and fibroblasts to topography in the nano–micro range. *Acta Biomater*. 2009;5(7):2460-2466. doi:10.1016/J.ACTBIO.2009.04.003
26. Liangliang Yang, Qi Gao, Lu Ge, et al. Topography induced stiffness alteration of stem cells influences osteogenic differentiation. *Biomater Sci*. 2020;8(9):2638-2652. doi:10.1039/D0BM00264J
27. Yeung T, Georges PC, Flanagan LA, et al. Effects of substrate stiffness on cell morphology, cytoskeletal structure, and adhesion. *Cell Motil Cytoskeleton*. 2005;60(1):24-34. doi:10.1002/cm.20041
28. Fusco S, Panzetta V, Netti PA. Mechanosensing of substrate stiffness regulates focal adhesions dynamics in cell. *Meccanica*. 2017;52(14):3389-3398. doi:10.1007/s11012-017-0676-3
29. Matte BF, Kumar A, Placone JK, et al. Matrix stiffness mechanically conditions EMT and migratory behavior of oral squamous cell carcinoma. *J Cell Sci*. 2019;132(1). doi:10.1242/JCS.224360
30. Yu Y, Ren LJ, Liu XY, Gong XB, Yao W. Effects of substrate stiffness on mast cell migration.

Eur J Cell Biol. 2021;100(7-8):151178. doi:10.1016/J.EJCB.2021.151178

31. Balcioglu HE, Balasubramaniam L, Stirbat TV, et al. A subtle relationship between substrate stiffness and collective migration of cell clusters. *Soft Matter.* 2020;16(7):1825-1839. doi:10.1039/C9SM01893J
32. Rice A, Cortes E, Lachowski D, et al. Matrix stiffness induces epithelial–mesenchymal transition and promotes chemoresistance in pancreatic cancer cells. *Oncog* 2017 67. 2017;6(7):e352-e352. doi:10.1038/oncis.2017.54
33. Li Z, Dranoff JA, Chan EP, Uemura M, Sévigny J, Wells RG. Transforming growth factor- β and substrate stiffness regulate portal fibroblast activation in culture. *Hepatology.* 2007;46(4):1246-1256. doi:10.1002/hep.21792
34. Koo LY, Irvine DJ, Mayes AM, Lauffenburger DA, Griffith LG. Co-regulation of cell adhesion by nanoscale RGD organization and mechanical stimulus. *J Cell Sci.* 2002;115(7):1423-1433. doi:10.1242/JCS.115.7.1423
35. Deeg JA, Louban I, Aydin D, Selhuber-Unkel C, Kessler H, Spatz JP. Impact of Local versus Global Ligand Density on Cellular Adhesion. *Nano Lett.* 2011;11(4):1469. doi:10.1021/NL104079R
36. Stanton AE, Tong X, Lee S, Yang F. Biochemical Ligand Density Regulates Yes-Associated Protein Translocation in Stem Cells through Cytoskeletal Tension and Integrins. *ACS Appl Mater Interfaces.* 2019;11(9):8849-8857. doi:10.1021/ACSAMI.8B21270
37. Kumar S. Cellular mechanotransduction: Stiffness does matter. *Nat Publ Gr.* 2014. doi:10.1038/nmat4094
38. Berger AJ, Linsmeier K, Kreeger PK, Masters KS. Decoupling the effects of stiffness and fiber density on cellular behaviors via an interpenetrating network of gelatin-methacrylate and collagen HHS Public Access. *Biomaterials.* 2017;141:125-135. doi:10.1016/j.biomaterials.2017.06.039
39. Shams H, Soheilypour M, Peyro M, Moussavi-Baygi R, Mofrad MRK. Looking “Under the Hood” of Cellular Mechanotransduction with Computational Tools: A Systems Biomechanics Approach across Multiple Scales. . *ACS Biomater Sci Eng.* 2017;3(11). doi:10.1021/acsbomaterials.7b00117
40. Michael M, Parsons M. New perspectives on integrin-dependent adhesions. *Curr Opin Cell Biol.* 2020;63:31-37. doi:10.1016/J.CEB.2019.12.008
41. Winograd-Katz SE, Fässler R, Geiger B, Legate KR. The integrin adhesome: from genes and proteins to human disease. *Nat Rev Mol Cell Biol* 2014 154. 2014;15(4):273-288. doi:10.1038/NRM3769
42. Kechagia JZ, Ivaska J, Roca-Cusachs P. Integrins as biomechanical sensors of the microenvironment. *Nat Rev Mol Cell Biol* 2019 208. 2019;20(8):457-473. doi:10.1038/S41580-019-0134-2
43. Kiosses WB, Shattil SJ, Pampori N, Schwartz MA. Rac recruits high-affinity integrin $\alpha v \beta 3$ to lamellipodia in endothelial cell migration. *Nat Cell Biol* 2001 33. 2001;3(3):316-320. doi:10.1038/35060120
44. Ballestrem C, Hinz B, Imhof BA, Wehrle-Haller B. Marching at the front and dragging

- behind: differential $\alpha\text{V}\beta\text{3}$ -integrin turnover regulates focal adhesion behavior. *J Cell Biol.* 2001;155(7):1319. doi:10.1083/JCB.200107107
45. Rottner K, Hall A, Small J V. Interplay between Rac and Rho in the control of substrate contact dynamics. *Curr Biol.* 1999;9(12):640-S1. doi:10.1016/S0960-9822(99)80286-3
 46. Chrzanowska-Wodnicka M, Burridge K. Rho-stimulated contractility drives the formation of stress fibers and focal adhesions. *J Cell Biol.* 1996;133(6):1403. doi:10.1083/JCB.133.6.1403
 47. Tan JL, Tien J, Pirone DM, Gray DS, Bhadriraju K, Chen CS. Cells lying on a bed of microneedles: An approach to isolate mechanical force. *Proc Natl Acad Sci.* 2003;100(4):1484-1489. doi:10.1073/PNAS.0235407100
 48. Tojkander S, Gateva G, Lappalainen P. Actin stress fibers - Assembly, dynamics and biological roles. *J Cell Sci.* 2012;125(8):1855-1864. doi:10.1242/JCS.098087/258435/AM/ACTIN-STRESS-FIBERS-ASSEMBLY-DYNAMICS-AND
 49. Khatau SB, Hale CM, Stewart-Hutchinson PJ, et al. A perinuclear actin cap regulates nuclear shape. *Proc Natl Acad Sci.* 2009;106(45):19017-19022. doi:10.1073/PNAS.0908686106
 50. Shiu JY, Aires L, Lin Z, Vogel V. Nanopillar force measurements reveal actin-cap-mediated YAP mechanotransduction. *Nat Cell Biol* 2017 203. 2018;20(3):262-271. doi:10.1038/s41556-017-0030-y
 51. Kim DH, Khatau SB, Feng Y, et al. Actin cap associated focal adhesions and their distinct role in cellular mechanosensing. *Sci Reports* 2012 21. 2012;2(1):1-13. doi:10.1038/srep00555
 52. Totaro A, Panciera T, Piccolo S. YAP/TAZ upstream signals and downstream responses. *Nat Cell Biol.* 2018;20(8):888-899. doi:10.1038/S41556-018-0142-Z
 53. Sun Z, Guo SS, Fässler R. Integrin-mediated mechanotransduction. *J Cell Biol.* 2016;215(4):445-456. doi:10.1083/JCB.201609037
 54. Elozegui-Artola A, Andreu I, Beedle AEM, et al. Force Triggers YAP Nuclear Entry by Regulating Transport across Nuclear Pores. *Cell.* 2017;171(6):1397-1410.e14. doi:10.1016/J.CELL.2017.10.008/ATTACHMENT/0ECE7707-6C47-455E-97E8-DAEC188FAEEC/MMC7.MP4
 55. Bonnans C, Chou J, Werb Z. Remodelling the extracellular matrix in development and disease. *Nat Rev Mol Cell Biol.* 2014;15(12):786. doi:10.1038/NRM3904
 56. Connelly JT, Gautrot JE, Trappmann B, et al. Actin and serum response factor transduce physical cues from the microenvironment to regulate epidermal stem cell fate decisions. *Nat Cell Biol* 2010 127. 2010;12(7):711-718. doi:10.1038/NCB2074
 57. Chiquet M, Gelman L, Lutz R, Maier S. From mechanotransduction to extracellular matrix gene expression in fibroblasts. *Biochim Biophys Acta - Mol Cell Res.* 2009;1793(5):911-920. doi:10.1016/J.BBAMCR.2009.01.012
 58. Bissell MJ, Barcellos-Hoff MH. The influence of extracellular matrix on gene expression: is structure the message? *J Cell Sci Suppl.* 1987;8(SUPPL. 8):327-343. doi:10.1242/JCS.1987.SUPPLEMENT_8.18
 59. Rokicki W, Rokicki M, Wojtacha J, Dželjili A. The role and importance of club cells (Clara

- cells) in the pathogenesis of some respiratory diseases. *Kardiochirurgia i Torakochirurgia Pol = Polish J Cardio-Thoracic Surg.* 2016;13(1):26. doi:10.5114/KITP.2016.58961
60. Whitsett JA, Kalin T V., Xu Y, Kalinichenko V V. Building and Regenerating the Lung Cell by Cell. <https://doi.org/10.1152/physrev000012018>. 2018;99(1):513-554. doi:10.1152/PHYSREV.00001.2018
 61. Basil MC, Katzen J, Engler AE, et al. Cell Stem Cell Review The Cellular and Physiological Basis for Lung Repair and Regeneration: Past, Present, and Future. *Cell Stem Cell.* 2020;26. doi:10.1016/j.stem.2020.03.009
 62. Sinclair K, Yerkovich ST, Chambers DC. Mesenchymal stem cells and the lung. *Respirology.* 2013;18(3):397-411. doi:10.1111/RESP.12050
 63. Li F, He J, Wei J, Cho WC, Liu X. Diversity of epithelial stem cell types in adult lung. *Stem Cells Int.* 2015;2015. doi:10.1155/2015/728307
 64. Schiller HB, Montoro DT, Simon LM, et al. The Human Lung Cell Atlas: A High-Resolution Reference Map of the Human Lung in Health and Disease. *Am J Respir Cell Mol Biol.* 2019;61(1):31-41. doi:10.1165/RCMB.2018-0416TR
 65. Bennet TJ, Randhawa A, Hua J, et al. Airway-On-A-Chip: Designs and Applications for Lung Repair and Disease. *Cells.* 2021;10. doi:10.3390/cells10071602
 66. Zepp JA, Zacharias WJ, Frank DB, et al. Distinct mesenchymal lineages and niches promote epithelial self-renewal and myofibrogenesis in the lung. *Cell.* 2017;170(6):1134. doi:10.1016/j.CELL.2017.07.034
 67. Sabatini F, Petecchia L, Taviani M, De Villeroché VJ, Rossi GA, Brouty-Boyé D. Human bronchial fibroblasts exhibit a mesenchymal stem cell phenotype and multilineage differentiating potentialities. *Lab Invest.* 2005;85(8):962-971. doi:10.1038/LABINVEST.3700300
 68. Dominici M, Le Blanc K, Mueller I, et al. Minimal criteria for defining multipotent mesenchymal stromal cells. The International Society for Cellular Therapy position statement. *Cytotherapy.* 2006;8(4):315-317. doi:10.1080/14653240600855905
 69. Chen XX, Tang L, Han ZH, Wang WJ, Meng JG. Coculture with bone marrow-derived mesenchymal stem cells attenuates inflammation and apoptosis in lipopolysaccharide-stimulated alveolar epithelial cells via enhanced secretion of keratinocyte growth factor and angiopoietin-1 modulating the Toll-like receptor-4 signal pathway. *Mol Med Rep.* 2019;19(3):1891-1902. doi:10.3892/MMR.2019.9836/HTML
 70. Fang X, Abbott J, Cheng L, et al. Human Mesenchymal Stem (Stromal) Cells Promote the Resolution of Acute Lung Injury in Part through Lipoxin A4. *J Immunol.* 2015;195(3):875-881. doi:10.4049/JIMMUNOL.1500244
 71. Karoubi G, Cortes-Dericks L, Breyer I, Schmid RA, Dutly AE. Identification of mesenchymal stromal cells in human lung parenchyma capable of differentiating into aquaporin 5-expressing cells. *Lab Investig 2009 8910.* 2009;89(10):1100-1114. doi:10.1038/labinvest.2009.73
 72. Russo MA, Santarelli DM, O'Rourke D. The physiological effects of slow breathing in the healthy human. *Breathe.* 2017;13(4):298-309. doi:10.1183/20734735.009817

73. Roan E, Waters CM. What do we know about mechanical strain in lung alveoli? *Am J Physiol - Lung Cell Mol Physiol*. 2011;301(5):L625. doi:10.1152/AJPLUNG.00105.2011
74. Thomas RA, Norman JC, Huynh TT, Williams B, Bolton SJ, Wardlaw AJ. Mechanical stretch has contrasting effects on mediator release from bronchial epithelial cells, with a rho-kinase-dependent component to the mechanotransduction pathway ARTICLE IN PRESS. *Respir Med*. 2006;100:1588-1597. doi:10.1016/j.rmed.2005.12.008
75. van Haften EE, Wissing TB, Kurniawan NA, Smits AIPM, Bouten CVC. Human In Vitro Model Mimicking Material-Driven Vascular Regeneration Reveals How Cyclic Stretch and Shear Stress Differentially Modulate Inflammation and Matrix Deposition. *Adv Biosyst*. 2020;4(6):1900249. doi:10.1002/ADBI.201900249
76. Hammerschmidt S, Kuhn H, Gessner C, Seyfarth H-J, Wirtz H. Stretch-Induced Alveolar Type II Cell Apoptosis Role of Endogenous Bradykinin and PI3K-Akt Signaling. *Am J Respir Cell Mol Biol*. 2007;37:699-705. doi:10.1165/rcmb.2006-0429OC
77. Mitsui Y, Koutsogiannaki S, Fujiogi M, Yuki K. In Vitro Model of Stretch-Induced Lung Injury to Study Different Lung Ventilation Regimens and the Role of Sedatives. *Transl Perioper pain Med*. 2020;7(3):258. /pmc/articles/PMC7295159/. Accessed May 10, 2022.
78. Davidovich N, DiPaolo BC, Lawrence GG, Chhour P, Yehya N, Margulies SS. Cyclic stretch-induced oxidative stress increases pulmonary alveolar epithelial permeability. *Am J Respir Cell Mol Biol*. 2013;49(1):156-164. doi:10.1165/RCMB.2012-0252OC/SUPPL_FILE/DISCLOSURES.PDF
79. Zhang B, Luo Q, Chen Z, et al. Cyclic mechanical stretching promotes migration but inhibits invasion of rat bone marrow stromal cells. *Stem Cell Res*. 2015;14(2):155-164. doi:10.1016/j.SCR.2015.01.001
80. Sanchez-Esteban J, Cicchiello LA, Wang Y, et al. Mechanical stretch promotes alveolar epithelial type II cell differentiation. <https://doi.org/10.1152/jappl.2001.91.2.589>. 2001;91(2):589-595. doi:10.1152/JAPPL.2001.91.2.589
81. Arold SP, Bartolák-Suki E, Suki B. Variable stretch pattern enhances surfactant secretion in alveolar type II cells in culture. *Am J Physiol - Lung Cell Mol Physiol*. 2009;296(4):L574. doi:10.1152/AJPLUNG.90454.2008
82. Martinez F, Lewis J, Copland I, et al. Mechanical Ventilation Effect on Surfactant Content, Function, and Lung Compliance in the Newborn Rat. 2004. doi:10.1203/01.PDR.0000128980.82797.29
83. Crowe DL, Ohannessian A. Recruitment of focal adhesion kinase and paxillin to $\beta 1$ integrin promotes cancer cell migration via mitogen activated protein kinase activation. *BMC Cancer*. 2004;4(1):1-8. doi:10.1186/1471-2407-4-18/FIGURES/4
84. Ding Q, Gladson CL, Wu H, Hayasaka H, Olman MA. Focal Adhesion Kinase (FAK)-related Non-kinase Inhibits Myofibroblast Differentiation through Differential MAPK Activation in a FAK-dependent Manner *. *J Biol Chem*. 2008;283(40):26839-26849. doi:10.1074/JBC.M803645200
85. Sun HY, Hu KZ, Yin ZS. Inhibition of the p38-MAPK signaling pathway suppresses the apoptosis and expression of proinflammatory cytokines in human osteoarthritis chondrocytes. *Cytokine*. 2017;90:135-143. doi:10.1016/j.CYTO.2016.11.002

86. Cui Y, Hameed FM, Yang B, et al. Cyclic stretching of soft substrates induces spreading and growth. *Nat Commun* 2015 61. 2015;6(1):1-8. doi:10.1038/ncomms7333
87. Heijink IH, Brandenburg SM, Noordhoek JA, Postma DS, Slebos D-J, Oosterhout AJM van. Characterisation of cell adhesion in airway epithelial cell types using electric cell–substrate impedance sensing. *Eur Respir J*. 2010;35(4):894-903. doi:10.1183/09031936.00065809
88. Bloodgood RA. Sensory reception is an attribute of both primary cilia and motile cilia. *J Cell Sci*. 2010;123(Pt 4):505-509. doi:10.1242/JCS.066308
89. Kishore U, Greenhough TJ, Waters P, et al. Surfactant proteins SP-A and SP-D: Structure, function and receptors. *Mol Immunol*. 2006;43(9):1293-1315. doi:10.1016/J.MOLIMM.2005.08.004
90. Beharka AA, Gaynor CD, Kang BK, Voelker DR, McCormack FX, Schlesinger LS. Pulmonary Surfactant Protein A Up-Regulates Activity of the Mannose Receptor, a Pattern Recognition Receptor Expressed on Human Macrophages. *J Immunol*. 2002;169(7):3565-3573. doi:10.4049/JIMMUNOL.169.7.3565
91. Crouch EC. Surfactant protein-D and pulmonary host defense. *Respir Res*. 2000;1(2):93-108. doi:10.1186/RR19
92. Mariathasan S, Monack DM. Inflammasome adaptors and sensors: intracellular regulators of infection and inflammation. *Nat Rev Immunol* 2007 71. 2007;7(1):31-40. doi:10.1038/NRI1997
93. Ye Z, Ting JPY. NLR, the nucleotide-binding domain leucine-rich repeat containing gene family. *Curr Opin Immunol*. 2008;20(1):3-9. doi:10.1016/J.COI.2008.01.003
94. Medzhitov R. Recognition of microorganisms and activation of the immune response. *Nat* 2007 4497164. 2007;449(7164):819-826. doi:10.1038/NATURE06246
95. Thorley AJ, Grandolfo D, Lim E, Goldstraw P, Young A. Innate Immune Responses to Bacterial Ligands in the Peripheral Human Lung-Role of Alveolar Epithelial TLR Expression and Signalling. *PLoS One*. 2011;6(7):21827. doi:10.1371/journal.pone.0021827
96. Thorley AJ, Ford PA, Giembycz MA, Goldstraw P, Young A, Tetley TD. Differential Regulation of Cytokine Release and Leukocyte Migration by Lipopolysaccharide-Stimulated Primary Human Lung Alveolar Type II Epithelial Cells and Macrophages. *J Immunol*. 2007;178(1):463-473. doi:10.4049/JIMMUNOL.178.1.463
97. Crestani B, Cornillet P, Dehoux M, Rolland C, Guenounou M, Aubier M. Alveolar type II epithelial cells produce interleukin-6 in vitro and in vivo. Regulation by alveolar macrophage secretory products. *J Clin Invest*. 1994;94(2):731. doi:10.1172/JCI117392
98. Hahon N, Castranova V. Interferon Production in Rat Type II Pneumocytes and Alveolar Macrophages. <http://dx.doi.org/10.3109/01902148909087869>. 2009;15(3):429-445. doi:10.3109/01902148909087869
99. Rolfe MW, Kunkel SL, Standiford TJ, et al. Expression and regulation of human pulmonary fibroblast-derived monocyte chemotactic peptide-1. *Am J Physiol - Lung Cell Mol Physiol*. 1992;263(5 7-5). doi:10.1152/AJPLUNG.1992.263.5.L536
100. Khalil N, O'Connor RN, Unruh HW, et al. Increased Production and Immunohistochemical Localization of Transforming Growth Factor- α in Idiopathic Pulmonary Fibrosis.

- <http://dx.doi.org/101165/ajrcmb/52155>. 2012;5(2):155-162. doi:10.1165/AJRCMB/5.2.155
101. Tazi A, Bouchonnet F, Grandsaigne M, Boumsell L, Hance AJ, Soler P. Evidence that granulocyte macrophage-colony-stimulating factor regulates the distribution and differentiated state of dendritic cells/Langerhans cells in human lung and lung cancers. *J Clin Invest*. 1993;91(2):566. doi:10.1172/JCI116236
 102. Jeyaseelan S, Manzer R, Young SK, et al. Induction of CXCL5 During Inflammation in the Rodent Lung Involves Activation of Alveolar Epithelium. <http://dx.doi.org/101165/rcmb2005-0063OC>. 2012;32(6):531-539. doi:10.1165/RCMB.2005-0063OC
 103. Aisiku IP, Yamal J-M, Doshi P, et al. Plasma cytokines IL-6, IL-8, and IL-10 are associated with the development of acute respiratory distress syndrome in patients with severe traumatic brain injury. *Crit Care*. 2016;288(20). doi:10.1186/s13054-016-1470-7
 104. Hiemstra P. Defensins and cathelicidins in inflammatory lung disease: beyond antimicrobial activity. *Biochem Soc Trans*. 2006;34(Pt 2):276-278. doi:10.1042/BST20060276
 105. Doss M, White MR, Teclé T, Hartshorn KL. Human defensins and LL-37 in mucosal immunity. *J Leukoc Biol*. 2010;87(1):79. doi:10.1189/JLB.0609382
 106. Teclé T, Tripathi S, Hartshorn KL. Review: Defensins and cathelicidins in lung immunity: <https://doi.org/101177/1753425910365734>. 2010;16(3):151-159. doi:10.1177/1753425910365734
 107. Smith RE. Chemotactic Cytokines Mediate Leukocyte Recruitment in Fibrotic Lung Disease. *Neurosignals*. 1996;5(4):223-231. doi:10.1159/000109194
 108. Chung KF. Cytokines in chronic obstructive pulmonary disease. *Eur Respir J*. 2001;18(34 suppl):50s-59s. doi:10.1183/09031936.01.00229701
 109. Liu S, Peng D, Qiu H, Yang K, Fu Z, Zou L. Mesenchymal stem cells as a potential therapy for COVID-19. *Stem Cell Res Ther*. 2020;11(1):1-4. doi:10.1186/S13287-020-01678-8/TABLES/1
 110. Huh JW, Kim WY, Park YY, et al. Anti-inflammatory Role of Mesenchymal Stem Cells in an Acute Lung Injury Mouse Model. 2018. doi:10.4266/acc.2018.00619
 111. Katsura H, Kobayashi Y, Tata PR, Hogan BLM. IL-1 and TNF α Contribute to the Inflammatory Niche to Enhance Alveolar Regeneration. *Stem Cell Reports*. 2019;12(4):657. doi:10.1016/J.STEMCR.2019.02.013
 112. Li Z, Mao Z, Lin Y, et al. Dynamic changes of tissue factor pathway inhibitor type 2 associated with IL-1 β and TNF- α in the development of murine acute lung injury. *Thromb Res*. 2008;123(2):361-366. doi:10.1016/J.THROMRES.2008.03.019
 113. Meduri GU, Headley S, Kohler G, et al. Persistent Elevation of Inflammatory Cytokines Predicts a Poor Outcome in ARDS: Plasma IL-1 β and IL-6 Levels Are Consistent and Efficient Predictors of Outcome Over Time. *Chest*. 1995;107(4):1062-1073. doi:10.1378/CHEST.107.4.1062
 114. Smith CA, Farrah T, Goodwin RG. The TNF receptor superfamily of cellular and viral proteins: activation, costimulation, and death. *Cell*. 1994;76(6):959-962. doi:10.1016/0092-8674(94)90372-7

115. Kalliolias GD, Ivashkiv LB. TNF biology, pathogenic mechanisms and emerging therapeutic strategies. *Nat Rev Rheumatol* 2015 121. 2015;12(1):49-62. doi:10.1038/NRRHEUM.2015.169
116. Wang J, Yang X, Li Y, Huang J an, Jiang J, Su N. Specific cytokines in the inflammatory cytokine storm of patients with COVID-19-associated acute respiratory distress syndrome and extrapulmonary multiple-organ dysfunction. *Virology*. 2021;18(1):1-12. doi:10.1186/s12985-021-01588-y
117. Stukas S, Hoiland RL, Cooper J, et al. The Association of Inflammatory Cytokines in the Pulmonary Pathophysiology of Respiratory Failure in Critically Ill Patients With Coronavirus Disease 2019. *Crit Care Explor*. 2020;2(9):e0203. doi:10.1097/cce.0000000000000203
118. Chen L Da, Zhang ZY, Wei XJ, et al. Association between cytokine profiles and lung injury in COVID-19 pneumonia. *Respir Res*. 2020;21(1):1-8. doi:10.1186/s12931-020-01465-2
119. Bernhard S, Hug S, Stratmann AEP, et al. Interleukin 8 Elicits Rapid Physiological Changes in Neutrophils That Are Altered by Inflammatory Conditions. *J Innate Immun*. 2021;13(4):225-241. doi:10.1159/000514885
120. Heidemann J, Ogawa H, Dwinell MB, et al. Angiogenic effects of interleukin 8 (CXCL8) in human intestinal microvascular endothelial cells are mediated by CXCR2. *J Biol Chem*. 2003;278(10):8508-8515. doi:10.1074/JBC.M208231200
121. Fiorentino DF, Zlotnik A, Mosmann TR, Howard M, Moore KW, O'Gara A. IL-10 acts on the antigen-presenting cell to inhibit cytokine production by Th1 cells. *The Journal of Immunology*. <https://www.jimmunol.org/content/146/10/3444>. Published 1991. Accessed May 10, 2022.
122. Mittal SK, Cho KJ, Ishido S, Roche PA. Interleukin 10 (IL-10)-mediated Immunosuppression: MARCH-I INDUCTION REGULATES ANTIGEN PRESENTATION BY MACROPHAGES BUT NOT DENDRITIC CELLS *. *J Biol Chem*. 2015;290(45):27158-27167. doi:10.1074/JBC.M115.682708
123. Abrams J, Figdor CG, De Waal Malefyt R, Bennett B, De Vries JE. Interleukin 10(IL-10) inhibits cytokine synthesis by human monocytes: an autoregulatory role of IL-10 produced by monocytes. *J Exp Med*. 1991;174(5):1209. doi:10.1084/JEM.174.5.1209
124. Park WY, Goodman RB, Steinberg KP, et al. Cytokine Balance in the Lungs of Patients with Acute Respiratory Distress Syndrome. <https://doi.org/10.1164/ajrccm.164.10.2104013>. 2012;164(10 I):1896-1903. doi:10.1164/AJRCCM.164.10.2104013
125. Liu CH, Kuo SW, Ko WJ, et al. Early measurement of IL-10 predicts the outcomes of patients with acute respiratory distress syndrome receiving extracorporeal membrane oxygenation. *Sci Rep*. 2017;7(1). doi:10.1038/S41598-017-01225-1
126. Mock JR, Tune MK, Dial CF, Torres-Castillo J, Hagan RS, Doerschuk CM. Effects of IFN- γ on immune cell kinetics during the resolution of acute lung injury. *Physiol Rep*. 2020;8(3). doi:10.14814/PHY2.14368
127. Arnaud C, Bochaton T, Pépin J-L, Belaidi E, Belaidi E. Obstructive sleep apnoea and cardiovascular consequences: Pathophysiological mechanisms. *Arch Cardiovasc Dis*. 2020;113(5):350-358. doi:10.1016/j.acvd.2020.01.003

128. Lucia Spicuzza DC and GDM. Obstructive sleep apnoea syndrome and its management. *Ther Adv Chronic Dis.* 2015;6(5):273-285. doi:10.1177/2040622315590318
129. Lévy P, Kohler M, McNicholas WT, et al. Obstructive sleep apnoea syndrome. *Nat Rev Dis Prim.* 2015;1(15015). doi:10.1038/nrdp.2015.15
130. Tuomilehto HPI, Seppä JM, Partinen MM, et al. Lifestyle Intervention with Weight Reduction. *Am J Respir Crit Care Med.* 2012;179(4):320-327. doi:10.1164/RCCM.200805-669OC
131. White DP, Shafazand S. Mandibular Advancement Device vs CPAP in the Treatment of Obstructive Sleep Apnea: Are they Equally Effective in Short Term Health Outcomes? *J Clin Sleep Med.* 2013;9(9):971. doi:10.5664/JCSM.3008
132. Patel D, Ash S, Evans J. The role of orthodontics and oral and maxillofacial surgery in the management of obstructive sleep apnoea-a single case report. *Br Dent J.* 2004;196(5):264-267. doi:10.1038/sj.bdj.4811032
133. I, Yu C, Chen R, et al. Obstructive Sleep Apnea: A Pathophysiology and Pharmacotherapy Approach. In: *Intech.* Vol i. ; 2019:13. doi:10.1016/j.colsurfa.2011.12.014
134. Horner RL. Contributions of passive mechanical loads and active neuromuscular compensation to upper airway collapsibility during sleep. *J Appl Physiol.* 2007;102(2):510-512. doi:10.1152/JAPPLPHYSIOL.01213.2006
135. Reale M, Velluto L, Di Nicola M, et al. Cholinergic Markers and Cytokines in OSA Patients. *Int J Mol Sci.* 2020;21(9). doi:10.3390/IJMS21093264
136. Pilkauskaite G, Miliuskas S, Sakalauskas R, et al. Clinical Study Reactive Oxygen Species Production in Peripheral Blood Neutrophils of Obstructive Sleep Apnea Patients. *Sci World J.* 2013;2013. doi:10.1155/2013/421763
137. Varadharaj S, Porter K, Pleister A, et al. Endothelial nitric oxide synthase uncoupling: A novel pathway in OSA induced vascular endothelial dysfunction. *Respir Physiol Neurobiol.* 2015;207:40-47. doi:10.1016/J.RESP.2014.12.012
138. Nair D, Dayyat EA, Zhang SX, Wang Y, Gozal D. Intermittent Hypoxia-Induced Cognitive Deficits Are Mediated by NADPH Oxidase Activity in a Murine Model of Sleep Apnea. *PLoS One.* 2011;6(5):e19847. doi:10.1371/JOURNAL.PONE.0019847
139. Allen AJH, Jen R, Mazzotti DR, et al. Symptom subtypes and risk of incident cardiovascular and cerebrovascular disease in a clinic-based obstructive sleep apnea cohort. *J Clin Sleep Med.* April 2022. doi:10.5664/JCSM.9986
140. Yeghiazarians Y, Jneid H, Tietjens JR, et al. Obstructive sleep apnea and cardiovascular disease a scientific statement from the American Heart Association. *Circulation.* 2021;144:E56-E67. doi:10.1161/CIR.0000000000000988
141. Bonsignore MR, Baiamonte P, Mazzuca E, Castrogiovanni A, Marrone O. Obstructive sleep apnea and comorbidities: a dangerous liaison. *Multidiscip Respir Med.* 2019;14(8). doi:10.1186/s40248-019-0172-9
142. Xu S, Wan Y, Xu M, et al. The association between obstructive sleep apnea and metabolic syndrome: A systematic review and meta-analysis. *BMC Pulm Med.* 2015;15(1):1-12. doi:10.1186/S12890-015-0102-3/FIGURES/5

143. Mesarwi OA, Sharma E V., Jun JC, Polotsky VY. Metabolic dysfunction in obstructive sleep apnea: A critical examination of underlying mechanisms. *Sleep Biol Rhythms*. 2015;13(1):2-17. doi:10.1111/SBR.12078/FULL
144. Cabezas E, Pérez-Warnisher MT, Troncoso MF, et al. Sleep disordered breathing is highly prevalent in patients with lung cancer: Results of the sleep apnea in lung cancer study. *Respiration*. 2019;97(2):119-124. doi:10.1159/000492273
145. Hao S, Zhu X, Liu Z, et al. Chronic intermittent hypoxia promoted lung cancer stem cell-like properties via enhancing Bach1 expression. *Respir Res*. 2021;22(1):1-12. doi:10.1186/S12931-021-01655-6/FIGURES/6
146. Jara SM, Phipps AI, Maynard C, Weaver EM. The Association of Sleep Apnea and Cancer in Veterans. *Otolaryngol - Head Neck Surg (United States)*. 2020;162(4):581-588. doi:10.1177/0194599819900487
147. Kendzerska T, Povitz M, Leung RS, et al. Obstructive Sleep Apnea and Incident Cancer: A Large Retrospective Multicenter Clinical Cohort Study. *Cancer Epidemiol Biomarkers Prev*. 2021;30(2):295. doi:10.1158/1055-9965.EPI-20-0975
148. Sillah A, Watson NF, Schwartz SM, Gozal D, Phipps AI. Sleep apnea and subsequent cancer incidence. *Cancer Causes Control*. 2018;29(10):987. doi:10.1007/S10552-018-1073-5
149. Justeau G, Gervès-Pinquier C, Le Vaillant M, et al. Association Between Nocturnal Hypoxemia and Cancer Incidence in Patients Investigated for OSA Data From a Large Multicenter French Cohort. *Chest*. 2020;158(6):2610-2620. doi:10.1016/j.chest.2020.06.055
150. Campos-Rodriguez F, Martinez-Garcia MA, Martinez M, et al. Association between Obstructive Sleep Apnea and Cancer Incidence in a Large Multicenter Spanish Cohort. <https://doi.org/10.1164/rccm.201209-1671OC>. 2013;187(1):99-105. doi:10.1164/RCCM.201209-1671OC
151. Dreher M, Krüger S, Schulze-Olden S, et al. Sleep-disordered breathing in patients with newly diagnosed lung cancer. *BMC Pulm Med*. 2018;18(72). doi:10.1186/s12890-018-0645-1
152. Zhang W, Shi X, Peng Y, et al. HIF-1 α Promotes Epithelial-Mesenchymal Transition and Metastasis through Direct Regulation of ZEB1 in Colorectal Cancer. *PLoS One*. 2015;10(6):e0129603. doi:10.1371/JOURNAL.PONE.0129603
153. Zhu J, Huang Z, Zhang M, et al. HIF-1 α promotes ZEB1 expression and EMT in a human bladder cancer lung metastasis animal model. *Oncol Lett*. 2018;15(3):3482-3489. doi:10.3892/OL.2018.7764/HTML
154. Hoffmann C, Mao X, Brown-Clay J, et al. Hypoxia promotes breast cancer cell invasion through HIF-1 α -mediated up-regulation of the invadopodial actin bundling protein CSRP2. *Sci Rep*. 2018;8(1):10191. doi:10.1038/S41598-018-28637-X
155. Hung JJ, Yang MH, Hsu HS, Hsu WH, Liu JS, Wu KJ. Prognostic significance of hypoxia-inducible factor-1 α , TWIST1 and Snail expression in resectable non-small cell lung cancer. *Thorax*. 2009;64(12):1082-1089. doi:10.1136/THX.2009.115691
156. Liu Y, Song X, Wang X, et al. Effect of chronic intermittent hypoxia on biological behavior and hypoxia-associated gene expression in lung cancer cells. *J Cell Biochem*.

- 2010;111(3):554-563. doi:10.1002/JCB.22739
157. Almendros I, Wang Y, Becker L, et al. Intermittent Hypoxia-induced Changes in Tumor-associated Macrophages and Tumor Malignancy in a Mouse Model of Sleep Apnea. *Am J Respir Crit Care Med*. 2014;189(5):593-601. doi:10.1164/rccm.201310-1830OC
 158. Wang T, Gilkes DM, Takano N, et al. Hypoxia-inducible factors and RAB22A mediate formation of microvesicles that stimulate breast cancer invasion and metastasis. *Proc Natl Acad Sci U S A*. 2014;111(31):E3234. doi:10.1073/PNAS.1410041111/-/DCSUPPLEMENTAL
 159. Almendros I, Gileles-Hillel A, Khalyfa A, et al. Adipose tissue macrophage polarization by intermittent hypoxia in a mouse model of OSA: Effect of tumor microenvironment. *Cancer Lett*. 2015;361:233-239. doi:10.1016/j.canlet.2015.03.010
 160. Cortinovis D, Abbate M, Bidoli P, Pelizzoni D, Canova S. Interpretation of lung cancer study outcomes. *J Thorac Dis*. 2015;7(11):E541. doi:10.3978/J.ISSN.2072-1439.2015.11.26
 161. Chen Z, Cheng K, Walton Z, et al. A murine lung cancer co-clinical trial identifies genetic modifiers of therapeutic response. *Nature*. 2012;483(7391):613. doi:10.1038/NATURE10937
 162. Harris JP, Fujimoto DK, Nagasaka M, et al. Controversies in Lung Cancer: Heterogeneity in Treatment Recommendations for Stage III NSCLC According to Disease Burden and Oncogenic Driver Alterations. *Clin Lung Cancer*. February 2022. doi:10.1016/J.CLLC.2022.02.001
 163. Santos ES, Castrellon A, Blaya M, Raez LE. Controversies in the management of stage IIIA non-small-cell lung cancer. *Expert Rev Anticancer Ther*. 2008;8(12):1913-1929. doi:10.1586/14737140.8.12.1913
 164. Inamura K. Lung Cancer: Understanding Its Molecular Pathology and the 2015 WHO Classification. *Front Oncol*. 2017;7(AUG):193. doi:10.3389/FONC.2017.00193
 165. Negewo NA, Gibson PG, McDonald VM. COPD and its comorbidities: Impact, measurement and mechanisms. *Respirology*. 2015;20(8):1160-1171. doi:10.1111/RESP.12642
 166. Taraseviciene-Stewart L, Voelkel NF. Molecular pathogenesis of emphysema. *J Clin Invest*. 2008;118(2):394-402. doi:10.1172/JCI31811
 167. Kim V, Criner GJ. Chronic Bronchitis and Chronic Obstructive Pulmonary Disease. <https://doi.org/10.1164/rccm.201210-1843CI>. 2013;187(3):228-237. doi:10.1164/RCCM.201210-1843CI
 168. Black PN, Ching PST, Beaumont B, Ransinghe S, Taylor G, Merrilees MJ. Changes in elastic fibres in the small airways and alveoli in COPD. *Eur Respir J*. 2008;31(5):998-1004. doi:10.1183/09031936.00017207
 169. Wagner PD, Dantzker DR, Dueck R, Clausen JL, West JB. Ventilation-perfusion inequality in chronic obstructive pulmonary disease. *J Clin Invest*. 1977;59(2):203-216. doi:10.1172/JCI108630
 170. Barbera JA, Ramirez J, Roca J, Wagner PD, Sanchez-Lloret J, Rodriguez-Roisin R. Lung Structure and Gas Exchange in Mild Chronic Obstructive Pulmonary Disease. *Am J Crit*

- Care Med.* 2012;141(4 I):895-901. doi:10.1164/AJRCCM/141.4_PT_1.895
171. Rovina N, Koutsoukou A, Koulouris NG. Inflammation and immune response in COPD: Where do we stand? *Mediators Inflamm.* 2013;2013. doi:10.1155/2013/413735
 172. Rahman I, Adcock IM. Oxidative stress and redox regulation of lung inflammation in COPD. *Eur Respir J.* 2006;28(1):219-242. doi:10.1183/09031936.06.00053805
 173. Mittal M, Siddiqui MR, Tran K, Reddy SP, Malik AB. Reactive oxygen species in inflammation and tissue injury. *Antioxidants Redox Signal.* 2014;20(7):1126-1167. doi:10.1089/ARS.2012.5149
 174. Yoshida M, Whitsett JA. Alveolar macrophages and emphysema in surfactant protein-D-deficient mice. *Respirology.* 2006;11(1). doi:10.1111/J.1440-1843.2006.00806.X
 175. Kassim SY, Fu X, Liles WC, Shapiro SD, Parks WC, Heinecke JW. NADPH oxidase restrains the matrix metalloproteinase activity of macrophages. *J Biol Chem.* 2005;280(34):30201-30205. doi:10.1074/JBC.M503292200
 176. Hogg JC, Chu F, Utokaparch S, et al. The Nature of Small-Airway Obstruction in Chronic Obstructive Pulmonary Disease. *N Engl J Med.* 2004;350(26):2645-2653. doi:10.1056/NEJM0A032158
 177. Dave C, Wharton S, Mukherjee R, Faqih BM, Stockley RA, Turner AM. Development and Relevance of Hypercapnia in COPD. *Can Respir J.* 2021;2021. doi:10.1155/2021/6623093
 178. Huang X, Guan W, Xiang B, Wang W, Xie Y, Zheng J. MUC5B regulates goblet cell differentiation and reduces inflammation in a murine COPD model. *Respir Res.* 2022;23(1):1-12. doi:10.1186/S12931-021-01920-8/FIGURES/6
 179. *Global Strategy for the Diagnosis, Management, and Prevention of Chronic Obstructive Pulmonary Disease;* 2020. www.goldcopd.org. Accessed May 15, 2020.
 180. Cazzola M, Page C. Long-acting bronchodilators in COPD: where are we now and where are we going? *Breathe.* 2014;10(2):110-120. doi:10.1183/20734735.014813
 181. Hannemann J, Böger R. Dysregulation of the Nitric Oxide/Dimethylarginine Pathway in Hypoxic Pulmonary Vasoconstriction—Molecular Mechanisms and Clinical Significance. *Front Med.* 2022;9:337. doi:10.3389/FMED.2022.835481/BIBTEX
 182. Wang JJ. Risk of Coronary Heart Disease in People with Chronic Obstructive Pulmonary Disease: A Meta-Analysis. *Int J Chron Obstruct Pulmon Dis.* 2021;16:2939-2944. doi:10.2147/COPD.S331505
 183. Sharma H, Kapur P, Jalali RK, Dubey K. Atherosclerosis risk assessment in patients with chronic obstructive pulmonary disease: a case-control study. *Ther Clin Risk Manag.* 2019;15:1061. doi:10.2147/TCRM.S216180
 184. Dauriat G, Reynaud-Gaubert M, Cottin V, et al. Severe pulmonary hypertension associated with chronic obstructive pulmonary disease: A prospective French multicenter cohort. *J Hear Lung Transplant.* 2021;40(9):1009-1018. doi:10.1016/J.HEALUN.2021.04.021
 185. Jaitovich A, Barreiro E. Skeletal muscle dysfunction in chronic obstructive pulmonary disease what we know and can do for our patients. *Am J Respir Crit Care Med.* 2018;198(2):175-186. doi:10.1164/RCCM.201710-2140CI/SUPPL_FILE/DISCLOSURES.PDF

186. Wang Y, Li X, Wei B, Tung TH, Tao P, Chien CW. Association between Chronic Obstructive Pulmonary Disease and Dementia: Systematic Review and Meta-Analysis of Cohort Studies. *Dement Geriatr Cogn Dis Extra*. 2019;9(2):250-259. doi:10.1159/000496475
187. Park HY, Kang D, Shin SH, et al. Chronic obstructive pulmonary disease and lung cancer incidence in never smokers: a cohort study. *Thorax*. 2020;75(6):506-509. doi:10.1136/THORAXJNL-2019-213732
188. Sekine Y, Katsura H, Koh E, Hiroshima K, Fujisawa T. Early detection of COPD is important for lung cancer surveillance. *Eur Respir J*. 2012;39(5):1230-1240. doi:10.1183/09031936.00126011
189. Wang H, Yang L, Zou L, et al. Association between Chronic Obstructive Pulmonary Disease and Lung Cancer: A Case-Control Study in Southern Chinese and a Meta-Analysis. *PLoS One*. 2012;7(9). doi:10.1371/JOURNAL.PONE.0046144
190. Ahn SV, Lee E, Park B, et al. Cancer development in patients with COPD: A retrospective analysis of the National Health Insurance Service-National Sample Cohort in Korea. *BMC Pulm Med*. 2020;20(1):1-10. doi:10.1186/S12890-020-01194-8/TABLES/4
191. Goffin JR, Pond GR, Puksa S, et al. Chronic obstructive pulmonary disease prevalence and prediction in a high-risk lung cancer screening population. *BMC Pulm Med*. 2020;20(1). doi:10.1186/S12890-020-01344-Y
192. Lin P, Fu S, Li W, Hu Y, Liang Z. Inhaled corticosteroids and risk of lung cancer: A systematic review and meta-analysis. *Eur J Clin Invest*. 2021;51(2):e13434. doi:10.1111/ECL.13434
193. Parris BA, O'Farrell HE, Fong KM, Yang IA. Chronic obstructive pulmonary disease (COPD) and lung cancer: common pathways for pathogenesis. *J Thorac Dis*. 2019;11(Suppl 17):S2155. doi:10.21037/JTD.2019.10.54
194. Pastor MD, Nogal A, Molina-Pinelo S, et al. Identification of proteomic signatures associated with lung cancer and COPD. *J Proteomics*. 2013;89:227-237. doi:10.1016/j.jprot.2013.04.037
195. Ellegaard PK, Poulsen HE. Tobacco smoking and oxidative stress to DNA: a meta-analysis of studies using chromatographic and immunological methods. *Scand J Clin Lab Invest*. 2016;76(2):151-158. doi:10.3109/00365513.2015.1127407
196. MØller P, Loft S. Oxidative damage to DNA and lipids as biomarkers of exposure to air pollution. *Environ Health Perspect*. 2010;118(8):1126-1136. doi:10.1289/EHP.0901725
197. Engels EA. Inflammation in the development of lung cancer: epidemiological evidence. <http://dx.doi.org/sire.ub.edu/101586/1473714084605>. 2014;8(4):605-615. doi:10.1586/14737140.8.4.605
198. Perera FP, Mooney LVA, Stampfer M, et al. Associations between carcinogen-DNA damage, glutathione S-transferase genotypes, and risk of lung cancer in the prospective Physicians' Health Cohort Study. *Carcinogenesis*. 2002;23(10):1641-1646. doi:10.1093/CARCIN/23.10.1641
199. Grudny J, Kołakowski J, Grudny MK, et al. Association of genetic dependences between lung

- cancer and chronic obstructive pulmonary disease | Grudny J. *Adv Respir Med*. 2013;81(4). https://journals.viamedica.pl/advances_in_respiratory_medicine/article/view/34790. Accessed April 15, 2022.
200. Pillai SG, Ge D, Zhu G, et al. A Genome-Wide Association Study in Chronic Obstructive Pulmonary Disease (COPD): Identification of Two Major Susceptibility Loci. *PLoS Genet*. 2009;5(3):e1000421. doi:10.1371/JOURNAL.PGEN.1000421
 201. Rojewski AM, Tanner NT, Dai L, et al. Tobacco Dependence Predicts Higher Lung Cancer and Mortality Rates and Lower Rates of Smoking Cessation in the National Lung Screening Trial. *Chest*. 2018;154(1):110. doi:10.1016/J.CHEST.2018.04.016
 202. Wang B, Xiao D, Wang C. Smoking and chronic obstructive pulmonary disease in Chinese population: a meta-analysis. *Clin Respir J*. 2015;9(2):165-175. doi:10.1111/CRJ.12118
 203. McNicholas WT. Chronic obstructive pulmonary disease and obstructive sleep apnoea—the overlap syndrome. *J Thorac Dis*. 2016;8(2):236-242. doi:10.3978/J.ISSN.2072-1439.2016.01.52
 204. Kent BD, Mitchell PD, Mcnicholas WT. Hypoxemia in patients with COPD: cause, effects, and disease progression. *Int J Chron Obstruct Pulmon Dis*. 2011;6(1):199. doi:10.2147/COPD.S10611
 205. Johnson MW, Remmers JE. Accessory muscle activity during sleep in chronic obstructive pulmonary disease. *J Appl Physiol*. 1984;57(4):1011-1017. doi:10.1152/JAPPL.1984.57.4.1011
 206. Lu H, Wu X, Fu C, Zhou J, Li S. Lung injury and inflammation response by chronic intermittent hypoxia in rats. *Sleep Sci Pract 2017 11*. 2017;1(1):1-7. doi:10.1186/S41606-016-0006-Z
 207. Bartels K, Grenz A, Eltzhig HK. Hypoxia and inflammation are two sides of the same coin. *Proc Natl Acad Sci U S A*. 2013;110(46):18351. doi:10.1073/PNAS.1318345110
 208. Papachatzakis, Velentza, Zarogoulidis, Kallianos, Trakada. Comorbidities in coexisting COPD and OSA – overlap syndrome. *Eur Rev Med Pharmacol Sci*. 2018;22:4325-4331.
 209. Ashbaugh DG, Bigelow DB, Petty TL, Levine BE. Acute Respiratory Distress in adults. *Lancet*. 1967;290(7511):319-323. doi:10.1016/S0140-6736(67)90168-7
 210. Mark D Siegel M. Acute respiratory distress syndrome: Epidemiology, pathophysiology, pathology, and etiology in adults - UpToDate. <https://www.uptodate.com/contents/acute-respiratory-distress-syndrome-epidemiology-pathophysiology-pathology-and-etiology-in-adults>. Published 2020. Accessed February 7, 2022.
 211. Ranieri VM, Rubenfeld GD, Thompson BT, et al. Acute respiratory distress syndrome: The Berlin definition. *JAMA - J Am Med Assoc*. 2012;307(23):2526-2533. doi:10.1001/jama.2012.5669
 212. Agarwal R, Srinivas R, Nath A, Jindal SK. Is the Mortality Higher in the Pulmonary vs the Extrapulmonary ARDS?: A Metaanalysis. *Chest*. 2008;133(6):1463-1473. doi:10.1378/CHEST.07-2182
 213. Pelosi P, D'Onofrio D, Chiumello D, et al. Pulmonary and extrapulmonary acute respiratory distress syndrome are different. *Eur Respir J*. 2003;22(42 suppl):48s-56s.

doi:10.1183/09031936.03.00420803

214. Matthay MA, Ware LB, Zimmerman GA. The acute respiratory distress syndrome. *J Clin Invest*. 2012;122(8):2731. doi:10.1172/JCI60331
215. Matthay MA, Zemans RL, Zimmerman GA, et al. Acute respiratory distress syndrome. *Nat Rev Dis Prim* 2019 51. 2019;5(1):1-22. doi:10.1038/s41572-019-0069-0
216. JN Gonzales 1,2,* R Lucas,1,3 and AD Verin. The Acute Respiratory Distress Syndrome: Mechanisms and Perspective Therapeutic Approaches. *Austin J Vasc Med*. 2013;2(1). doi:10.5772/52701
217. Spadaro S, Park M, Turrini C, et al. Biomarkers for Acute Respiratory Distress syndrome and prospects for personalised medicine. *J Inflamm (United Kingdom)*. 2019;16(1):1-11. doi:10.1186/S12950-018-0202-Y/TABLES/4
218. Qin M, Qiu Z. Changes in TNF- α , IL-6, IL-10 and VEGF in rats with ARDS and the effects of dexamethasone. *Exp Ther Med*. 2019;17(1):383-387. doi:10.3892/ETM.2018.6926
219. Chen CM, Lu HC, Tung YT, Chen W. Antiplatelet Therapy for Acute Respiratory Distress Syndrome. *Biomed* 2020, Vol 8, Page 230. 2020;8(7):230. doi:10.3390/BIOMEDICINES8070230
220. Vohwinkel CU, Lecuona E, Sun H, et al. Elevated CO₂ Levels Cause Mitochondrial Dysfunction and Impair Cell Proliferation. *J Biol Chem*. 2011;286(43):37067. doi:10.1074/JBC.M111.290056
221. Homas T, Uckton JN, Ames J, et al. PULMONARY DEAD-SPACE FRACTION AS A RISK FACTOR FOR DEATH IN THE ACUTE RESPIRATORY DISTRESS SYNDROME A BSTRACT Background No single pulmonary-specific vari. *N Engl J Med*. 2002;346(17). www.nejm.org. Accessed February 7, 2022.
222. WHO Coronavirus (COVID-19) Dashboard . <https://covid19.who.int/>. Accessed May 24, 2022.
223. van Paassen J, Vos JS, Hoekstra EM, Neumann KMI, Boot PC, Arbous SM. Corticosteroid use in COVID-19 patients: a systematic review and meta-analysis on clinical outcomes. *Crit care*. 2020;24(1). doi:10.1186/S13054-020-03400-9
224. Webb HH, Tierney DF. Experimental pulmonary edema due to intermittent positive pressure ventilation with high inflation pressures. Protection by positive end expiratory pressure. *AMERREVRESPIRDIS*. 1974;110(5):556-565. doi:10.1164/ARRD.1974.110.5.556
225. Forel JM, Roch A, Marin V, et al. Neuromuscular blocking agents decrease inflammatory response in patients presenting with acute respiratory distress syndrome. *Crit Care Med*. 2006;34(11):2749-2757. doi:10.1097/01.CCM.0000239435.87433.0D
226. Augy JL, Aissaoui N, Richard C, et al. A 2-year multicenter, observational, prospective, cohort study on extracorporeal CO₂ removal in a large metropolis area. *J Intensive Care*. 2019;7(1):1-8. doi:10.1186/S40560-019-0399-8/TABLES/5
227. Sameed M, Meng Z, Marciniak ET. EOLIA trial: the future of extracorporeal membrane oxygenation in acute respiratory distress syndrome therapy? *Breathe*. 2019;15(3):244-246. doi:10.1183/20734735.0363-2018

228. KP S, LD H, RB G, et al. Efficacy and safety of corticosteroids for persistent acute respiratory distress syndrome. *N Engl J Med*. 2006;354(16):1671-1684. doi:10.1056/NEJMOA051693
229. Fuller BM, Mohr NM, Skrupky L, Fowler S, Kollef MH, Carpenter CR. The Use of Inhaled Prostaglandins in Patients With ARDS: A Systematic Review and Meta-analysis. *Chest*. 2015;147(6):1510. doi:10.1378/CHEST.14-3161
230. Meduri GU, Bridges L, Shih MC, Marik PE, Siemieniuk RAC, Kocak M. Prolonged glucocorticoid treatment is associated with improved ARDS outcomes: analysis of individual patients' data from four randomized trials and trial-level meta-analysis of the updated literature. *Intensive Care Med* 2015 425. 2015;42(5):829-840. doi:10.1007/S00134-015-4095-4
231. Barnes PJ, Bonini S, Seeger W, Belvisi MG, Ward B, Holmes A. Barriers to new drug development in respiratory disease. *Eur Respir J*. 2015;45(5):1197-1207. doi:10.1183/09031936.00007915
232. Seyhan AA. Lost in translation: the valley of death across preclinical and clinical divide – identification of problems and overcoming obstacles. *Transl Med Commun* 2019 41. 2019;4(1):1-19. doi:10.1186/S41231-019-0050-7
233. Stuart JA, Fonseca J, Moradi F, et al. How supraphysiological oxygen levels in standard cell culture affect oxygen-consuming reactions. *Oxid Med Cell Longev*. 2018;2018. doi:10.1155/2018/8238459
234. Woo KW, Yeo SI. Dalton's Law vs, Amagat's Law for the Mixture of Real Gases. *SNU J Educ Reseach*. 1995;5:127-134.
235. Metzen E, Wolff M, Fandrey J, Jelkmann W. Pericellular PO₂ and O₂ consumption in monolayer cell cultures. *Respir Physiol*. 1995;100(2):101-106. doi:10.1016/0034-5687(94)00125-j
236. Grimaldi D, Hraiech S, Boutin E, et al. Hypoxemia in the ICU: prevalence, treatment, and outcome. *Ann Intensive Care*. 2018;8(1):1-11. doi:10.1186/S13613-018-0424-4/TABLES/5
237. Kacmarek RM, Villar J. Management of refractory hypoxemia in ARDS. *Minerva Anesthesiol*. 2013;79(10):1173-1179. <https://europepmc.org/article/med/23857446>. Accessed May 10, 2022.
238. Rashid NHA, Zaghi S, Scapuccin M, Camacho M, Certal V, Capasso R. The Value of Oxygen Desaturation Index for Diagnosing Obstructive Sleep Apnea: A Systematic Review. *Laryngoscope*. 2021;131(2):440-447. doi:10.1002/LARY.28663
239. Chen B, Longtine MS, Nelson DM. Pericellular oxygen concentration of cultured primary human trophoblasts. *Placenta*. 2013;34(2):106. doi:10.1016/J.PLACENTA.2012.11.011
240. Oze H, Hirao M, Ebina K, et al. Impact of medium volume and oxygen concentration in the incubator on pericellular oxygen concentration and differentiation of murine chondrogenic cell culture. *Vitr Cell Dev Biol - Anim*. 2012;48(2):123-130. doi:10.1007/S11626-011-9479-3/FIGURES/5
241. Pavlacky J, Polak J. Technical Feasibility and Physiological Relevance of Hypoxic Cell Culture Models. *Front Endocrinol (Lausanne)*. 2020;11:57. doi:10.3389/FENDO.2020.00057/BIBTEX

242. Wree A, Mayer A, Westphal S, et al. Adipokine expression in brown and white adipocytes in response to hypoxia. *J Endocrinol Invest.* 2012;35(5):522-527. doi:10.3275/7964
243. Lam RHW, Kim M-C, Thorsen T. Culturing Aerobic and Anaerobic Bacteria and Mammalian Cells with a Microfluidic Differential Oxygenator. *Ann Chemistry.* 2009;81:5918-5924. doi:10.1021/ac9006864
244. Polinkovsky M, Gutierrez E, Levchenko A, Groisman A. Fine temporal control of the medium gas content and acidity and on-chip generation of series of oxygen concentrations for cell cultures. *Lab Chip.* 2009;9(8):1073-1084. doi:10.1039/B816191G
245. Gao Y, Stybayeva G, Revzin A. Fabrication of composite microfluidic devices for local control of oxygen tension in cell cultures. *Lab Chip.* 2019;19(2):306-315. doi:10.1039/C8LC00825F
246. Baumgardner JE, Otto CM. In vitro intermittent hypoxia: challenges for creating hypoxia in cell culture. *Respir Physiol Neurobiol.* 2003;136(2-3):131-139. doi:10.1016/S1569-9048(03)00077-6
247. Tsapikouni T, Garreta E, Melo E, Navajas D, Farré R. A bioreactor for subjecting cultured cells to fast-rate intermittent hypoxia. *Respir Physiol Neurobiol.* 2012;182:47-52. doi:10.1016/j.resp.2012.01.001
248. Oppedard SC, Blake AJ, Williams JC, Eddington DT. Precise control over the oxygen conditions within the Boyden chamber using a microfabricated insert. *Lab Chip.* 2010;10(18):2366-2373. doi:10.1039/C004856A
249. Polak J, Studer-Rabeler K, Mchugh H, Hussain MA, Shimoda LA. System for exposing cultured cells to intermittent hypoxia utilizing gas permeable cultureware. *Gen Physiol Biophys.* 2015;34:235-247. doi:10.4149/gpb_2014043
250. Campillo N, Jorba I, Schaedel L, et al. A Novel Chip for Cyclic Stretch and Intermittent Hypoxia Cell Exposures Mimicking Obstructive Sleep Apnea. *Front Physiol | www.frontiersin.org.* 2016;1:319. doi:10.3389/fphys.2016.00319
251. Campillo N, Falcones B, Montserrat JM, et al. Frequency and magnitude of intermittent hypoxia modulate endothelial wound healing in a cell culture model of sleep apnea. *J Appl Physiol.* 2017;123:1047-1054. doi:10.1152/jappl
252. McAdams RM, Mustafa SB, Shenberger JS, Dixon PS, Henson BM, DiGeronimo RJ. Cyclic stretch attenuates effects of hyperoxia on cell proliferation and viability in human alveolar epithelial cells. <https://doi.org/10.1152/ajplung001602005>. 2006;291(2):166-174. doi:10.1152/AJPLUNG.00160.2005
253. Nguyen TM, van der Merwe J, Elowsson Rendin L, et al. Stretch increases alveolar type 1 cell number in fetal lungs through ROCK-Yap/Taz pathway. *Am J Physiol Lung Cell Mol Physiol.* 2021;321(5):L814-L826. doi:10.1152/AJPLUNG.00484.2020/ASSET/IMAGES/LARGE/AJPLUNG.00484.2020_F004.JPG
254. Zhang W, Huang G, Xu F. Engineering Biomaterials and Approaches for Mechanical Stretching of Cells in Three Dimensions. *Front Bioeng Biotechnol.* 2020;8:1151. doi:10.3389/FBIOE.2020.589590/BIBTEX

255. Vandenburg H, Kaufman S. In vitro model for stretch-induced hypertrophy of skeletal muscle. *Science (80-)*. 1979;203(4377):265-268. doi:10.1126/SCIENCE.569901
256. Wirtz HRW, Dobbs LG. Calcium mobilization and exocytosis after one mechanical stretch of lung epithelial cells. *Science (80-)*. 1990;250(4985):1266-1269. doi:10.1126/science.2173861
257. Gutierrez JA, Gonzalez RF, Dobbs LG. Mechanical distension modulates pulmonary alveolar epithelial phenotypic expression in vitro. *Am J Physiol - Lung Cell Mol Physiol*. 1998;274(218-2):196-202. doi:10.1152/AJPLUNG.1998.274.2.L196
258. Foster CD, Varghese LS, Gonzales LW, Margulies SS, Guttentag SH. The Rho Pathway Mediates Transition to an Alveolar Type I Cell Phenotype During Static Stretch of Alveolar Type II Cells. *Pediatr Res* 2010 676. 2010;67(6):585-590. doi:10.1203/pdr.0b013e3181dbc708
259. Pugin J, Dunn-Siegrist I, Dufour J, Tissières P, Charles PE, Comte R. Cyclic Stretch of Human Lung Cells Induces an Acidification and Promotes Bacterial Growth. <https://doi.org/10.1165/rcmb.2007-0114OC>. 2012;38(3):362-370. doi:10.1165/RCMB.2007-0114OC
260. Wu J, Yan Z, Schwartz DE, Yu J, Malik B, Hu G. Activation of NLRP3 in Alveolar Macrophages Contributes to Mechanical Stretch-Induced Lung Inflammation and Injury. *J Immunol*. 2013;190(7):3591-3599. doi:10.4049/jimmunol.1200860
261. Ferreira JMC, Huhle R, Müller S, et al. Static Stretch Increases the Pro-Inflammatory Response of Rat Type 2 Alveolar Epithelial Cells to Dynamic Stretch. *Front Physiol*. 2022;13(April):1-12. doi:10.3389/fphys.2022.838834
262. Xie Y, Qian Y, Wang Y, Liu K, Li X. Mechanical stretch and LPS affect the proliferation, extracellular matrix remodeling and viscoelasticity of lung fibroblasts. *Exp Ther Med*. 2020;20(5):1-1. doi:10.3892/ETM.2020.9133
263. Andersen T, Auk-Emblem P, Dornish M. 3D Cell Culture in Alginate Hydrogels. *Microarrays*. 2015;4(2):133. doi:10.3390/MICROARRAYS4020133
264. Oh SA, Lee HY, Lee JH, et al. Collagen three-dimensional hydrogel Matrix carrying basic fibroblast growth factor for the cultivation of mesenchymal stem cells and osteogenic differentiation. *Tissue Eng - Part A*. 2012;18(9-10):1087-1100. doi:10.1089/TEN.TEA.2011.0360/ASSET/IMAGES/LARGE/FIGURE12.JPG
265. Shah MK, Leary EA, Darling EM. Integration of hyper-compliant microparticles into a 3D melanoma tumor model. *J Biomech*. 2019;82. doi:10.1016/J.JBIOMECH.2018.10.018
266. Mercey E, Obeid P, Glaise D, Calvo-Muñoz ML, Guguen-Guillouzo C, Fouqué B. The application of 3D micropatterning of agarose substrate for cell culture and in situ comet assays. *Biomaterials*. 2010;31(12):3156-3165. doi:10.1016/J.BIOMATERIALS.2010.01.020
267. Hong Y, Song H, Gong Y, Mao Z, Gao C, Shen J. Covalently crosslinked chitosan hydrogel: Properties of in vitro degradation and chondrocyte encapsulation. *Acta Biomater*. 2007;3(1):23-31. doi:10.1016/J.ACTBIO.2006.06.007
268. Rode MP, Batti Angulski AB, Gomes FA, et al. Carrageenan hydrogel as a scaffold for skin-derived multipotent stromal cells delivery. *J Biomater Appl*. 2018;33(3):422-434.

doi:10.1177/0885328218795569

269. Ye Q, Zünd G, Benedikt P, et al. Fibrin gel as a three dimensional matrix in cardiovascular tissue engineering. *Eur J Cardio-Thoracic Surg*. 2000;17(5):587-591. doi:10.1016/S1010-7940(00)00373-0
270. Joo S, Oh SH, Sittadjody S, et al. The effect of collagen hydrogel on 3D culture of ovarian follicles. *Biomed Mater*. 2016;11(6):065009. doi:10.1088/1748-6041/11/6/065009
271. Hiraki HL, Nagao RJ, Himmelfarb J, Zheng Y. Fabricating a Kidney Cortex Extracellular Matrix-Derived Hydrogel. *JoVE (Journal Vis Exp)*. 2018;(140):e58314. doi:10.3791/58314
272. Pouliot RA, Link PA, Mikhael NS, et al. Development and characterization of a naturally derived lung extracellular matrix hydrogel. *J Biomed Mater Res A*. 2016;104(8):1922. doi:10.1002/JBM.A.35726
273. Khosravizadeh Z, Razavi S, Bahramian H, Kazemi M. The beneficial effect of encapsulated human adipose-derived stem cells in alginate hydrogel on neural differentiation. *J Biomed Mater Res Part B Appl Biomater*. 2014;102(4):749-755. doi:10.1002/JBM.B.33055
274. Olderøy M, Lilledahl MB, Beckwith MS, et al. Biochemical and Structural Characterization of Neocartilage Formed by Mesenchymal Stem Cells in Alginate Hydrogels. *PLoS One*. 2014;9(3):e91662. doi:10.1371/JOURNAL.PONE.0091662
275. Pascual-Garrido C, Aisenbrey EA, Rodriguez-Fontan F, Payne KA, Bryant SJ, Goodrich LR. Photopolymerizable Injectable Cartilage Mimetic Hydrogel for the Treatment of Focal Chondral Lesions: A Proof of Concept Study in a Rabbit Animal Model. *Am J Sports Med*. 2019;47(1):212-221. doi:10.1177/0363546518808012
276. Cho MO, Li Z, Shim HE, et al. Bioinspired tuning of glycol chitosan for 3D cell culture. *NPG Asia Mater* 2016 89. 2016;8(9):e309-e309. doi:10.1038/am.2016.130
277. Arunraj TR, Rejinold NS, Kumar NA, Jayakumar R. Doxorubicin-chitin-poly(caprolactone) composite nanogel for drug delivery. *Int J Biol Macromol*. 2013;62:35-43. doi:10.1016/j.ijbiomac.2013.08.013
278. Rejinold N S, Chennazhi KP, Tamura H, Nair S V., Rangasamy J. Multifunctional chitin nanogels for simultaneous drug delivery, bioimaging, and biosensing. *ACS Appl Mater Interfaces*. 2011;3(9):3654-3665. doi:10.1021/AM200844M/SUPPL_FILE/AM200844M_SI_001.PDF
279. Cambria E, Brunner S, Heusser S, et al. Cell-Laden Agarose-Collagen Composite Hydrogels for Mechanotransduction Studies. *Front Bioeng Biotechnol*. 2020;8:346. doi:10.3389/FBIOE.2020.00346/BIBTEX
280. Su T, Zhang M, Zeng Q, et al. Mussel-inspired agarose hydrogel scaffolds for skin tissue engineering. *Bioact Mater*. 2021;6(3):579-588. doi:10.1016/j.BIOACTMAT.2020.09.004
281. Martínez A, Blanco MD, Davidenko N, Cameron RE. Tailoring chitosan/collagen scaffolds for tissue engineering: Effect of composition and different crosslinking agents on scaffold properties. *Carbohydr Polym*. 2015;132:606-619. doi:10.1016/j.carbpol.2015.06.084
282. Hesse E, Hefferan TE, Tarara JE, et al. Collagen type I hydrogel allows migration, proliferation, and osteogenic differentiation of rat bone marrow stromal cells. *J Biomed Mater Res Part A*. 2010;94A(2):442-449. doi:10.1002/JBM.A.32696

283. Almelkar S, Patwardhan A, Divate S, Agrawal N, Bhonde R, Chaukar A. Fibrin matrix supports endothelial cell adhesion and migration in culture. *OA Biol.* 2014;2. https://www.researchgate.net/publication/272170899_Fibrin_matrix_supports_endothelial_cell_adhesion_and_migration_in_culture. Accessed March 10, 2022.
284. Antoine EE, Vlachos PP, Rylander MN. Review of collagen i hydrogels for bioengineered tissue microenvironments: Characterization of mechanics, structure, and transport. *Tissue Eng - Part B Rev.* 2014;20(6):683-696. doi:10.1089/TEN.TEB.2014.0086/ASSET/IMAGES/LARGE/FIGURE10.JPG
285. Silvipriya KS, Kumar KK, Bhat AR, Dinesh Kumar B, John A, James S. Collagen: Animal Sources and Biomedical Application. *J Appl Pharm Sci.* 2015;5(03):123-127. doi:10.7324/JAPS.2015.50322
286. Doyle AD. Fluorescent Labeling of Rat-tail Collagen for 3D Fluorescence Imaging. *Bio-protocol.* 2018;8(13). doi:10.21769/BIOPROTOCOL.2919
287. Bosnakovski D, Mizuno M, Kim G, Takagi S, Okumura M, Fujinaga T. Chondrogenic differentiation of bovine bone marrow mesenchymal stem cells (MSCs) in different hydrogels: Influence of collagen type II extracellular matrix on MSC chondrogenesis. *Biotechnol Bioeng.* 2006;93(6):1152-1163. doi:10.1002/BIT.20828
288. Ding L, Li A, Sun H, et al. Transplantation of bone marrow mesenchymal stem cells on collagen scaffolds for the functional regeneration of injured rat uterus. *Biomaterials.* 2014;35:4888-4900. doi:10.1016/j.biomaterials.2014.02.046
289. Voytik-Harbin SL, Brightman AO, Waisner BZ, Robinson JP, Lamar CH. Small intestinal submucosa: A tissue-derived extracellular matrix that promotes tissue-specific growth and differentiation of cells in vitro. *Tissue Eng.* 1998;4(2):157-174. doi:10.1089/TEN.1998.4.157
290. Ozpinar EW, Frey AL, Arthur GK, et al. Dermal Extracellular Matrix-Derived Hydrogels as an in Vitro Substrate to Study Mast Cell Maturation. *Tissue Eng - Part A.* 2021;27(15-16):1008-1022. doi:10.1089/TEN.TEA.2020.0142/ASSET/IMAGES/LARGE/TEN.TEA.2020.0142_FIGURE4.JPG
291. Mashayekhan S, Jafarkhani M, Moghadam S. Reinforcement of a Decellularized Extracellular Matrix-Derived Hydrogel Using Nanofibers for Cardiac Tissue Engineering. *Int J Adv Biol Biomed Res.* 2020;8(3):302-313. doi:10.33945/SAMI/IJABBR.2020.3.8
292. Huleihel L, Hussey GS, Naranjo JD, et al. Matrix-bound nanovesicles within ECM bioscaffolds. *Science (80-).* 2016;2. doi:10.1126/sciadv.1600502
293. Agrawal V, Tottey S, Johnson SA, Freund JM, Siu BF, Badylak SF. Recruitment of progenitor cells by an extracellular matrix cryptic peptide in a mouse model of digit amputation. *Tissue Eng - Part A.* 2011;17(19-20):2435-2443. doi:10.1089/TEN.TEA.2011.0036/FORMAT/EPUB
294. Londono R, Badylak SF. Biologic Scaffolds for Regenerative Medicine: Mechanisms of In vivo Remodeling. *Ann Biomed Eng.* 2015;43(3):577-592. doi:10.1007/S10439-014-1103-8/FIGURES/6
295. Badylak SF. The extracellular matrix as a scaffold for tissue reconstruction. *Cell Dev Biol.* 2002;13:377-383. doi:10.1016/S1084-9521(02)00094-0

296. Saldin LT, Cramer MC, Velankar SS, White LJ, Badylak SF. Extracellular Matrix Hydrogels from Decellularized Tissues: Structure and Function. *Acta Biomater.* 2017;49:1. doi:10.1016/j.ACTBIO.2016.11.068
297. Freytes DO, Martin J, Velankar SS, Lee AS, Badylak SF. Preparation and rheological characterization of a gel form of the porcine urinary bladder matrix. *Biomaterials.* 2008;29:1630-1637. doi:10.1016/j.biomaterials.2007.12.014
298. Petrou CL, D'Ovidio TJ, Bölükbas DA, et al. Clickable decellularized extracellular matrix as a new tool for building hybrid-hydrogels to model chronic fibrotic diseases in vitro. *J Mater Chem B.* 2020;8(31):6814-6826. doi:10.1039/D0TB00613K
299. Shannon JM, Emrie PA, Fisher JH, Kuroki Y, Jennings SD, Mason RJ. Effect of a reconstituted basement membrane on expression of surfactant apoproteins in cultured adult rat alveolar type II cells. *Am J Respir Cell Mol Biol.* 1990;2(2):183-192. doi:10.1165/ajrcmb/2.2.183
300. Loebel C, Weiner AI, Katzen JB, et al. Microstructured hydrogels to guide self-assembly and function of lung alveolospheres. *bioRxiv.* September 2021:2021.08.30.457534. doi:10.1101/2021.08.30.457534
301. Hoffman ET, Pouliot R, Alysandratos K, Ikononou L, Kotton D, Weiss DJ. Alveolar Extracellular Matrix Hydrogels Facilitate Proliferation of Induced Pluripotent Stem Cell-Derived Alveolar Epithelial Spheroids. *Cytotherapy.* 2020;22(5):S204. doi:10.1016/j.JCYT.2020.04.082
302. Jung M, Han Y, Woo C, Ki CS. Pulmonary tissue-mimetic hydrogel niches for small cell lung cancer cell culture. *J Mater Chem B.* 2021;9(7):1858-1866. doi:10.1039/D0TB02609C
303. Jiang R, Huang J, Sun X, et al. Construction of in vitro 3-D model for lung cancer-cell metastasis study. *BMC Cancer.* 2022;22(1):1-9. doi:10.1186/S12885-022-09546-9
304. Hermanns MI, Unger RE, Kehe K, Peters K, Kirkpatrick CJ. Lung epithelial cell lines in coculture with human pulmonary microvascular endothelial cells: development of an alveolo-capillary barrier in vitro. *Lab Investig 2004 846.* 2004;84(6):736-752. doi:10.1038/labinvest.3700081
305. Haghgi M, Hittinger M, Zeng Q, et al. Mono- and Cocultures of Bronchial and Alveolar Epithelial Cells Respond Differently to Proinflammatory Stimuli and Their Modulation by Salbutamol and Budesonide. *Mol Pharm.* 2015;12(8):2625-2632. doi:10.1021/ACS.MOLPHARMACEUT.5B00124/SUPPL_FILE/MP5B00124_SI_001.MP4
306. Wang G, Zhang X, Liu X, Zheng J. Co-culture of human alveolar epithelial (A549) and macrophage (THP-1) cells to study the potential toxicity of ambient PM2.5: a comparison of growth under ALI and submerged conditions. *Toxicol Res (Camb).* 2020;9(5):636-651. doi:10.1093/TOXRES/TFAA072
307. Humayun M, Chow CW, Young EWK. Microfluidic lung airway-on-a-chip with arrayable suspended gels for studying epithelial and smooth muscle cell interactions. *Lab Chip.* 2018;18(9):1298-1309. doi:10.1039/C7LC01357D
308. Park JY, Ryu H, Lee B, et al. Development of a functional airway-on-a-chip by 3D cell printing. *Biofabrication.* 2018;11(1):015002. doi:10.1088/1758-5090/AAE545
309. Barkal LJ, Procknow CL, Álvarez-García YR, et al. Microbial volatile communication in

- human organotypic lung models. *Nat Commun* 2017 81. 2017;8(1):1-10.
doi:10.1038/S41467-017-01985-4
310. Huh D, Matthews BD, Mammoto A, Montoya-Zavala M, Yuan Hsin H, Ingber DE. Reconstituting organ-level lung functions on a chip. *Science (80-)*. 2010;328(5986):1662-1668. doi:10.1126/SCIENCE.1188302/SUPPL_FILE/HUH_SOM.PDF
 311. Stucki AO, Stucki JD, Hall SRR, et al. A lung-on-a-chip array with an integrated bio-inspired respiration mechanism. *Lab Chip*. 2015;15(5):1302-1310. doi:10.1039/C4LC01252F
 312. Zamprogno P, Wüthrich S, Achenbach S, et al. Second-generation lung-on-a-chip with an array of stretchable alveoli made with a biological membrane. *Commun Biol* . 2021;4(1):1-10. doi:10.1038/s42003-021-01695-0
 313. Benam KH, Villenave R, Lucchesi C, et al. Small airway-on-a-chip enables analysis of human lung inflammation and drug responses in vitro. *Nat Methods*. 2015;13(2):151-157. doi:10.1038/NMETH.3697
 314. Huang D, Liu T, Liao J, et al. Reversed-engineered human alveolar lung-on-a-chip model. *Proc Natl Acad Sci U S A*. 2021;118(19). doi:10.1073/PNAS.2016146118/SUPPL_FILE/PNAS.2016146118.SM04.MP4
 315. Campillo N, Jorba I, Schaedel L, et al. A novel chip for cyclic stretch and intermittent hypoxia cell exposures mimicking obstructive sleep apnea. *Front Physiol*. 2016;7(JUL). doi:10.3389/fphys.2016.00319
 316. Rouschop KMA, Van Den Beucken T, Dubois L, et al. The unfolded protein response protects human tumor cells during hypoxia through regulation of the autophagy genes MAP1LC3B and ATG5. *J Clin Invest*. 2010;120(1):127. doi:10.1172/JCI40027
 317. Ortmann BM, Burrows N, Lobb IT, et al. The HIF complex recruits the histone methyltransferase SET1B to activate specific hypoxia-inducible genes. *Nat Genet*. 2021;53(7):1022-1035. doi:10.1038/S41588-021-00887-Y
 318. Li Q, Ma R, Zhang M. CoCl₂ increases the expression of hypoxic markers HIF-1 α , VEGF and CXCR4 in breast cancer MCF-7 cells. *Oncol Lett*. 2017;15(1):1119-1124. doi:10.3892/OL.2017.7369/HTML
 319. Cabezas E, Teresa M, Maria P, Troncoso F, Gotera C, Mahillo I. Sleep Disordered Breathing Is Highly Prevalent in Patients with Lung Cancer : Results of the Sleep Apnea in Lung Cancer Study. 2019:119-124. doi:10.1159/000492273
 320. Papi A, Casoni G, Caramori G, et al. COPD increases the risk of squamous histological subtype in smokers who develop non-small cell lung carcinoma. *Thorax*. 2004;59(8):679-681. doi:10.1136/THX.2003.018291
 321. Dreher M, Krüger S, Schulze-olden S, et al. Sleep-disordered breathing in patients with newly diagnosed lung cancer. 2018:1-6.
 322. Keeley TP, Mann GE. Defining Physiological Normoxia for Improved Translation of Cell Physiology to Animal Models and Humans. *Physiol Rev*. 2018;99:161-234. doi:10.1152/PHYSREV.00041.2017
 323. Kim Y, Kim HS, Cui ZY, et al. Clinicopathological Implications of EpCAM Expression in Adenocarcinoma of the Lung. *Anticancer Res*. 2009;29(5). doi:10.3322/canjclin.53.1.5

324. Zhu T, Peng X, Cheng Z, Xing D, Zhang M. Diagnostic rather than prognostic markers-relationship between EpCAM overexpression and lung cancer: a meta-analysis. *Ann Palliat Med*. 2021;10(4):4025036-4024036. doi:10.21037/APM-20-2013
325. Inoue H, Ohnishi Y, Nakajima M, Kakudo K, Nozaki M. A novel function of EpCAM in oral squamous cell carcinoma cells under anchorage-independent conditions. *Int J Oncol*. 2011;39(6):1401-1405. doi:10.3892/ijo.2011.1137
326. Sarrach S, Huang Y, Niedermeyer S, et al. Spatiotemporal patterning of EpCAM is important for murine embryonic endo- and mesodermal differentiation. *Sci Reports 2018* 81. 2018;8(1):1-18. doi:10.1038/s41598-018-20131-8
327. Münz M, Kieu C, Mack B, Schmitt B, Zeidler R, Gires O. The carcinoma-associated antigen EpCAM upregulates c-myc and induces cell proliferation. *Oncogene 2004* 2334. 2004;23(34):5748-5758. doi:10.1038/sj.onc.1207610
328. Soysal SD, Muenst S, Barbie T, et al. EpCAM expression varies significantly and is differentially associated with prognosis in the luminal B HER2+, basal-like, and HER2 intrinsic subtypes of breast cancer. *Br J Cancer 2013* 1087. 2013;108(7):1480-1487. doi:10.1038/bjc.2013.80
329. Moin AT, Sarkar B, Ullah MA, Araf Y, Ahmed N, Rudra B. In silico assessment of EpCAM transcriptional expression and determination of the prognostic biomarker for human lung adenocarcinoma (LUAD) and lung squamous cell carcinoma (LUSC). *Biochem Biophys Reports*. 2021;27:101074. doi:10.1016/j.bbrep.2021.101074
330. Petrova V, Annicchiarico-Petruzzelli M, Melino G, Amelio I. The hypoxic tumour microenvironment. *Oncogenesis*. 2018;7(1):10. doi:10.1038/s41389-017-0011-9
331. Hubbi ME, Kshitiz, Gilkes DM, et al. A nontranscriptional role for HIF-1 α as a direct inhibitor of DNA replication. *Sci Signal*. 2013;6(262). doi:10.1126/SCISIGNAL.2003417/SUPPL_FILE/6_RA10_SM.PDF
332. Gordan JD, Bertout JA, Hu CJ, Diehl JA, Simon MC. HIF-2 α Promotes Hypoxic Cell Proliferation by Enhancing c-Myc Transcriptional Activity. *Cancer Cell*. 2007;11(4):335-347. doi:10.1016/j.ccr.2007.02.006/ATTACHMENT/70ED8117-86E7-431D-B08B-9A70AC349836/MMC1.PDF
333. Koshiji M, Kageyama Y, Pete EA, Horikawa I, Barrett JC, Huang LE. HIF-1 α induces cell cycle arrest by functionally counteracting Myc. *EMBO J*. 2004;23(9):1949-1956. doi:10.1038/sj.emboj.7600196
334. Zhong H, De Marzo AM, Laughner E, et al. Overexpression of Hypoxia-inducible Factor 1 in Common Human Cancers and Their Metastases 1. *CANCER Res*. 1999;59:5830-5835. <http://aacrjournals.org/cancerres/article-pdf/59/22/5830/2472894/5830.pdf>. Accessed March 21, 2022.
335. Eilertsen M, Pettersen I, Andersen S, et al. In NSCLC, VEGF-A Response to Hypoxia May Differ between Squamous Cell and Adenocarcinoma Histology. *Anticancer Res*. 2012;32:4729-4736.
336. Stegeman H, Span PN, Peeters WJM, et al. Interaction between hypoxia, AKT and HIF-1 signaling in HNSCC and NSCLC: Implications for future treatment strategies. *Futur Sci OA*. 2016;2(1). doi:10.4155/FSO.15.84/SUPPL_FILE/SUPPL_FIGURE1.TIF

337. Li C, Yang N, Chen Z, et al. Hypoxia-induced Tie1 drives stemness and cisplatin resistance in non-small cell lung carcinoma cells. *Cancer Cell Int.* 2021;21(1):1-12. doi:10.1186/S12935-020-01729-3/FIGURES/6
338. Kim H, Lin Q, Glazer PM, Yun Z. The hypoxic tumor microenvironment in vivo selects the cancer stem cell fate of breast cancer cells. *Breast Cancer Res.* 2018;20(1):1-15. doi:10.1186/S13058-018-0944-8/FIGURES/6
339. Mahoney MJ, Anseth KS. Three-dimensional growth and function of neural tissue in degradable polyethylene glycol hydrogels. *Biomaterials.* 2006;27:2265-2274. doi:10.1016/j.biomaterials.2005.11.007
340. Das M, Sharabani-Yosef O, Eliaz N, Mandler D. Hydrogel-integrated 3D-printed poly(lactic acid) scaffolds for bone tissue engineering. *J Mater Res.* 2021;36(19):3833-3842. doi:10.1557/S43578-021-00201-W/FIGURES/5
341. Jara CP, Wang O, Paulino do Prado T, et al. Novel fibrin-fibronectin matrix accelerates mice skin wound healing. *Bioact Mater.* 2020;5(4):949-962. doi:10.1016/j.BIOACTMAT.2020.06.015
342. Zhao L, Yee M, O'Reilly MA. Transdifferentiation of alveolar epithelial type II to type I cells is controlled by opposing TGF- β and BMP signaling. *Am J Physiol - Lung Cell Mol Physiol.* 2013;305(6):L409. doi:10.1152/ajplung.00032.2013
343. Bove PF, Dang H, Chelvaraju C, et al. Breaking the in vitro alveolar type II cell proliferation barrier while retaining ion transport properties. *Am J Respir Cell Mol Biol.* 2014;50(4):767-776. doi:10.1165/rcmb.2013-0071OC
344. Rice WR, Conkright JJ, Na C-L, Ikegami M, Shannon JM, Weaver TE. Maintenance of the mouse type II cell phenotype in vitro. <https://doi.org/10.1152/ajplung003022001>. 2002;283(27-2):256-264. doi:10.1152/AJPLUNG.00302.2001
345. Wang J, Edeen K, Manzer R, et al. Differentiated human alveolar epithelial cells and reversibility of their phenotype in vitro. *Am J Respir Cell Mol Biol.* 2007;36(6):661-668. doi:10.1165/rcmb.2006-0410OC
346. Falcones B, Sanz-Fraile H, Marhuenda E, et al. Bioprintable Lung Extracellular Matrix Hydrogel Scaffolds for 3D Culture of Mesenchymal Stromal Cells. *Polymers (Basel).* 2021;13(14). doi:10.3390/POLYM13142350
347. Sidhu JS, Farin FM, Kavanagh TJ, Omiecinski CJ. Effect of Tissue-Culture Substratum and Extracellular Matrix Overlay on Liver-Selective and Xenobiotic Inducible Gene Expression in Primary Rat Hepatocytes. *In Vitro Toxicol.* 1994;7(3):225. [/pmc/articles/PMC4012392/](https://pubmed.ncbi.nlm.nih.gov/12392/). Accessed May 29, 2022.
348. Dunn JCY, Tompkins RG, Yarmush ML. Hepatocytes in collagen sandwich: evidence for transcriptional and translational regulation. *J Cell Biol.* 1992;116(4):1043. doi:10.1083/JCB.116.4.1043
349. Fujita M, Spray DC, Choi H, et al. Glycosaminoglycans and proteoglycans induce gap junction expression and restore transcription of tissue-specific mRNAs in primary liver cultures. *Hepatology.* 1987;7(1 Suppl):1S-9S. doi:10.1002/HEP.1840070702
350. Buckley S, Driscoll B, Anderson KD, Warburton D. Cell cycle in alveolar epithelial type II

- cells: Integration of Matrigel and KGF. *Am J Physiol.* 1997;273(3 PART 1).
351. Fujino N, Kubo H, Suzuki T, et al. Isolation of alveolar epithelial type II progenitor cells from adult human lungs. *Lab Invest.* 2011;91:363. doi:10.1038/labinvest.2010.187
 352. Ken-Ichi Wada, Kazuyoshi Itoga, Okano, Teruo, Yonemura, Shigenobu HS. Hippo pathway regulation by cell morphology and stress fibers. *Development.* 2011;138(18):3907-3914. doi:10.1242/DEV.070987
 353. Aragona M, Panciera T, Manfrin A, et al. A mechanical checkpoint controls multicellular growth through YAP/TAZ regulation by actin-processing factors. *Cell.* 2013;154(5):1047-1059. doi:10.1016/j.CELL.2013.07.042
 354. Liu Z, Wu H, Jiang K, et al. MAPK-Mediated YAP Activation Controls Mechanical-Tension-Induced Pulmonary Alveolar Regeneration. *Cell Rep.* 2016;16(7):1810-1819. doi:10.1016/j.CELREP.2016.07.020/ATTACHMENT/CC4B651F-AF4C-477E-BEFC-69E6A946B657/MMC2.XLSX
 355. LaCanna R, Liccardo D, Zhang P, et al. Yap/Taz regulate alveolar regeneration and resolution of lung inflammation. *J Clin Invest.* 2019;129(5):2107-2122. doi:10.1172/JCI125014
 356. Chen Q, Rehman J, Chan M, et al. Angiocrine Sphingosine-1-Phosphate Activation of S1PR2-YAP Signaling Axis in Alveolar Type II Cells Is Essential for Lung Repair. *Cell Rep.* 2020;31(13). doi:10.1016/j.celrep.2020.107828
 357. Dupont S, Morsut L, Aragona M, et al. Role of YAP/TAZ in mechanotransduction. *Nature.* 2011;474(7350):179-184. doi:10.1038/nature10137
 358. Ning Q-M, Sun X-N, Zhao X-K. Role of mechanical stretching and lipopolysaccharide in early apoptosis and IL-8 of alveolar epithelial type II cells A549. *Asian Pac J Trop Med.* 2012:638-644. doi:10.1016/S1995-7645(12)60131-X
 359. Liu Z, Li S, Qian X, Li L, Zhang H, Liu Z. RhoA/ROCK-YAP/TAZ Axis Regulates the Fibrotic Activity in Dexamethasone-Treated Human Trabecular Meshwork Cells. *Front Mol Biosci.* 2021;0:859. doi:10.3389/FMOLB.2021.728932
 360. Nardone G, Oliver-De La Cruz J, Vrbsky J, et al. YAP regulates cell mechanics by controlling focal adhesion assembly. *Nat Commun.* 2017;8(1):1-13. doi:10.1038/ncomms15321
 361. Manicone AM. Role of the pulmonary epithelium and inflammatory signals in acute lung injury. *Expert Rev Clin Immunol.* 2009;5(1):63. doi:10.1586/177666X.5.1.63
 362. Fehrenbach H. Alveolar epithelial type II cell: Defender of the alveolus revisited. *Respir Res.* 2001;2(1):33-46. doi:10.1186/RR36/FIGURES/6
 363. Vlahakis NE, Schroeder MA, Limper AH, Hubmayr RD. Stretch induces cytokine release by alveolar epithelial cells in vitro. <https://doi-org.sire.ub.edu/101152/ajplung19992771L167>. 1999;277(1 21-1). doi:10.1152/AJPLUNG.1999.277.1.L167
 364. Rentzsch I, Santos CL, Huhle R, et al. Variable stretch reduces the pro-inflammatory response of alveolar epithelial cells. *PLoS One.* 2017;12(8):e0182369. doi:10.1371/JOURNAL.PONE.0182369
 365. Ito H, Uchida T, Makita K. Interactions between rat alveolar epithelial cells and bone

- marrow-derived mesenchymal stem cells: an in vitro co-culture model. *Intensive Care Med Exp*. 2015;3(15). doi:10.1186/s40635-015-0053-2
366. Romieu-Mourez R, François M, Boivin M-N, Bouchentouf M, Spaner DE, Jacques G. Cytokine Modulation of TLR Expression and Activation in Mesenchymal Stromal Cells Leads to a Proinflammatory Phenotype. *J Immunol*. 2009;182:7963-7973. doi:10.4049/jimmunol.0803864
 367. Mani A, Hotra JW, Blackwell SC, Goetzl L, Refuerzo JS. Mesenchymal Stem Cells Attenuate Lipopolysaccharide-Induced Inflammatory Response in Human Uterine Smooth Muscle Cells. *Reprod Sci*. 2020;10:335-341. doi:10.1055/s-0040-1715166
 368. Chen YC, Chang YW, Tan KP, Shen YS, Wang YH, Chang CH. Can mesenchymal stem cells and their conditioned medium assist inflammatory chondrocytes recovery? *PLoS One*. 2018;13(11):e0205563. doi:10.1371/JOURNAL.PONE.0205563
 369. Schwede M, Wilfong EM, Zemans RL, et al. Effects of bone marrow-derived mesenchymal stromal cells on gene expression in human alveolar type II cells exposed to TNF- α , IL-1 β , and IFN- γ . *Physiol Rep*. 2018;6(16):e13831. doi:10.14814/phy2.13831
 370. Lee JW, Fang X, Krasnodembskaya A, Howard JP, Matthay MA. Concise review: Mesenchymal stem cells for acute lung injury: Role of paracrine soluble factors. *Stem Cells*. 2011;29(6):913-919. doi:10.1002/stem.643
 371. Qiao R, Yan W, Clavijo C, et al. Effects of KGF on Alveolar Epithelial Cell Transdifferentiation Are Mediated by JNK Signaling. <https://doi.org/10.1165/rcmb.2007-0172OC>. 2012;38(2):239-246. doi:10.1165/RCMB.2007-0172OC
 372. Borok Z, Lubman RL, Danto SI, et al. Keratinocyte Growth Factor Modulates Alveolar Epithelial Cell Phenotype In Vitro: Expression of Aquaporin 5. <https://doi.org/10.1165/ajrcmb.1842838>. 2012;18(4):554-561. doi:10.1165/AJRCMB.18.4.2838
 373. Kyurkchiev D, Bochev I, Ivanova-Todorova E, et al. Secretion of immunoregulatory cytokines by mesenchymal stem cells. *World J Stem Cells*. 2014;6(5):552. doi:10.4252/WJSC.V6.I5.552
 374. Gaggar A, Weathington N. Bioactive extracellular matrix fragments in lung health and disease. *J Clin Invest*. 2016;126(9):3176-3184. doi:10.1172/JCI83147
 375. Salesse S, Odoul L, Chazée L, et al. Elastin molecular aging promotes MDA-MB-231 breast cancer cell invasiveness. *FEBS Press*. 2018. doi:10.1002/2211-5463.12455i
 376. Hope C, Emmerich PB, Papadas A, et al. Versican-Derived Matrikines Regulate Batf3–Dendritic Cell Differentiation and Promote T Cell Infiltration in Colorectal Cancer. *J Immunol*. 2017;199(5):1933-1941. doi:10.4049/JIMMUNOL.1700529/-/DCSUPPLEMENTAL
 377. Robison SW, Gaggar A, Xu X. A mechanism for matrikine regulation in acute inflammatory lung injury. 2021. doi:10.1172/jci.insight.140750
 378. Wells JM, Xing D, Viera L, et al. The matrikine acetyl-proline-glycine-proline and clinical features of COPD: Findings from SPIROMICS. *Respir Res*. 2019;20(1):1-9. doi:10.1186/S12931-019-1230-8/FIGURES/2
 379. Sparding N, Genovese F, Guldager D, et al. Endotrophin, a collagen type VI-derived

- matrikine, reflects the degree of renal fibrosis in patients with IgA nephropathy and in patients with ANCA-associated vasculitis. *Nephrol Dial Transplant*. April 2021:1-10. doi:10.1093/NDT/GFAB163
380. Lin P, Zhao Y, Li X, Jiang F, Liang Z. Decreased mortality in acute respiratory distress syndrome patients treated with corticosteroids: an updated meta-analysis of randomized clinical trials with trial sequential analysis. *Crit Care*. 2021;25(1). doi:10.1186/S13054-021-03546-0
 381. Agarwal R, Nath A, Aggarwal AN, Gupta D. Do glucocorticoids decrease mortality in acute respiratory distress syndrome? A meta-analysis. *Respirology*. 2007;12(4):585-590. doi:10.1111/J.1440-1843.2007.01060.X
 382. Qin M, Qiu Z. Changes in TNF- α , IL-6, IL-10 and VEGF in rats with ARDS and the effects of dexamethasone. *Exp Ther Med*. 2018;17:383-387. doi:10.3892/etm.2018.6926
 383. Mikolka P, Kosutova P, Kolomaznik M, et al. Effect of Different Dosages of Dexamethasone Therapy on Lung Function and Inflammation in an Early Phase of Acute Respiratory Distress Syndrome Model. *Physiol Res*. 2019;68(S3):S253-S263. doi:10.33549/physiolres.934364
 384. Patil RH, Naveen Kumar M, Kiran Kumar KM, et al. Dexamethasone inhibits inflammatory response via down regulation of AP-1 transcription factor in human lung epithelial cells. *Gene*. 2018;645:85-94. doi:10.1016/J.GENE.2017.12.024
 385. Chen Y, Zhang C, Xiao C xue, et al. Dexamethasone can attenuate the pulmonary inflammatory response via regulation of the lncH19/miR-324-3p cascade. *J Inflamm (United Kingdom)*. 2021;18(1):1-12. doi:10.1186/S12950-020-00266-0/FIGURES/6
 386. Chen X, Gan Y, Li W, et al. The interaction between mesenchymal stem cells and steroids during inflammation. *Cell Death Dis* 2014 51. 2014;5(1):e1009-e1009. doi:10.1038/cddis.2013.537
 387. Wang D, Sun YQ, Gao WX, Fan XL, Shi JB, Fu QL. An in Vitro and in Vivo Study of the Effect of Dexamethasone on Immunoinhibitory Function of Induced Pluripotent Stem Cell-Derived Mesenchymal Stem Cells. *Cell Transplant*. 2018;27(9):1340. doi:10.1177/0963689718780194
 388. Huh D, Matthews BD, Mammoto A, Montoya-Zavala M, Yuan Hsin H, Ingber DE. Reconstituting Organ-Level Lung Functions on a Chip. *Science (80-)*. 2010;328:1662-1668. doi:10.1126/science.1189401
 389. Zeng S, Qiao H, Lv XW, Fan D, Liu T, Xie D. High-dose dexamethasone induced LPS-stimulated rat alveolar macrophages apoptosis. *Drug Des Devel Ther*. 2017;11:3097. doi:10.2147/DDDT.S147014
 390. Yan J, Wang W-B, Fan Y-J, et al. Cyclic Stretch Induces Vascular Smooth Muscle Cells to Secrete Connective Tissue Growth Factor and Promote Endothelial Progenitor Cell Differentiation and Angiogenesis. *Front Cell Dev Biol*. 2020;0:1460. doi:10.3389/FCCELL.2020.606989
 391. Zhang B, Luo Q, Chen Z, et al. Cyclic mechanical stretching promotes migration but inhibits invasion of rat bone marrow stromal cells. *Stem Cell Res*. 2015;14(2):155-164. doi:10.1016/J.SCR.2015.01.001

392. Huang J, Zhang L, Wan D, et al. Extracellular matrix and its therapeutic potential for cancer treatment. *Signal Transduct Target Ther* 2021 61. 2021;6(1):1-24. doi:10.1038/s41392-021-00544-0
393. Katsumiti A, Ruenraroengsak P, Cajaraville MP, Thorley AJ, Tetley TD. Immortalisation of primary human alveolar epithelial lung cells using a non-viral vector to study respiratory bioreactivity in vitro. *Sci Reports* 2020 101. 2020;10(1):1-13. doi:10.1038/s41598-020-77191-y
394. Wang H, He L, Liu B, et al. Establishment and comparison of air-liquid interface culture systems for primary and immortalized swine tracheal epithelial cells. *BCM Cell Biol*. 2018;19(10). doi:10.1186/s12860-018-0162-3
395. Witherden IR, Vanden Bon EJ, Goldstraw P, Ratcliffe C, Pastorino U, Tetley TD. Primary Human Alveolar Type II Epithelial Cell Chemokine Release. *Am J Cell Mol Biol*. 2012;30(4):500-509. doi:10.1165/RCMB.4890
396. Swain RJ, Kemp SJ, Goldstraw P, Tetley TD, Stevens MM. Assessment of Cell Line Models of Primary Human Cells by Raman Spectral Phenotyping. *Biophysj*. 2010;98:1703-1711. doi:10.1016/j.bpj.2009.12.4289
397. Lou Z, Lin W, Zhao H, et al. Alkaline phosphatase downregulation promotes lung adenocarcinoma metastasis via the c-Myc/RhoA axis. *Cancer Cell Int*. 2021;21(1):1-13. doi:10.1186/S12935-021-01919-7/FIGURES/8
398. Godfrey RW. Human airway epithelial tight junctions. *Microscopy Research and Technique*. <https://analyticalsciencejournals-onlinelibrary-wiley-com.sire.ub.edu/doi/epdf/10.1002/%28SICI%291097-0029%2819970901%2938%3A5%3C488%3A%3AAID-JEMT5%3E3.0.CO%3B2-E>. Published 1997. Accessed April 13, 2022.
399. Vasan K, Werner M, Chandel NS. Mitochondrial Metabolism as a Target for Cancer Therapy. *Cell Metab*. 2020;32:341-352. doi:10.1016/j.cmet.2020.06.019

Chapter XI.
APPENDICES

APPENDIX A: FABRICATION AND CALIBRATION OF CHIPS

The use of chips for culturing cells has been a basic tool in the accomplishment of this thesis. The main advantage of this type of culture is that allows to subject the cells to certain gas concentrations and to a cyclic stretch like that occurring in the lungs. In the figure 1, we can observe the two models employed.

The static chip is composed of two parts: the upper part is the culture chamber, and the lower part is gas chamber. They are separated by a 380 μm thick PDMS membrane permeable to gases. The air goes inside the chip through the inlet tube (ID = 1.06 mm), it distributes radially through the channels, becomes in contact with the membrane -and therefore with the cells- in the gas chamber, and leaves the device through the channels that connect the air chamber with the exterior.

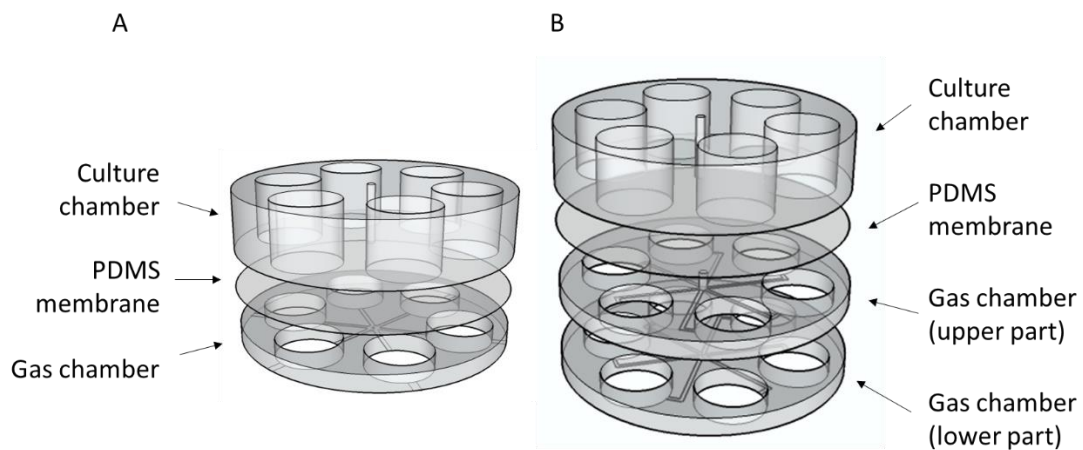


Figure 1. Three-dimensional representation of the static chip (A) is formed by two PDMS parts separated by the PDMS membrane. The stretching chip (B) is formed by three parts and the PDMS membrane separating the upper one from the other two.

The stretching chip is composed of three parts. The upper part, like in the static chip, composes the culture chamber, where cells are cultured, and the middle and the lower part compose the gas chamber. It also has an inlet tube and an outlet tube in order to control the flow of the air that abandons the chip.

1. Fabrication of chips for culturing cells at different oxygenation patterns or oxygenation patterns and stretch

MATERIALS

Reagents

- Polydimethylsiloxane (PDMS) (Dow Corning, Sylgard 184 kit, cat. no. 01064291)
- Ethanol 70% (Sigma Aldrich, Misuri)

Equipment

- Spoon (DD BioLab, cat. no. 442195)
- Plastic Pasteur pipette
- Weighing scale (PCE Instruments, Germany, PCE-BSH-6000)
- Ultimaker S5 3D printer (Ultimaker, Utrecht, Netherlands)
- Oven (Selecta, cat. no.2000200)
- Desiccator (Dynalab, NY, cat. no. 243045)
- Hand-held corona treater (Electro Technic Products, BD-20AC model)
- 200 μ l pipette tips (Eppendorf, cat. no 4130075)
- Weighing boats (VWR International, cat. no. 611-0094)
- Scalpel (Swann Morton, cat. no. 0206)
- Tweezers (VWR International, cat. no. 232-0111)
- Gel-Pak membranes (Gel-Pak, cat. no. PF-40x40-0065-X4)
- Punch (Harris Uni-Core)
- Petri dish (TPP, Switzerland, cat. no. 93100)
- Tube ID = 1.06mm; OD = 1.67 mm (Cole Parmer, cat. no. 06417-41)
- Drill (Dormer, cat. no. A100 1.0)

PROCEDURE

A) Design and fabrication of the molds to create the PDMS pieces.

In order to construct the chips, the first step is to design a mold with the negative shape of the parts needed to build the chip. For doing that, the Ultimaker Cura software is employed. The parts are printed with the Ultimaker 3D printer in polylactic acid (PLA).

For the stretching chip, an additional part should be printed. It is a funnel-like piece that will be placed in the bottom part of the petri dish where the chip is adhered. Its function is to allow the connection of a tube to the chip outlet to release the air.

B) Construction of the chip.

The construction of the static and stretching chip is mainly the same. There are some steps (7, 14) that only take place in the stretching chip.

1. The desired amount of polydimethylsiloxane is poured into a weighting boat and add the curing agent in a proportion 1/10 (w/w).
2. Mix it vigorously with the help of a plastic Pasteur pipette. **CAUTION:** the mixture obtained should be homogeneous to allow a correct polymerization.
3. Once it is well mixed, the weighting boats are placed in the desiccator to remove the bubbles for around 30 minutes.

4. The mixture is poured into the printed PLA molds and placed again in the desiccator for another 30 minutes.
5. The molds containing the PDMS are placed in the oven for 2 hours at 60 °C.
6. They are removed from the molds with the help of a spatula. **NOTE:** 70% ethanol can be added to make the detachment easier.
7. This step is only applicable to the stretching chip. Before attaching the lower and the middle part together to form the gas chamber, the middle part must be pierced with a punch in the center. The surface of the lower part (with the channels upside down) and the surface of the middle part are treated for two minutes each with the hand-held corona. Afterward, they are attached together so that the wells of both parts coincide perfectly. All the edge is sealed with non-polymerized PDMS and allowed to polymerize for 30 minutes at 60 °C. **NOTE:** to improve the adherence of both parts, put some weight on them for 15 minutes approximately, prior the edge sealing.
8. The commercial PDMS membranes are protected between two pieces of plastic. The thinner one is removed so the PDMS membrane is exposed. Treat the surface with the hand-held corona for two minutes.
9. The surface of the gas chamber (composed by the lower part in the case of the static chip and by the lower and the middle part in the stretching chip) is also treated for 2 minutes with the hand-held Corona. After that, it is placed over the already treated PDMS membrane and pressure is made to ensure the correct adhesion of the whole surface.
10. All the perimeter of the PDMS part attached to the membrane is sealed with non-polymerized PDMS with the help of a 200 μ L pipette tip and placed in the oven at 60 °C for 30 minutes.
11. With the help of a scalpel, the remaining parts of the PDMS membrane are removed. The membrane and the lower part attached to it are pulled apart from the PDMS membrane protective plastic.
12. The surface of the upper part is covered with non-polymerized PDMS and placed carefully on the membrane attached to the lower part, making the wells of the upper and lower part coincide. **NOTE:** the amount of non-polymerized PDMS should be enough to adhere the two parts correctly but not too much because the membrane inside the wells could result "flood".

13. Both chambers are pierced with a punch in the case of the static chip. In the case of the stretching chip, the culture chamber is pierced making the new hole coincide with the one made previously in the step 7.
14. Next, chip will be adhered to a petri dish. For the stretching-chip, a 1 cm diameter hole should be previously done in the middle of the petri dish.
15. The lower part of the chip is covered with non-polymerized PDMS and placed over a petri dish and let it 30 minutes at 60°C
16. 10 cm of tube (1.06 mm ID × 1.68 mm OD) are introduced in the pierced chip and the hole is sealed with non-polymerized PDMS and let it 30 minutes at 60°C
17. The lid of the petri dish is pierced with drill to let the tube out.

2. Assessment of gas equilibrium kinetics

Once the chips are fabricated, they must be verified for correct oxygen diffusion, especially in the static chip, where rapid changes in the PO_2 are required. For assessing this issue, a fiber-optic oxygen meter is employed. This sensor, which is based on the REDFLASH technology, has an ultra-fast response time (< 0.3 s), allowing to perform the measurements of the hypoxia and reoxygenation cycles in an accurate way. The REDFLASH indicator is placed on the sensor tip, which is excitable at 610-630 nm (orange-red light) and has an oxygen-dependent emission at 760-790 nm (near-infrared). In an oxygenated environment, oxygen molecules will collide with the sensor tip and quench the emission of luminescence, while in an anoxic environment, the emission of the fluorescence in the near-infrared (NIR) will reach the maximum (figure 2). The phase shift between the orange-red light and the NIR fluorescence is measured by the Profix Software and converted into oxygen units according to the Stern-Volmer theory. Also, precise temperature compensation is performed using an external temperature sensor for correct measurement and conversion to oxygen units.

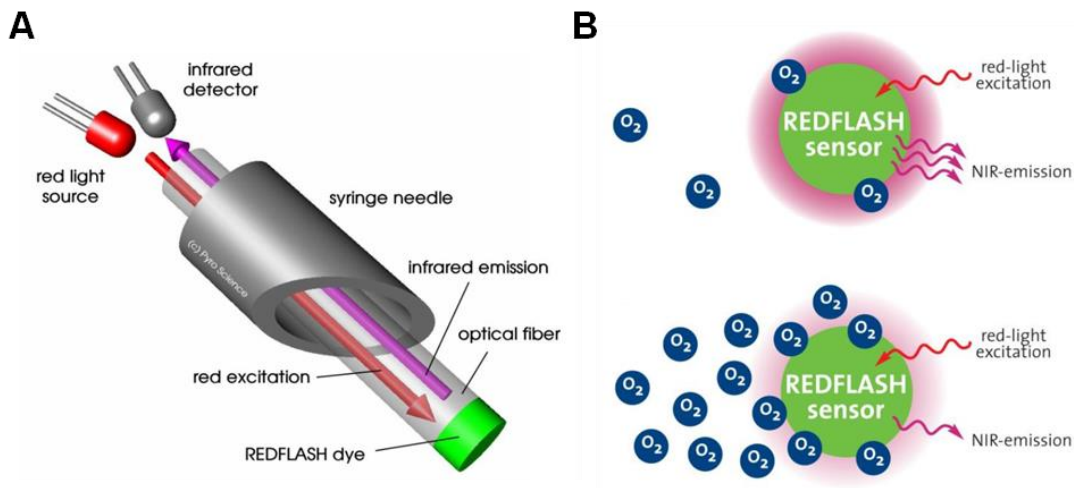


Figure 2. Optical fiber oxygen sensor and its measuring principle. The REDFLASH dye is excited by the red light and its emission is detected by the infrared detector (A). The resulting REDFLASH emission is quenched by the oxygen molecules in the sample, so the emission is indirectly proportional to the oxygen concentration. (B)

MATERIALS

Reagents

- Distilled water
- MilliQ water
- PBS 1X (Gibco, Massachusetts, cat. no. 10010-015)
- Sodium Hydroxide (Sigma, cat no 1310-73-2)
- Sodium Ascorbate (Sigma, cat no 134-03-2)

Equipment

- Fiber-optic oxygen meter, FireSting-O₂ (PyroScience, cat. no. FSO2-x)
- Profix software (PyroScience)
- Retractable needle-type optical oxygen sensor (PyroScience, cat. no. OX50)
- Submersible temperature sensor (PyroScience, cat. no. TSub21)
- Laptop computer
- Z micromanipulator (Thorlabs Inc., cat. no. MT1/M)
- MCQ Gas Mixture Creator Software (MCQ Instruments)
- Gas Blender mixer (MCQ Instruments, Gas blender 100 Series model)
- Pressurized N₂, O₂ and CO₂ sources

- 50 ml falcon tube (Corning, cat. no. 352070)
- Weighting boats (VWR International, cat. no. 611-0094)
- 100 ml Erlenmeyers (VWR, cat. no. 214-1156)
- 100-1000 μ l micropipette
- 1000 μ l pipette tips (Eppendorf, cat. no. 4130135)
- Precision balance scale (PCE Instruments, Germany, PCE-BSK 310)
- Spoon (DD BioLab, cat. no. 442195)
- Vortex (Scientific Industries, Vortex Genie 2 model)

Reagent Setup

- Sodium hydroxide and sodium ascorbate solution (0.1 M): using two weighting boats, weight 0.2 g of NaOH and 1 g of sodium ascorbate. Transfer both of them to a 50 mL conical tube and add 50 mL of milliQ water. Vortex vigorously until obtaining a homogeneous solution.
- Oxygenated water: employing a gas blender and the MCQ Gas Mixer Software, bubble milliQ water

contained in an Erlenmeyer flask with a gas mixture containing 20% O₂ and 0% CO₂ at the maximum

flow provided by the device (400 mL/min) for 10 minutes.

PROCEDURE

1. Before performing the oxygen measurements in the chips, the calibration of the oxygen probe should be carried out.
 - 1.1 Connect the FireSting-O₂ oxygen sensor and the optical temperature sensor to their connectors in the FireSting-O₂ device after removing the protective caps.
 - 1.2 Connect the FireSting-O₂ read-out device with the USB cable to the computer and run the Profix Software.
 - 1.3 Introduce the Sensor Settings (sensor code, oxygen unit and temperature compensation).
 - 1.4 Select the 2-point sensor calibration in aqueous samples. For setting the 20% O₂ point a water solution previously bubbled with 20% O₂ and 0% CO₂ is employed. For setting the point at 0% of O₂, a 0.1 M sodium hydroxide and sodium ascorbate solution is employed. **CAUTION:** it is photosensitive, protect it from light to avoid the degradation of the components.
 - 1.5 Protective cap should be removed from the oxygen sensor prior to introduction in the solution. The probe should be ejected and completely introduced into the sodium sulfate solution, together with the temperature sensor. Wait until the oxygen measurement is stable and select "Set 0%". **NOTE:** For ensuring a correct calibration, before setting both points, the temperature sensor measurement must be stable too and no bubbles should be in the solution.
 - 1.6 Repeat the previous step with the oxygenated solution this time. Once the measurement is stable, press "Set air" button.
 - 1.7 For finishing the calibration, select "Finish".
2. Open the N₂, CO₂ and O₂ sources, connect the gas blender to the computer with the USB cable and switch on the computer and the device.
3. Connect the outlet from the gas blender device to the chip inlet tube employing an ID=1.67 mm diameter flexible tube.
4. Using the MCQ Gas Mixture Creator Software select the desired concentration of gases (13% O₂, 5% CO₂ and 82% N₂ or 7% O₂ and 5% CO₂ and 88% N₂) or design a program

to reproduce the oxygenation-deoxygenation cycles (swings every 30 seconds from 13% O₂, 5% CO₂, 82% N₂ to 7% O₂, 5% CO₂, 88% N₂, or swings every 30 seconds from 7% O₂, 5% CO₂, 88% N₂ to 4% O₂, 5% CO₂, 92% N₂).

5. Place the oxygen probe in a holder that allows micromanipulation on Z axis.
6. Cover the wells with 1 mL of PBS 1X.
7. Extract the retractable tip from the oxygen sensor, and place it carefully, with the help of the micromanipulator on the surface of the PDMS membrane. Place the temperature probe inside the well.
8. The measurement will take place when pressing the buttons “Measurement start” and “Log to file” in the Profix Software

3. Assessment of membrane strain

The design of the stretch chip and the elastic properties of the PDMS membrane, allows it to deflect and subject the cells seeded on the surface of the membrane to strain. As previously explained, it is composed by the culture chamber (upper part) and the gas chamber (middle and lower part), and an inlet tube, through which the desired gas mixture from the gas blenders goes inside the device, and an outlet tube, that will be connected to a proportional valve that opens and closes every 5 seconds (0.2 Hz), which is the physiological breathing frequency. Placed just before the valve, a tube with a small diameter can be found. It works as a leakage, releasing part of the air in the system when the valve is closed. That way, the pressure inside the system can be modulated by increasing the size of the tube (the resistance will increase so less air will be able to abandon the system and the pressure will increase) or decreasing it (the resistance will decrease, and the air will be able to leave the system more easily). Before going inside the chip, with the aim of humidifying the air, it will go inside a water trap (50 mL falcon tube with an inlet tube that is submerged in water and an outlet tube that will be in contact with the air chamber inside the falcon). Also, when abandoning the chip, the air will find another water trap in this case for getting rid of all the humidity before arriving to the small tube working as leakage and the valve (figure 3). **CAUTION:** If there is some humidity in the air, the water will condensate inside the tubes when abandoning the incubator due to the change of temperature and can block the way out. In that case, the pressure in the system will increase and the previously set values of strain will change.

Connected between the water trap to dry the air and the leakage, there is a pressure transductor connected to an oscilloscope to measure the pressure of the system.

The itinerary that the air follows is:

1. The gas mixture coming from the gas blender gets humid in the water trap inside the incubator.
2. Humid air goes inside the chip through the inlet tube.
3. It expands radially through the channels of the middle part.
4. It gets in contact with the inferior part of the membrane in the gas chamber and inflates it (if the valve is closed) or not (if the valve is opened).
5. It leaves the gas chamber through the channels of the lower part.
6. It leaves the chip through the outlet tube.
7. It gets dry in the water trap outside the incubator.
8. When the valve is opened, it leaves the system through the open valve.
9. When the valve is closed, it leaves the system through the resistance, causing the stretch of the membrane.

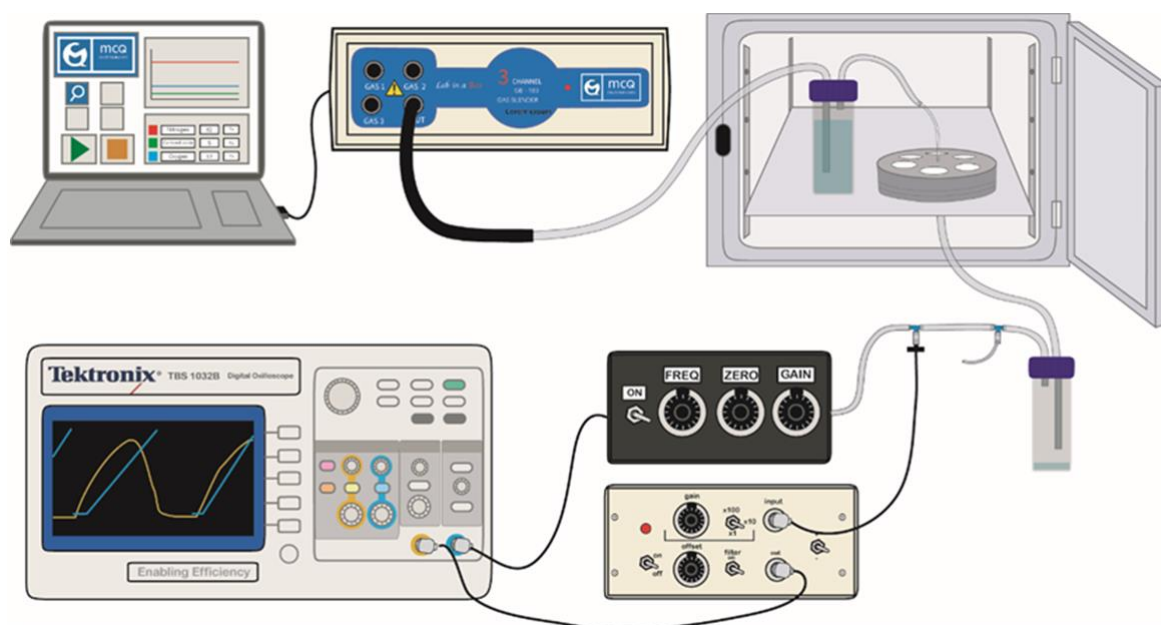


Figure 3. Experimental setup. The drawing shows how the air path from the gas blender, controlled by the software, to the valve, through the chip and the two water traps to initially humidify and finally de-humidify the gas. Cyclic stretch-generating pressure is measured along the experiment with the pressure sensor, the signal transducer and the oscilloscope

4. Calibration of stretching-chips

The stretch of the membranes of the chips depends on the pressure inside the system, which can be modulated in two different ways: by changing the length of the leakage or by increasing the airflow. In this case, every chip should be connected to the same airflow (180 mL/min), so the length of the leakage is adjusted for them to experience a 10% of surface strain.

The strain of the membrane can be calculated with the formula below, where h is the height of the strained membrane (calculated as the difference in the z position between the relaxed position of the membrane and the deflected one), and r is the radius of the well.

$$\varepsilon = \frac{2}{3} \cdot \left(\frac{h}{r}\right)^2$$

APPENDIX B: ISOLATION OF PRIMARY LUNG CELLS

1. Isolation of alveolar type II cells

Alveolar type II cells are the most abundant type of cells that forms the alveoli. The study of their behavior is crucial for the understanding of the development of many respiratory diseases. However, these cells present an important limitation which is the impossibility of subculturing them. For that reason, the number of studies in the literature employing primary ATII are limited. Here I explain the process to isolate primary ATII that is required in order to carry out every replicate of the ARDS model.

MATERIALS

Reagents

- Urethane (Sigma, cat. no. 51-79-6)
- DCCM-1 medium (Biological Industries, cat. no. 05-010-1A)
- Penicillin/streptomycin solution (Sigma, cat. no P4333)
- Amphotericin B solution (Sigma, cat. no. A2942)
- PBS 1X (Gibco, Massachusetts, cat. no. 10010-015)
- Glutamine 2.5 mM (Gibco, Massachusetts)
- Trypan Blue (Sigma, cat. no. T8154)
- Fetal Bovine Serum (Gibco, cat. no. 10270106)
- Trypsin (Sigma, cat. no T4799)
- DNase (Sigma, cat no 04536282001)

- Percoll (GE HealthCare, Illinois)
- Phenol Red (Sigma, 143-74-8)
- NaCl (Sigma, cat no S9888)
- KCl (Sigma, cat no P5405)
- CaCl₂ (Sigma, cat no C1016)
- MgSO₄ (Sigma, cat no 63136)
- KH₂PO₄ (Sigma, cat no P5655)
- NaH₂PO₄ (Sigma, cat no 243663)
- HEPES (Sigma, cat no 7365-45-9)
- Glucose (Gibco, cat no G8270)

Equipment

- Centrifuge (Heraeus Instruments, Labofuge 400R model)
- Cell culture incubator (Thermo Scientific Heracell 150i CO₂ incubator)

- Laminar flow cabinet for cell culture (Scanlaf Mars Safety Class 2)
- Centrifuge (Heraeus Instruments, Labofuge 400R model)
- Optical microscope (Olympus Life Science, CKX31 model)
- Vortex (Scientific Industries, Vortex-Genie 2 model)
- Hemocytometer (VWR, MARI0640011)
- 250 ml sterile borosilicate bottle (VWR 590-0834)
- 5 ml sterile serological pipettes (Greiner Bio-One, cat. no. 606180)
- 10 ml sterile serological pipettes (Greiner Bio-One, cat. no. 607180)
- 25 ml sterile serological pipettes (Greiner Bio-One, 760180)
- Pipettor (Pipet-Aid, XP model)
- 15 ml sterile Falcon tube (Corning, cat. no. 652095)
- 0.5 ml sterile tube (Eppendorf, cat. no 022363611)
- 0.5-10 μ l micropipette (Eppendorf, cat. no. ES-10)
- 20-200 μ l micropipette (Eppendorf, cat. no., ES-200)
- 100-1000 μ l micropipette (Eppendorf, cat. no., ES-1000)
- 10 μ l pipette tips (Eppendorf, cat. no 0030000854)
- 200 μ l pipette tips (Eppendorf, cat. no 0030000897)
- 1000 μ l pipette tips (Eppendorf, cat. no 0030000927)
- Magnetic stirrer (Velp Scientifica, MST, model 100-240 V / 50-60 Hz)
- Precision balance scale (PCE Instruments, Germany, PCE-BSK 310)
- 23 G needle (BD, cat no 300800)
- Scalpel (Swann Morton, cat. no. 0206)
- 2.5 mL syringe (BD, cat no 309658)
- 10 mL syringe (BD, cat no 305959)
- Suture (Silkam, cat no 0762075)
- Petri dishes (TPP, Switzerland, cat. no. 93100)
- 50 mL conical tubes (Corning, cat. no. 352070)
- Sterile Pasteur pipettes (Deltalab, cat. no. 200006C)
- 100 μ m cell strainer (Thermo Scientific; 22-363-549)
- 40 μ m cell strainer (Thermo Scientific; 22-363-547)
- Vacuum filters (Nalgene, cat no Z358207-1CS)

Reagent Setup

- **Urethane 20%:** weight in a scale 20 grams of urethane. Add 100 mL of ultrapure distilled sterile water and agitate with a magnetic stirrer until the urethane is completely dissolved.
- **Free Ca^{2+} and Mg^{2+} solution:** this solution is employed for preparing the DNase solutions. The reagents in the table below are weighted and diluted in ultrapure sterile distilled water. The pH is adjusted to 7.4 and it is filtrated and kept at room temperature.
- **Solution containing Ca^{2+} and Mg^{2+} :** this solution is employed for preparing the Trypsin solution. The reagents in the table below are weighted and diluted in ultrapure sterile distilled water. The pH is adjusted to 7.4 and it is filtrated and kept at room temperature.
- **Trypsin solution 0.25%:** 125 mg of trypsin are weighted and dissolved in 50 mL of the solution containing Ca^{2+} and Mg^{2+} previously prepared.
- **DNase solution (I):** 6.16 mg of DNase are weighted and diluted in 25 mL of the free Ca^{2+} and Mg^{2+} solution prepared previously. The final concentration is 0.24624 mg/mL.
- **DNase solution (II):** 2.5 mg of DNase are weighted and diluted in 50 mL of the free Ca^{2+} and Mg^{2+} solution prepared previously. The final concentration is 0.05 mg/mL.
- **DCCM-1 complete medium:** DCCM-1 medium is supplemented with a 10% FBS, 1% glutamine 2,5

mM and 1% of antibiotics mix (streptomycin, penicillin and amphotericin). **NOTE:** It is stored at 4°C up to a month.

- **Percoll solutions (high/low):** add the volumes of the reagents in the table to create the high-concentrated Percoll solution and the low-concentrated Percoll solution.
- **Phosphate Buffer Solution:** this is the solution employed for preparing the Percoll gradients. The solutes in the table below should be weighted and then diluted in ultrapure distilled

water through magnetic agitation. pH should be adjusted until 7.4 and finally, the solution is autoclaved and stored at 4°C.

- **10x solution:** this solution is also employed for preparing the Percoll gradients. The solutes in the table below should be weighed and then diluted in ultrapure distilled water through magnetic agitation. pH should be adjusted until 7.4 and finally, the solution is filtrated and stored at room temperature.

Solution containing Ca ²⁺ and Mg ²⁺	
NaCl	4.5 g
CaCl ₂	0.24 g
KCl	0.222 g
MgSO ₄	0.12 g
Glucose	0.63 g
HEPES	1.432 g
Phosphate Buffer Solution	15 mL
H ₂ O	500 mL

Solution Ca ²⁺ and Mg ²⁺ free	
NaCl	4.5 g
KCl	0.222 g
Glucose	0.63 g
HEPES	1.432 g
Phosphate Buffer Solution	15 mL
H ₂ O	500 mL

10x Solution	
NaCl	4.5 g
KCl	0.22 g
Glucosa	0.42 g
KH ₂ PO ₄	0.212 g
HEPES	1.432 g
H ₂ O	50 mL

Phosphate Buffer Solution	
NaCl	8.72 g
KCl	0.20 g
KH ₂ PO ₄	0.20 g
Na ₂ HPO ₄	0.15 g
H ₂ O	1 L

Percoll Gradients				
Gradient	X10	FBS	H ₂ O	Percoll
Heavy	1.5 mL	0.075 mL	3.75 mL	9.75 mL
Light	1.5 mL	0.075 mL	9.45 mL	4.05 mL

PROCEDURE

1. The rat (200 grams) is anesthetized with an intraperitoneal injection of 7.5 mL/kg of animal weight of urethane at 20%.
2. Check the animal reflexes by pressing with some tweezers on the feet. If it has still reflexes, administrate half of the previous dose and check again the reflexes after some minutes.
3. It is placed in the supine position and ethanol soaked. The abdominal cavity is opened, and the vena cava is cut off to release the blood. **CAUTION:** the speed is crucial from this point since the heart beating is needed to perform proper perfusion of the lungs.
4. The diaphragm is cut off and the chest cavity is opened to show the lungs and the heart. The right ventricle is sectioned off to introduce through the pulmonary artery a 16 G cannula that is connected to a saline solution dropper.
5. A tracheotomy is performed to introduce a 14 G cannula through the trachea.
6. While the key of the dropper is opened and the lungs are being perfused, lungs are inflated 5 times with 10 mL of air with a syringe through the trachea.
7. Once lungs are free of blood, they are excised in bloc keeping the trachea. The heart is removed.
8. Five bronchioalveolar lavages are performed to get rid of the alveolar macrophages. To do so, the lungs are fluxed with 10 mL of saline and then are placed upside down on an opened 50 mL conical tube with a piece of paper -bent so it looks like a W- around them to avoid them falling inside the tube once they are empty.
9. Lungs are placed inside a 500 mL glass bottle containing 200 mL of PBS 1x. A 14 G cannula is tightly tied to the trachea with a suture and 50 mL of trypsin solution is perfused by gravity for 30 minutes with a 10 mL syringe. All this process is carried out inside the water bath at 37°C. **NOTE:** the speed of the perfusion can be altered by the volume of the lung submerged in the PBS. The more submerged it is, the slower the trypsin will perfuse.
10. Inside the laminar flow cabinet, lungs are placed on petri dishes, and non-alveolar parts are removed. Trypsin reaction is stopped with 5 mL of Fetal Bovine Serum (FBS). **CAUTION:** when working with more than one lung at the same time, it is important to make some big cuts in the lungs to allow the FBS go inside the tissue before going to the next step in order to avoid the over-digestion of the lungs by the trypsin.

11. Lobes are cut into 1 mm² piece and are placed inside 50 mL conical tubes. DNase solution I is added until the total volume is 20 mL. This solution is agitating for 4 minutes at room temperature.
12. The solution is strained twice consecutively, the first time with a 100 µm strainer, and the second one with a 40 µm strainer.
13. Percoll gradient is prepared by placing the low-concentrated Percoll solution on the high-concentrated Percoll solution. **NOTE:** it is important to prepare the gradient in the very moment of using it to avoid the phases mixing.
14. Double-filtered cell suspension is placed on the Percoll gradient **NOTE:** It is crucial to make steps 13 and 14 carefully in order to form a perfect gradient (13) and not to disturb it (14)
15. Percoll gradients are centrifuged during 20 minutes at 500 G at room temperature with no acceleration or brake.
16. After centrifugation, a white line is formed between the two gradients, which should be collected with a Pasteur pipette and placed in a conical tube. DNase solution II should be added until the final volume is 40 mL.
17. The solution is centrifuged at 500 G for 15 minutes at room temperature, with acceleration, and breaks at 9.
18. Supernatant is discarded and pellet is resuspended in complete DCCM-1 medium. The cell suspension is placed in petri dishes for 1 hour to allow the interstitial macrophages to adhere to the surface. **NOTE 1:** if after one hour the petri dish surface is completely covered by cells, place the suspension in a new petri dish for an extra hour. **NOTE 2:** the presence of ciliated cells seen at the phase contrast microscope in this step is a signal that the extraction is made properly.
19. Centrifuge the cell suspension at 500 G for 8 minutes at room temperature
20. After that centrifugation, cells are ready to culture.

2. Isolation of lung mesenchymal stem cells

Mesenchymal stem cells are cells with multipotent differentiation capacity that can be isolated from bone marrow, adipose, and other tissues. In this case, these cells are isolated from lungs. Unlike ATII, they have the ability to proliferate in vitro.

MATERIALS

Reagents

- Urethane (Sigma, cat. no. 51-79-6)

- DCCM-1 medium (Biological Industries, cat. no. 05-010-1A)
- Penicillin/streptomycin solution (Sigma, cat. no. P4333)
- Amphotericin B solution (Sigma, cat. no. A2942)
- PBS 1X (Gibco, Massachusetts, cat. no. 10010-015)
- Glutamine 2.5 mM (Gibco, Massachusetts)
- Trypan Blue (Sigma, cat. no. T8154)
- Fetal Bovine Serum (Gibco, cat. no. 10270106)
- Trypsin (Gibco, Massachusetts, cat. no. 25200056)
- DMEM (Gibco, cat. no. 10313021)
- Collagenase
- HEPES (Sigma, cat. no. 7365-45-9)

Equipment

- Centrifuge (Heraeus Instruments, Labofuge 400R model)
- Cell culture incubator (Thermo Scientific Heracell 150i CO₂ incubator)
- Laminar flow cabinet for cell culture (Scanlaf Mars Safety Class 2)
- Centrifuge (Heraeus Instruments, Labofuge 400R model)
- Optical microscope (Olympus Life Science, CKX31 model)
- Vortex (Scientific Industries, Vortex-Genie 2 model)
- Hemocytometer (VWR, MARI0640011)
- 250 ml sterile borosilicate bottle (VWR 590-0834)
- 5 ml sterile serological pipettes (Greiner Bio-One, cat. no. 606180)
- 10 ml sterile serological pipettes (Greiner Bio-One, cat. no. 607180)
- 25 ml sterile serological pipettes (Greiner Bio-One, 760180)
- Pipettor (Pipet-Aid, XP model)
- 15 ml sterile Falcon tube (Corning, cat. no. 652095)
- 0.5 ml sterile tube (Eppendorf, cat. no. 022363611)
- 0.5-10 µl micropipette (Eppendorf, cat. no. ES-10)
- 20-200 µl micropipette (Eppendorf, cat. no., ES-200)
- 100-1000 µl micropipette (Eppendorf, cat. no., ES-1000)
- 10 µl pipette tips (Eppendorf, cat. no. 0030000854)
- 200 µl pipette tips (Eppendorf, cat. no. 0030000897)
- 1000 µl pipette tips (Eppendorf, cat. no. 0030000927)
- 18 G needle (BD, 400070)
- 23 G needle (BD, cat. no. 300800)
- 2.5 mL syringe (BD, cat. no. 309658)
- 10 mL syringe (BD, cat. no. 305959)
- 50 mL syringe (BD, cat. no. 309653)
- Petri dishes (TPP, Switzerland, cat. no. 93100)
- Scalpel (Swann Morton, cat. no. 0206)
- 50 mL conical tubes (Corning, cat. no. 352070)
- Sterile Pasteur pipettes (Deltalab, cat. no. 200006C)
- Glass Pasteur pipettes (VWR, Pennsylvania, cat. no. 612-3814)
- 100 µm cell strainer (Thermo Scientific; 22-363-549)
- 250 µm tissue strainers (Thermo Scientific; 87791)
- 75 cm² flasks (Techno Plastic Products, cat. no. 90025)

Reagent Setup

- **Urethane 20%:** weigh in a scale 20 grams of urethane. Add 100 mL of ultrapure distilled sterile water and agitate with a magnetic stirrer until the urethane is completely dissolved.
- **DMEM complete medium:** DMEM medium is supplemented with a 10% FBS and 1% of antibiotics mix (streptomycin, penicillin and amphotericin). **NOTE:** It is stored at 4°C up to a month.
- **Collagenase solution 250 U/mL:** mix 15 mg of collagenase in 9 mL of DMEM and 1 mL of HEPES.

- **Red Blood Lysis Buffer (RBC)**: dilute 1:10 the RBC in distilled water.

PROCEDURE

1. The rat (200 grams) is anesthetized with an intraperitoneal injection of 7.5 mL/kg of animal weight of urethane at 20%.
2. Check the animal reflexes by pressing with some tweezers the feet. If it has still reflexes, administrate half of the previous dose and check again the reflexes after some minutes.
3. It is placed in supine position and ethanol soaked. The abdominal cavity is opened, and the vena cava is cut off to release the blood. **CAUTION**: the speed is crucial from this point since it is needed the heart beating to perform a proper perfusion of the lungs.
4. The diaphragm is cut off and the chest cavity is opened to show the lungs and the heart. A 19 G needle is introduced in the right ventricle and 50 mL of PBS 1X are fluxed inside.
5. Once lungs are free of blood, they are excised in bloc keeping the trachea. The heart is removed.
6. Lungs are cut in small pieces around 1 mm² and the collagenase solution is added.
7. The solution is filtrated with the tissue strainer and the reaction acts for 30 minutes at 37°C.
8. After that time, the reaction is stopped with 5 mL of FBS and it is filtrated again using a 100 µm filter.
9. The solution is centrifugated at 800 G for 10 minutes.
10. The supernatant is discarded and the pellet is resuspended for 8 minutes in RBC.

APPENDIX C: CELL CULTURE ON CHIPS AND ON LUNG HYDROGELS ADHERED TO THE CHIP SURFACE

1. Culture of cancer cells on PDMS membranes

MATERIALS

Reagents

- Trypsin (Gibco, Massachusetts, cat. no. 25200056)
- Collagen (Cultrex, cat. no. 3440-100-01)
- Fibronectin (Sigma, 10838039001)
- Penicillin/streptomycin solution (Sigma, cat. no P4333)
- Amphotericin B solution (Sigma, cat. no. A2942)
- PBS 1X (Gibco, Massachusetts, cat. no. 10010-015)
- Trypan Blue (Sigma, cat. no. T8154)

- RPMI medium (Thermo Fisher, cat. no. 21875091)
- Fetal Bovine Serum (FBS) (Gibco, cat. no. 10270106)

Equipment

- Plasma Cleaner (Harrick Scientific Products Inc., PDC-002 model)
- Centrifuge (Heraeus Instruments, Labofuge 400R model)
- Cell culture incubator (Thermo Scientific Heracell 150i CO₂ incubator)
- Laminar flow cabinet for cell culture (Scanlaf Mars Safety Class 2)
- Centrifuge (Heraeus Instruments, Labofuge 400R model)
- Optical microscope (Olympus Life Science, CKX31 model)
- Vortex (Scientific Industries, Vortex-Genie 2 model)
- Hemocytometer (VWR, MARI0640011)
- 250 ml sterile borosilicate bottle (VWR 590-0834)
- 5 ml sterile serological pipettes (Greiner Bio-One, cat. no. 606180)
- 10 ml sterile serological pipettes (Greiner Bio-One, cat. no. 607180)
- 25 ml sterile serological pipettes (Greiner Bio-One, 760180)
- Pipettor (Pipet-Aid, XP model)
- 15 ml sterile Falcon tube (Corning, cat. no. 652095)
- 0.5 ml sterile tube (Eppendorf, cat. no. 022363611)
- 0.5-10 μ l micropipette (Eppendorf, cat. no. ES-10)
- 20-200 μ l micropipette (Eppendorf, cat. no., ES-200)
- 100-1000 μ l micropipette (Eppendorf, cat. no., ES-1000)
- 10 μ l pipette tips (Eppendorf, cat. no. 0030000854)
- 200 μ l pipette tips (Eppendorf, cat. no. 0030000897)
- 1000 μ l pipette tips (Eppendorf, cat. no. 0030000927)

PROCEDURE

Treatment of the PDMS surface

1. PDMS surface is activated by introducing the chip in the Plasma Cleaner for 2 minutes at maximum voltage for making the surface hydrophilic. CAUTION: next step should be performed immediately to avoid the loss of the surface activation (maximum time 1 hour)
2. Then, the chip is introduced in the culture chamber and irradiated with UV light for 10 minutes to accomplish sterilization. The chip should be placed near the source of the light (~20 cm).
3. PDMS surface is covered with 0.1 mg/mL collagen or 0.01 mg/mL fibronectin solution, alternatively for 45 minutes in an incubator. During this time, the trypsinization of cancer cells can be performed. NOTE: make sure that the whole surface is covered by the coating.

Cell seeding

4. Trypsinize the cancer cells (H522, H1437, H520, H1975) following the next steps:
 - 4.1 Remove the medium with a sterile glass Pasteur pipette.
 - 4.2 Add 5 mL of PBS 1x to remove the rest of the medium.
 - 4.3 Add 0.5 mL of Trypsin/EDTA and leave it for 5 minutes in the cell culture incubator
 - 4.4 Add 5 mL of culture medium to stop the reaction. **CAUTION:** Before stopping the reaction, check in the optical microscope that all the cells have detached.
 - 4.5 Transfer the content into a 15 mL falcon and centrifuge it at 350 G for 5 minutes.
5. Count the cells in a hemocytometer
 - 5.1 Take a small aliquote of the cell suspension and dilute it in 1:1 v/v with trypan blue. Mix it well with micropipette.
 - 5.2 Place 10 μ L of the solution and place it carefully in the hemocytometer chamber
 - 5.3 Count the cells and calculate the cell concentration.
6. Seed the cells on the wells
 - 6.1 Take the chips from the incubator, aspire the fibronectin solution, and perform three washes with PBS 1X. **CAUTION:** leave the third wash to avoid the membrane to dry.
 - 6.2 Take the desired volume of the initial cell solution and place it in a 15 mL falcon. Dilute it with RPMI medium so the final concentration is 600.000 cells/mL
 - 6.3 Add 500 ul from the just prepared cell solution, so the final amount of cells in each well is 300.000.
7. Leave it in the incubator overnight for cells to adhere to the surface. Next day, proceed to the connection to the desired gas parameters.

2. Culture of cells in and on hydrogels adhered to the PDMS membranes

MATERIALS

Reagents

- DCCM-1 medium (Biological Industries, cat. no. 05-010-1A)
- Trypsin neutralization solution (Thermo Scientific, R002100)
- Tryple trypsin (Thermo Scientific, 12605036)
- Penicillin/streptomycin solution (Sigma, cat. no P4333)
- Amphotericin B solution (Sigma, cat. no. A2942)
- PBS 1X (Gibco, Massachusetts, cat. no. 10010-015)
- Trypan Blue (Sigma, cat. no. T8154)
- APTES (Sigma, 440140)
- NaOH (Sigma, cat no 1310-73-2)
- HCl (Sigma, cat no 320331)

Equipment

- Centrifuge (Heraeus Instruments, Labofuge 400R model)
- Cell culture incubator (Thermo Scientific Heracell 150i CO2 incubator)
- Laminar flow cabinet for cell culture (Scanlaf Mars Safety Class 2)
- Centrifuge (Heraeus Instruments, Labofuge 400R model)
- Optical microscope (Olympus Life Science, CKX31 model)
- Vortex (Scientific Industries, Vortex-Genie 2 model)
- Magnetic stirrer (Velp Scientifica, MST, model 100-240 V / 50-60 Hz)
- Hemocytometer (VWR, MARI0640011)
- 250 ml sterile borosilicate bottle (VWR 590-0834)
- 5 ml sterile serological pipettes (Greiner Bio-One, cat. no. 606180)
- 10 ml sterile serological pipettes (Greiner Bio-One, cat. no. 607180)
- 25 ml sterile serological pipettes (Greiner Bio-One, 760180)
- Pipettor (Pipet-Aid, XP model)
- 15 ml sterile Falcon tube (Corning, cat. no. 652095)
- 0.5 ml sterile tube (Eppendorf, cat. no 022363611)
- 0.5-10 μ l micropipette (Eppendorf, cat. no. ES-10)
- 20-200 μ l micropipette (Eppendorf, cat. no., ES-200)
- 100-1000 μ l micropipette (Eppendorf, cat. no., ES-1000)
- 10 μ l pipette tips (Eppendorf, cat. no 0030000854)
- 200 μ l pipette tips (Eppendorf, cat. no 0030000897)
- 1000 μ l pipette tips (Eppendorf, cat. no 0030000927)
- pH strips (Metria, cat no. CSPH-002-001)

Reagent Setup

- **APTES 10%:** 10 mL of (3-aminopropyl) triethoxysilane is added to 90 mL of absolute ethanol.
- **Genipin 5 mM:** 25 mg/mL of stock solution is prepared by diluting 125 mg of genipin in 5 mL of DMSO. 2.5mL of this stock solution is taken and dissolved in 45.5 mL of PBS 1x

PROCEDURE

Treatment of the PDMS surface

The day before the experiment, the treatment of the PDMS surface should be performed.

1. PDMS surface is activated by introducing the chip in the Plasma Cleaner for 2 minutes at maximum voltage for making the surface hydrophilic. **CAUTION:** next step should be performed immediately to avoid the loss of the surface activation (maximum time 1 hour)
2. Then, the chip is introduced in the culture chamber and irradiated with UV light for 10 minutes to accomplish sterilization. The chip should be placed near the source of the light (~20 cm).

3. PDMS surface is covered with APTES 10% for 1 h. After that, 3 washes of PBS 1X of 5 minutes each are performed. Genipin 5 mM is added to the wells for 45 minutes.
CAUTION: genipin should be protected from light exposure during the experiment and during its storage. The chips are left overnight to dry.

Preparation of the pregel

The afternoon before the experiment, the pregel must be prepared to be digested overnight.

4. 5 mg of pepsin is weighted in a 50 mL conical tube.
5. In the same tube, 100 mg of freeze-dried and milled lung ECM powder is weighted.
6. 5 mL of 0.1M HCl is added. **NOTE:** with a sterile Pasteur pipette, flush the solution up and down until no clots are seen.
7. A small magnetic stirrer is placed in the tube and is left on a magnetic agitator overnight at 400 rpm.

Neutralization of the pregel

To stop the enzymatic digestion and allow jellification the next steps are followed:

8. In order to equilibrate salts concentration to a physiological level, 500 μ L of PBS 10X is added
9. To neutralize the solution, 250 μ L of 0.2 M NaOH is added to the solution. Solution is vortex for a few seconds and pH is checked using pH strips. Some extra microliters of 0.1 M NaOH can be added in order to adjust the pH to a physiological level (7.4).
CAUTION: No more than 10 μ L should be added at once. Every time a new amount of NaOH is added, the solution should be vortexed and pH should be checked.
10. The neutralized solution is kept in ice to avoid jellification while LMSC are being trypsinized.

Trypsinization of LMSC

10. Trypsinize lung stem cells following the next steps:
 - 10.1 Remove the medium with a sterile glass Pasteur pipette.
 - 10.2 Add 5 mL of PBS 1x to remove the rest of the medium.
 - 10.3 Add 2 mL of Tryple Trypsin and leave it for 7 minutes in the cell culture incubator

- 10.4 Add 5 mL of TNS to stop the reaction. **CAUTION:** Before stopping the reaction, check in the optical microscope that all the cells have detached.
- 10.5 Transfer the content into a 15 mL falcon and centrifuge it at 350 G for 5 minutes.
- 10.6 Aspirate the TNS and resuspend the pellet in 1 mL of DCCM-1 medium. **NOTE:** pellet should be resuspended in a small volume in order to not dilute de cell suspension so we need a small volume to get the desired amount of cells.
11. Count the cells in a hemocytometer
 - 11.1 Take a small aliquote of the cell suspension and dilute it in 1:10 v/v with trypan blue. Mix it well with micropipette.
 - 11.2 Place 10 μ L of the solution and place it carefully in the hemocytometer chamber
 - 11.3 Count the cells and calculate the cell concentration.
12. Take the needed volume of cell suspension to have a final concentration of 300.000 cells/mL of hydrogel and dilute with DCCM-1 medium until having a 10% of the volume of hydrogel.

LMSC 3D culture

13. Add the prepared suspension of LMSC to the hydrogel
14. With the help of the 1000 μ L micropipette, homogenize the hydrogel solution.
15. Centrifugate the cells at 400 G for 2 minutes at 4 °C. To eliminate the bubbles.
16. Again, mix the suspension carefully this time to avoid the formation of new bubbles with the help of the micropipette.
17. Three PBS 1x washes are performed to the chips that are in the incubator to wash the collagen coating.
18. 300 μ L of hydrogel is placed on every well. **CAUTION:** avoid the formation of bubbles when pipetting
19. Chips are let in the incubator for 20 minutes for the hydrogel to jellify. Afterward, 500 μ L of DCCM-1 is added to each well.